

# **DESIGN OF A SECURE ELECTROMAGNETIC BUILDING**

A THESIS CONDUCTED AT

**THE UNIVERSITY OF SHEFFIELD**

IN THE DEPARTMENT OF

**ELECTRONIC AND ELECTRICAL ENGINEERING**

SUBMITTED FOR THE DEGREE OF

**DOCTOR OF PHILOSOPHY**

BY

Jiayin Roberts

-June 2014-

# ABSTRACT

This research explores the design of a secure electromagnetic building, focusing on buildings such as hospitals, embassies, cinemas and prisons. The novelty in this research was the investigation of a surface, which can be embedded into a wall or a window of a room/building, which is “smart”. In this case “smart” relates to the surfaces ability to reconfigure itself depending on the environment required for wireless signals that are present in the local surrounding area.

For the purpose of designing a “smart” surface, classical passive Frequency Selective Surface (FSS) designs attenuating more than 60dB being very difficult, due to this poor filtering obtained by current passive FSS designs with limited options to reconfigure it practically.

By introducing tuning elements, such as varactor diodes which are embedded into the FSS structure, vast improvements can be seen which can impair mobile phone signal without the need of greater attenuation levels. The outcome of this is a reconfigurable FSS, where the power transmitted through the FSS is a function of the bias voltage across the diodes. The reconfigurable nature of the FSS allows us to rapidly switch the complex transmission response such that the mobile phone signal passing through the FSS is corrupted. This is the first time that such a system has been tested against the GSM protocol.

Simulations and measurements of the system verified that this concept can achieve the required performance. To test the performance of the new FSS, state of the art signal generators and receivers were employed to evaluate the Bit Error Rate (BER), which is a measure of the quality of a communications signal. BER of greater than 35% were achieved, which is significantly higher than that needed to successfully receive a signal.

Original work has also been carried out investigating the diffraction effects of FSS for secure building applications in order to understand the practical implications of this technology. In summary all aspects of the design of a secure building have been investigated, from the FSS design and the scattering from the room/building which it is intended to be used in.

# ACKNOWLEDGMENTS

My PhD study here at Sheffield University has enhanced and widened my skills and knowledge throughout the development of my study. It has shown me new ways of thinking, adding concepts and ideas learned from the communication group in Electronic and Electrical Engineering, which has matured my already well-established engineering background.

I would like express my deepest thanks to all the people who have guided me throughout the writing of this Thesis, especially to those who are acknowledged below.

Many thanks to my supervisors Dr. Jonathan Rigelsford and Dr. Lee Ford who have supported me at every step, providing useful knowledge to aid this dissertation as well as their support and encouragement throughout my PhD study. Without their help I wouldn't have been able to flourish in completing my study.

Additional thanks, goes to my pervious supervisor Professor Richard Langley for funding my scholarship. When I started my PhD, he was able to provide me with a lot of valuable ideas throughout my first year's progression.

I've appreciated my full support from my husband Matthew Stephen Roberts, who during my study has always stood by and looked after me. My parents have also been important during this time, helping me out with difficulties and supporting me. Without their support wouldn't have been able to finish my study as they looked after my little son Tony as well.

Finally, I would like to extend my sincere gratitude to all staffs and colleagues from my department.

# LIST OF CONTENTS

|  |    |
|--|----|
| Abstract .....   | 2  |
| Acknowledgments .....  | 3  |
| List of Contents .....   | 4  |
| List of Publications .....                                       | 7  |
| List of Figures .....  | 8  |
| List of Tables .....   | 12 |
| List of Acronyms .....   | 13 |
| List of Symbols .....  | 14 |
| Chapter 1 Introduction .....                                     | 15 |
| 1.1 Background .....   | 15 |
| 1.2 Motivation and Objectives .....                              | 16 |
| 1.3 Summary of the Work Presented in this Thesis .....           | 22 |
| Chapter 2 Literature Review .....                                | 24 |
| 2.1 The need for Privacy .....                                   | 24 |
| 2.2 FSS Theory .....   | 25 |
| 2.3 Types of FSS .....   | 28 |
| 2.3.1 Reconfigurable Switching FSS .....                         | 28 |
| 2.3.2 The Transparent Frequency Selective Surface .....          | 31 |
| 2.3.3 Convolved Frequency Selective Structures .....             | 33 |
| 2.4 Use of FSS on Building Structures .....                      | 34 |
| 2.5 Digital Modulation Schemes .....                             | 36 |
| 2.5.1 Binary Phase-Shift Keying (BPSK) .....                     | 38 |
| 2.5.2 Quadrature Phase-Shift keying (QPSK) .....                 | 38 |
| 2.5.3 Offset Quadrature Phase-Shift keying (OQPSK) .....         | 39 |
| 2.5.4 Gaussian Minimum-Shift Keying (GMSK) .....                 | 40 |
| Chapter 3 Basic FSS Structure Simulations and Measurements ..... | 41 |
| 3.1 Band-Stop Filters .....                                      | 41 |
| 3.1.1 Band-Stop FSS Unit Cell Tuned at 1.8GHz .....              | 41 |
| 3.1.2 Band-Stop FSS Unit Cell Tuned at 2.1GHz .....              | 44 |
| 3.1.3 Band-Stop FSS Panel Tuned at 2.1GHz .....                  | 46 |

|           |   |     |
|-----------|---|-----|
| 3.2       | Modelled Prison Cell using Signal Layer FSS.....                          | 48  |
| 3.3       | Summary.....  | 50  |
| Chapter 4 | Numerical Modelling Development.....                                      | 51  |
| 4.1       | GSM Protocol Modelling.....   | 51  |
| 4.1.1     | GSM Background.....   | 51  |
| 4.1.2     | Speech Signal Convolution Coding.....                                     | 53  |
| 4.1.3     | Interleave Simulation.....  | 53  |
| 4.1.4     | Differential Encoding Simulation.....                                     | 55  |
| 4.1.5     | GMSK Modulation Simulation.....   | 57  |
| 4.1.6     | Channel Simulation.....   | 62  |
| 4.1.7     | Low-Pass Filter Simulation.....   | 62  |
| 4.1.8     | GSM Demodulation Simulation.....  | 62  |
| 4.1.9     | MLSE Detection.....   | 65  |
| 4.1.10    | Differential Decoder Simulation.....                                      | 66  |
| 4.1.11    | De-interleave Simulation.....   | 67  |
| 4.1.12    | Convolution Decoding.....   | 68  |
| 4.2       | Software Environment.....   | 69  |
| 4.3       | Summary.....  | 71  |
| Chapter 5 | Reconfigurable FSS for use in Secure Electromagnetic Building.....        | 72  |
| 5.1       | GSM Simulator Using MATLAB.....   | 74  |
| 5.2       | Frequency Spectrum of Channel with Interleaving.....                      | 79  |
| 5.3       | 2-D Surface Plots of BER with Interleaving.....                           | 86  |
| 5.4       | Frequency Spectrum of Channel without Interleaving.....                   | 88  |
| 5.5       | 2-D Surface Plots of BER without Interleaving.....                        | 90  |
| 5.6       | Summary.....  | 93  |
| Chapter 6 | System Measurement to Test Switching FSS with GSM Signals.....            | 94  |
| 6.1       | Reconfigurable Single Polarization FSS Unit Cell Design.....              | 94  |
| 6.2       | Reconfigurable Single Polarization FSS Panel Design.....                  | 97  |
| 6.3       | Reconfigurable Single Polarization FSS System Measurement.....            | 98  |
| 6.4       | BER Measurement for the Reconfigurable Signal Polarization FSS Panel..... | 101 |
| 6.5       | Reconfigurable Dual Polarization FSS Unit Cell Design.....                | 103 |

|           |   |     |
|-----------|---|-----|
| 6.6       | Reconfigurable Dual Polarization FSS Panel Design .....                             | 106 |
| 6.7       | Reconfigurable Dual Polarization FSS System Measurement .....                       | 108 |
| 6.8       | BER Measurement for the Reconfigurable Dual Polarization FSS .....                  | 113 |
| 6.9       | Frequency Spectrum Measurements for the Reconfigurable Dual Polarization FSS .....  | 116 |
| 6.10      | Summary .....   | 119 |
| Chapter 7 | Diffraction from Frequency Selective Surfaces for Secure Building Application ..... | 120 |
| 7.1       | FSS Non-Specular Scattering Scenario .....  | 120 |
| 7.2       | FSS Non-Specular Scattering Radiation Pattern Analysis .....                        | 123 |
| 7.3       | Summary .....   | 142 |
| Chapter 8 | Conclusion .....  | 143 |
| Chapter 9 | Future Work .....   | 147 |
| 9.1       | Smart FSS design .....  | 147 |
| 9.2       | 3D building simulation .....  | 147 |
| 9.3       | Verifying theoretical results with measurement results .....                        | 147 |
| 9.4       | Measurement of different concrete materials .....                                   | 148 |
| 9.5       | Investigate Diffraction Scattering from FSS Panel with Missing Elements .....       | 148 |
| 9.6       | Reconfigurable Switching FSS Switch over Different Modulation Schemes .....         | 148 |
|           | Bibliography .....  | 149 |
|           | Appendix I: Prison List .....   | 154 |
|           | Appendix II: Prison Cell with FSS on the Window .....                               | 166 |
|           | Appendix III: BB857 Diode Data Sheet .....  | 167 |
|           | Appendix IV: BB131 Diode Data Sheet .....   | 168 |

# LIST OF PUBLICATIONS

[1] J Roberts, J. Rigelsford and K. L. Ford “Diffraction From Frequency Selective Surfaces for Secure Building Applications,” in European Conference on Antennas and Propagation (EuCAP 2012), Prague, Czech Republic, 2012.

[2] J Roberts, K. L. Ford and J. Rigelsford "Secure Electromagnetic Buildings," in European Conference on Antennas and Propagation (EuCAP 2014), Hague, Netherlands, 2014.

[3] K.L. Ford, J. Roberts, S. Zhou, G. Fong and J. Rigelsford “Reconfigurable Frequency Selective Surface for use in Secure Electromagnetic Buildings” *Electronic Letters, IET*, Vol.49 ,No.14, July 2013.

# LIST OF FIGURES

|   |    |
|---|----|
| Figure 1-1: Signal Quality for Category M .....   | 18 |
| Figure 1-2: Signal Quality for Category A .....   | 18 |
| Figure 1-3: Signal Quality for Category B .....   | 18 |
| Figure 1-4: Signal Quality for Category C .....   | 19 |
| Figure 1-5: Signal Quality for Category D .....   | 19 |
| Figure 1-6: Front and Top view of Mappin Building .....                                 | 20 |
| Figure 1-7: Monopole antennas .....   | 20 |
| Figure 1-8: Marked Locations of Mobile Base Stations .....                              | 21 |
| Figure 2-1: Periodic Surface of Elements of Length $2l$ .....                           | 25 |
| Figure 2-2: Plane Wave Incident FSS and the Electrons Effect .....                      | 26 |
| Figure 2-3: Frequency Selective Surface .....   | 27 |
| Figure 2-4: FSS with their Equivalent Circuit and Transmission Response .....           | 27 |
| Figure 2-5: Front Close-Up View of a Switchable FSS Prototype .....                     | 29 |
| Figure 2-6: Frequency Spectrum of Reflected Signal from PSS .....                       | 30 |
| Figure 2-7: A Single-layer Planer PSS .....   | 31 |
| Figure 2-8: Circular Patch (a) and Slot Rings (b) In a Square Lattice Arrangement ..... | 32 |
| Figure 2-9: (a) 1.9GHz Single Shield Type (b) 1.9GHz, 2.4GHz Dual Shield Type .....     | 32 |
| Figure 2-10: Structure of the Convolved Transparent FSS Structure .....                 | 34 |
| Figure 2-11: Binary Phase-Shift Keying .....  | 38 |
| Figure 2-12: Quadrature Phase-Shift Keying .....  | 39 |
| Figure 2-13: Offset Quadrature Phase-Shift Keying .....                                 | 39 |
| Figure 2-14: Gaussian Minimum-Shift Keying .....  | 40 |
| Figure 3-1: Band-stop Single Square Loop FSS at 1.8 GHz .....                           | 42 |
| Figure 3-2: Transmission Response of the FSS at 1.8GHz .....                            | 42 |
| Figure 3-3: Transmission Responses of the FSS at 1.8GHz in TE Mode .....                | 43 |
| Figure 3-4: Transmission Responses of the FSS at 1.8GHz in TM Mode .....                | 43 |
| Figure 3-5: Band-stop Single Square Loop FSS at 2.1 GHz .....                           | 44 |
| Figure 3-6: Transmission Response of the FSS at 2.1GHz .....                            | 44 |
| Figure 3-7: Transmission Responses of the FSS at 2.1GHz in TE Mode .....                | 45 |
| Figure 3-8: Transmission Responses of the FSS at 2.1GHz in TM Mode .....                | 45 |
| Figure 3-9: FSS Panel .....   | 46 |
| Figure 3-10: Measurement Set Up for FSS Panel .....                                     | 47 |
| Figure 3-11: FSS Panel Measurement Result .....   | 48 |
| Figure 3-12: (a) Metal Box without FSS and (b) Metal Box Model .....                    | 48 |
| Figure 3-13: Simulation Result for Metal Box without FSS .....                          | 49 |
| Figure 3-14: Metal Box with FSS .....   | 49 |
| Figure 3-15: Simulation Result for Metal Box with FSS .....                             | 50 |
| Figure 4-1: Structure of a GSM TDMA Frame .....   | 52 |

|  |    |
|--|----|
| Figure 4-2: Model of GSM System.....   | 52 |
| Figure 4-3: Convolutional Coding .....   | 53 |
| Figure 4-4: Interleaving Process .....   | 54 |
| Figure 4-5: Input Data of the Differential Encoder .....                                     | 56 |
| Figure 4-6: Output Data of Differential Encoder .....  | 56 |
| Figure 4-7: GMSK Modulator.....  | 57 |
| Figure 4-8: Impulse Response of Gaussian Filter .....  | 58 |
| Figure 4-9: Data Stream after Encoder in Matlab .....  | 59 |
| Figure 4-10: Stream of Bits Added After Passing through the Gaussian Filter .....            | 60 |
| Figure 4-11: Integrated Stream of Bits in MATLAB .....                                       | 60 |
| Figure 4-12: In Phase Sequence I(t) in MATLAB .....  | 61 |
| Figure 4-13: Quadrature Phase Sequence Q(t) in MATLAB .....                                  | 61 |
| Figure 4-14: An example of TSC1 .....  | 63 |
| Figure 4-15: Estimated Channel Impulse Response.....   | 64 |
| Figure 4-16: The Peak of the CIR within the Window Size.....                                 | 65 |
| Figure 4-17: Input Data of the Differential Decoder .....                                    | 67 |
| Figure 4-18: Output Data of the Differential Decoder .....                                   | 67 |
| Figure 4-19: De-interleave Process .....   | 68 |
| Figure 4-20: Convolutional Decoding.....   | 69 |
| Figure 4-21: TEM, TE and TM Polarisation .....   | 70 |
| Figure 5-1: Illustration of FSS Embedded with the Wall of a Building .....                   | 73 |
| Figure 5-2: Phase before Switching, Interleaving and Convolutional Coding .....              | 75 |
| Figure 5-3: Phase Switching at 2.71MHz, Interleaving and Convolutional Coding .....          | 75 |
| Figure 5-4: Phase Switching at 271kHz, Interleaving and Convolutional Coding .....           | 76 |
| Figure 5-5: Frequency Spectrum before Switching, Interleaving and Convolutional Coding ..... | 77 |
| Figure 5-6: Frequency Spectrum of the Signal Switching by 2.71MHz .....                      | 77 |
| Figure 5-7: The Frequency Spectrum of the Signal Switching at 271kHz.....                    | 78 |
| Figure 5-8: The Signal as Switching Frequency at 2.71MHz .....                               | 79 |
| Figure 5-9: The Signal as Switching Frequency at 271kHz.....                                 | 80 |
| Figure 5-10: The Signal as Switching Frequency at 135.5kHz.....                              | 80 |
| Figure 5-11: The Signal as Switching Frequency at 67.75 kHz.....                             | 81 |
| Figure 5-12: The Signal as Switching Frequency at 2.71MHz .....                              | 82 |
| Figure 5-13: The Signal as Switching Frequency at 271kHz .....                               | 82 |
| Figure 5-14: The Signal as Switching Frequency at 135.5kHz.....                              | 83 |
| Figure 5-15: The Signal as Maximum Switching Frequency at 67.75kHz .....                     | 83 |
| Figure 5-16: A 2-D Surface Plot of BER for 1 Random Seed.....                                | 84 |
| Figure 5-17: A 2-D Surface Plot of BER for 10 Random Seeds .....                             | 85 |
| Figure 5-18: A 2-D Surface Plot of BER for 100 Random Seeds .....                            | 85 |
| Figure 5-19: BER (%) using Bandwidth Filter of 135kHz with Interleaving .....                | 86 |
| Figure 5-20: BER (%) using Bandwidth Filter of 270kHz with Interleaving .....                | 86 |

|   |     |
|---|-----|
| Figure 5-21: BER (%) using Bandwidth Filter of 405kHz with Interleaving .....                   | 87  |
| Figure 5-22: BER (%) using Bandwidth Filter of 540kHz with Interleaving .....                   | 87  |
| Figure 5-23: The Signal as Switching Frequency at 271 kHz .....                                 | 88  |
| Figure 5-24: The Signal as Switching Frequency at 135.5kHz .....                                | 89  |
| Figure 5-25: The Signal as Switching Frequency at 67.75kHz .....                                | 89  |
| Figure 5-26: BER (%) using Bandwidth Filter of 135kHz without Interleaving .....                | 90  |
| Figure 5-27: BER (%) using Bandwidth Filter of 270kHz without Interleaving .....                | 91  |
| Figure 5-28: BER (%) using Bandwidth Filter of 405kHz without Interleaving .....                | 91  |
| Figure 5-29: BER (%) using Bandwidth Filter of 540kHz without Interleaving .....                | 92  |
| Figure 6-1: Front and Side View of the Reconfigurable Signal Polarization FSS Unit Cell .....   | 94  |
| Figure 6-2: Transmission Response for Reconfigurable Signal Polarization FSS Unit Cell .....    | 95  |
| Figure 6-3: Phase Response for Reconfigurable Signal Polarization FSS Unit Cell .....           | 95  |
| Figure 6-4: Transmission Response of FSS Unit Cell Tuned at 1.8GHz .....                        | 96  |
| Figure 6-5: Phase Response of FSS Unit Cell Tuned at 1.8GHz .....                               | 97  |
| Figure 6-6: Phase Response of FSS Unit Cell at varying Capacitances .....                       | 97  |
| Figure 6-7: Reconfigurable Single Polarization FSS Panel .....                                  | 98  |
| Figure 6-8: Measurement Set Up for Reconfigurable FSS Panel .....                               | 99  |
| Figure 6-9: Transmission Response for Reconfigurable Single Polarization FSS Panel .....        | 100 |
| Figure 6-10: Phase Response for Reconfigurable Single Polarization FSS Panel .....              | 100 |
| Figure 6-11: BER Measurement Set Up for Reconfigurable Single Polarization FSS Panel .....      | 101 |
| Figure 6-12: GSM Signal BER (%) of Reconfigurable Single Polarization FSS Panel .....           | 102 |
| Figure 6-13: Front and Side View of the Reconfigurable Dual Polarization FSS Unit Cell .....    | 103 |
| Figure 6-14: Transmission Response for Reconfigurable Dual Polarization FSS Unit Cell .....     | 104 |
| Figure 6-15: Phase Response for Reconfigurable Dual Polarization FSS Unit Cell .....            | 104 |
| Figure 6-16: Transmission Response of FSS Unit Cell Tuned at 1.8GHz .....                       | 105 |
| Figure 6-17: Phase Response of FSS Unit Cell Tuned at 1.8GHz .....                              | 106 |
| Figure 6-18: Phase Response of FSS Unit Cell at varying Capacitances .....                      | 106 |
| Figure 6-19: Reconfigurable Dual Polarization FSS Panel .....                                   | 107 |
| Figure 6-20: The structure of the FSS Panel .....   | 107 |
| Figure 6-21: Transmission Response for Initial Position of the FSS Panel .....                  | 109 |
| Figure 6-22: Phase Response for Initial Position of the FSS Panel .....                         | 109 |
| Figure 6-23: Transmission Response against Frequencies at Initial Position of FSS Panel .....   | 110 |
| Figure 6-24: Phase Response against Frequencies at Initial Position of FSS Panel .....          | 110 |
| Figure 6-25: The Transmission Response of FSS Panel Rotate 90° .....                            | 112 |
| Figure 6-26: The Phase Response of the FSS Panel Rotate 90° .....                               | 112 |
| Figure 6-27: Transmission Response against Frequencies after FSS Panel Rotated 90° .....        | 112 |
| Figure 6-28: Phase Response against Frequencies after FSS Panel Rotated 90° .....               | 113 |
| Figure 6-29: Received Signal power against Frequencies .....                                    | 114 |
| Figure 6-30: GSM Signal BER (%) of Reconfigurable Dual Polarization FSS Panel .....             | 115 |
| Figure 6-31: GSM Signal BER (%) of Reconfigurable Dual Polarization FSS Panel rotated 90° ..... | 115 |

|  |     |
|--|-----|
| Figure 6-32 Frequency Spectrum for Reconfigurable Dual Polarization FSS – No Switching .....           | 117 |
| Figure 6-33 Frequency Spectrum for Reconfigurable Dual Polarization FSS – Switching At 2.71 MHz.....   | 117 |
| Figure 6-34 Frequency Spectrum for Reconfigurable Dual Polarization FSS – Switching At 1 MHz.....      | 118 |
| Figure 6-35 Frequency Spectrum for Reconfigurable Dual Polarization FSS – Switching At 271 kHz .....   | 118 |
| Figure 6-36 Frequency Spectrum for Reconfigurable Dual Polarization FSS – Switching At 135.5 kHz ..... | 119 |
| Figure 7-1: The Signal Received by Base Station .....  | 121 |
| Figure 7-2: Illustration of an FSS in a Secure Room .....  | 121 |
| Figure 7-3: The Transmission Response for the Unit Cell.....   | 122 |
| Figure 7-4: 3-D Wall Surface.....  | 123 |
| Figure 7-5: 20° Incident Angle from the Wall Surface with 3-D Simulation Result.....                   | 124 |
| Figure 7-6: Radiation Pattern Flat PEC Sheet at Different Incident Angles .....                        | 125 |
| Figure 7-7: Incident Angle at 20° for the scatter field.....   | 126 |
| Figure 7-8: Incident Angle at 40° for the scatter field.....   | 126 |
| Figure 7-9: Incident Angle at 60° for the scatter field.....   | 127 |
| Figure 7-10: Incident Angle at 80° for the scatter field.....  | 127 |
| Figure 7-11: Comparison of Incident Angle at 20° and 80° .....   | 128 |
| Figure 7-12: The Transmission Responses of the Large Unit Cell .....                                   | 128 |
| Figure 7-13: Comparison Metal Wall with FSS and With Aperture Cases at Specular Angle at 60° .....     | 130 |
| Figure 7-14: Comparison Metal Wall with FSS and With Aperture Cases at Specular Angle at 80° .....     | 130 |
| Figure 7-15: Small Unit Cell.....  | 131 |
| Figure 7-16: Transmission Response for a Smaller Unit Cell.....  | 131 |
| Figure 7-17: Comparison of 25mm and 50mm Unit Cell at incident angle of 20° .....                      | 132 |
| Figure 7-18: Comparison of 25mm and 50mm Unit Cell at incident angle of 40° .....                      | 132 |
| Figure 7-19: Comparison of 25mm and 50mm Unit Cell at incident angle of 60° .....                      | 133 |
| Figure 7-20: Comparison of 25mm and 50mm Unit Cell at incident angle of 80° .....                      | 133 |
| Figure 7-21: Transmission Responses for the Small Unit Cell .....                                      | 134 |
| Figure 7-22: Rotate Unit Cell 45°.....   | 135 |
| Figure 7-23: Transmission Response for Rotate FSS 45° .....  | 135 |
| Figure 7-24: Comparison of Original and Rotated Unit Cell at Incident Angle of 20° .....               | 136 |
| Figure 7-25: Comparison of Original and Rotated Unit Cell at Incident Angle of 40° .....               | 136 |
| Figure 7-26: Comparison of Original and Rotated Unit Cell at Incident Angle of 60° .....               | 137 |
| Figure 7-27: Comparison of Original and Rotated Unit Cell at Incident Angle of 80° .....               | 137 |
| Figure 7-28: The Transmission Response for the Rotate FSS Panel.....                                   | 138 |
| Figure 7-29: FSS Panel with Metal Teeth attached to a Metal Wall .....                                 | 139 |
| Figure 7-30: Comparison of FSS Panel , with and without Metal Teeth at Incident Angle of 20° .....     | 140 |
| Figure 7-31: Comparison of FSS Panel , with and without Metal Teeth at Incident Angle of 40° .....     | 140 |
| Figure 7-32: Comparison of FSS Panel , with and without Metal Teeth at Incident Angle of 60° .....     | 141 |
| Figure 7-33: Comparison of FSS Panel , with and without Metal Teeth at Incident Angle of 80° .....     | 141 |

# LIST OF TABLES

|  |     |
|--|-----|
| Table 1-1: The categories of prison .....  | 17  |
| Table 1-2: The Category A Prison List .....  | 17  |
| Table 1-3: Measured Signal Strengths at Various Locations .....  | 21  |
| Table 2-1: ISO/OSI 7 layers protocol .....   | 37  |
| Table 4-1: The Frequency Ranges, Offset, and Number of Physical Chanel for GSM900/1800 .....                 | 51  |
| Table 4-2: True Table for Logical XOR Operator .....   | 55  |
| Table 4-3: Logical Table for Differential Encoding .....   | 55  |
| Table 4-4: A Binary Data Stream.....   | 59  |
| Table 4-5: Eight Types of GSM training sequences .....   | 63  |
| Table 4-6: Logical Table for Differential Encoding.....  | 66  |
| Table 5-1: Comparison of the 'on' and 'off' Mode of Interleaving.....  | 92  |
| Table 6-1: The Transmission and Phase Response for the FSS against Voltage.....                              | 99  |
| Table 6-2: The Transmission and Phase Response for the FSS against Voltage at initial position.....          | 108 |
| Table 6-3: The Transmission and Phase Response for the FSS against Voltage after rotated 90° .....           | 111 |
| Table 7-1: Specular Scattering and Normalised Scattered Field .....  | 129 |
| Table 7-2: Specular Scattering and Normalised Scattered Field of Small and Large Unit Cell .....             | 134 |
| Table 7-3: Specular Scattering and Normalised Scattered Field of Rotated and Large Unit Cell FSS .....       | 138 |
| Table 7-4: Specular Scattering and Normalised Scattered Field of Metal Teeth and Large Unit Cell Panel ..... | 142 |

# LIST OF ACRONYMS

|             |  |
|-------------|--|
| BER         | Bit Error Rate                         |
| CST         | Computer Simulation Technology         |
| CAI         | Common Air Interface                   |
| CDMA        | Code Division Multiple Access          |
| 1D          | One Dimensional                        |
| 2D          | Two Dimensional                        |
| 3D          | Three Dimensional                      |
| E Field     | Electric Field                         |
| FIT         | Finite Integration Technique           |
| FSS         | Frequency Selective Surface            |
| FDTD        | Finite-Difference Time-domain          |
| 2G          | Second-Generation                      |
| 3G          | Three-Generation                       |
| GSM         | Global System for Mobile Communication |
| MLSE        | Maximum Likelihood Sequence Estimator  |
| NLOS        | Non Line of Sight                      |
| PEC         | Perfect Electric Conductor             |
| PN          | Pseudo Noise                           |
| PSS         | Phase-Switch Screen                    |
| RCS         | Radar Cross Section                    |
| RAM         | Radar-Absorbent Material               |
| S Parameter | Scattering Parameter                   |

|       |   |
|-------|---|
| TE    | Transverse Electric                         |
| TM    | Transverse Magnetic                         |
| TEM   | Transverse Electromagnetic                  |
| TETRA | Terrestrial Trunked Radio                   |
| UMTS  | Universal Mobile Telecommunications Service |
| UWB   | Ultra Wideband                              |
| WLAN  | Wireless Local Area Network                 |

## **LIST OF SYMBOLS**

|            |                                      |
|------------|--------------------------------------|
| F          | Frequency (Hz)                       |
| T          | Time (s)                             |
| W/C        | The Mass Ratio of Water to Cement    |
| $Z_0$      | Free Space Impedance ( $377\Omega$ ) |
| $\epsilon$ | Electric Permittivity                |
| $\lambda$  | Wave Length                          |
| c          | Speed of Light in Vacuum             |

# CHAPTER 1 INTRODUCTION

## 1.1 Background

The mobile telecommunication industry is undergoing an increasing rate of market growth, combined with the advancement of technological change[1]. In the early stages, mobile services only saw small numbers of subscribers, but now many mobile phone users in the UK have more than one phone. This means mobile phones are heavily used in the UK, which will cause problems in locations where they need to be prohibited, such as prisons, theatres, hospitals, embassies and so on. For example, in a prison, a prisoner might smuggle a phone to do criminal activities including arranging a jailbreak, threaten someone or supply drugs to other prisoners. If mobile phones are used in hospitals they may interfere with medical equipment which is stated in NHS website [2], such as pacemakers, electronic monitoring devices, pumps etc. In cinemas or theatres, silent environments are required, these are just a handful of applications, where the location requires a method to block the transmitted phone signals and novel solutions need to be obtained.

The restriction of devices is still quite difficult to enforce, with many mobile phones still being brought inside restricted areas. Therefore, alternative methods need to be explored preventing the usage of these devices inside a building. Current research and development into this field has developed at a rapid pace, exploring different methods, e.g. mobile phone jammers, RF signal shielding materials or a Frequency Selective Surface (FSS).

Some European countries allow the use of mobile phone jamming in certain public places, e.g. France has decided to jam phone signals in cinemas to allow audiences to enjoy films without interruption. Many countries actually prohibit the use of jammers, like in the UK where mobile phone jammers are illegal according to the Wireless Telegraph Act 1949 [3].

RF signal shielding materials attenuate signals up to 90dB over a spectrum ranging from 50MHz to over 20GHz. This is a lightweight and easy method for isolating RF signals [4]. However this would block all signals, including emergency service.

Frequency Selective Surfaces (FSS) have been researched for many years for their ever increasing use in antennas and Radar Cross Section (RCS) reduction applications [5].

Recently theoretical and experimental work have demonstrated that a FSS could be applied to a building, changing the propagation for different frequencies (GSM, UMTS, Bluetooth and WLAN) which could be controlled to affect its surrounding environments [6]. The advantage of this solution is that a chosen frequency range can be selected to be blocked, so that not all wireless signals are lost within entering the building.

## 1.2 Motivation and Objectives

This research focuses on the use of FSS to design a secure electromagnetic building, where there is a need to control a mobile phone's signal in/out of the building. An example of a prison is given in this research, with prison operators searching for different ways of preventing prisoners covertly using smuggled mobile phones in their cells. The issues they face are that they also need to allow emergency service frequencies to enter the building so they can still communicate freely using internal radio systems. Various possible FSS solutions have been designed to potentially meet this requirement [7, 8].

In order to design a FSS for this building application, the power levels need to be assessed inside the building to make sure it can meet the 'secure' requirement. This would be worked out using various modelling techniques and measurement campaigns which will be discussed in 0 and Chapter 7. When very high attenuation levels are required for the FSS design, Non-specular scattering will become important for Non Line Of Site (NLOS) transmission where diffraction can be significant, and which also needs to be assessed.

To evaluate the influence of diffraction scattering from the edge of an FSS panel on the window aperture, an understanding is required of how the FSS performs in high signal strength areas. Using geographical locations, 2G cellular network signal quality was assessed for all UK prisons, using data provided by the network operators. This information is only indicative and does not provide values of actual signal strength but rather gives an approximation to the level of service in areas that we may wish to remain secure. During the analysis a total of 249 prisons were assessed across the UK. These prisons can be categorised into five different types as shown in Table 1-1: category M, A, B, C, and D, where category A has the highest security and category D has the least.

|          |   |
|----------|---|
| <b>M</b> | Maximum security: paradoxically these can be B as well as A. Specialist attention is paid here, and they are not many in number.                                      |
| <b>A</b> | Closed prison: prisoners are those whose escape would be highly dangerous to the public or national security. A type prisons are designed to make escape impossible . |
| <b>B</b> | Closed prison: prisoners are those whose do not require maximum security, but for whom escape needs to be made very difficult.  |
| <b>C</b> | Closed prison: prisoners cannot be trusted in open conditions but are considered to be prisoners who are unlikely to make a determined escape attempt.                |
| <b>D</b> | Open Prison, prisoners can be trusted in open conditions.   |

*Table 1-1: The categories of prison [9]*

All UK prisons from the extracted prison list have been categorized into their security level type and the associated claimed by the signal strengths for known mobile operators (Appendix I). Table 1-2 contains example of category A prison.

| Prison Name          | Address   | Post Code | Category | OP-A | OP-B | OP-C | OP-D |
|----------------------|---|-----------|----------|------|------|------|------|
| HMP MANCHESTER       | Southall Street, Strangeways, MANCHESTER                | M60 9AH   | A        | 5    | 5    | 2    | 5    |
| HMP ALTCOURSE        | Higher Lane, Fazakerley, LIVERPOOL                      | L9 7LH    | A        | 5    | 5    | 2    | 5    |
| HMP/YOI DONCASTER    | Off North Bridge, Marshgate, DONCASTER, South Yorkshire | DN5 8UX   | A        | 5    | 5    | 2    | 5    |
| HMP BOWHOUSE         | Mauchline Road, Bowhouse, KILMARNOCK, East Ayrshire     | KA1 5AA   | A        | 5    | 3    | 1    | 5    |
| HMP & IDC MAGHABERRY | 17, Old Road, Upper Ballinderry, LISBURN, Co.Antrim     | BT28 2PT  | A        | 5    | 4    | 2    | 5    |

*Table 1-2: The Category A Prison List*

Table 1-2 shows the first few rows of category A prisons outlining the signal strength rating on a scale of 1-5 where 1 is weakest for each mobile phone provider in that area by postcode. Graphs to compare these results are then generated to analyse the signal strength across different categories as shown in Figure 1-1.

Figure 1-1 to Figure 1-5 shows the percentage of prisons grouped by their expected received signal quality in a given prison category. OP-A to OP-D are network operators.

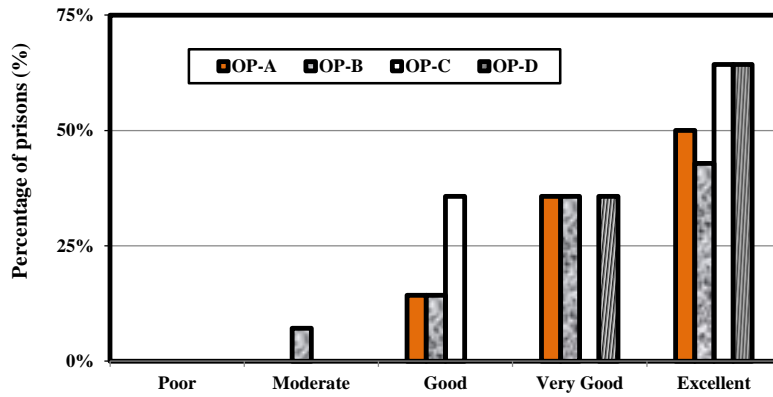


Figure 1-1: Signal Quality for Category M

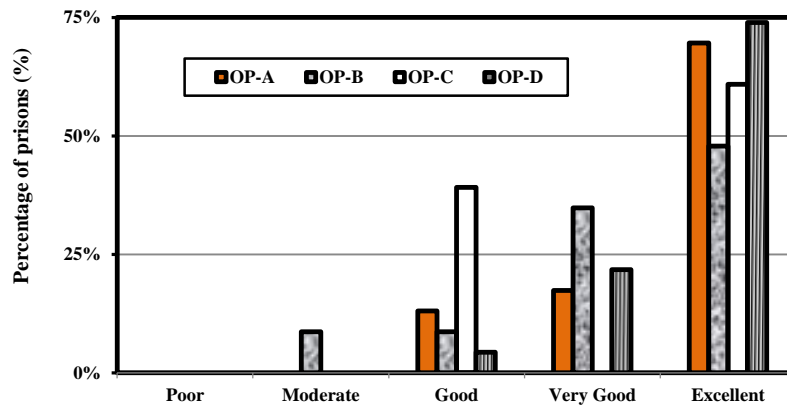


Figure 1-2: Signal Quality for Category A

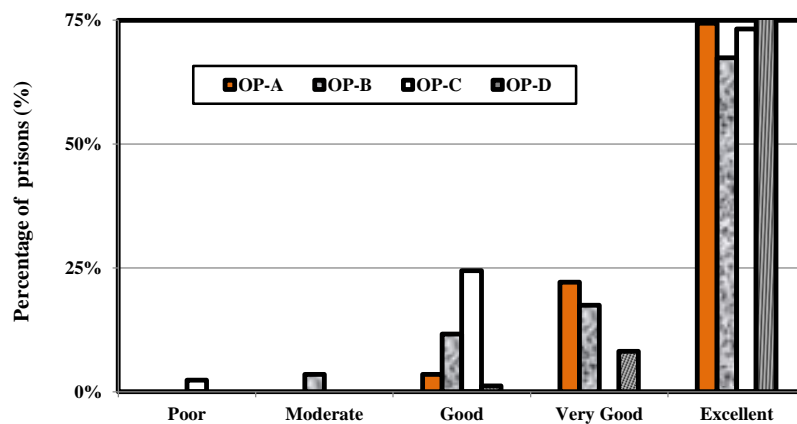


Figure 1-3: Signal Quality for Category B

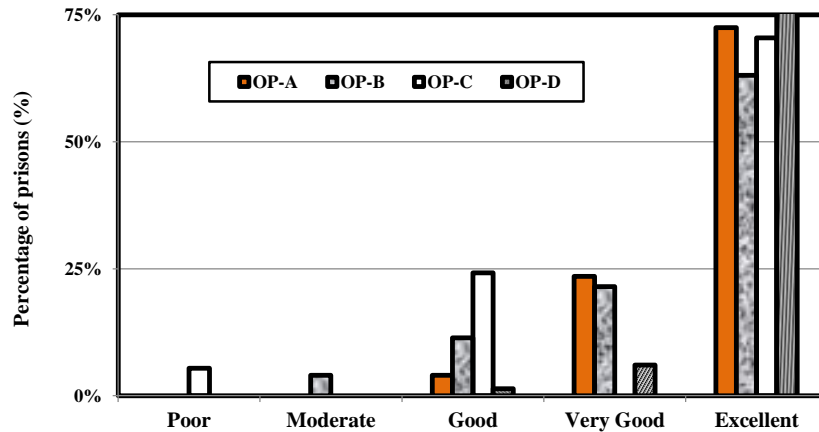


Figure 1-4: Signal Quality for Category C

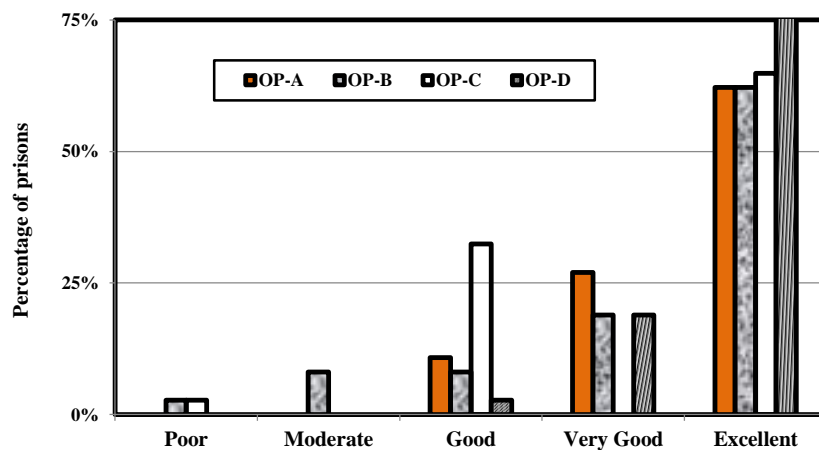
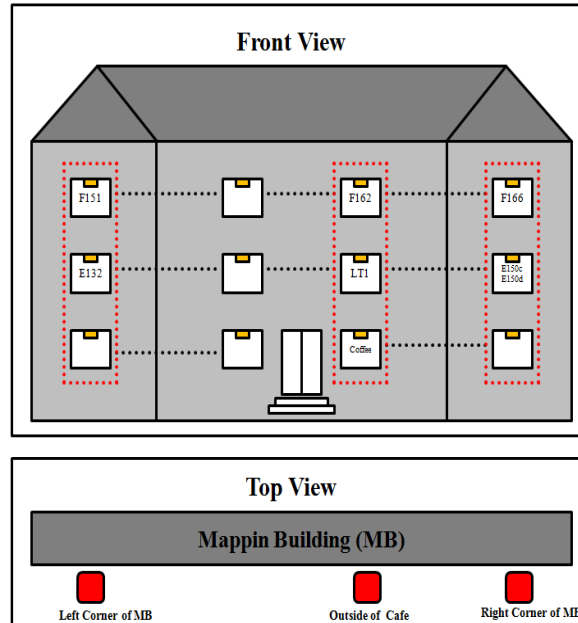


Figure 1-5: Signal Quality for Category D

The results shown in Figure 1-1 to Figure 1-5 illustrate the potential problem that is faced when designing a secure building, where the indicated signal levels can be very high and may require a high level of attenuation from an FSS solution. In such a situation, non-specular scattering could also provide a viable communication channel independent of the specular FSS performance.

In order to understand the FSS attenuation which may be required in a high signal area, several reference measurements were conducted both outside and inside the Sir Frederick Mappin Building at the University of Sheffield.

This location was selected due to it being in an area of excellent signal strength for all network operators so obtaining a good benchmark. Figure 1-6 shows an illustration of the building tested, highlighting the locations which were measured.



*Figure 1-6: Front and Top view of Mappin Building*

To perform the measurements, the three monopole antennas shown in Figure 1-7 were manufactured to operate at 400MHz, 900MHz and 1800MHz, with their lengths being 187.5mm, 83.3mm and 41mm respectively. The antennas were connected to a portable spectrum analyser (Rohde & Schwarz FSH3), which can operate over a frequency range of 100kHz to 3GHz with a resolution bandwidth being from 100Hz to 1MHz. The power measurement capability on this device is from -125dBm to +2 dBm.

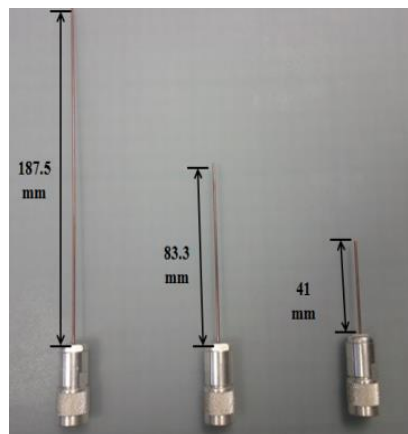


*Figure 1-7: Monopole antennas*

At each location, power measurements were carried out over the full TETRA band and the GSM 900/1800 downlink frequency bands (935MHz - 960MHz and 1805–1880 MHz). The measurements were carried out during dry conditions, with an external temperature of approximately 6 °C. Three samples were taken for each location, with a summary of the results being shown in Table 1-3.

| Location                  | Power (dBm) |            |            |
|---------------------------|-------------|------------|------------|
|                           | 400MHz      | 900MHz     | 1800MHz    |
| <b>Left Corner of MB</b>  | <b>-57</b>  | <b>-62</b> | <b>-56</b> |
| E132                      | -55         | -52        | -65        |
| F151                      | -46         | -61        | -62        |
| <b>Outside of Cafe</b>    | <b>-57</b>  | <b>-60</b> | <b>-45</b> |
| Inside of Cafe            | -63         | -69        | -48        |
| LT1                       | -61         | -62        | -54        |
| F162                      | -55         | -64        | -60        |
| <b>Right Corner of MB</b> | <b>-55</b>  | <b>-53</b> | <b>-51</b> |
| E150c                     | -62         | -44        | -55        |
| E150d                     | -59         | -49        | -61        |
| F166                      | -56         | -51        | -57        |

*Table 1-3: Measured Signal Strengths at Various Locations*

Table 1-3 denotes bold for outdoor locations with Figure 1-8 showing the locations of the base station antennas in relation to the building. Throughout this area, the signal strength is classified by all mobile operators as being of excellent signal quality. The maximum power for the TETRA band is -46dBm, with a variation of 17dB. The maximum power for the GSM900 band is -44dBm, with a variation of 25dB. The maximum power for the GSM1800 band is -45dBm with a variation of 20dB.

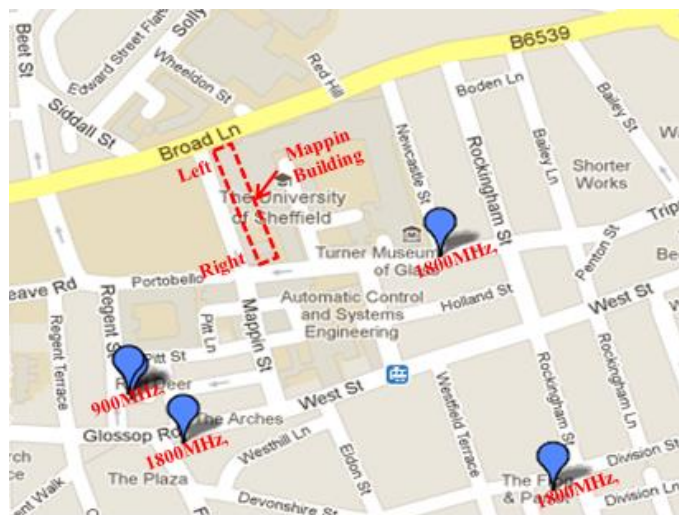


*Figure 1-8: Marked Locations of Mobile Base Stations*

From the measurements taken and analysed, it is possible that a secure room would require above 60dB of attenuation to successfully stop a wireless communication channel. Due to this reason, these research objectives are set as follows:

- Non-specular scattering from a FSS need to be analysed in more detail.
- Different methods need to be investigated to reduce non-specular scattering.
- Due to the use of passive FSS designs attenuating more than 60dB being very difficult to design in practice, a reconfigurable switching FSS to be designed and measured to corrupt a received mobile phone signal inside a building by change the complex transmission response, causing the receiver inside a building being unable to determine the data which was transmitted from outside the building.

### **1.3 Summary of the Work Presented in this Thesis**

The areas of this thesis are sectioned into nine chapters:

The first chapter is an introduction of research, introducing the project background and objectives.

The second chapter explains FSS theory, showing different types of FSS and how FSS interact with building structures. It also outlines the need for privacy within a building structure as well as brief look into several digital modulation schemes used for RF carriers.

The third chapter provides simple FSS simulation results to familiarize the use of the CST simulation environment by designing a simple prison cell structure which is later used in subsequent chapters.

The forth chapter covers the development of numerical modelling, outlining the model of the GSM system which would be built using MATLAB. This chapter explains details for how each module element works in a GSM system, as well as introducing CST as a software environment being used for the simulation in the following chapter.

The fifth chapter shows the design of a reconfigurable frequency selective surface that can be utilised to corrupt a mobile phone signal over the channel. This is achieved by making the receiver being unable to determine the sent data which is transmitted by the

base station. This chapter will also show the simulation results of a 2-D BER surface plot comparing against the phase shifts and switching frequencies.

The sixth chapter contains the measurement set up and results for a single polarization and dual polarization reconfigurable switching FSS.

The seventh chapter presents research into diffraction from a FSS in the application of a secure building, to prevent a signal from entering or leaking from a room. Non-specular scattering will be of importance for Non Line of Site when very high attenuation levels are required. For this reason, the levels of diffraction scattering from a FSS need to be investigated to meet the attenuation needed by the FSS solution.

The eighth chapter is a conclusion, summarising the research finding, including a discussion of the research contributions and illustrating the research limitations.

The ninth chapter briefly outlines further possible research developments that may be expanded upon from this research area.

The contribution of this work is:

- Introducing a reconfigurable switching FSS can impair a GSM signal without the need of greater attenuation levels.
- 2D surface plots and measurement results of the reconfigurable switching FSS presented, showing a BER of over 30% for a wide range of input parameters.
- Illustrates the importance of FSS diffraction for secure building applications in high signal strength areas.
- Three methods for reducing the non-specular scattering mechanism being introduced.

## CHAPTER 2 LITERATURE REVIEW

This section reviews theory behind the basics of an FSS model, in order to understand their equivalent circuit and their transmission response. After this, research into different types of FSS which could be utilised on a buildings structure such as active or transparent FSS. The convoluted FSS also has been looked into to reduce FSS unit cell size.

Previous work from other researchers are also investigated to see how the uses of a FSS are used to control the propagation in/out of a building at different frequencies which includes the consideration of signal propagation within a building which is influenced by specific features. Following that, a more feasible reconfigurable switching FSS would be reviewed. Finally, different digital modulation schemes has been introduced.

### 2.1 The need for Privacy

The demand of utilising radio spectrum is increased rapidly causing degrade wireless communication with channel congestion within indoor environments, especially unlicensed bands, were users privacy could be effected by nearby receivers eavesdropping on their conversation illegally [10]. FSS can be used as an isolator in an indoor environment by providing band selective screening which can selectively reject unwanted frequency range within buildings to reduce interference between adjacent co-channel and reject interfering signal from surrounding building [11].

FSS could improve frequency reuse in building which can lead to increase of network capacity, where incorporating FSS would control the Electromagnetic Architecture of Buildings (EAoB) [12]. According to inverse square law approximation, it recommends just 10 dB reduction decreases cell size required for frequency reuse by a factor of 3, and reuse becomes feasible within buildings and the efficiency of use of the radio spectrum would be potential by enhanced [13].

## 2.2 FSS Theory

Frequency Selective Surfaces (FSS) have been researched for many years for their ever increasing use in reflector antennas and Radar Cross Section (RCS) reduction applications[5]. Historically, it can be traced back as far as the 18th century, where the American physicist David Rittenhouse discovered light spectrum from a street lamp can be filtered through a silk handkerchief [14]. This became the frequency selective property used for this FSS application. One of the earliest patents was granted in 1919 as shown in Figure 2-1, in which an array of elements of finite length  $2\ell$  which should be preferably  $\lambda/2$ , but may be made shorter or longer by inserting in it either a condenser or an inductance with the same spacing  $D_x$ . This periodic surface structure has been intensely studied since the mid-1960s due its large interest in military applications [15].

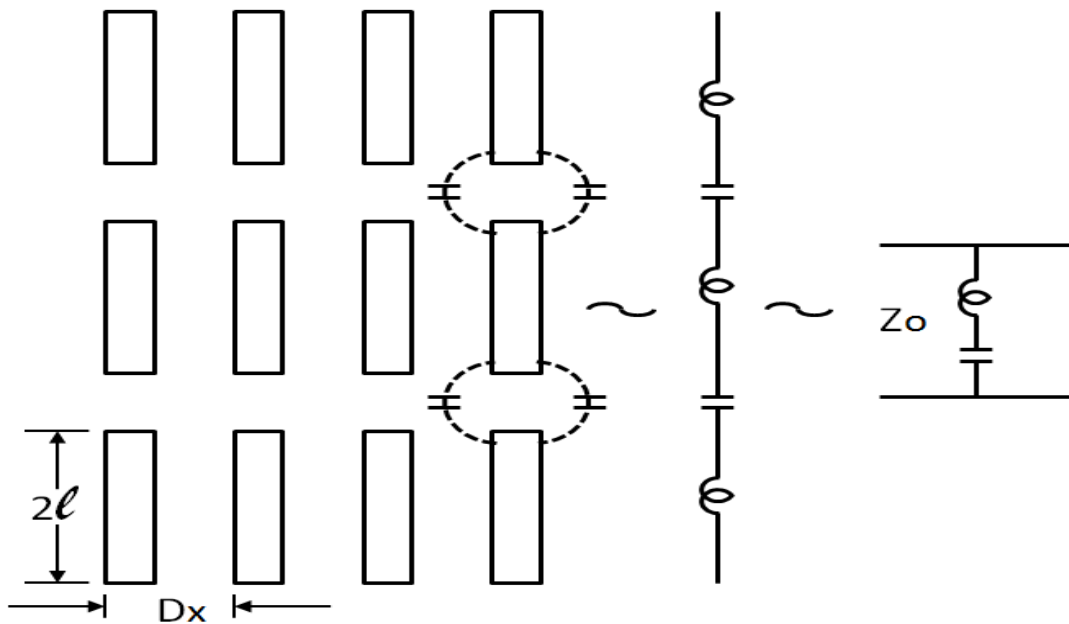
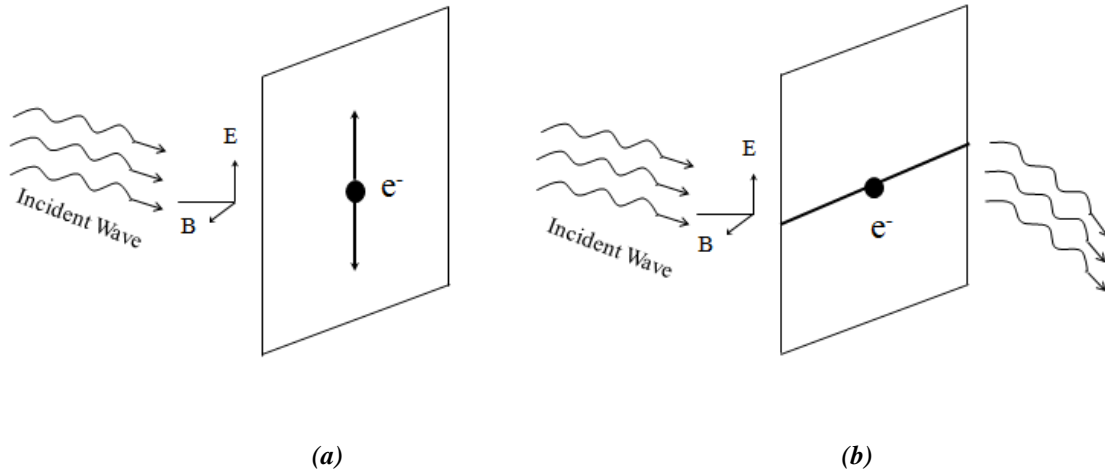


Figure 2-1: Periodic Surface of Elements of Length  $2\ell$

[15]

Before starting analysis of a FSS structure, the relevant concepts in electromagnetic theory has been reviewed to understand how a FSS can perform as a filter.



**Figure 2-2: Plane Wave Incident FSS and the Electrons Effect [16]**

In Figure 2-2 (a), the excitation signal incident to the FSS from left is propagating at a normal incidence angle. The black spot represent a single electron, with the FSS being orthogonal to the incident wave propagation direction. The E-Vector of the incident wave is located on the FSS which bring a force to bear on the electron, causing it to oscillate. A portion of the energy from the incident signal will be absorbed by the oscillating electrons, causing the energy to be converted into kinetic energy [16]. After the electrons absorbed the energy, the electrons start to oscillate, which behave like an electric dipole, with their radiation patterns being emitted on both sides of the FSS. The radiation emitted on the right hand side of the surface will interfere with the incident wave, causing their E-fields to cancel each other out. The left hand side of the radiation is the reflected wave [16].

In the Figure 2-2 (b), the FSS element which is orthogonal to the E-Vector of the incident wave. If the electron is restrained to only go along this wire, the energy from the incident wave will not be absorbed by electron due to it being orthogonal to the direction in which the electron is oscillating. Therefore the incident wave wouldn't be affected by the electron and causing the wave to be transmitted through the surface. A incident wave transmission therefore depends on the pattern of a surface, which will decide the FSS behaviour [16].

A regular FSS is a flat two dimensional planer periodic resonant structure consisting of one or more metallic designs, which are backed by a dielectric substrate in Figure 2-3. These structures are usually arranged periodically [17]. The FSS behaves as a passive electromagnetic filter, which may have a low-pass, band-pass, band-stop or high-pass property[18], attenuating or reflecting a selected frequency band. An elements 'shape

and size' can affect the response of the FSS as well as its 'angle of incidence', 'polarisation', 'permittivity' and 'thickness of the substrate' [19].

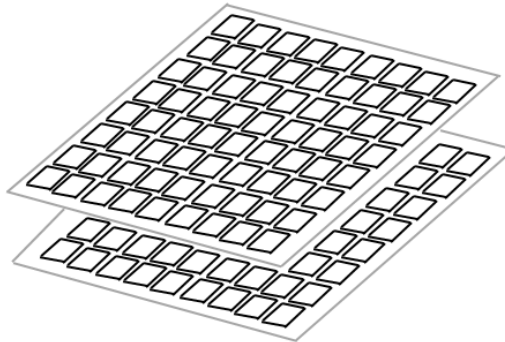


*Figure 2-3: Frequency Selective Surface*

A FSS behaves as a spatial filter, with an equivalent LC circuit being used to represent its overall response characteristics. A band stop filter and a band pass filter are used as an example in Figure 2-4, which is to show their equivalent circuits and transmission response.

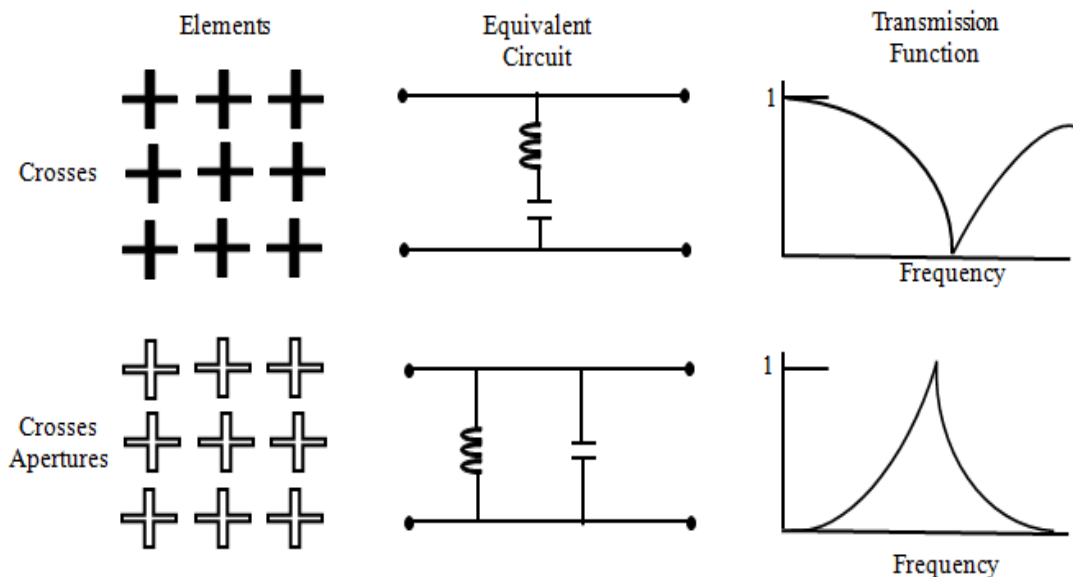


*Figure 2-4: FSS with their Equivalent Circuit and Transmission Response*

The advantage of these two models is that the transmittance propagating pass the filter is independent of the sources polarization due to the filters being symmetrical under rotation. If for example the FSS is rotated  $90^\circ$ , both components of polarization would “see” the same grid geometry [16].

To extend the FSS functions, additional electronic devices were embedded into classical periodic FSS structure to create active grid arrays [18]. Lee and Fong in their paper in 1971 mentioned an active corrugated structure that can control the phase of the reflected wave but also its magnitude of the reflection coefficient which has potential applications, e.g. in phase array radar and microwave amplification [21].

Recently theoretical and experimental work have demonstrated that FSS could be applied to a building, changing the propagation for different frequencies (GSM, UMTS, Bluetooth and WLAN) which could be controlled to effect its surrounding environments [6].

## 2.3 Types of FSS

In this section three types of FSS are introduced which could be used on a building structure, attempting to secure it over different unwanted frequency bands.

### 2.3.1 Reconfigurable Switching FSS

Reconfigurable active FSS are widely used in current communication systems for a FSS design which can provide a better reconfigurable solution for a given building architecture. It adds additional bias circuitry to the traditional passive FSS which can vary the frequency response with time to change its characteristics [22]. These active FSS are designed with varactor diodes that can be adjusted by altering the DC voltage across the varactor diodes connections to directly control the reflection and transmission response of the active tuned FSS [23]-[24].

Switching FSS can also be used to switch between reflective and transparent states for a building application, which is to switch the EM coupling between individual rooms inside a building or to an external environment [25]. Figure 2-5 is an example for a switching FSS which has been fabricated using a square loop FSS design with each unit cell having four PIN diodes placed symmetrically [26].

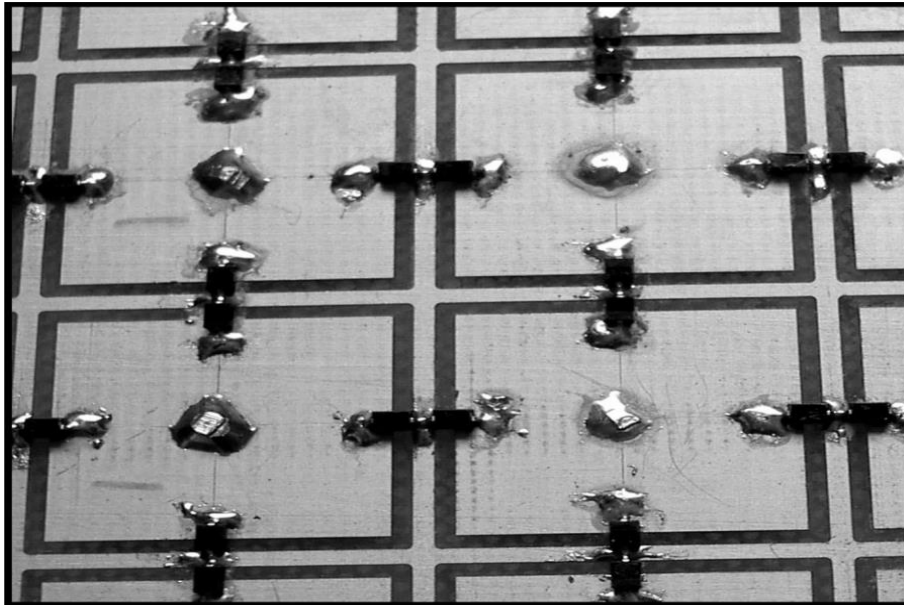


*Figure 2-5: Front Close-Up View of a Switchable FSS Prototype [26]*

Reconfigurable switching FSS using a spread spectrum system can be traced back to 1984, with a patent paper mentioning it as a ‘covert communication system’ which employs an extensive bandwidth to improve its signal to noise ratio [27]. “The term “covert communication system” means a communication system that prevents unauthorized detection of the communication traffic”. It includes four arrangements: first, translate bit '1' and '0' into PN (Pseudo Noise) code sequence which spread over a large bandwidth. Second, the PN sequence has been transmitted at a low power level environmental noise of propagation medium. Third, received the PN sequence with the environmental noise. Fourth, recovered the binary signal from the PN sequence [27].

Recently, this technology has been used in a Phase-Switch Screen (PSS) as well. Chambers and Tennant explored a lot of research in this area [28-35], with a PSS being a device that can reduce a target's Radar-Cross Section (RCS) by reflections and redistributing electromagnetic energy of the incident signal outside the bandwidth of the detection systems so that only a proportion of energy can be received [32]; Figure 2-6 illustrates an example for the signal incident for a PSS. The grey coloured trace represent the PSS screen ON which the scattered signal from the unmodulated PSS shows a classic  $\sin x/x$  response centred on the 11GHz carrier. The black coloured trace represents the PSS screen OFF which the modulated FSS shows the energy of the

response has been redistributed into sidebands at every 20MHz [35]. This functionality is very useful for military applications which ultimately aims to make an object undetectable on radar.

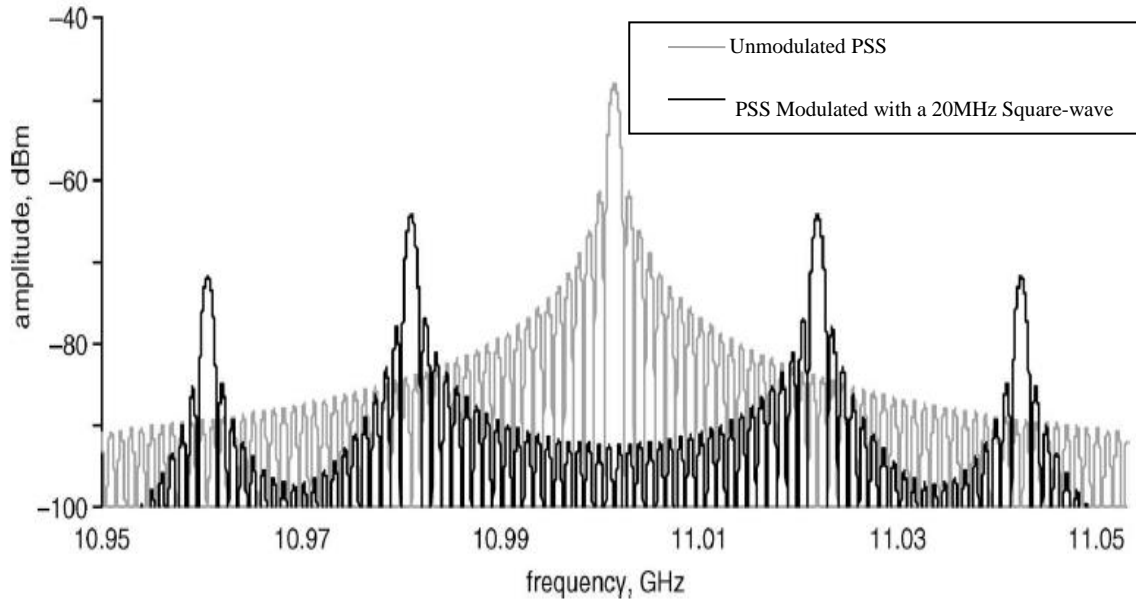


*Figure 2-6: Frequency Spectrum of Reflected Signal from PSS [35]*

PSS has different designs: single-layer, dual-layer and dual-polarised. To understand the structure, the simplest single-layer planar PSS will be used as an example in Figure 2-7. It has a switchable active front layer and a PEC backplane, the impedance states of the active layer can be switched very rapidly from high to low. When  $R = \infty\Omega$ , the layer is switched off, it can be switched to totally transparent states to the incident signal, when  $R = 0\Omega$ , the layer is switched on, with the incident signal being reflected back [36]. If the illuminating signal is a unit amplitude normalised plane wave with an angular frequency of  $\omega$ , the reflected signal back can be expressed as  $\cos(\omega t)$  when the active screen is ON and  $\cos(\omega t + 2\beta d)$  when the active screen is OFF, where  $\beta = 2\pi/\lambda$  and  $\lambda = C/f$ . The term  $2\beta d$  describes the phase shift between the two reflected waves from the front active layer and PEC backplane, when the distance  $d$  between these two layers equal to  $\lambda/4$ , the phase difference is  $180^\circ$ . So if the active layer is switched between ON and OFF states for a response to a modulating function being applied, a phase modulated reflected signal would be produced [37].

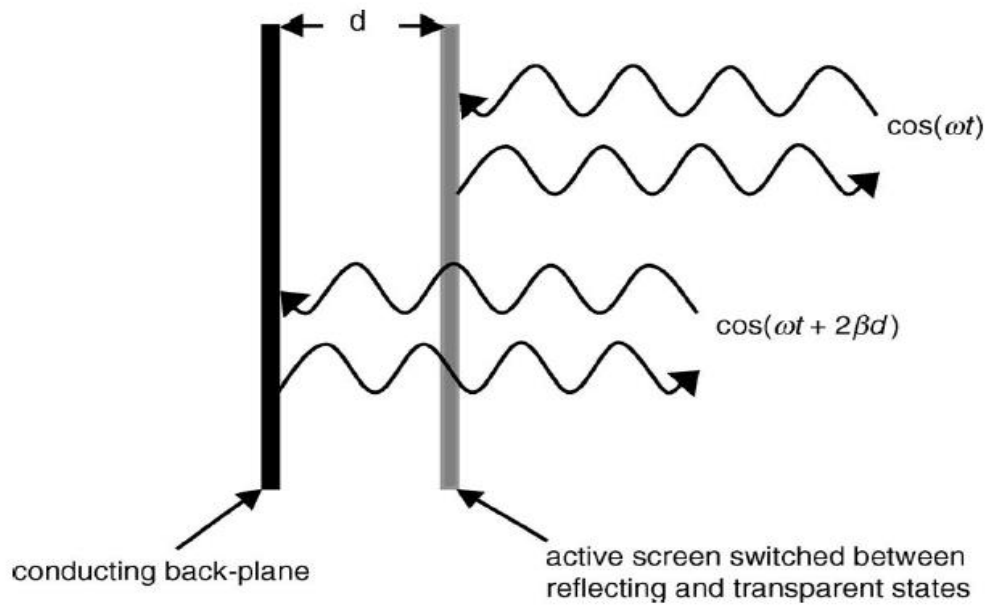


*Figure 2-7: A Single-layer Planar PSS [35]*

### 2.3.2 The Transparent Frequency Selective Surface

When rooms need to be screened to stop a signal in or out the windows also need to be shielded. This requires the FSS to be optically transparent to let light through with the following research on transparent FSS being carried out.

Parker et al. [38] first investigated FSS structures that used optically transparent conductive elements. In his work, circular patch (band-stop FSS) and slot ring (band-pass FSS) patterns were employed as shown in Figure 2-8. A square lattice structure of elements is arranged, fabricated using a resistance sheet of 4-8 ohm-sq thin-film silver, bonded onto a thin film of polyester [38].

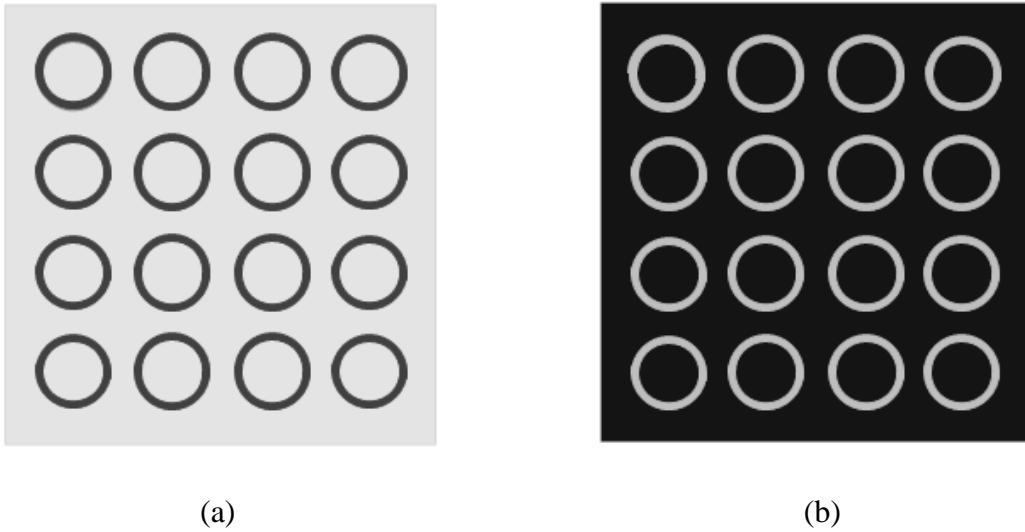


*Figure 2-8: Circular Patch (a) and Slot Rings (b) In a Square Lattice Arrangement [39]*

FSS glass has also been developed, being an Electro-magnetic wave reflector, containing a collection of thin antennas manufactured onto it. Silver (95% Ag) was chosen as the element material that can be deposited directly on glass. Two band- stop FSS structures are employed for this application. Both being of a Y type antenna design, the first is illustrated in Figure 2-9(a) which is designed to be an FSS element having an attenuation peak at 1.9GHz. The second illustrated in Figure 2-9(b) adds the added ability of shielding for two different bands at the same time with its attenuation stretching to being more than 40dB at 1.9GHz and 2.4 GHz. Measurements concluded a 0.5mm diameter silver antenna and prove it had satisfactory performance [40].

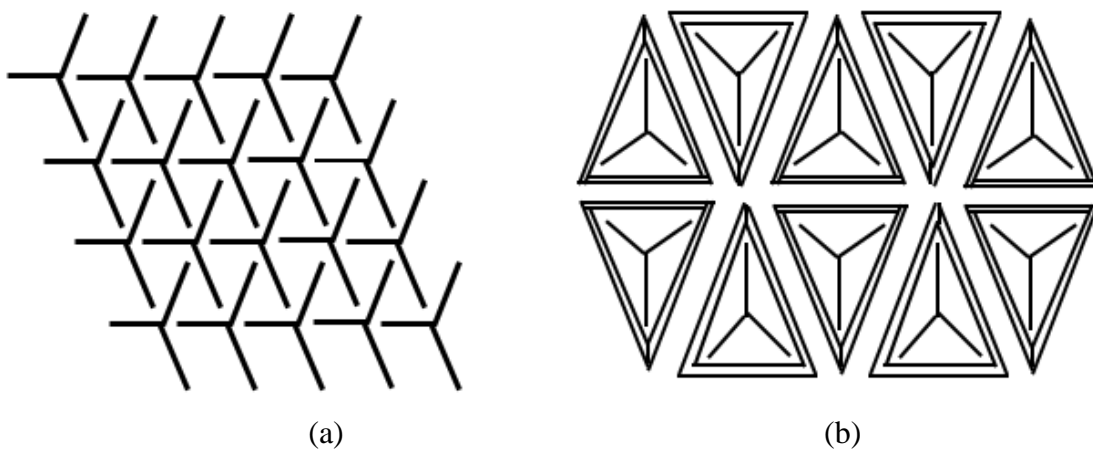


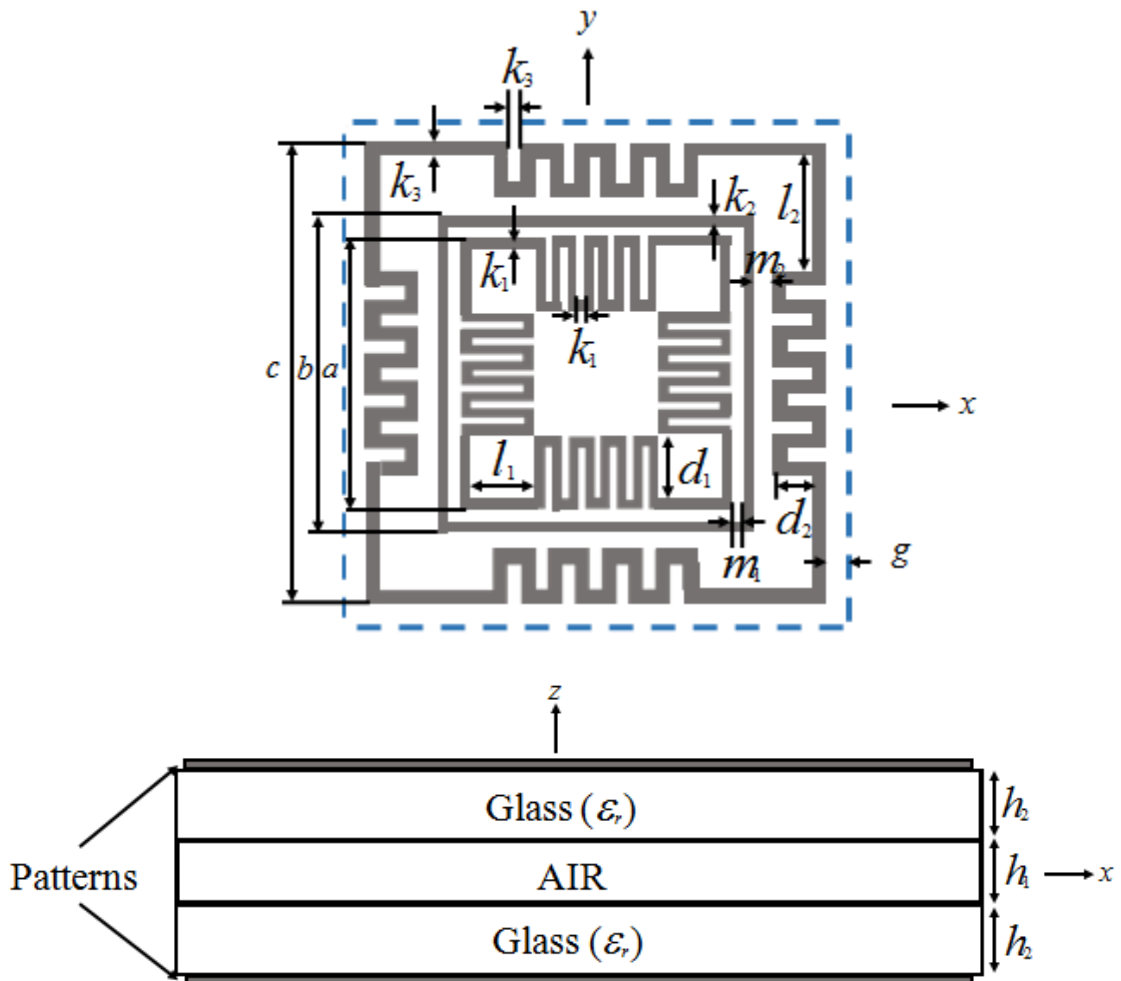
*Figure 2-9: (a) 1.9GHz Single Shield Type (b) 1.9GHz, 2.4GHz Dual Shield Type [39]*

### 2.3.3 Convolved Frequency Selective Structures

In the process of designing a FSS which operates below the frequency range of 3GHz, the size of a unit cell can become quite large depending on the range of frequencies of interested [41]. Using a larger conducting screen, a finite smaller sized FSS panel could be placed within a cut aperture, if a larger panel is required using a reduced sized FSS to save on manufacturing costs. One of the benefits of using an element which is reduced in size is an enhanced stability in the transmission or reflection frequency response when different angles of incidence from the exciting wave [7]. Therefore convoluted FSS designs can be used to produce resonating structures with a smaller unit cell dimension, which improves the angular stability of the frequency responses of the surface [42].

A FSS panel that can be used on the window of each prison cell that can be designed to block signals between base stations and mobile phones (Appendix II). A key requirement of the FSS panel needs to be the continuity of optical field through the FSS, so the choice of material for the substrate is glass ( $\epsilon_r = 7.5, \tan\delta = 0.02$ ). In the paper [43], two single layer FSS with modified multiple-loop elements are printed on the top and bottom of a glass panes, which is a pair of glass panes each 5mm thick with a 6mm air gap between them in Figure 2-10. This design also can reduce heat emission and to block noise in the building. When a triple-band FSS with three independent band-stop responses are needed, the single-band single-layer FSS must be placed in such a way that three resonant structures reside on the same surface. This is the reason why three loops are printed on each both of the glass substrate.

The design operates at three bands for (890MHz - 960MHz, 1710MHz - 1875MHz and 1920MHz - 2170 MHz), rejecting all three mobile bands at over -30dB attenuation.



|                    |                     |                     |                     |                     |
|--------------------|---------------------|---------------------|---------------------|---------------------|
| $a=18.82\text{mm}$ | $b=21.96\text{mm}$  | $c=32\text{mm}$     | $d_1=4.43\text{mm}$ | $d_2=2.82\text{mm}$ |
| $g=1\text{mm}$     | $k_1=0.55\text{mm}$ | $k_2=0.61\text{mm}$ | $k_3=0.94\text{mm}$ | $l_1=4.71\text{mm}$ |
| $l_2=8\text{mm}$   | $m_1=0.96\text{mm}$ | $m_2=1.26\text{mm}$ | $h_1=6\text{mm}$    | $h_2=5\text{mm}$    |

Figure 2-10: Structure of the Convolved Transparent FSS Structure [43]

## 2.4 Use of FSS on Building Structures

This area concentrates on large scale simulation methods both experimental and development validation, assessing characteristics of electromagnetic fields due to radio transmissions in large cavities, using building based case studies.

From the papers which have been studied, they typically build very simple cavities as a building model, which only have basic walls, doors and windows. The propagation within

each building are influenced strongly by the layout of the building creating specific feature points [44], the construction materials [45], and the building type i.e. Flat, Office Building, House, etc. To summarise this work, they can be categorised into several areas:

Transformation of building walls making them into a frequency selective surface, which not only filters out unwanted interference or radio frequencies, but also allows desired radio spectrum to pass through. Additionally, the frequency selectivity is closely related to the incident angle and dielectric properties of the building's material [46].

For accurate propagation channel modelling, knowledge of reflective properties of building materials is required for future pico-cellular indoor THz communication systems [47]. THz time-domain spectroscopy is used to measure reflection coefficient and calculating the reflection coefficients using Fresnel's equations. Also the roughness of a surface has an impact on attenuation of the reflection depending on the location from the transmitter as opposed to a smooth surface [47].

In construction of large buildings, rebar is commonly used to reinforce concrete. Over a frequency range of 100-6000MHz, transmission and electronic magnetic reflection coefficients are calculated for reinforced concrete walls as a function of rebar geometry and wall thickness using finite-difference time-domain techniques [48]. The methods used to reinforce concrete walls depend on the structural requirements of the building, with three general rebar configurations being analysed [48]. By changing the rebar lattice period, wall thickness, rebar diameter or the rebar geometry, its electrical properties change, causing the transmission coefficient and reflection coefficient to change. Concrete and rebar separated have their own very different properties when subject to radio frequencies, but these effects change completely when integrated together making it more difficult to model [48].

Using the FDTD method, a 2D model of a nearby building has been analysed; with the results indicating that a reflection from the nearby buildings can increase the received power on lower floors [49]. Adjacent floors in a multi-storey building are dominated by power penetrating through the floors and reflection by close by building. Assuming isotropic spreading in the third dimension, this 2D simulation can be extended to 2.5D [49].

There are different ways in which to make a material act as a wave absorber:

- Magnetic wood made of the wood and magnetic powder which can be easily processed due to characteristics similar to other woods and has a texture just like wood, it can absorb electromagnetic wave[50].
- Three-layer wave absorber which is made of common building materials; an advantage of this is that it can save costs and easy to construct [51].

Research has shown the penetration loss and time dispersion on building materials for UWB (Ultra Wideband) ranging over a spectrum of 3.1GHz to 10.6GHz; where dry wood, partition board, gypsum and glass are considered as obstruction materials. The higher the material thickness becomes causes more penetration loss, so the UWB receiver design needs adapted to achieve the high accuracy of the performance on the receiver when using such materials [52].

## **2.5 Digital Modulation Schemes**

For a GSM system, its services only need first three layers of the well-defined ISO/OSI 7 (International Standards Organization Open Systems Interconnection) layer protocol which is a standardised protocol on networking accepted by nations around the world. This protocol has 7 layers, with each layer having a specific function [53]. Table 2-1 compares the ISO/OSI layers with the equivalent layer in the GSM standards. For this section of interest to be researched, the modulation layer is part of the first layer, being the physical layer; used for RF connection between a mobile phone device and the base station. This modulation layer is responsible for the modulation scheme employed in order to send the information over a given RF channel [36].

| <b>ISO/OSI Model</b>     |                       |                                 | <b>Equivalent Layer in GSM</b>      |                              |
|--------------------------|-----------------------|---------------------------------|-------------------------------------|------------------------------|
| <b>Upper Layers</b>      | <b>7</b>              | <b>Application Layer</b>        |                                     | <b>Task of User</b>          |
|                          | <b>6</b>              | <b>Presentation Layer</b>       |                                     |                              |
|                          | <b>5</b>              | <b>Session Layer</b>            |                                     | <b>Task of Fixed Network</b> |
| <b>Transport Service</b> | <b>4</b>              | <b>Transport Layer</b>          |                                     |                              |
|                          | <b>3</b>              | <b>Network Layer</b>            | <b>Call Control</b>                 | <b>Task of GSM-Network</b>   |
|                          |                       |                                 | <b>Mobility Management</b>          |                              |
|                          |                       |                                 | <b>Radio Resource Management</b>    |                              |
|                          | <b>2</b>              | <b>Data Link Layer</b>          | <b>Segmentation / Concatenation</b> |                              |
|                          |                       |                                 | <b>Acknowledgement</b>              |                              |
| <b>1</b>                 | <b>Physical Layer</b> | <b>Forward Error Correction</b> |                                     |                              |
|                          |                       | <b>Channel Coding</b>           |                                     |                              |
|                          |                       | <b>Modulation</b>               |                                     |                              |

*Table 2-1: ISO/OSI 7 layers protocol [36]*

In order to pass digital binary information over a RF channel we need to superimpose the binary waveform onto a RF carrier. This process is known as digital modulation where the information can be carried over a channel by means of altering any of the carrier's characteristics. This can be achieved by varying one or several of the carrier's phase (PM), frequency (FM) or amplitude (AM), where a few of these modulation schemes will be described below for reference. If a carrier channel is primarily considered as a frequency-selective fading channel, then PM or FM are used instead of AM, since amplitude changes are more sensitive than angle modulation that could occur in a fading channel[54].

Various methods known as keying methods are used to represent the binary on-off status of the digital modulation, which are: phase-shift keying (PSK), frequency-shift keying (FSK) and amplitude-shift keying (ASK) [54]. A few example of these keying methods will be briefly described as bellow:

### 2.5.1 Binary Phase-Shift Keying (BPSK)

BPSK is PSK that has two carriers out of phase with each other at the given data rate. They differ in phase by  $180^\circ$  and are represented easily on an I/Q diagram as shown in Figure 2-11.

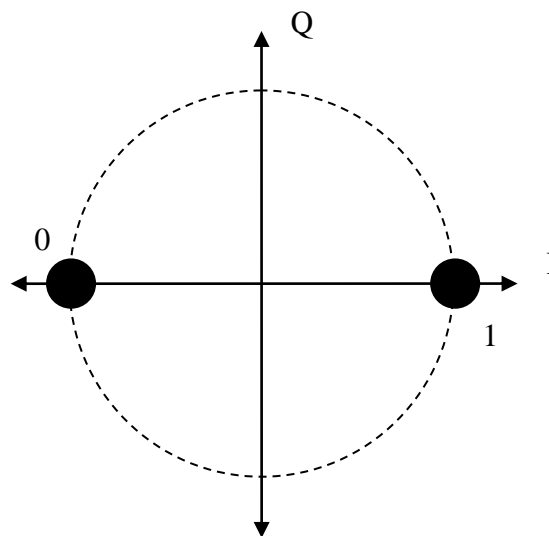


*Figure 2-11: Binary Phase-Shift Keying [54]*

### 2.5.2 Quadrature Phase-Shift keying (QPSK)

QPSK expands on BPSK by allowing phase changes split into four different quadrants. This allows for four carrier phases to be utilised as opposed to two carriers using BPSK. For maximum gain resolution when demodulating the waveform, all four of the carriers are exactly  $90^\circ$  out of phase from each other. All possible changes between phase states are shown in Figure 2-12 as well as the smaller circle states, indicating a no-change condition from the previous state. It is also noted that this modulation scheme now represents two bits where each state is referred to as a symbol. As each carrier is  $90^\circ$  out of phase from another, QPSK can be formed by taking two BPSK waveforms which have been shifted  $90^\circ$  from each other.

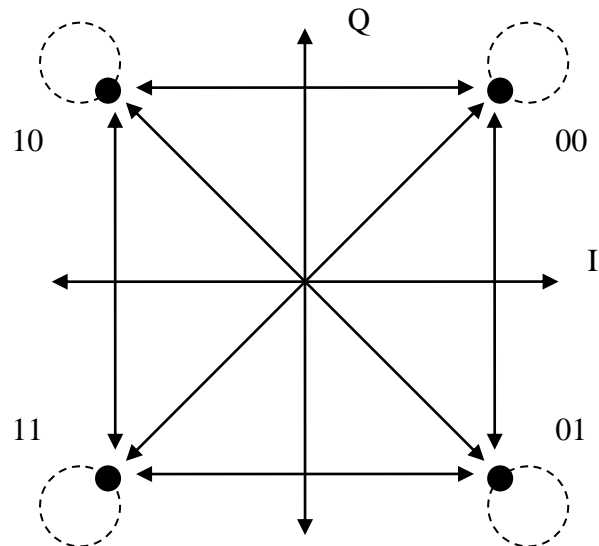


Figure 2-12: Quadrature Phase-Shift Keying [54]

### 2.5.3 Offset Quadrature Phase-Shift keying (OQPSK)

OQPSK follow similar principles for QPSK, using a two bits per symbol modulation scheme but only allows one of those bits to change at any given time by offsetting the data going into the BPSK generators by half a symbol, which in this case is one bit. By doing this the carrier states are changed so that a symbol cannot cause a  $180^\circ$  phase change as shown in Figure 2-13.

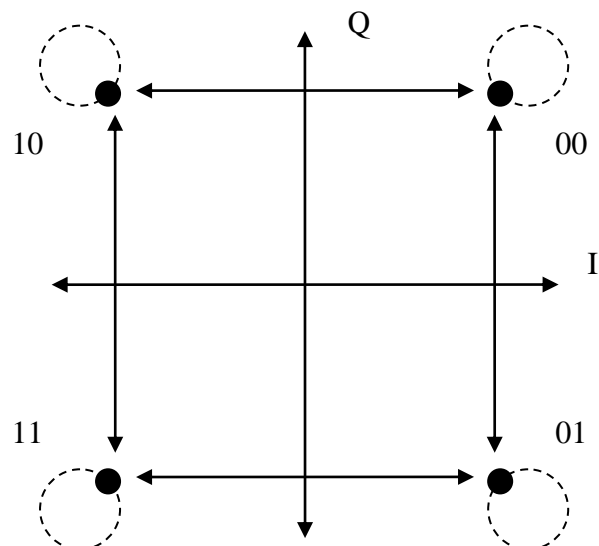
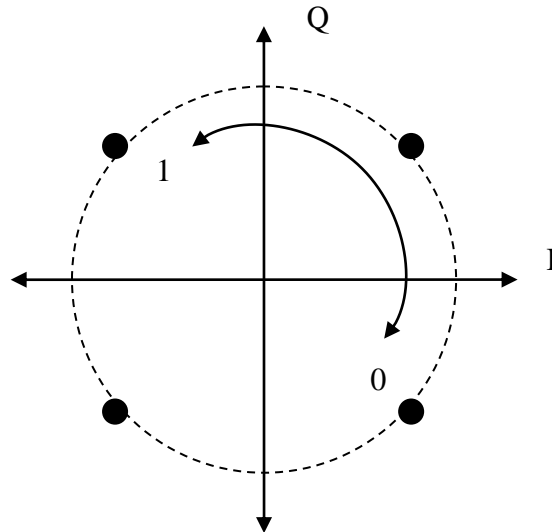


Figure 2-13: Offset Quadrature Phase-Shift Keying [54]

### 2.5.4 Gaussian Minimum-Shift Keying (GMSK)

For GSM, the modulation scheme specified is GMSK, therefore this research will focus on simulating this modulation scheme in later chapters. GMSK is an enhancement a MSK modulated waveform where the signal is filtered with a Gaussian filter of the correct bandwidth. This bandwidth is defined by the BT product. The states for GMSK can be seen in Figure 2-14.



*Figure 2-14: Gaussian Minimum-Shift Keying [54]*

# CHAPTER 3 BASIC FSS STRUCTURE SIMULATIONS AND MEASUREMENTS

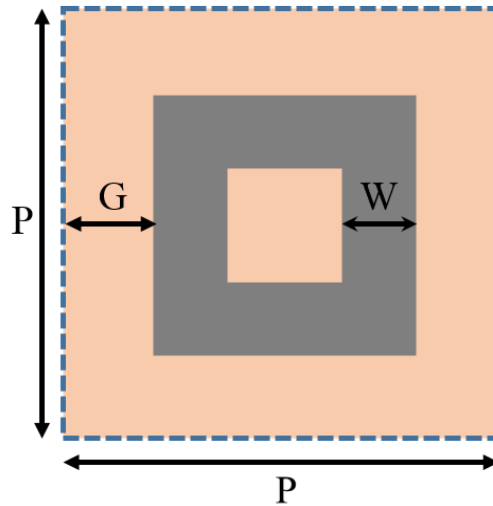
This research explores the design of a secure electromagnetic building, focusing on buildings such as hospitals, embassies, cinemas and prisons. The novelty in this research was the investigation of a surface, which can be embedded into a wall or a window of a room/building to stop unwanted frequency bands. So the basic passive band-stop FSS has been researched to understand the FSS structure and also to familiarize the use of the CST simulation environment by designing a simple prison cell structure. This basic FSS design would be used for a secure building application in the following chapters, with the prison cell being explored as an example.

## 3.1 Band-Stop Filters

Band-Stop FSS can filter out unwanted frequency bands which will be frequently used in this research; two examples are given to stop frequencies at 1.8GHz and 2.1GHz. Most a theoretical analysis methods for FSS, is not take into account arrays with finite size. These methods are often based on approximated arrays of infinite size using Floquet modes reducing to a single cell computation area, which used within the frequency domain solver in CST [55]. The unit cell boundary simulates conditions in the x and y directions and derives Floquet mode excitation. The use of these boundary conditions allows a rapid and accurate simulation of an infinite FSS in the directions of periodicity. For this reason we only need to construct a FSS geometry of single unit cell [56].

### 3.1.1 Band-Stop FSS Unit Cell Tuned at 1.8GHz

A square loop FSS unit cell (50mm x 50mm) tuned at 1.8GHz was designed and fabricated on 1.6mm FR4 dielectric ( $\epsilon_r= 4.5$ ,  $\tan\delta= 0.01$ ) substrate as shown in Figure 3-1. These materials were chosen mainly because they are relatively inexpensive.



| FSS Type               | P(mm) | G(mm) | W(mm) |
|------------------------|-------|-------|-------|
| Single Square Loop FSS | 50    | 5     | 2.6   |

*Figure 3-1: Band-stop Single Square Loop FSS at 1.8 GHz*

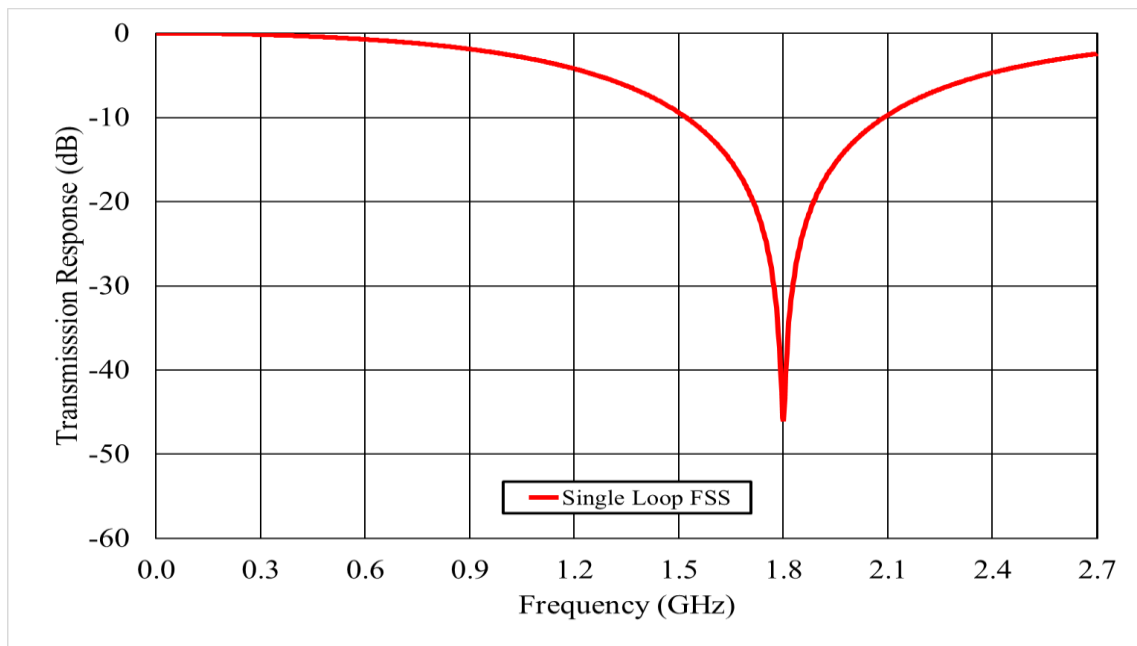


*Figure 3-2: Transmission Response of the FSS at 1.8GHz*

The simulation results were generated using the CST frequency domain solver showing that the FSS is tuned at 1.8GHz for a normal incidence angle ( $\theta$ ) of  $0^\circ$  with attenuation 46dB in the TE and TM mode in Figure 3-2. By varying the incidence angle ( $\theta$ ) in  $10^\circ$  intervals until  $50^\circ$ , the attenuation ranges between 27dB to 46dB in the TE mode as shown on graph in Figure 3-3.

A similar attenuation was seen ranging between 31dB to 46dB in the TM mode shown in Figure 3-4. All the simulated results have similar resonant frequencies with attenuations of greater than 27dB at different varying incidence angles.

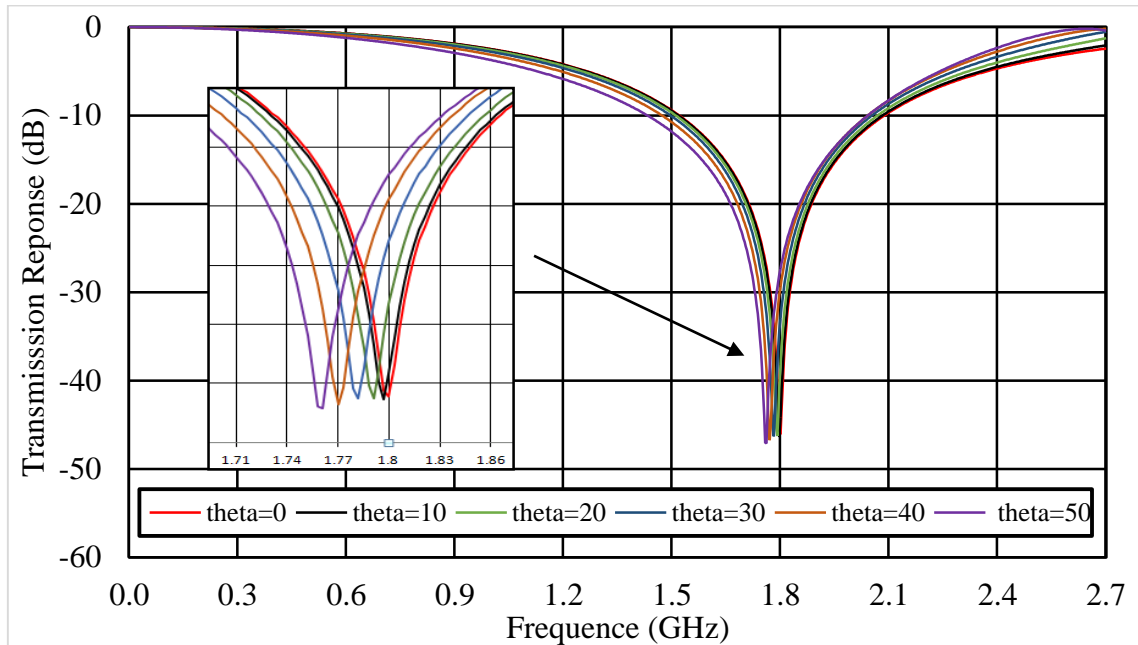


*Figure 3-3: Transmission Responses of the FSS at 1.8GHz in TE Mode*

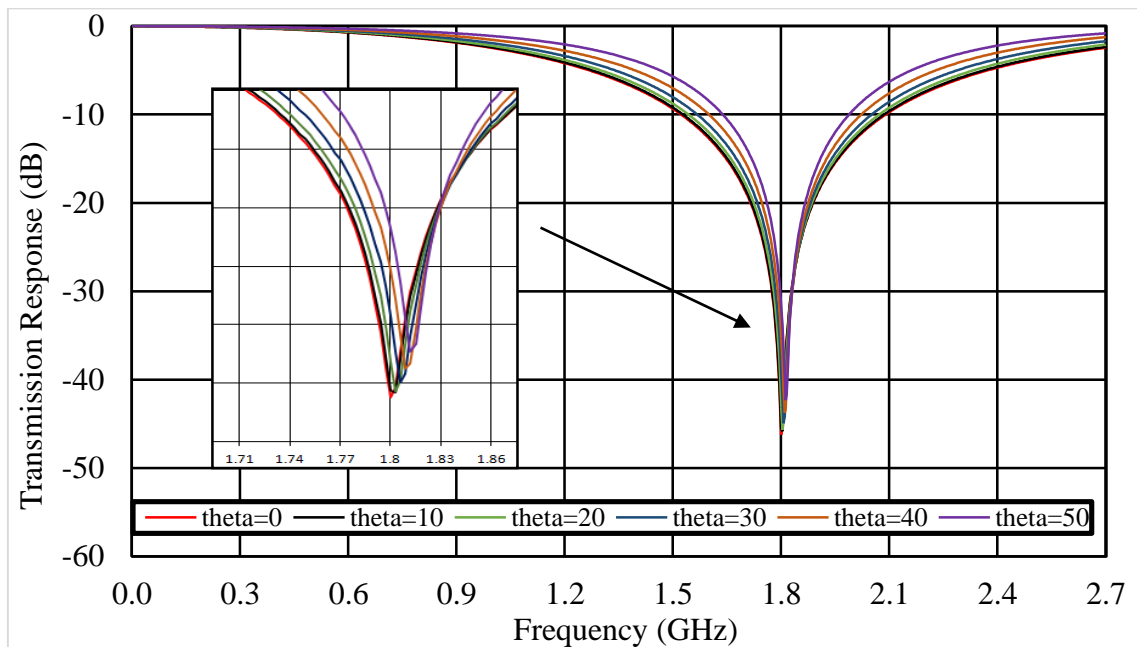
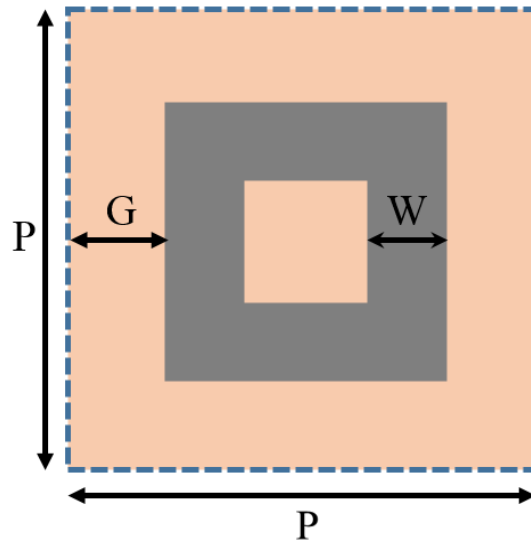


*Figure 3-4: Transmission Responses of the FSS at 1.8GHz in TM Mode*

### 3.1.2 Band-Stop FSS Unit Cell Tuned at 2.1GHz

A square loop FSS unit cell (50mm x 50mm) tuned at 2.1 GHz was designed and fabricated on 1.6mm FR4 dielectric ( $\epsilon_r = 4.5$ ,  $\tan\delta = 0.01$ ) substrate with a 5mm plastic board ( $\epsilon_r = 2.5$ ,  $\tan\delta = 0.05$ ) attached to its back surface as shown in Figure 3-5.



| FSS Type               | P(mm) | G(mm) | W(mm) |
|------------------------|-------|-------|-------|
| Single Square Loop FSS | 50    | 5     | 5.95  |

Figure 3-5: Band-stop Single Square Loop FSS at 2.1 GHz

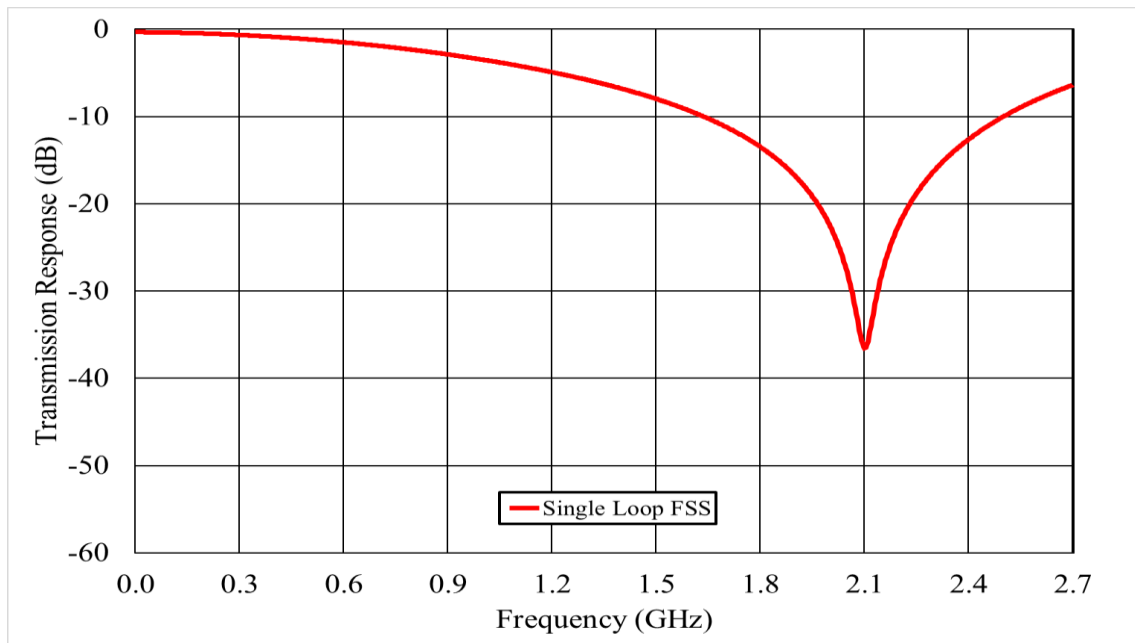
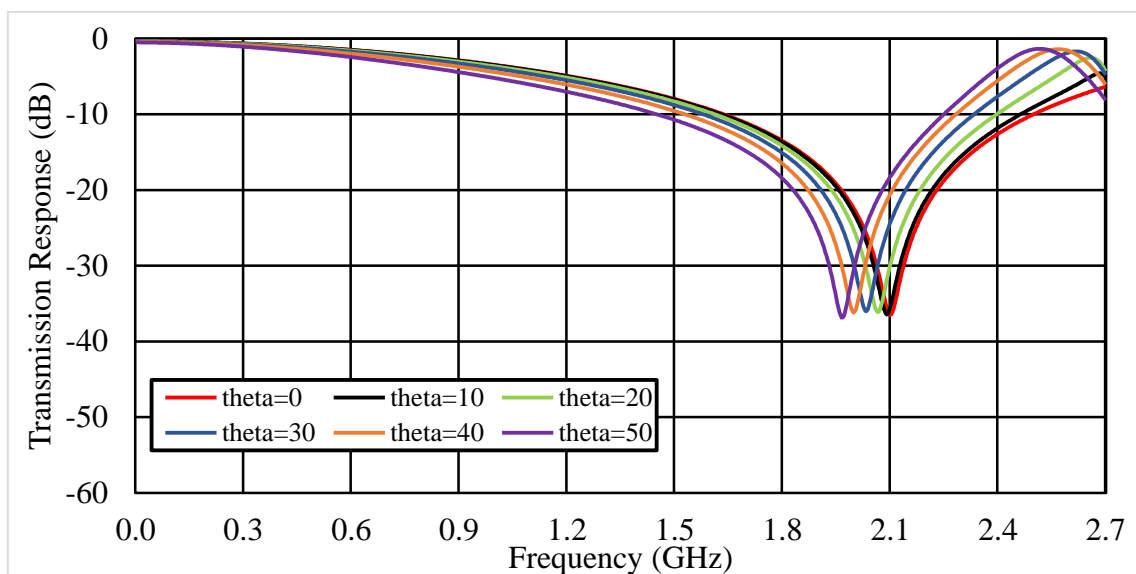
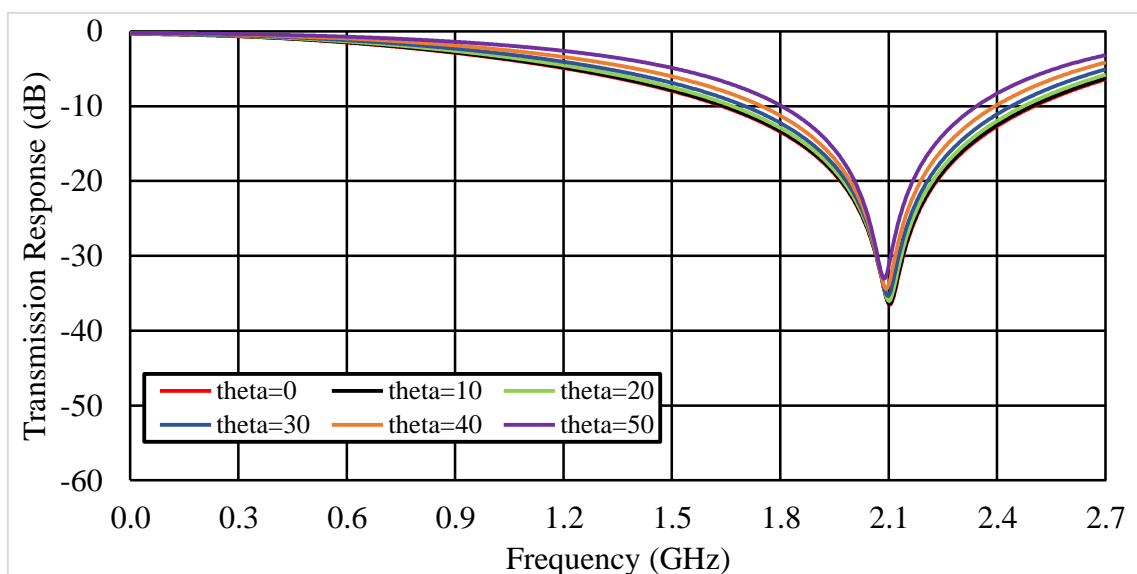


Figure 3-6: Transmission Response of the FSS at 2.1GHz

The simulation results were generated using the CST frequency domain solver showing that the FSS is tuned at 2.1GHz for a normal incidence angle ( $\theta$ ) of  $0^\circ$  with attenuation 36dB in the TE and TM mode in Figure 3-6. By varying the incidence angle ( $\theta$ ) in  $10^\circ$  intervals until  $50^\circ$ , the attenuation ranges between 18dB to 36dB in the TE mode showing a slight shift of the resonant frequency to the left as the incidence angles increases, Figure 3-7. A better performance of 31dB to 36dB in the TM mode was seen in Figure 3-8 with minimal shift of the resonant frequency. All the results simulated perform with similar resonant frequencies attenuations of greater than 18dB at different varying incidence angles.



*Figure 3-7: Transmission Responses of the FSS at 2.1GHz in TE Mode*



*Figure 3-8: Transmission Responses of the FSS at 2.1GHz in TM Mode*

The frequency characteristics of the FSS can be tuned by modifying the parameters of the substrate material. Manipulating the FSS layers reactive characteristics by incorporating tuning elements or re-arranging the structure geometry are also methods that can be employed [9]. In this single loop FSS design, changes to the thickness of the loop are used to alter the frequency response. Additionally, due to this symmetrically designed structure with respect to both x and y axes, its response of TM mode only slightly shifted from the desired resonant frequency.

### 3.1.3 Band-Stop FSS Panel Tuned at 2.1GHz

This research focuses on special buildings requirements which can stop unwanted frequencies entering the building. In the example of a prison, the assumption has been made for a prison cell window being of dimension 1m x 1m, and therefore the FSS panel dimensions were chosen to be 1.2m x 1.2m, so that it can be attached to the surrounding frame. The purpose of this panel is to stop signals at 2.1GHz. To make the panel straightforward to manufacture and construct, the FSS was split into sixteen identical panels, each with a width of 0.3m and a height of 0.3m. On each small panel is an FSS with a 6x6 unit cell structure as shown in Figure 3-9.

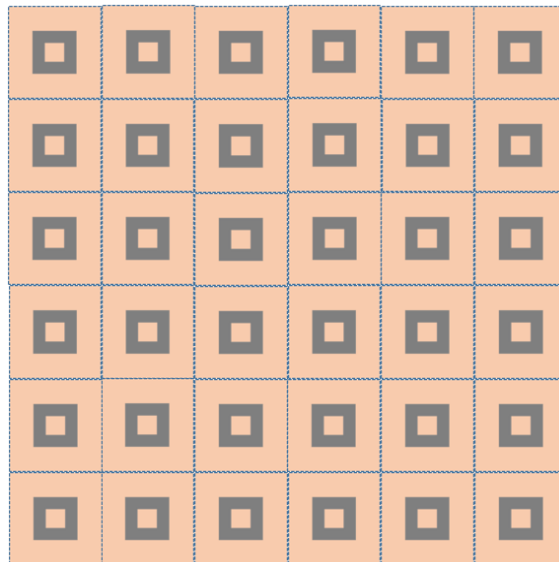


*Figure 3-9: FSS Panel*

After CST simulations were carried out, actual measurements use a pair of transmitting and receiving horn antenna (Rohde & Schwarz HF906) which have a bandwidth between 1GHz to 18GHz, they connect with a vector network analyser were carried as a comparison to confirm the simulation results; the vector network analyser have been calibrated before take this measurement, this setup as shown in Figure 3-10. For each measurement a reference calibration was taken without the FSS and using the same procedure. For the transmission frequency range of interested, the instrument was then calibrated. The measurement results in Figure 3-11 compared closely with the simulated result of the unit cell in Figure 3-6 which both showing a band-stop response at 2.1GHz with an attenuation of 36dB.

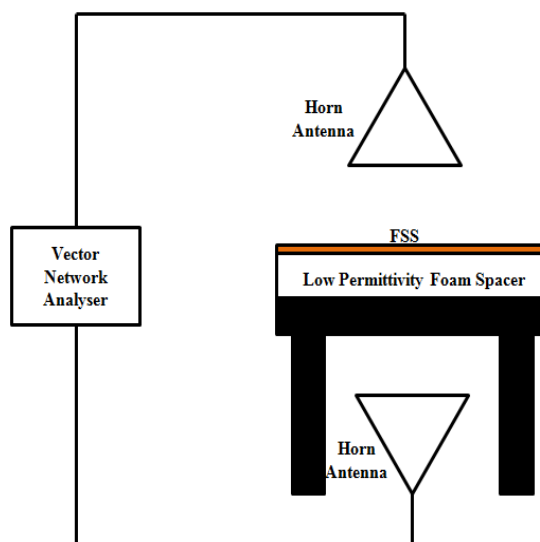


*Figure 3-10: Measurement Set Up for FSS Panel*

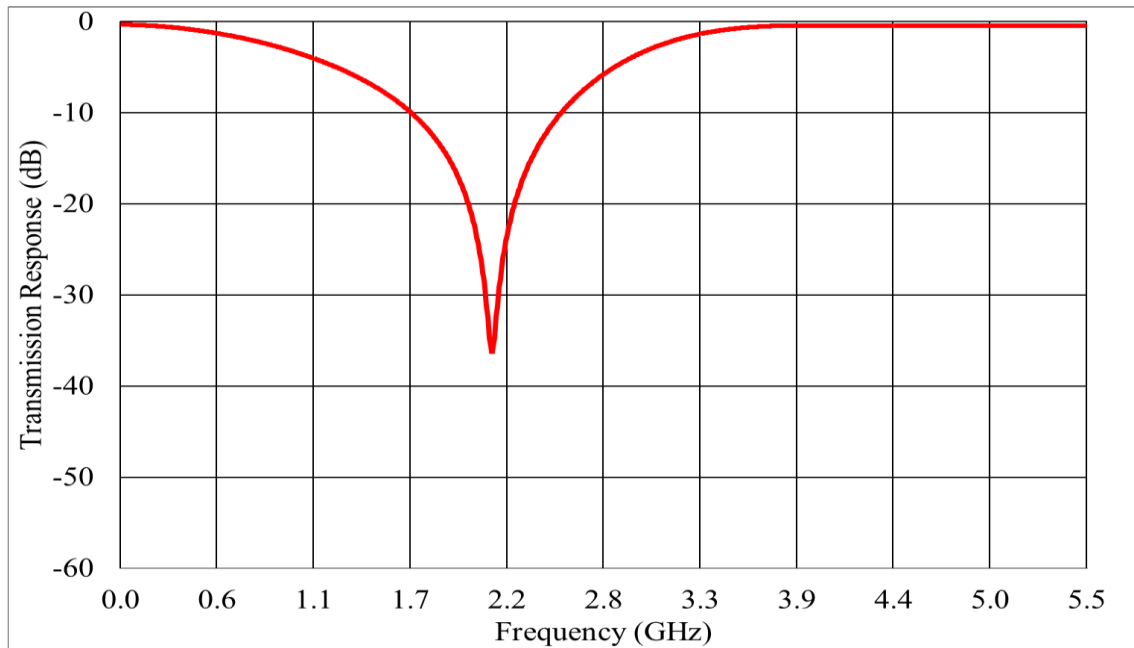


*Figure 3-11: FSS Panel Measurement Result*

### 3.2 Modelled Prison Cell using Signal Layer FSS

A 3.0m x 3.0m x 3.0m metal box is constructed as an empty prison cell model using CST simulation software. For the purposes of this simulation the outer shell is assumed to be made of metal a 1.0m x 1.0m aperture window in the front wall of the box as in Figure 3-12 (a). A plane wave is used as the excitation signal, with the probe being used to receive signals located in the middle of the room as illustrated by Figure 3-12 (b). The prison cell was first simulated without an FSS in place as a reference by using the CST time domain solver giving the response in Figure 3-13.

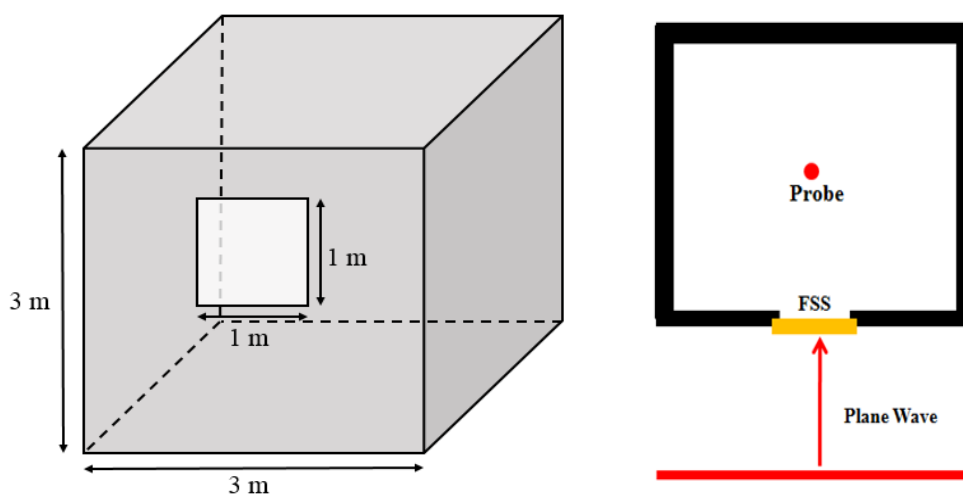


*Figure 3-12: (a) Metal Box without FSS and (b) Metal Box Model*

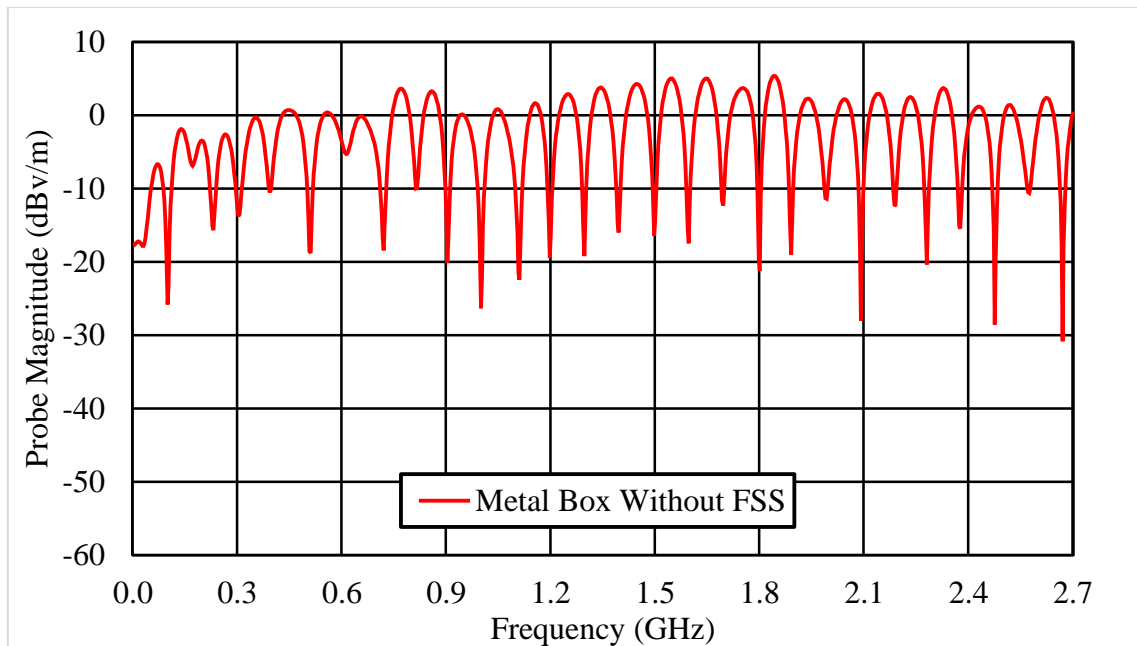


*Figure 3-13: Simulation Result for Metal Box without FSS*

A 1.0m x 1.0m band-stop FSS panel tuned at 2.1GHz was then placed in the aperture as in Figure 3-14, and the same simulation conditions were used for comparison with the reference result. The frequency range of interest is between 0Hz and 2.7GHz.

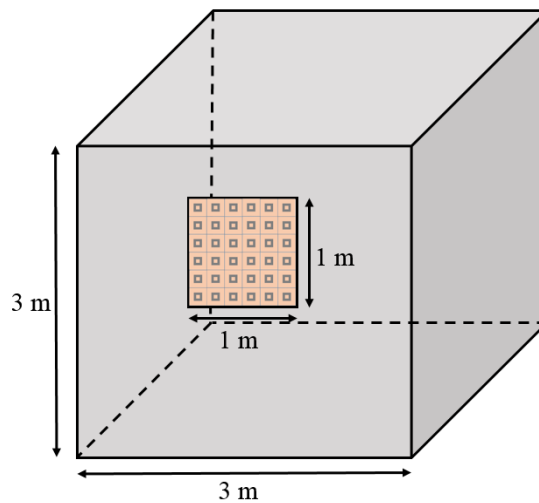


*Figure 3-14: Metal Box with FSS*

Figure 3-15 shows the simulated electric field signal attenuation as being around 26dB at 2.1GHz after the FSS was added.

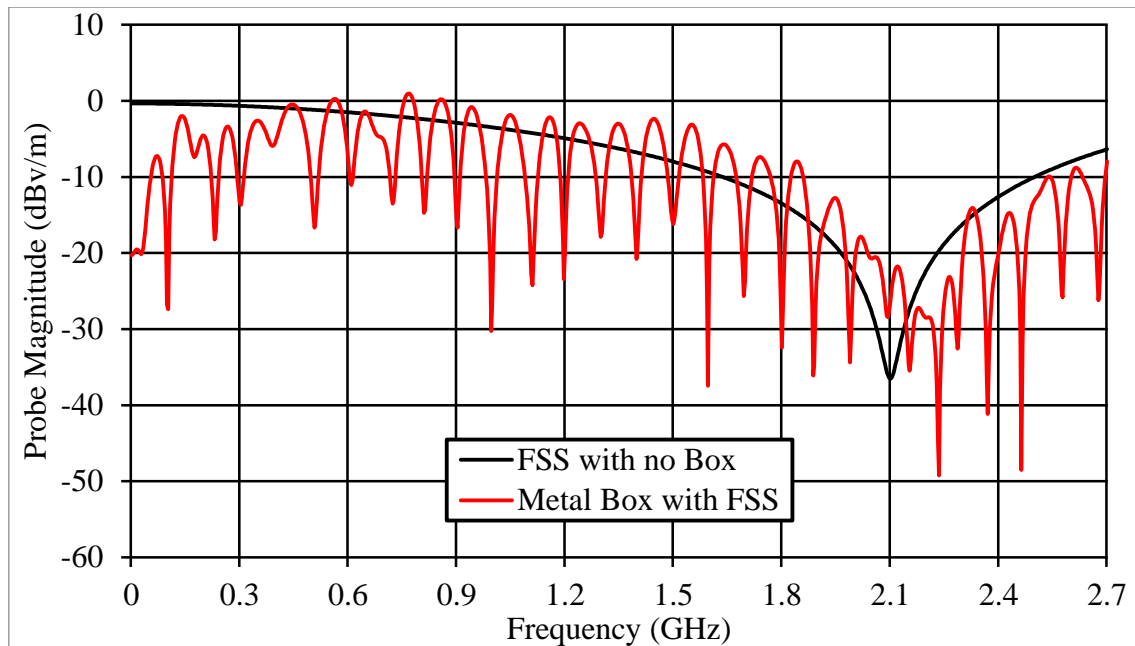


*Figure 3-15: Simulation Result for Metal Box with FSS*

The resonant frequency has been shifted slightly to the right and there is a broadening of the attenuating bandwidth around the resonant frequency. This is due to the nature of the structure interacting with the FSS design.

### 3.3 Summary

Two basic passive band-stop FSS have been analysed; The first one attenuates signals by upto 46dB for normal incidence ( $\theta=0$ ,  $\phi=0$ ) at 1.8GHz. By varying the incidence angles, the attenuation ranges between 27dB and 46dB, which indicates that if the incident signal is stronger than 27dB, this FSS would be unable to filter out all the unwanted signal at some incidence angles. The second FSS can attenuate signal to 36dB for a normal incidence angle at 2.1GHz. By varying its incidence angle the attenuation range seen is between 18dB and 36dB. These FSS are both straightforward to manufacture and low in cost; so if a building does not require a high attenuation, they are the good choices. To validate the simulation results, the FSS panels are manufactured, with their measurement results have good agreement with the simulation results. Additionally, a metal box with a single layer FSS has been simulated to assess FSS performance at 2.1 GHz. The results concluded that this signal layer FSS panel can attenuate a signal by upto 26dB at the required frequency.

# CHAPTER 4      NUMERICAL MODELLING

## DEVELOPMENT

This chapter is intended to explain the framework of GSM as implemented for simulation in MATLAB, and to compare the simulation results with those reported in previous work. This GSM framework will be used to test reconfigurable switching FSS performance in Chapter 5. In order to speed up the modelling processing of this research, the use of software CST and Matlab will also be explored.

### 4.1 GSM Protocol Modelling

#### 4.1.1 GSM Background

To begin the design of a simulation model in MATLAB the framework of GSM needs to be understood. GSM is an example of the second generation (2G), it brought the switch over from analogue to digital systems, which vastly improved voice calls in terms of privacy and quality. GSM operates on both 900MHz and 1800MHz frequency bands throughout the UK [57], with Vodafone and O2 networks using GSM 900 and Orange and T-Mobile networks using GSM 1800. GSM carrier frequencies are separated by 200 kHz have an uplink and downlink frequency range which is shown in Table 4-1. The uplink transmits from mobile device to base station, the downlink is vice versa.

|                        | <i>Uplink</i> | <i>Downlink</i> | <i>No. of physical channels</i> |
|------------------------|---------------|-----------------|---------------------------------|
| <b><i>GSM 900</i></b>  | 890--915MHz   | 935--960MHz     | 125                             |
| <b><i>GSM 1800</i></b> | 1710--1785MHz | 1805--1880MHz   | 375                             |

**Table 4-1: The Frequency Ranges, Offset, and Number of Physical Chanel for GSM900/1800**

GSM technology uses the radio spectrum more efficiently than previous generations, so that users could transmit text/data and voice, with the optional choice of using their mobile phone abroad as well if required [58]. To do this it employs narrow band TDMA (time-division multiple-access), with each TDMA frame shown in Figure 4-1 being divided into eight bursts. These bursts consist of several trail and guard bits with the important 26 bit training sequence which is used as a timing reference and for multipath equalisation at the centre of burst, it being in the middle surrounded by data of 58 bits on each side [59].

The duration of a TDMA frame is 4.615ms, so each burst will take 576.9  $\mu$ s, and it has a bit rate of 271kbit/s giving 3.69  $\mu$ s for each bit duration in the burst [60].

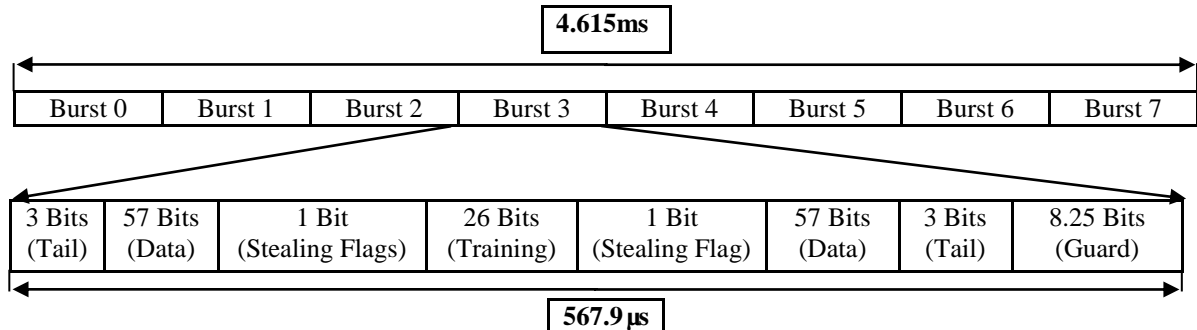


*Figure 4-1: Structure of a GSM TDMA Frame*

From the GSM TDMA frame structure shown in Figure 4-1, the transmission part of the Matlab model is constructed by first encoding the speech data combining interleaving and differential encoding followed by GSMK (Gaussian Minimum Shift Keying) modulation of the signal [61]. The modulated signal is transmitted through the CAI (Common Air Interface) after up conversion by a frequency multiplier. The receiver part of the GSM model is implemented in reverse with a de-modulator followed by decoding with interleaving and differential techniques to reconstruct the original data sent. A model of the GSM system used in this research is shown as follows:

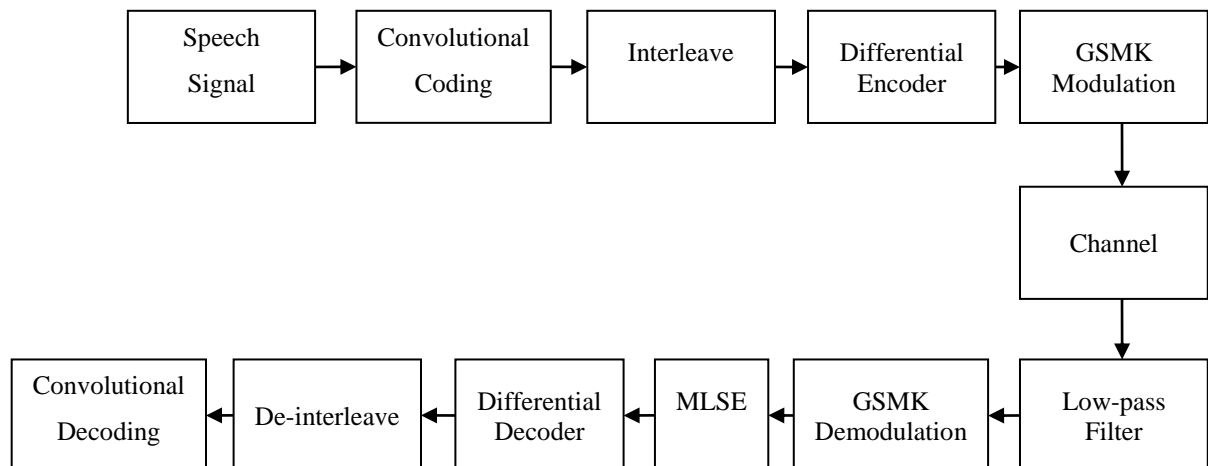


*Figure 4-2: Model of GSM System*

### 4.1.2 Speech Signal Convolution Coding

Speech samples are analysed and processed in 20ms audio blocks by a speech encoder which compresses the data of a speech signal. This process is referred to as the Regular Pulse Excitation and Linear Predictive Coding (RPE-LPC) module in a GSM model. The speech encoder operates at 13 kbit/s which corresponds to 260 bits every 20ms [62].

These 260 bits are divided into two classes: Class I (182bits) and Class II (78bits) with Class I being split into two categories (Ia and Ib). This is due to the bits in Class Ia being more important than the bits contained in Class Ib and require extra encoding protection to prevent data errors before convolutional coding. To do this three parity bits are calculated for error detection using Class Ia and are added to the end of the Class Ia before being combined with Ib and an additional four tail bits to make the full Class I.

This now makes the frame of size 267 bits with only the Class I part requiring encoding using convolutional coding techniques. Once the Class I is input into the convolutional coder it adds redundant bits for every bit that enters it, so that it can be less prone to errors which can be better recovered by the receiver compared with systems that do not use convolution coding. After the convolutional coding, the Class I in the frame will come to 378 bits to make a total frame size of 456 bits [63] as shown in Figure 4-3.

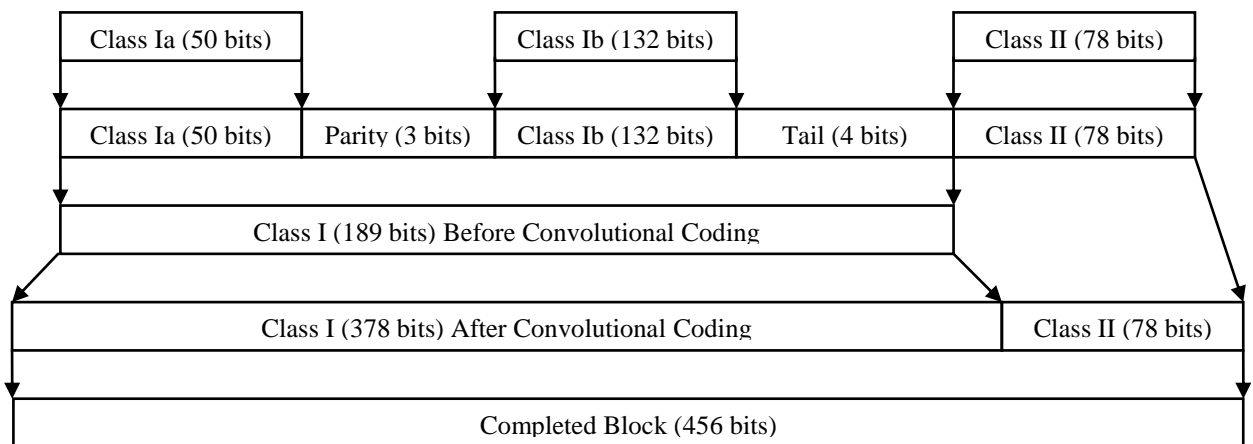


*Figure 4-3: Convolutional Coding*

### 4.1.3 Interleave Simulation

The 456 bits which are output from convolutional coding are divided into eight equal time slots of 57 bits each, which are reordered. This has an advantage as if one time slot

burst is corrupted, then only one-eighth of each time slot burst is lost rather than a full time slot burst segment. Also this data still has a potential of being recovered successfully at the received end. This process is known as data interleaving. The convolutional coder and interleaving protects against the fading phenomenon that might happen over the channel.

In the GSM standard, each time slot burst has 114 data bits which consists of two 57 bit data blocks. In a frame these eight time slots bursts are interleaved with data from three consecutive data blocks referred to as A, B and C. If you take the example of the current four time slots and the next four time slots with Block B being the current data the following logic can be applied. The first four time slot bursts are allocated with starting data from Block B only populating the odds bits. The even bits come from the last part of data Block A. The remaining last part of data Block B is populated into then even sections of the next four time slot [62]. This is illustrated in Figure 4-4 showing where each data element gets divided into each time slot.

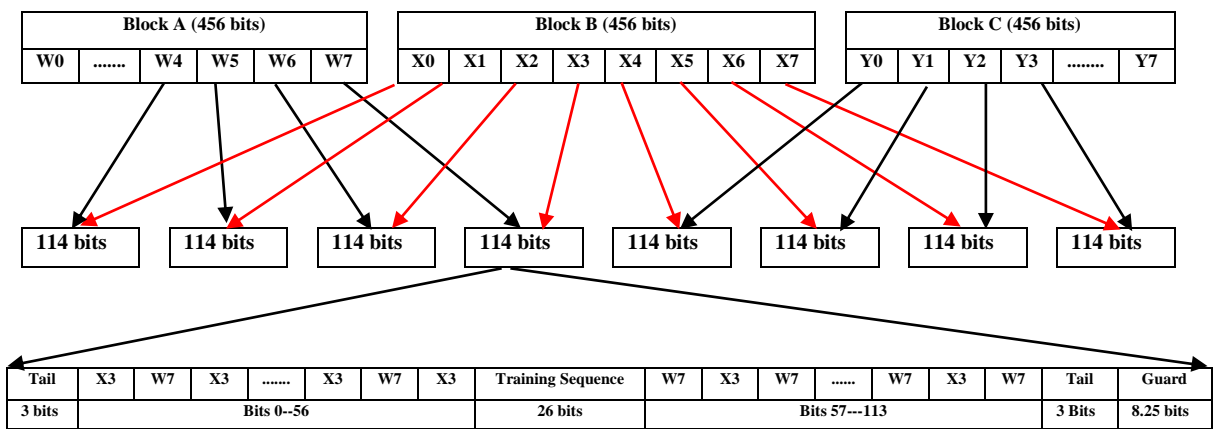


Figure 4-4: Interleaving Process

#### 4.1.4 Differential Encoding Simulation

Differential encoder assigns a polarity to the symbols. It converts the '0' and '1' symbols into equally distant aptitudes '+1' and '-1' respectively. Firstly, the '0' and '1' symbols in the burst input are fed into an XOR logical operator which produces a value of '1' only when the two input values are different and produces a value of '0' only when the two input values are the same [54] as shown in Table 4-2.

| <i>Input A</i> | <i>Input B</i> | <i>Output (X)</i> |
|----------------|----------------|-------------------|
| 0              | 0              | 0                 |
| 0              | 1              | 1                 |
| 1              | 0              | 1                 |
| 1              | 1              | 0                 |

*Table 4-2: True Table for Logical XOR Operator [54]*

After this process the '0' and '1' symbols from this output are converted into '+1' and '-1' by the equation shown (4-1) below:

$$Y = 1 - 2X \quad (4-1)$$

Where  $X \in (0, 1)$

| <i>X</i> | <i>Y</i> |
|----------|----------|
| 0        | +1       |
| 1        | -1       |

*Table 4-3: Logical Table for Differential Encoding [54]*

Each frame includes eight bursts in GSM. For simplicity, one of the eight bursts in MATLAB is used as an example to show the difference between the input and output of the differential encoder in Figure 4-5 and Figure 4-6. The burst shows all 157 bits. This is broken down with two 57 bit data sections being set to zero as well as the bits required for tail and steal flags. The actual 26 bits training sequence required are kept to be the true values and all 9 guard bits are set to one.

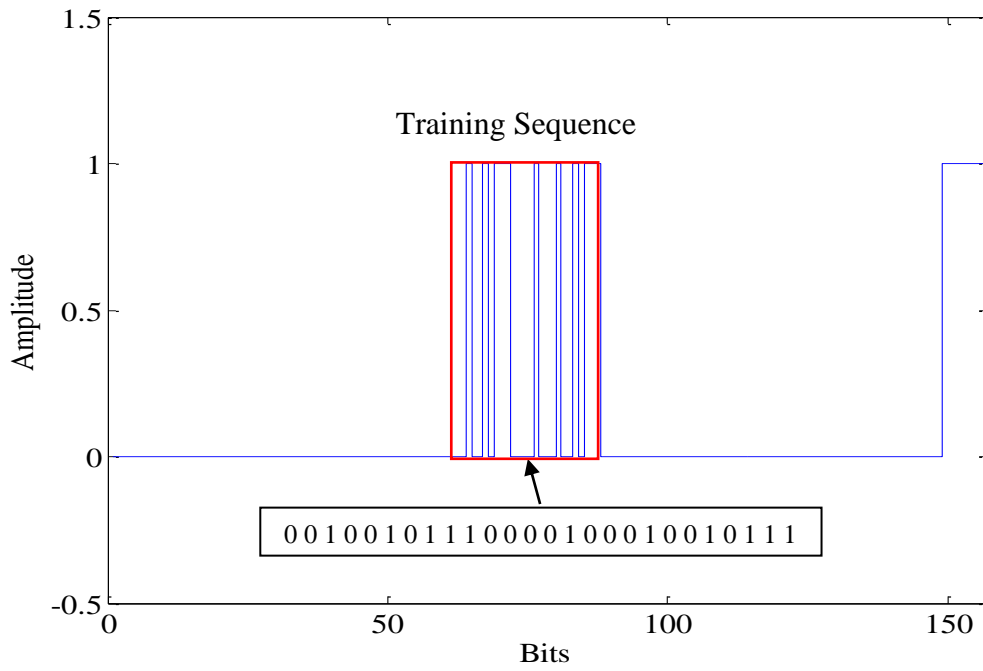


*Figure 4-5: Input Data of the Differential Encoder*

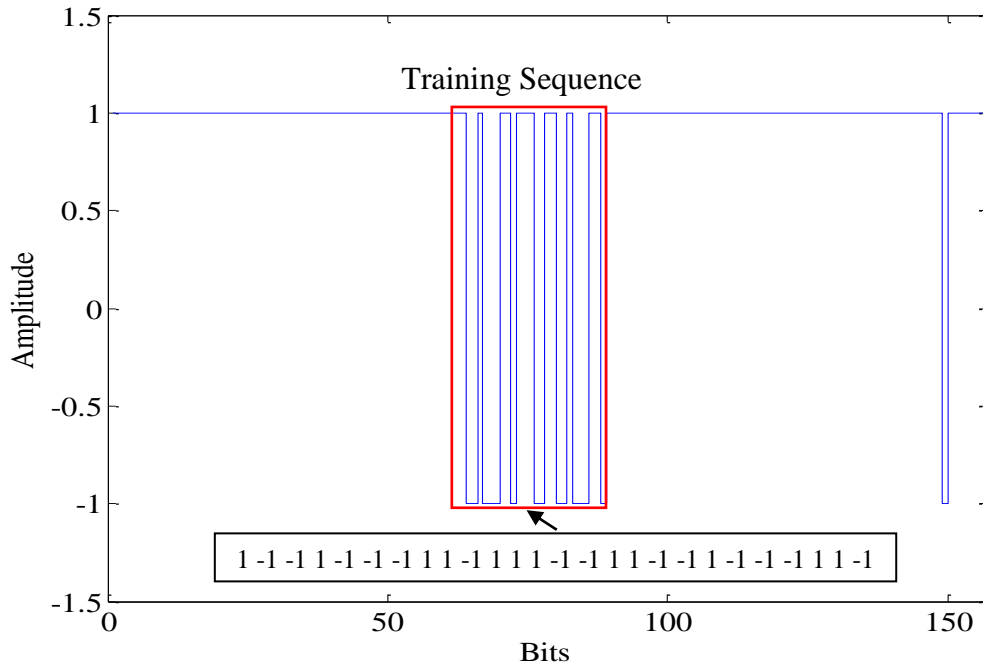


*Figure 4-6: Output Data of Differential Encoder*

### 4.1.5 GMSK Modulation Simulation

After the differential encoder, the data needs to be modulated with GMSK (Gaussian Minimum-shift Keying) which is widely used in GSM systems as a constant-envelope modulation method. To achieve this, data from the differential encoder is input into the Gaussian filter which is shown in Figure 4-7 below:

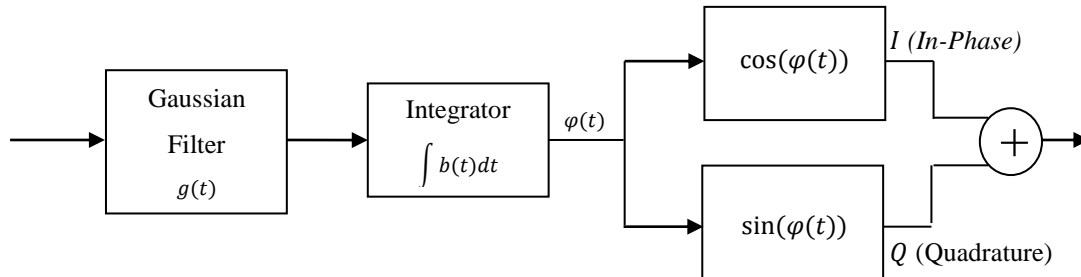


Figure 4-7: GMSK Modulator

A Gaussian impulse response in the Gaussian Filter is typically used for GMSK modulation which is designed for filtering out interference between adjacent signals in the frequency spectrum. This is calculated using the following (4-2) below.

$$G(t) = \frac{1}{2T} \left[ Q \left( 2\pi B \frac{t - \frac{T}{2}}{\sqrt{\ln 2}} \right) - Q \left( 2\pi B \frac{t + \frac{T}{2}}{\sqrt{\ln 2}} \right) \right] \quad (4-2)$$

Where B is the bandwidth of the Gaussian filter. The bit interval product (BT) is 0.3 in GSM which is used as the normalised bandwidth [60].

The Q function for the Gaussian impulse response can be obtained as shown,

$$Q(t) = \int_t^{\infty} \frac{1}{\sqrt{2}} \exp(-r^2/2) dr \quad (4-3)$$

Where r is the output data from the differential encoder.

For a Gaussian Filter in GSM, a bit duration of  $T$  is given as follows

$$T = \frac{\text{The duration of a TDMA frame}}{\text{The bits contain in a TDMA frame}}$$

$$T = \frac{4.615\text{ms}}{1250\text{bits}} \quad (4-4)$$

$$T = 3.692\mu\text{s}$$

For a BT of 0.3, the Gaussian impulse response is truncated, symmetrically around zero on the x axis, to four bits periods from  $-2T$  to  $2T$ . In Figure 4-8 a graphical representation of the impulse response from the MATLAB simulation is shown.

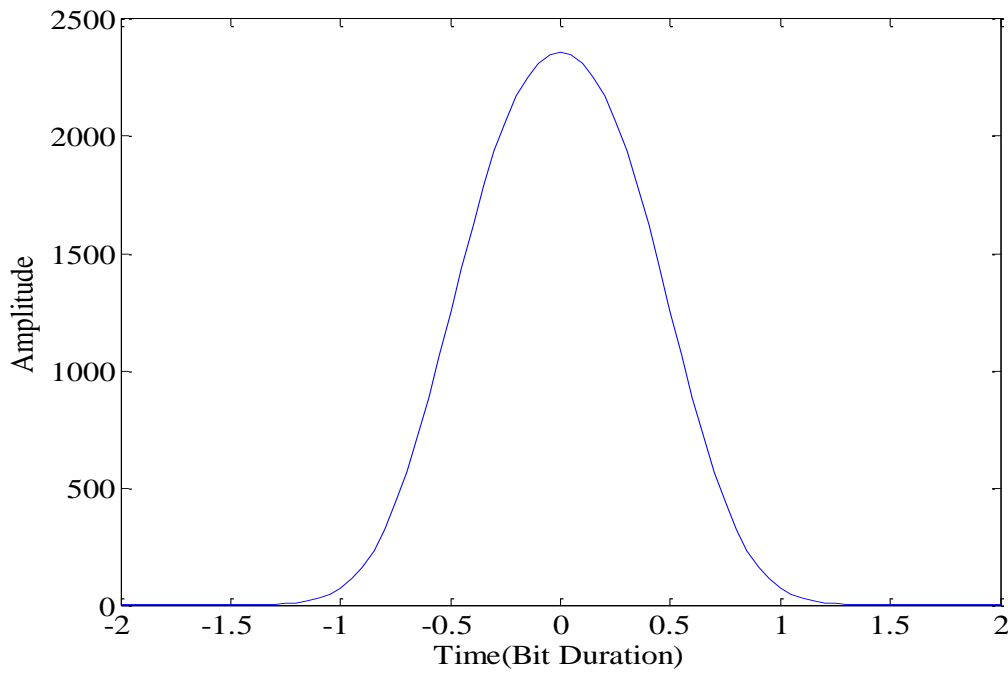


*Figure 4-8: Impulse Response of Gaussian Filter*

After the signal passes through the Gaussian filter  $g(t)$  this would yield a function of  $b(t)$ . In GMSK modulation the signal is made up of In phase and Quadrature phase components from the Gaussian impulse response where the phase shift function is given by:

$$\Phi(t) = \int_t^{\infty} b(t)dt \quad (4-5)$$

Combining both the in-phase  $\cos(\varphi(t))$  and quadrature phase  $\sin(\varphi(t))$  the output of GMSK modulation can be obtained as follows:

$$\cos(\varphi(t)) + j \sin(\varphi(t)) \quad (4-6)$$

To validate the GSM modulation simulation in MATLAB, a 12 bit repeating stream shown in Table 4-4 is used and which has been extracted from a report available on the Link Collaborative Research website [64].

|   |   |    |   |   |    |    |   |    |   |    |    |   |   |    |   |   |    |    |   |    |   |    |    |     |
|---|---|----|---|---|----|----|---|----|---|----|----|---|---|----|---|---|----|----|---|----|---|----|----|-----|
| 1 | 1 | -1 | 1 | 1 | -1 | -1 | 1 | -1 | 1 | -1 | -1 | 1 | 1 | -1 | 1 | 1 | -1 | -1 | 1 | -1 | 1 | -1 | -1 | ... |
|---|---|----|---|---|----|----|---|----|---|----|----|---|---|----|---|---|----|----|---|----|---|----|----|-----|

*Table 4-4: A Binary Data Stream*

The Data stream is represented graphically below Figure 4-9 using MATLAB.

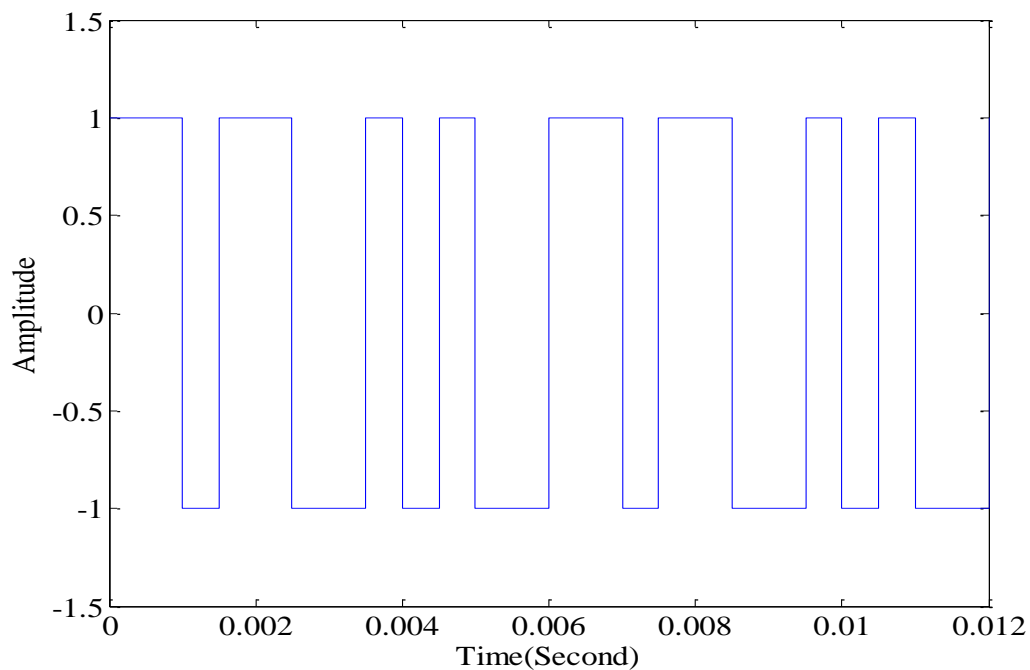


*Figure 4-9: Data Stream after Encoder in Matlab*

After the data stream passes through the Gaussian filter, the individual Gaussian shaped pulses are added together, obtaining function  $b(t)$ . The bit interval product is set at 0.5 with bit duration of  $T = 1/2000$  in the report, so these parameters are also used in the MATLAB to generate the same graph in Figure 4-10.



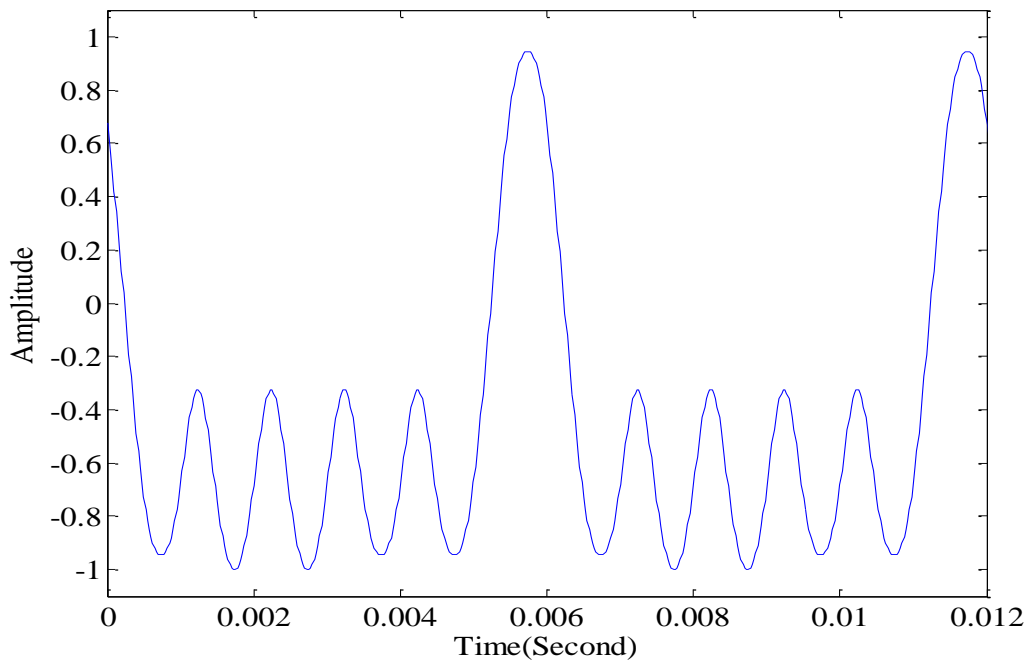


**Figure 4-12: In Phase Sequence  $I(t)$  in MATLAB**

The Quadrature phase  $Q(t) = \sin(\varphi(t))$  is represented graphically from MATLAB in Figure 4-13.

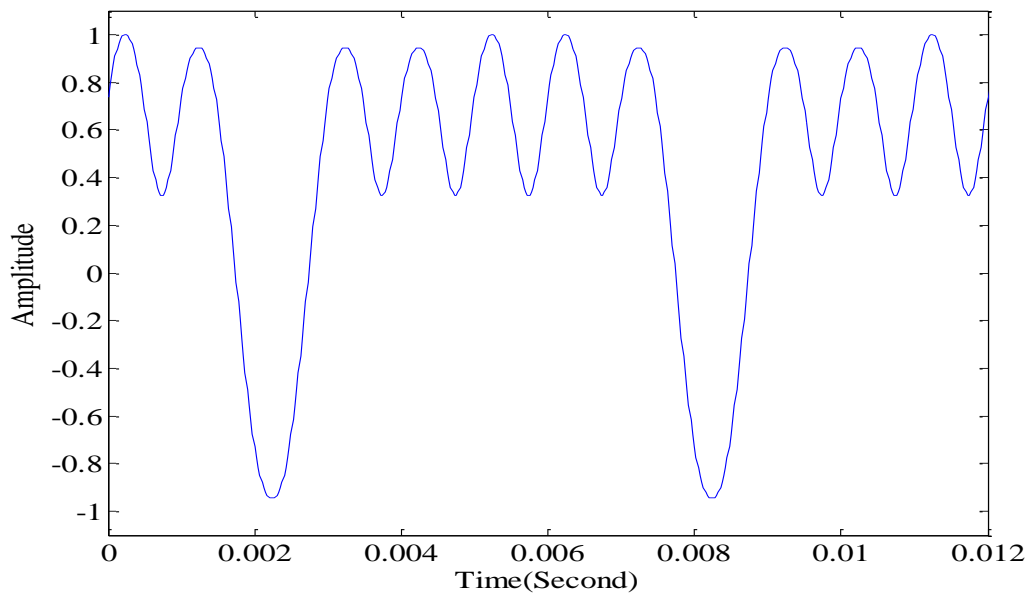


**Figure 4-13: Quadrature Phase Sequence  $Q(t)$  in MATLAB**

Figure 4-9 to Figure 4-13, illustrate the same results as the original report [64]. This validates the modulation part of the GSM MATLAB model.

#### **4.1.6 Channel Simulation**

In order to simulate a realistic channel for an active switched FSS, three things need to be considered; Phase, Amplitude and Noise. Noise can currently be ignored in the simulation as any BER (Bit Error Rate) in this system will be produced by time varying transmission phase of the FSS. Note that the BER in this thesis is the data before interleave compared to the data after de-interleave. This calculates how many bits are in error which is then divided by the length of the data transmitted to get the ratio.

The phase and attenuation can be switched by dividing up the signal channel into digitised samples. Depending on how many samples are used to divide up the signal when switching between phase and attenuation states, a switching frequency for the FSS can be determined, and this will be analysed in Chapter 5.

#### **4.1.7 Low-Pass Filter Simulation**

A low-pass digital filter is used to filter out the energy within the side bands in frequency spectrum of the different switching frequency plot. For the case of this research, the cut off frequency will be tested at four different filter bandwidths, where a Hamming Window function has been employed in the low-pass filter to obtain a zero gain value outside of the chosen frequency band in the Fourier spectrum. More details about these will be explained in Chapter 5.

#### **4.1.8 GSM Demodulation Simulation**

The Channel Impulse Response (CIR) in the demodulation process ensures successful equalisation which can remove Inter-Symbol Interference (ISI) in the received signal. The CIR is based on the special 26 bits known as training sequences [65]. In GSM there are eight different training sequences which can be used depending on the time slot used as follows:

| <i>Training Sequence Code (TSC)</i> | <i>Training Sequence Bits</i>                             |
|-------------------------------------|---|
| 0                                   | 0,0,1,0,0,1,0,1,1,1,0,0,0,0,1,0,0,0,1,0,0,1,0,0,1,0,1,1,1 |
| 1                                   | 0,0,1,0,1,1,0,1,1,1,0,1,1,1,1,0,0,0,1,0,1,1,0,1,1,1,1     |
| 2                                   | 0,1,0,0,0,0,1,1,1,0,1,1,1,0,1,0,0,1,0,0,0,0,1,1,1,0       |
| 3                                   | 0,1,0,0,0,1,1,1,1,0,1,1,0,1,0,0,0,1,0,0,0,1,1,1,1,0       |
| 4                                   | 0,0,0,1,1,0,1,0,1,1,1,0,0,1,0,0,0,0,0,1,1,0,1,0,1,1       |
| 5                                   | 0,1,0,0,1,1,1,0,1,0,1,1,0,0,0,0,0,1,0,0,1,1,1,0,1,0       |
| 6                                   | 1,0,1,0,0,1,1,1,1,1,0,1,1,0,0,0,1,0,1,0,0,1,1,1,1,1       |
| 7                                   | 1,1,1,0,1,1,1,1,0,0,0,1,0,0,1,0,1,1,1,0,1,1,1,1,0,0       |

*Table 4-5: Eight Types of GSM training sequences [66]*

The different training sequences help to distinguish between similar simultaneous signals arriving at the receiver at the same time. A training sequence consists of 16 bits to constitute the frame synchronization word in the middle and 5 bits at each ends to keep auto-correlation and frequency oscillation low. The first 5 bits at the beginning of the training sequence are copied from the last 5 bits in the centre 16 bits. The last 5 bits at the end of the training sequence are copied from the beginning 5 bits in the centre 16 bits. An example of a Training Sequence Code 1 (TSC1) is shown in Figure 4-14.

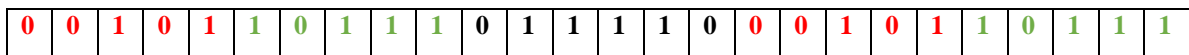


*Figure 4-14: An example of TSC1*

An estimate of CIR shown in Figure 4-15 can be obtained by correlating the received training sequence (16 bits) with a replica training sequence (26 bits) known at the receiver.

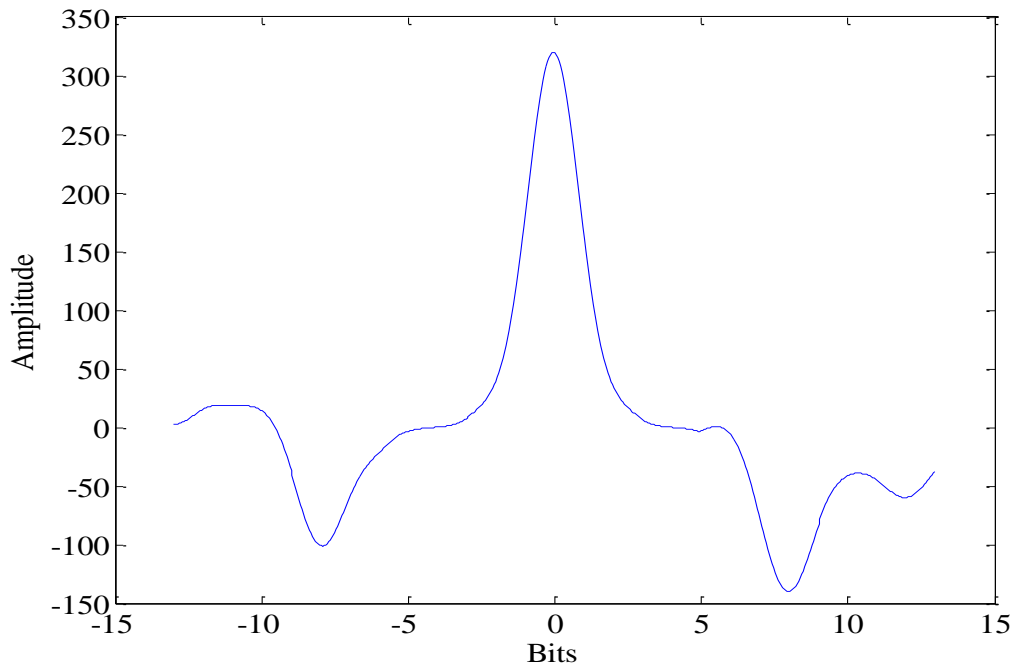


**Figure 4-15: Estimated Channel Impulse Response**

A rectangular window is slid over the estimated CIR across the length over the whole estimated response to calculate the energy in the window and find the maximum energy location [60].

$$E_i = \sum_{k=0}^{K-1} |h_{i+k}|^2 \quad (4-7)$$

Where  $K$  is the window size, and typical GSM equalization use  $K = 5$  [60].

When  $E_i$  in (4-7) reaches the maximum value, the maximum energy window start location  $i$  is obtained. Then the peak section of the CIR ( $h_n^{est}$ ) can be calculated in (4-8) and shown in Figure 4-16.

$$h_n^{est} = h_{i+n} \quad (4-8)$$

Where  $n = 0, 1, \dots, K - 1$

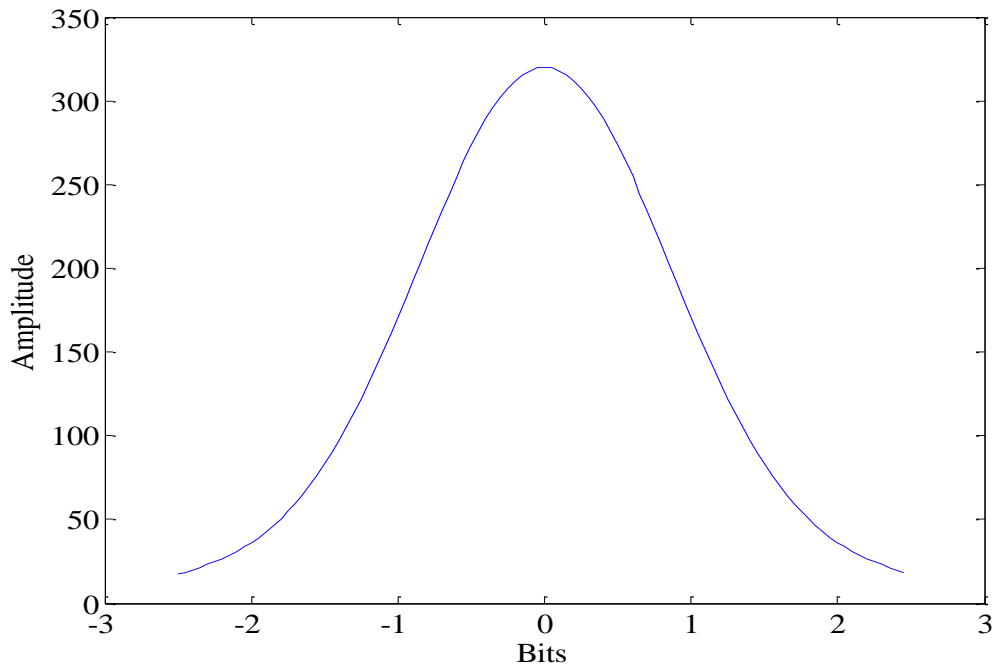


*Figure 4-16: The Peak of the CIR within the Window Size*

The location of this peak can then be used for the matched filtering process in equation (4-9) along with locating the start position of the received burst for synchronising the received input data due to the peak position being the centre point of the training sequence in any given burst.

$$s = r * h^{est'} \quad (4-9)$$

where  $r$  is the received input data synchronised from the located start position and  $h^{est'}$  is the transposed CIR used by the filtering process.

The output  $s$  from the matched filtering process is the down sampled MSK symbols required for further decoding. The received input data  $r$  contains  $x$  samples compared to  $s$  due to the down sampling of the filtering process.  $x$  is also referred to as the sample rate.

#### 4.1.9 MLSE Detection

The Maximum Likelihood Sequence Estimator (MLSE) is implemented as a Viterbi equaliser which is based on the modified Ungerboeck algorithm [67]. This section of the

receiver handles the actual detection of the received sequence which is fed from the matched filtered and down sampled signal. This input signal is a sequence of samples which contains one sample for each transmitted symbol due to being down sampled first. The other information required by the Viterbi equaliser is the autocorrelation of the estimated CIR obtained during the matched filtering process. Using this information with a Viterbi equaliser can produce an output which is an estimate of the most probable sequence of the transmitted binary symbols.

#### 4.1.10 Differential Decoder Simulation

A differential decoder converts the '-1' and '+1' symbols into '0' and '1' respectively. Firstly, the '1' and '-1' symbols from the output of demodulation are converted into '0' and '1' by equation (4-10) as shown below:

$$Y = \frac{1 - x}{2} \quad (4-10)$$

Where  $X \in (-1, 1)$

| $X$ | $Y$ |
|-----|-----|
| -1  | 1   |
| +1  | 0   |

*Table 4-6: Logical Table for Differential Encoding*

The '0' and '1' symbols in the burst input are fed into an XOR logical operator which produces a value of '1' only when the two input values are different and produces a value of '0' only when the two input values are same [54] as shown in above Table 4-6. The same burst in the differential encoding simulation (Section 4.1.4) is simulated in MATLAB as an example to show the difference between in the input and output of the differential Decoder in Figure 4-17 and Figure 4-18.

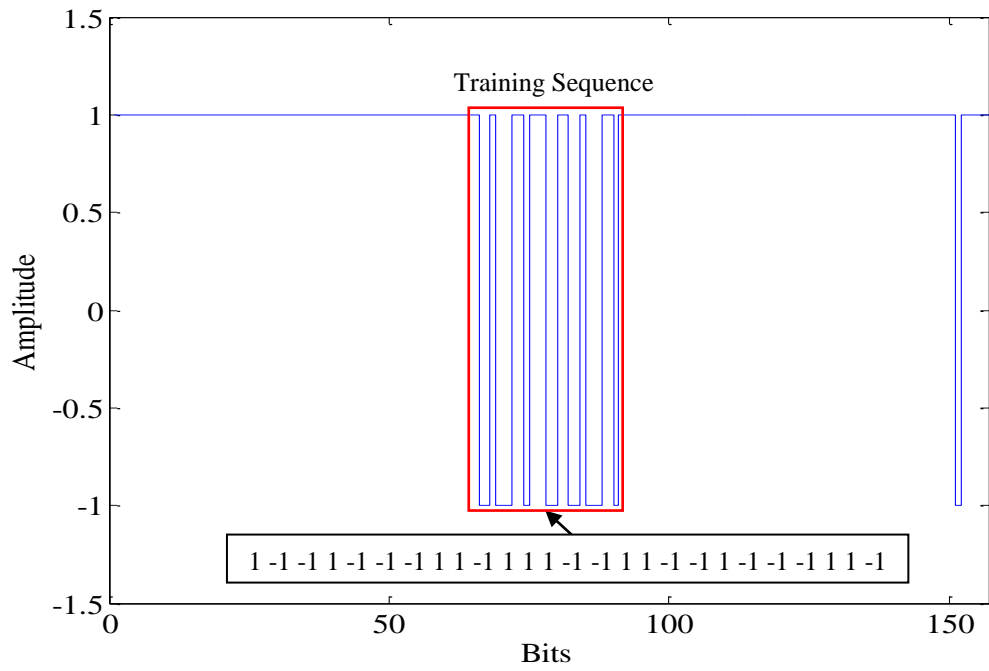


*Figure 4-17: Input Data of the Differential Decoder*

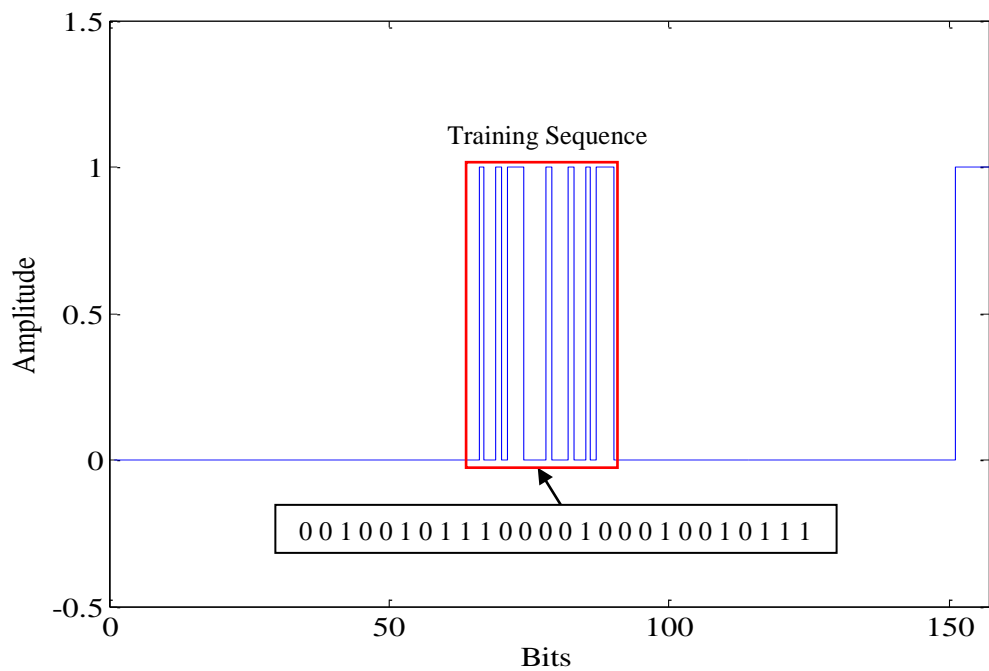


*Figure 4-18: Output Data of the Differential Decoder*

#### 4.1.11 De-interleave Simulation

In the interleave simulation (section 4.1.3), the 456 bits are portioned into eight time slots of 57 bits each. The slots are then reordered and allocated into two 57 bits sections in one

burst to avoid the data being corrupted. In the de-interleave simulation, using the first 114 data slot as an example, the block is divided into even and odd bits. All even bits go to W4 in block A and all odd bits go to X0 in block B. This is illustrated in Figure 4-19 .

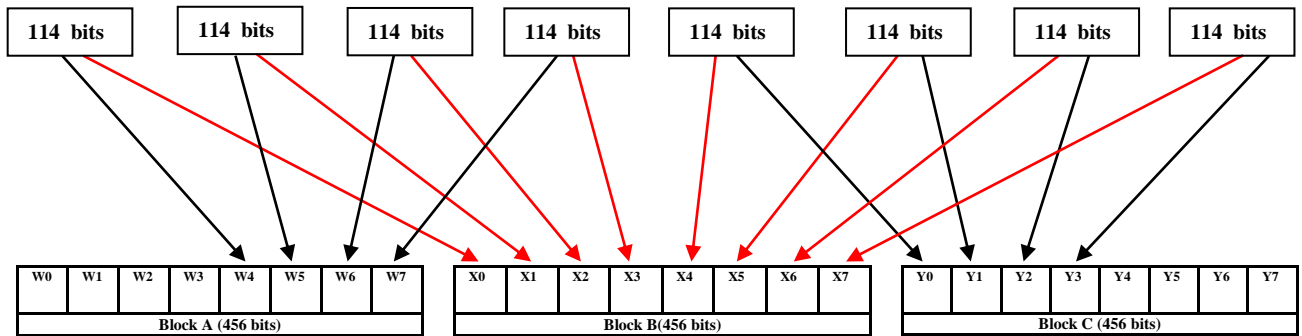


*Figure 4-19: De-interleave Process*

#### 4.1.12 Convolution Decoding

After performing de-interleaving, each block contains 456 bits which are divided into two classes: Class I (378 bits) and Class II (78 bits) before it can be further processed. Only Class I requires decoding using convolutional decoding as Class II is used directly in the encoding process described in Section 4.1.2.

Once the data from Class I is input into the convolutional decoder it will reduce the redundant bits for every bit that enters it, with Class I becoming 189 bits from its received 378 bits. Following this process, Class I is further split into two categories (Ia and Ib), due to Class Ia being more important than the information contained in Class Ib.

Class Ia contains three parity bits which can be used to check if any data has been corrupted and further correction can be applied if required but are not used in this simulation.

At the end of Class Ib the extra four tail bits which were added by the sending system can be ignored and are no longer required. Finally Class Ia of 50 bits and Class Ib of 132 bits can be reconstructed with Class II which remains at 78 bits to recover back the original speech signal of 260 bits.

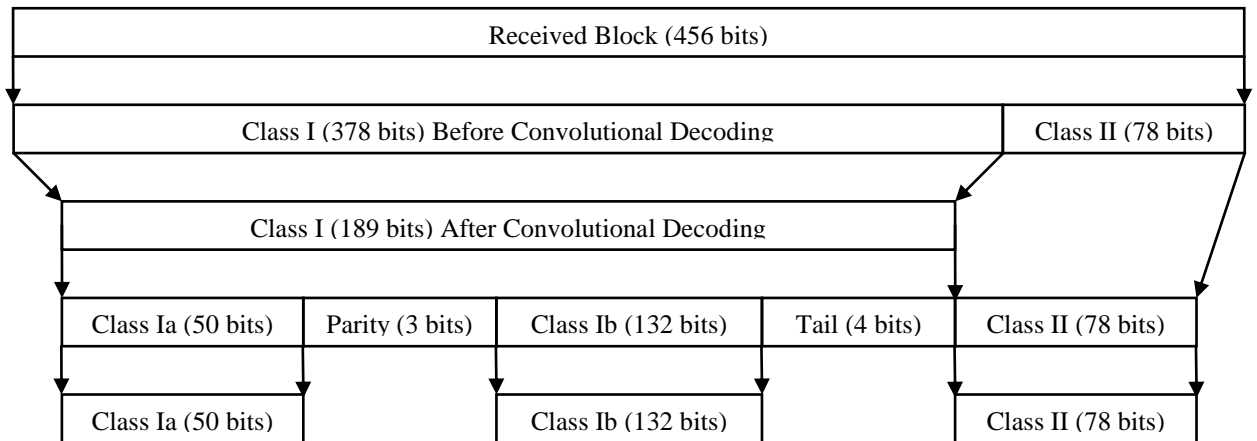


*Figure 4-20: Convolutional Decoding*

## 4.2 Software Environment

In this research, modelling simulation work plays an essential role regarding the evaluation of the design created for a FSS and the BER for a reconfigurable switching FSS. Commercial tool for the FSS design are utilised within a software suite called CST Microwave Studio. The sophisticated software can carry out electromagnetic static, low-frequency and high-frequency simulations based on the Finite Integration Technique (FIT). The FSS models have been designed in CST which can output 1D or 2D/3D results. The Scattering Parameters (S-Parameters) in the 1D result are very important. There is the reflection (S11) and transmission (S12) coefficients between the incident and reflection waves. Each parameter can be represented by real/imaginary parts, absolute and decibel value and phase. The results in decibels for the S-parameter are  $20 \log(S_{i,j})$ . The excitation wave travels in the ports with a variety of patterns called modes. Normally, there are three types of modes in a waveguide: Transverse Electric and Magnetic (TEM) mode, TE (Transverse Electric) mode and TM (Transverse Magnetic) mode. TEM mode is the direction of propagation, perpendicular to the electric field and magnetic field. TE mode is the direction of propagation, being only perpendicular to the electric field. TM mode which is opposite to TE mode, where the direction of propagation is only perpendicular to the magnetic field [68]. In the Figure 4-21, the 3-D wall surface are used as example to demonstrate these three modes.

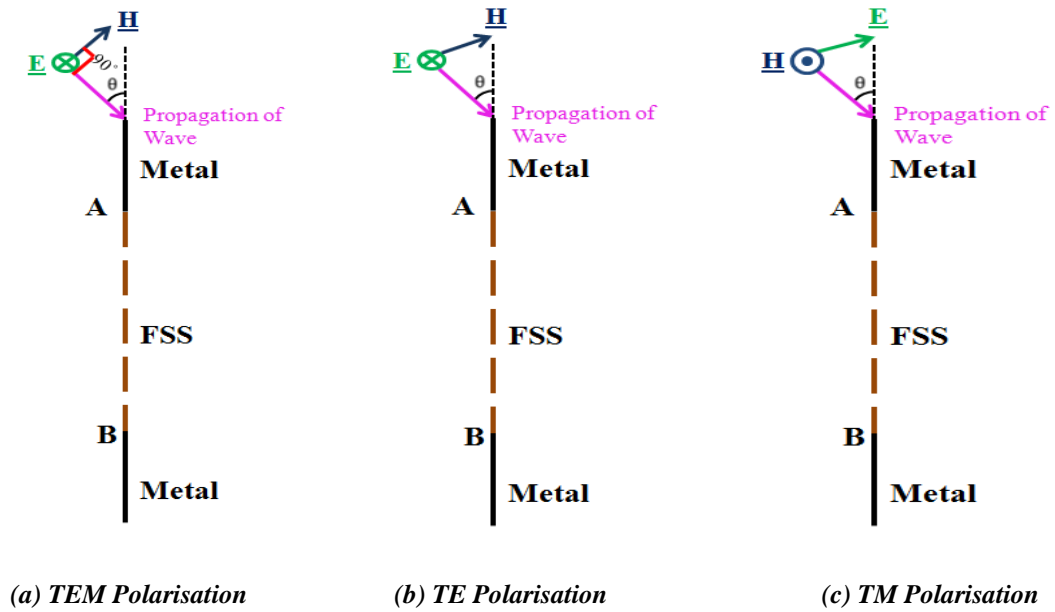


*Figure 4-21: TEM, TE and TM Polarisation*

CST Microwave Studio can be used as a tool for accurate responsive 3D simulations of high frequency models which operate over a vast range of frequencies [18]. It will be utilised to observe the propagation of a radio wave through a FSS wall in an external to internal 3D environment. CST is also used to analyse plane wave incidence fired at the chosen FSS model obtaining its reflection and transmission characteristics [56].

The software used to simulate and analyse the BER for the reconfigurable switching FSS is MATLAB, which is an interactive environment used for numerical computation, visualization and programming. Programming scripts were developed to model a simulation of a GSM channel which could be used to measure the total BER of any given test input data sent over the simulated channel. This was further enhanced by exploring the characteristics of the channel by emulating the switching active FSS design with the results being clearly represented in 2D surface graphical form.

### **4.3 Summary**

This chapter firstly introduced the background of GSM, to understand uplink and downlink for GSM 900 and GSM 1800, with the use of TDMA to transmit text, data and voice and the structure of a TDMA Frame being illustrated.

Secondly, the structure of the whole GSM system model has been shown with each part of the structure explained in detail. Also, the simulation results from MATLAB has been compared with the results extracted from an interest report to prove the GSM system created in MATLAB is correct and can be employed to test the reconfigurable switching FSS performance.

The major commercial software used for this research are CST Microwave Studio and MATLAB, with a brief outline of their functions being given for each in this chapter.

# CHAPTER 5 RECONFIGURABLE FSS FOR USE IN SECURE ELECTROMAGNETIC BUILDING

Frequency Selective Surfaces (FSS) have been a topic of research for many decades, for applications in large area filters [69-71], absorbing materials [72], and for use in the building environment [73]. There has been significant interest in designing reconfigurable periodic surfaces.

Generally, FSS are designed to either pass or stop electromagnetic waves over a range of frequencies. Reconfigurable FSS offer the advantage of flexibility by changing the FSS frequency response using an external bias signal i.e. voltage/current.

In this research, FSS has been investigated to act as impairment to mobile/cell phone signals for applications where communication is not wanted (i.e. hospitals, prisons etc.), where full electrical shielding of such signals may not be practical. It was shown in [74], that in areas of good mobile/cell phone coverage there would need to be >60dB of attenuation of the signal before the phone would not be able to communicate with the Base Station Transceiver (BTS). To use FSS with these requirements is very difficult in practice, due to manufacturing tolerances, angle of incidence and polarization effects.

The proposed solution is to make use of reconfigurable FSS in a manner that will corrupt the mobile/cell phone signal, such that the receiver cannot determine the data which is transmitted. This research will examine how this may be carried out for the GSM protocol even when a desirable >60dB attenuation cannot be achieved. Figure 5-1 illustrates the scenario of an FSS inserted into a perfectly conducting wall of a room or building. It is assumed that no energy can propagate into the room except through the FSS.

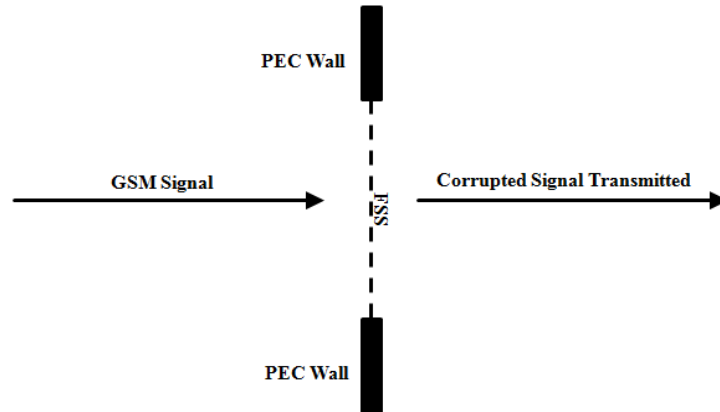


*Figure 5-1: Illustration of FSS Embedded with the Wall of a Building*

The FSS transmission properties are such that the transmission coefficient is time varying and complex, given as (5-1).

$$\tau(t) = |\tau(t)|e^{j\phi(t)} \quad (5-1)$$

Where  $\tau$  the transmission coefficient and  $\phi$  is the phase of the transmission coefficient.

The GSM protocol uses a combination of spatial, frequency and time domain multiplexing, however, for simplicity we will only consider the TDMA aspect of GSM. It is well known that a GSM “frame” is split into eight “bursts”. The frame time is 4.6ms and the burst time is 0.577ms. It is assumed that each phone is allocated one burst per frame. Within each burst the signal that is transmitted is made up of binary information, which conveys the data as well as synchronization bits and training sequence bits at a data rate of approximately 270.8kbits/s. As previously described in Chapter 4.1 the binary signal is differentially encoded then modulated using Gaussian Minimum Shift Keying (GMSK) creating a baseband signal before being RF modulated to the appropriate transmission frequency.

The proposed technique is to use the time varying transmission response of the FSS to corrupt the GMSK modulated signal. The GSM protocol assumes that the channel in which the signal is propagating through is relatively constant, so if the channel response can be impaired appropriately with use of a FSS, it should be possible to corrupt the signal. For simplicity it is assumed that the FSS transmission response will vary periodically with time at a switching frequency  $f_s$ , with the concept first being modelled using the GSM simulator described previously in Chapter 4.1.

## 5.1 GSM Simulator Using MATLAB

In Chapter 4.1, the model of a GSM system has been created in MATLAB, with the model being able to simulate different scenarios required. Firstly, this model enables fast simulation times to sweep all the different combinations of switching frequencies with corresponding phase values. Secondly, this model will allow for optimum values to be obtained, maximising BER which are required when designing phase characteristics of the active switching FSS model. Finally, this model is further verified once a physical FSS model is built for true environment testing which should closely match the simulated results from MATLAB.

In Chapter 4.1.6 the channels simulation mentioned that the phase and attenuation can be switched by dividing up the signal channel into digitised samples. Depending on how many samples are used to divide up the signal when switching between phase and attenuation states of the FSS, a switching frequency can be determined. The maximum switching frequency of the FSS is given below:

$$f_{\text{Maximum Switching Frequency}} = \frac{1}{2 * \text{Bit Duration/Sample Rate}} \quad (5-2)$$

Where the bit duration is given by  $3.69\mu\text{s}$  from a previously calculated Equation (4-4) in Chapter 4.1.5. For each signal switched from one state to another state the minimum of one bit duration per state is required to obtain maximum switching. For example if the sample rate was equal to 20, the maximum switching frequency of the FSS would be  $2.71\text{MHz}$ .

One of the eight burst are employed as an example for the switching technique which originally is 156 bits. After the data has been divided into digitised samples, if the sample rate is 20, then a total of 3120 sample points are used. In this research, two cases will be compared. First where in the data is not interleaved and second where the data has been interleaved before entering into the differential encoder which is introduced in Chapter 4.1.3.

When a randomly generated data stream with interleaving and convolutional coding, passes through the GSM modulation and enters the GSM Channel the phase represented graphically from MATLAB can be seen in Figure 5-2 to Figure 5-4. The signal is transmitted through a FSS with a transmission coefficient magnitude of 0dB and the

transmission phase varying from  $\pm 60^\circ$ . Figure 5-2 shows the phase before the channel switching; Figure 5-3 is the phase switching at the maximum switching frequency of 2.71MHz and Figure 5-4 is the phase switching at switching frequency of 271kHz.

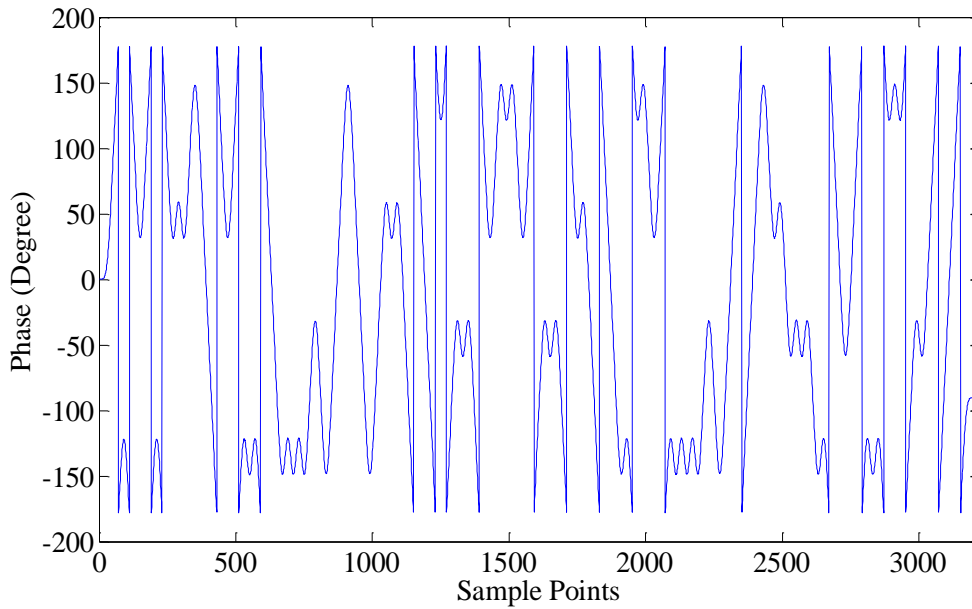


*Figure 5-2: Phase before Switching, Interleaving and Convolutional Coding*

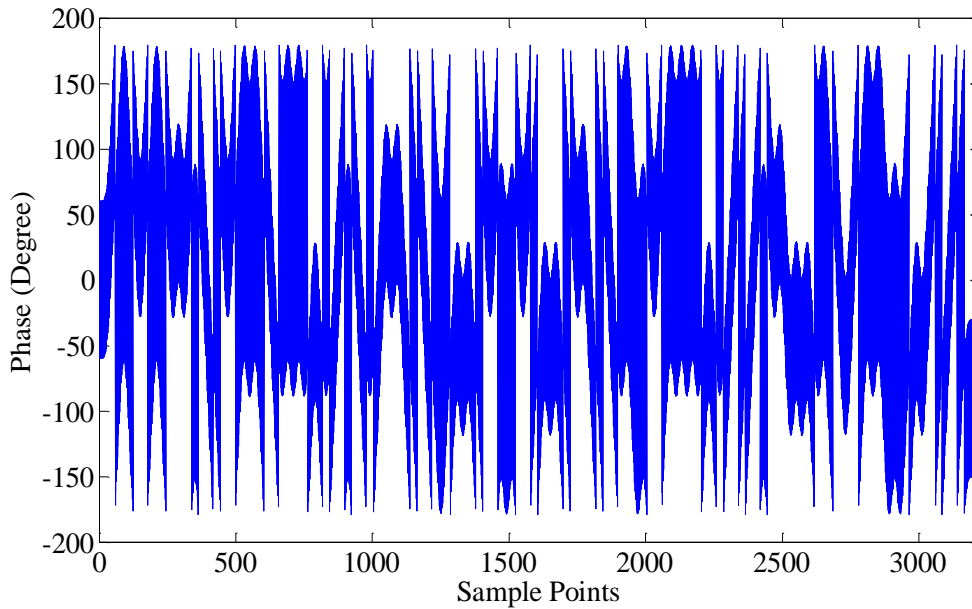


*Figure 5-3: Phase Switching at 2.71MHz, Interleaving and Convolutional Coding*

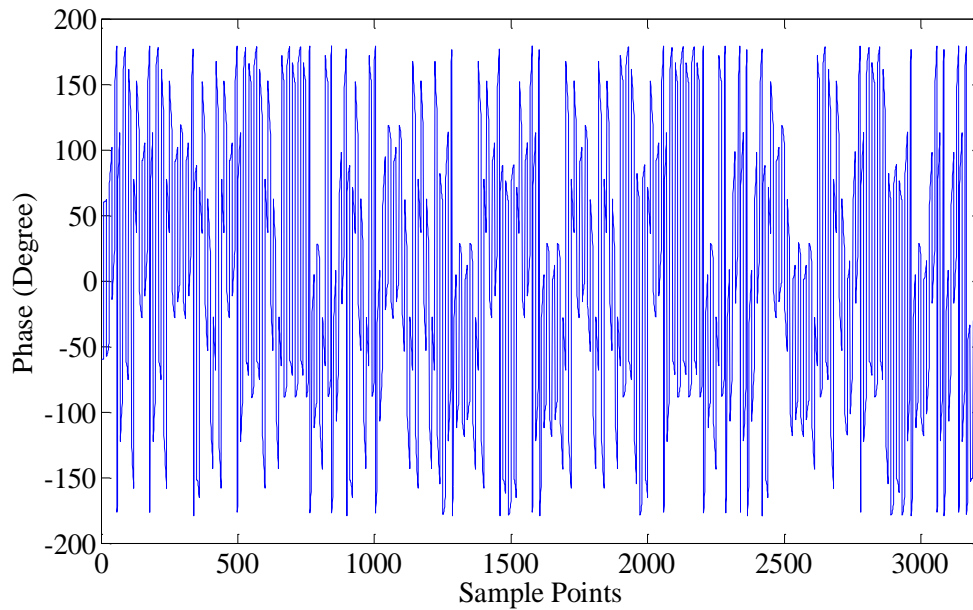


*Figure 5-4: Phase Switching at 271kHz, Interleaving and Convolutional Coding*

Now the discrete time domain of the signal for its phase is understood by the two phase states being switched, the frequency spectrum of channel can be analysed before switching which is shown in Figure 5-5. When a randomly generated data stream is switched by the maximum switching frequency, the frequency spectrum is shown in Figure 5-6 with the spectrum comprising of the original baseband data plus the sidebands are odd multiples of the switching frequency, making the first sideband at 2.71MHz. The frequency spectrum at the middle of Figure 5-6 compared with the frequency spectrum before the switching in Figure 5-5 has been attenuated 41%.

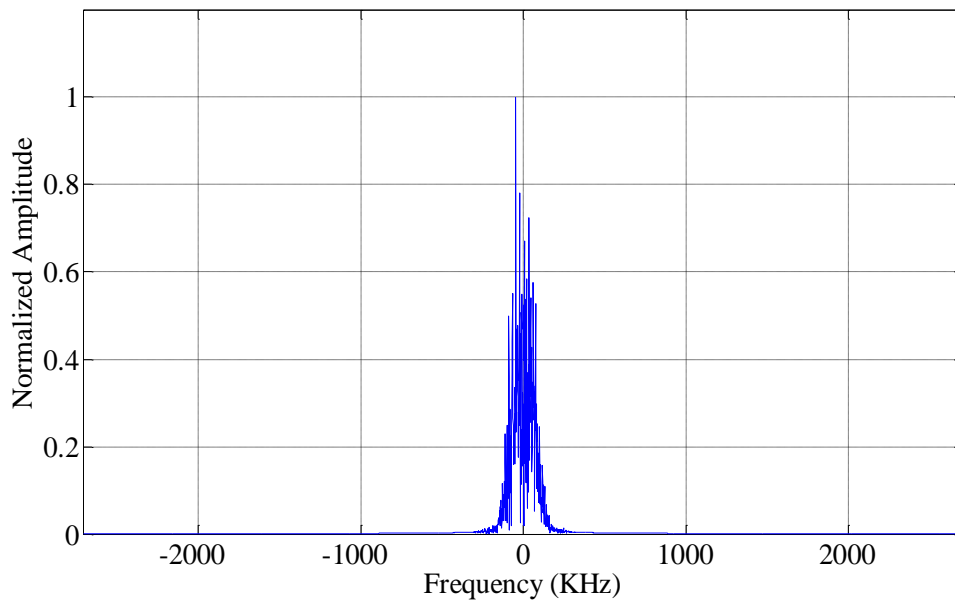


*Figure 5-5: Frequency Spectrum before Switching, Interleaving and Convolutional Coding*

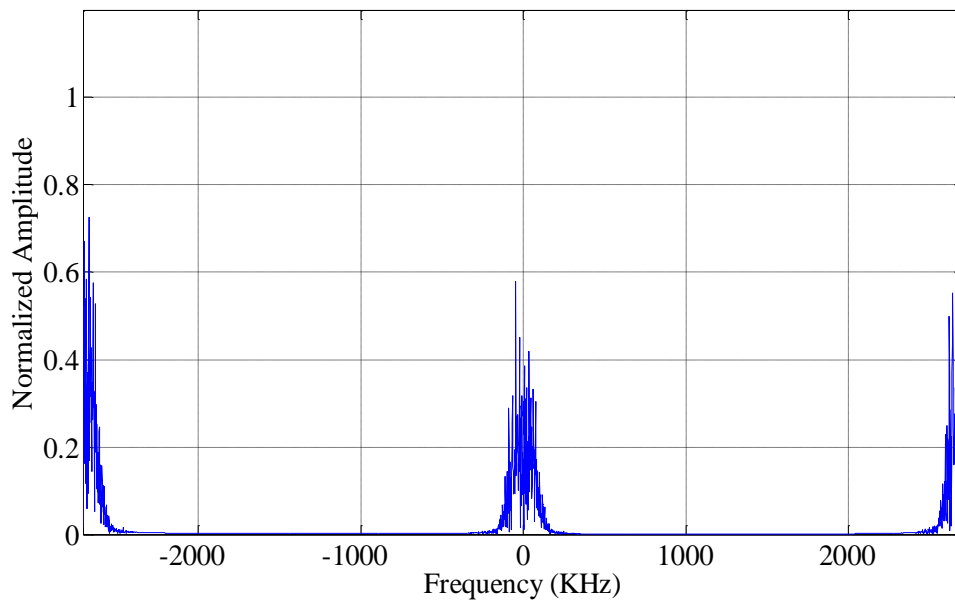


*Figure 5-6: Frequency Spectrum of the Signal Switching by 2.71MHz*

When the signal is switched at 271kHz, the frequency spectrum can be shown as in Figure 5-7 with the spectrum comprising of the original baseband data plus harmonics spaced  $n \cdot 271\text{kHz}$  apart, where  $n$  is an odd integer in the ideal case, making the first harmonics at 271kHz and second harmonics at 813kHz and so on. The frequency

spectrum at the middle of the Figure 5-7 compared with the signal before the switching in Figure 5-5 has been attenuated 10%.

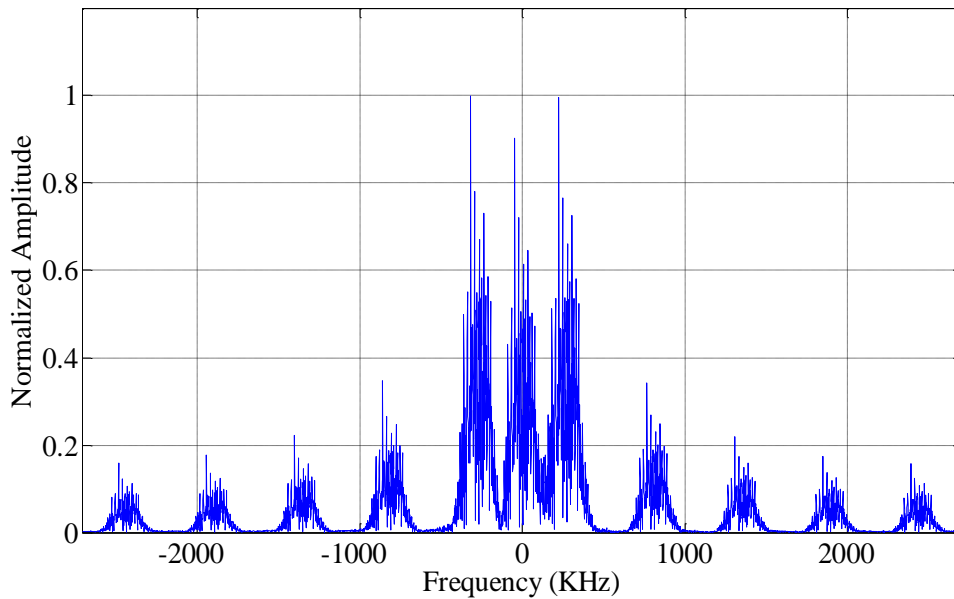


*Figure 5-7: The Frequency Spectrum of the Signal Switching at 271kHz*

As illustrated in Figure 5-7, if the signal of the channel has been switched high enough, the significant sidebands of energy which could distort the recovering of the signal are beyond the predefined bandwidth of the receivers filter, making the process easy to be filtered out by the GSM receiver. The bandwidth of filter may vary depending on the receiver topology used which is very important as impacts the overall BER. When the filter is applied the signal is easily demodulated, assuming there is no significant noise on the signal. So in this research, a few bandwidths are chosen to give examples for their BER which are:

- Half the GSM bandwidth (135kHz)
- GSM bandwidth (270kHz)
- One and an half times the GSM bandwidth (405kHz)
- Two times the GSM bandwidth (540kHz)

For the above bandwidths a set hamming window will be used for all the digital filters. The hamming window is represented as follows,

$$\omega(n) = 0.54 - 0.46 \cos\left(2\pi \frac{n}{N}\right) \quad (5-3)$$

Where  $0 \leq n \leq N$ , the window length is  $L=N+1$ .

## 5.2 Frequency Spectrum of Channel with Interleaving

Firstly, from Figure 5-8 to Figure 5-11 the frequency spectrum of the channel with an applied bandwidth filter of 135kHz will be used as an example for its BER. For the following it is assumed as above that the switching frequency would be the maximum switching frequency at 2.71MHz. In Figure 5-8 the red line represents the filter in the receiver which can filter out the ‘in band’ signal with its amplitude being dropped 43% from the original transmission channel before switching. Assuming that it had not been attenuated beyond the sensitivity of the receiver, this would allow for the attenuated baseband signal to be recovered easily, with the signal which is received by the GSM receiver being the same as the signal being sent through the GSM channel, therefore creating no bit errors in this case i.e. a BER equal to zero.

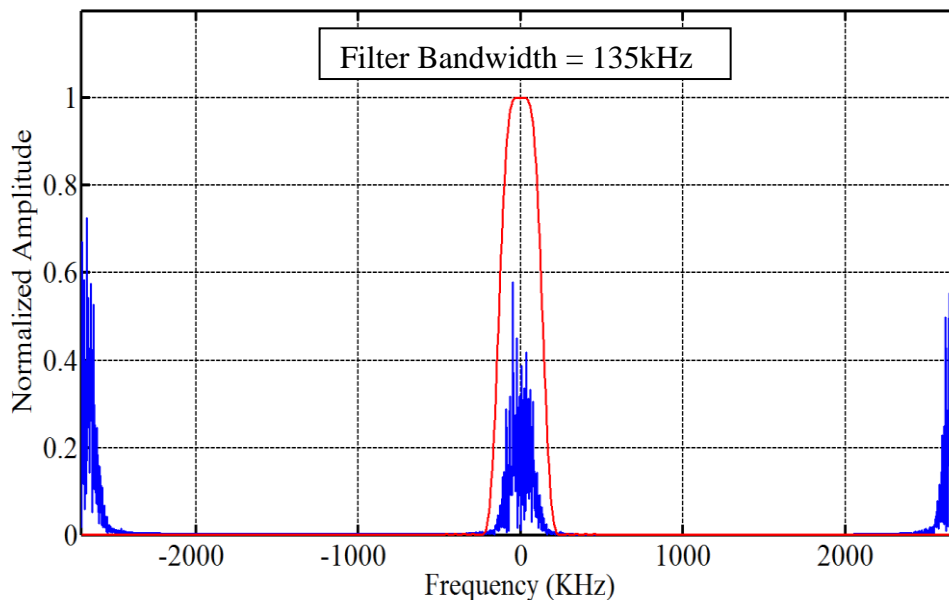


*Figure 5-8: The Signal as Switching Frequency at 2.71MHz*

If the switching frequency is changed to 271kHz as in Figure 5-9 the sidebands of energy are slightly overlapping within the bandwidth of the receiver filter, after the signal is filtered the sidebands remain inside the receiver filter bandwidth which makes the receiver difficult to filter out the unwanted sideband energy by the GSM receiver. This can cause the attenuated baseband signal to be received in-correctly. In this case there is only a reduced amount of sideband signals which has not been filtered out, meaning that the signal can still be recovered by the Viterbi Algorithm used by GSM, giving a BER of 0% being obtained with the energy level dropping 10%.

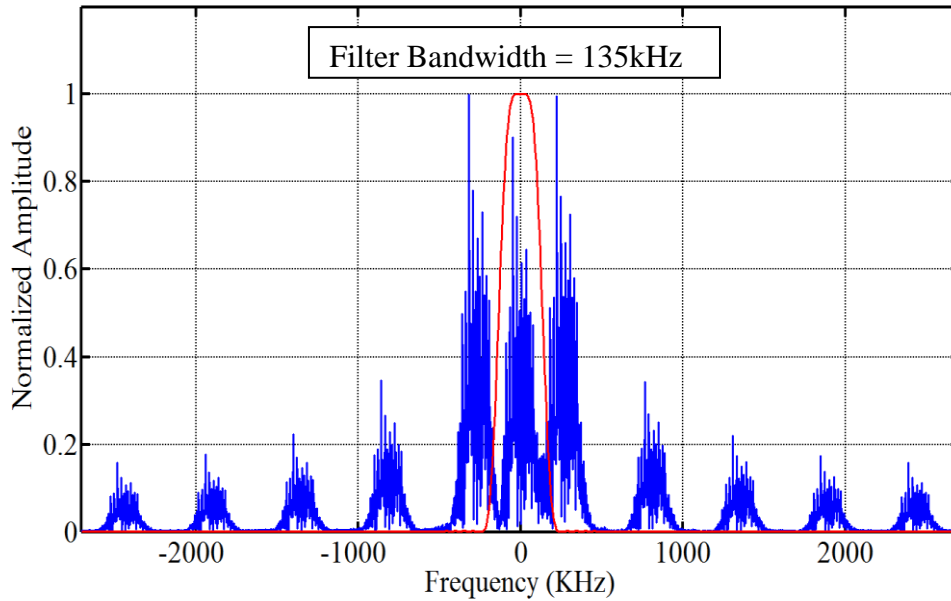


*Figure 5-9: The Signal as Switching Frequency at 271kHz*

If the switching frequency is changed to 135.5kHz, a different observation can be seen from Figure 5-10 which shows the sidebands of energy interrupting significantly the ‘in band’ signal when the switching frequency is at 135.5kHz. The sidebands now contained in the bandwidth of the receiver filter, and combined with the ‘in band’ signal, which distorts the recovery of the signal giving a BER of 6.1% with the signal energy level being dropped by 5.3%.

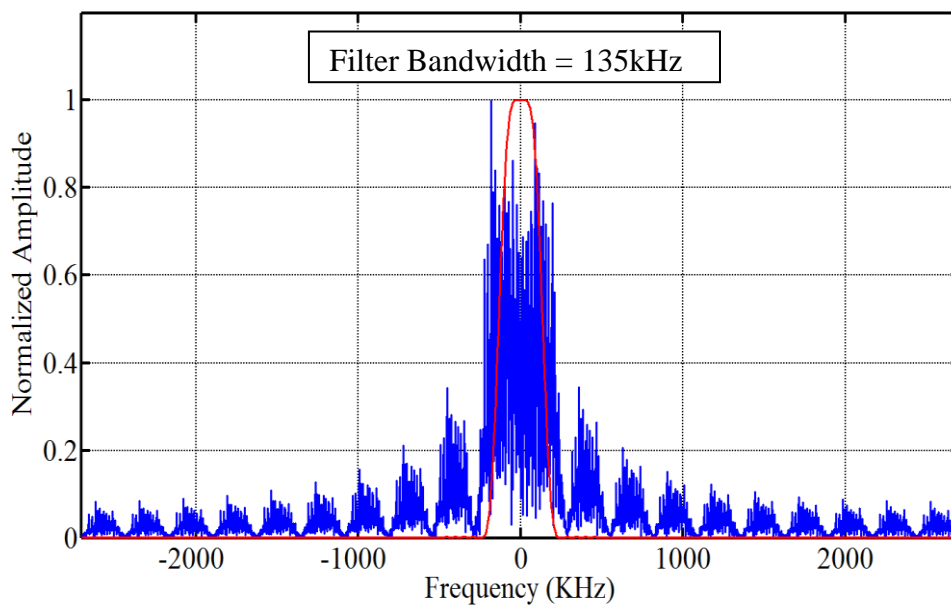


*Figure 5-10: The Signal as Switching Frequency at 135.5kHz*

Figure 5-11 shows the switching frequency now being changed to 67.75kHz. The sidebands signal are contained in the bandwidth of the receiver filter, which distorts the recovery of the signal giving a BER of 46.5% with the signal energy level being dropped by 2%.

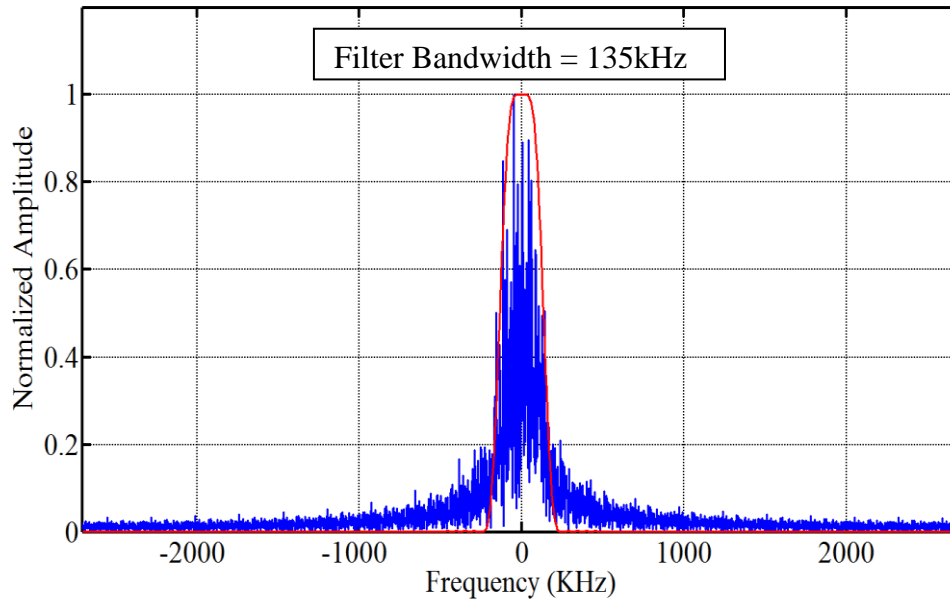


*Figure 5-11: The Signal as Switching Frequency at 67.75 kHz*

Comparing the BER of the switching frequency changing between 2.71MHz to 67.75kHz from Figure 5-8 to Figure 5-11, when the switching frequency decreases, the sidebands of energy interrupts significantly the ‘in band’ signal, causing the BER to be increased. Whereas the ‘in band’ signal’s amplitude when compared to the original transmission channel decreases as the switching frequency increases.

Secondly, from Figure 5-12 to Figure 5-15 the frequency spectrum of a channel with an applied bandwidth filter of 270kHz is used as an example for its BER.

If the switching frequency is 2.71MHz, a BER of 0% is obtained with the energy level dropping 43%.

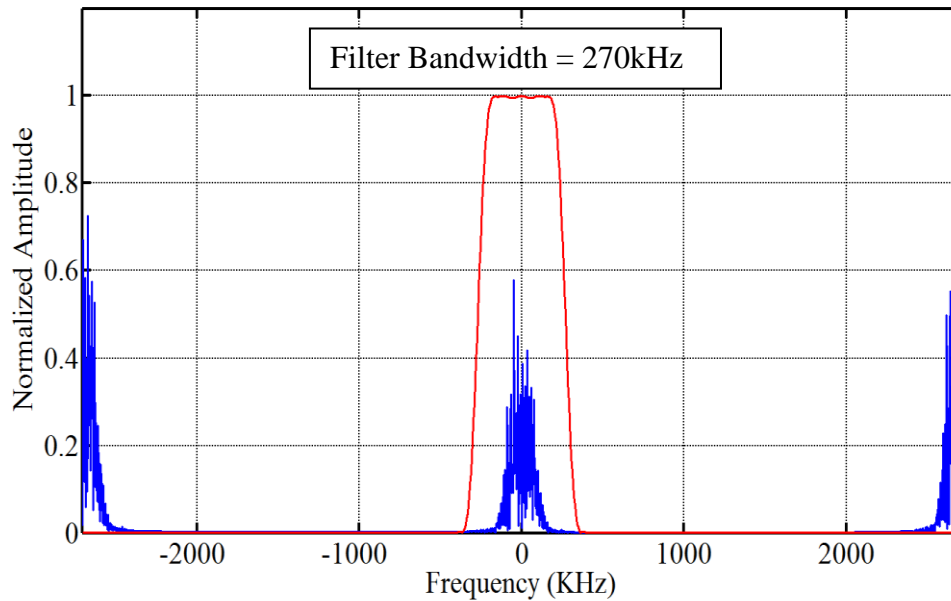


*Figure 5-12: The Signal as Switching Frequency at 2.71MHz*

If the switching frequency is changed to 271kHz, a BER of 0% is obtained with the energy level dropping 10%.

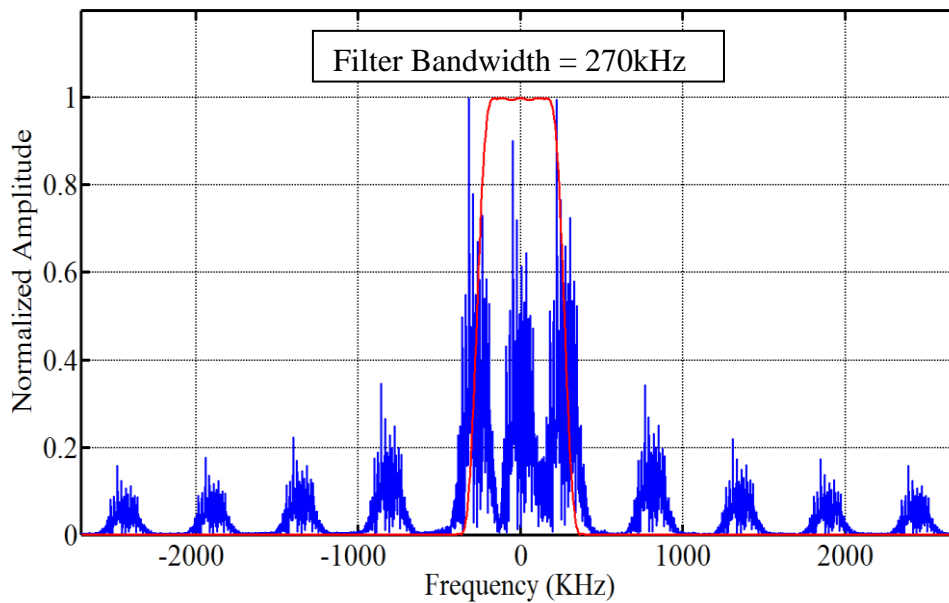


*Figure 5-13: The Signal as Switching Frequency at 271kHz*

If the switching frequency is changed to 135kHz, a BER of 42% is obtained with the energy level dropping 1%.

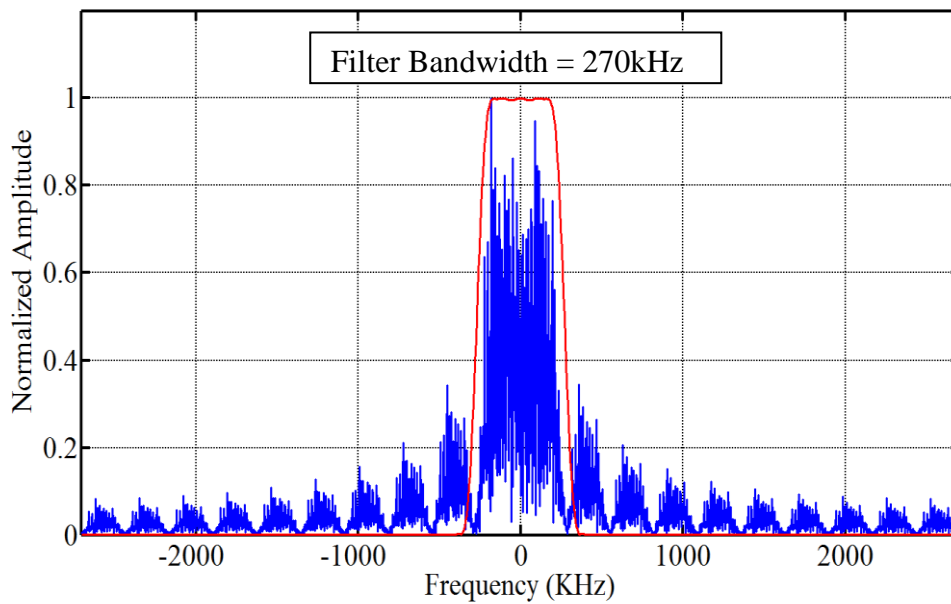


*Figure 5-14: The Signal as Switching Frequency at 135.5kHz*

If the switching frequency is changed to 67.5 kHz, the BER of 44.6% is obtained with the energy level dropping 0.5%.

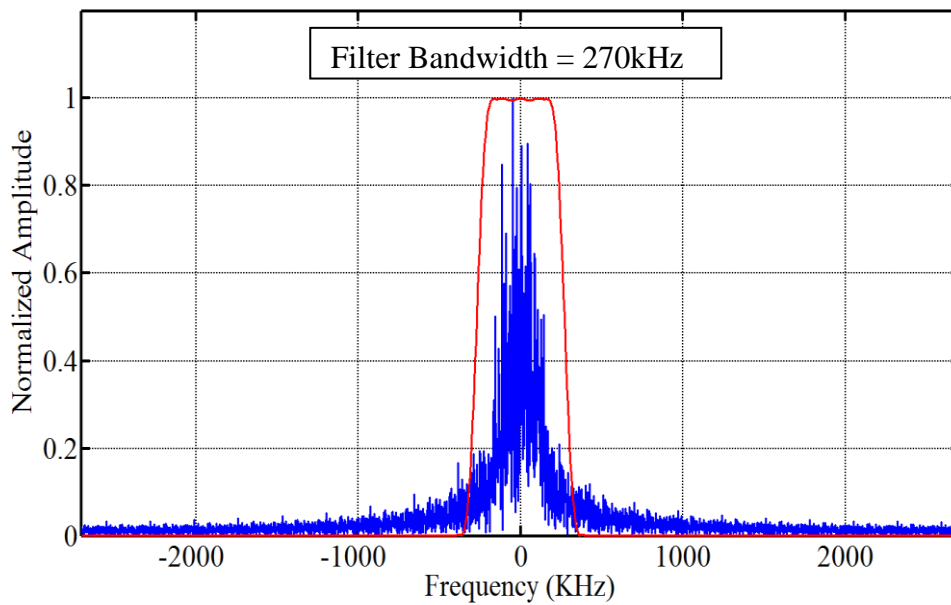


*Figure 5-15: The Signal as Maximum Switching Frequency at 67.75kHz*

From Figure 5-12 to Figure 5-15, the BER follows the same trend as a filter bandwidth of 135kHz. As the switching frequency decreases, the BER rate is increased. As previously stated the BER using a switching frequency of 135.5kHz applied with a bandwidth filter of 135 kHz is 6.1%. If compared with as bandwidth of a filter changed to 270kHz, the BER increases to 42%, which indicates the importance of the bandwidth used in the filter which will decide the effect on the BER received.

The above were examples of switching with a two state FSS between phase of  $60^\circ$  and  $-60^\circ$  do not show the wide range of effects at different switching phases across different switching frequencies. To achieve this, the BER of a number of randomly generated GSM signals were transmitted through a surface by varying the switching frequency and transmission phase to plot a 2-D surface of BER. The x-axis is the phase difference in degrees between two states e.g.  $\pm 60^\circ$  equals  $120^\circ$  phase difference, the y-axis is the switching frequency in kHz and the z-axis is the BER which is represented as a percentage. The BER shown is the average taken from a set number of randomly generated GSM signals tested at a given frequency and phase switching sample. The 2-D surfaces of BER plotted in Figure 5-16 to Figure 5-18 are simulated in MATLAB using 1 random seed, 10 random seeds and 100 random seeds respectively. Comparing these three figures, the figure that uses 10 random seeds is very similar with 100 random seeds, concluding that the figure using 100 random seeds has already converged to a stable average result, making it accurate enough to analyse the BER.

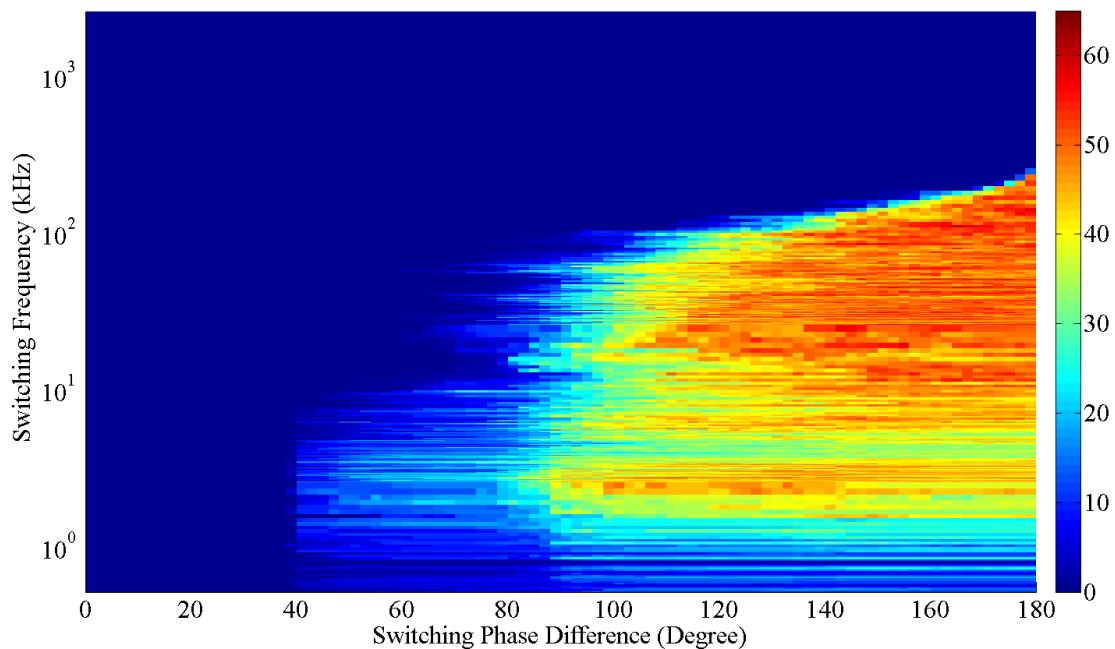


*Figure 5-16: A 2-D Surface Plot of BER for 1 Random Seed*

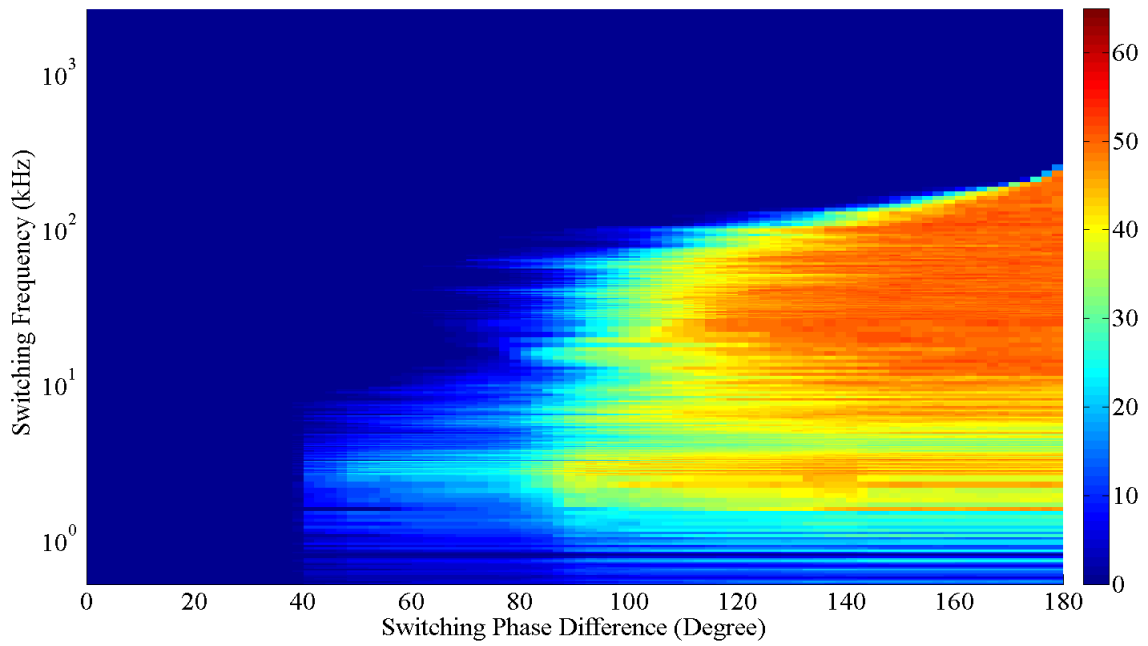


*Figure 5-17: A 2-D Surface Plot of BER for 10 Random Seeds*

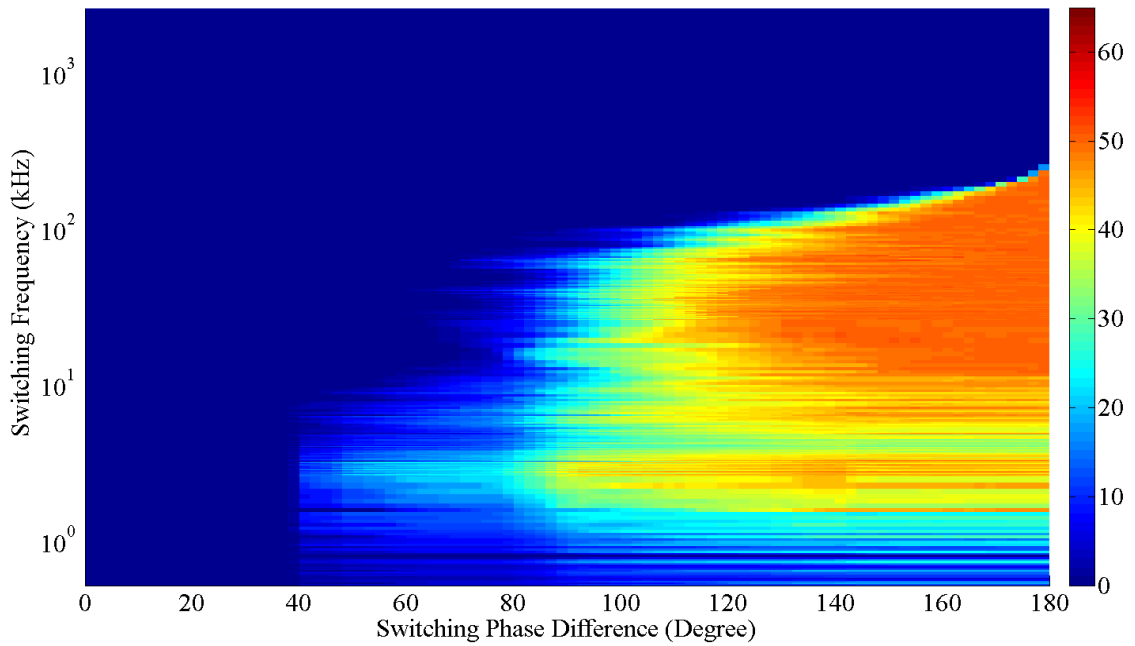


*Figure 5-18: A 2-D Surface Plot of BER for 100 Random Seeds*

All the following results have been generated using 100 pre-set random seeds so that the same data is used to compare the BER between different filter bandwidths, phases and switching frequencies.

### 5.3 2-D Surface Plots of BER with Interleaving

When the bandwidth of the receiver filter is half of the GSM bandwidth (135 kHz), the resulting 2-D BER is shown in Figure 5-19.

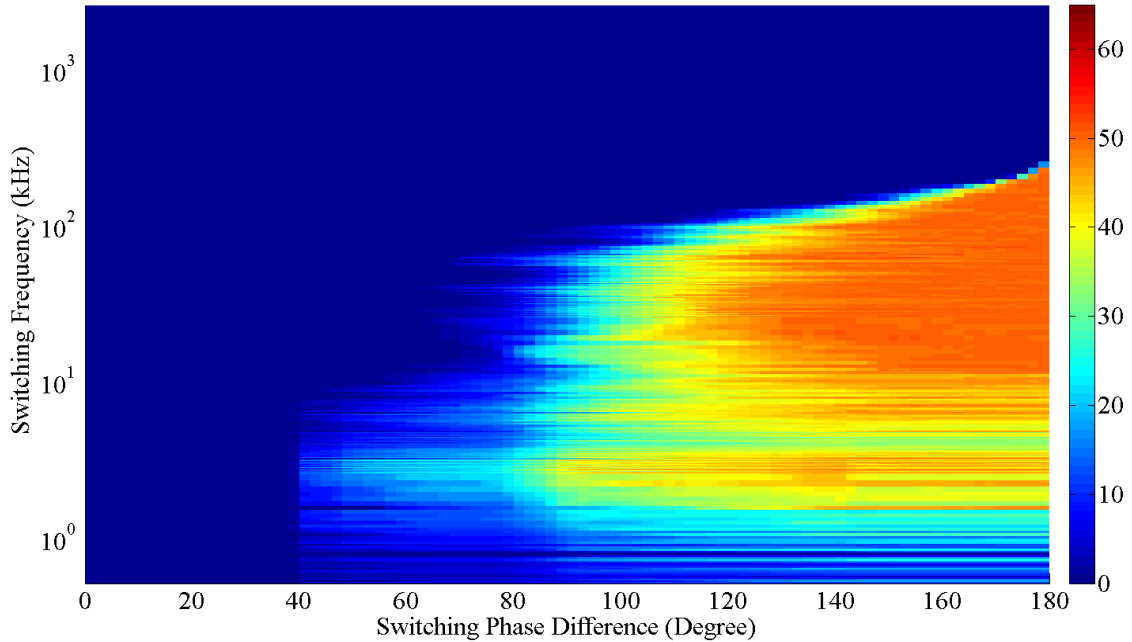


*Figure 5-19: BER (%) using Bandwidth Filter of 135kHz with Interleaving*

When the bandwidth of receiver filter is the GSM bandwidth (270kHz), the resulting 2-D BER is shown in Figure 5-20.

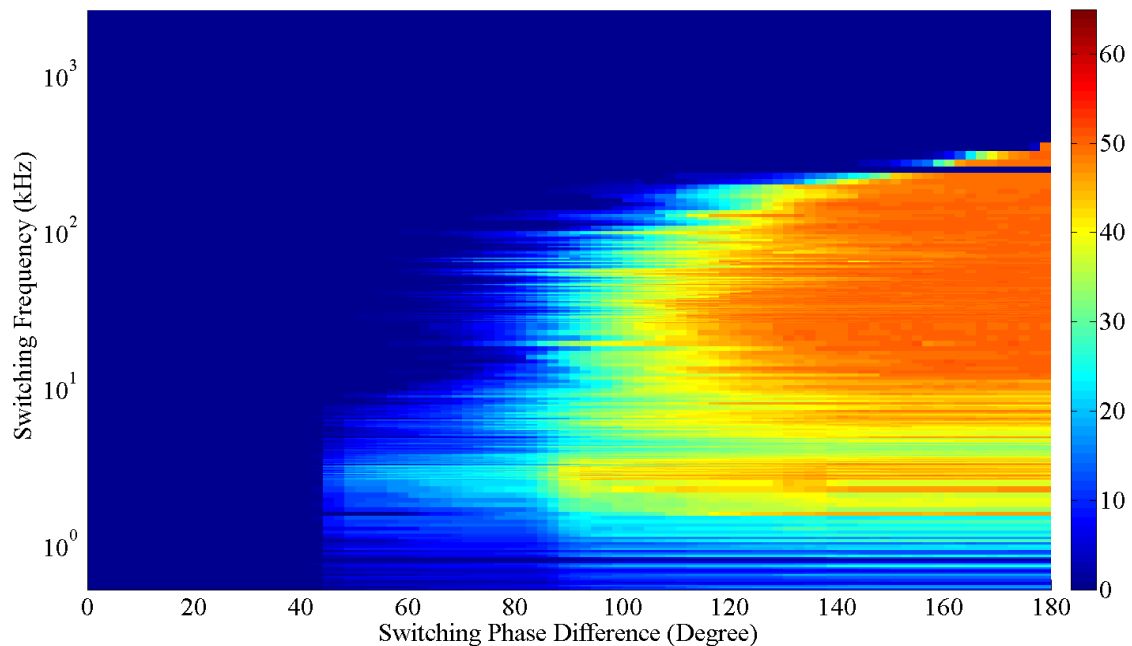


*Figure 5-20: BER (%) using Bandwidth Filter of 270kHz with Interleaving*

When the bandwidth of receiver filter is one and a half times the GSM bandwidth (405kHz), the resulting 2-D BER is shown in Figure 5-21.

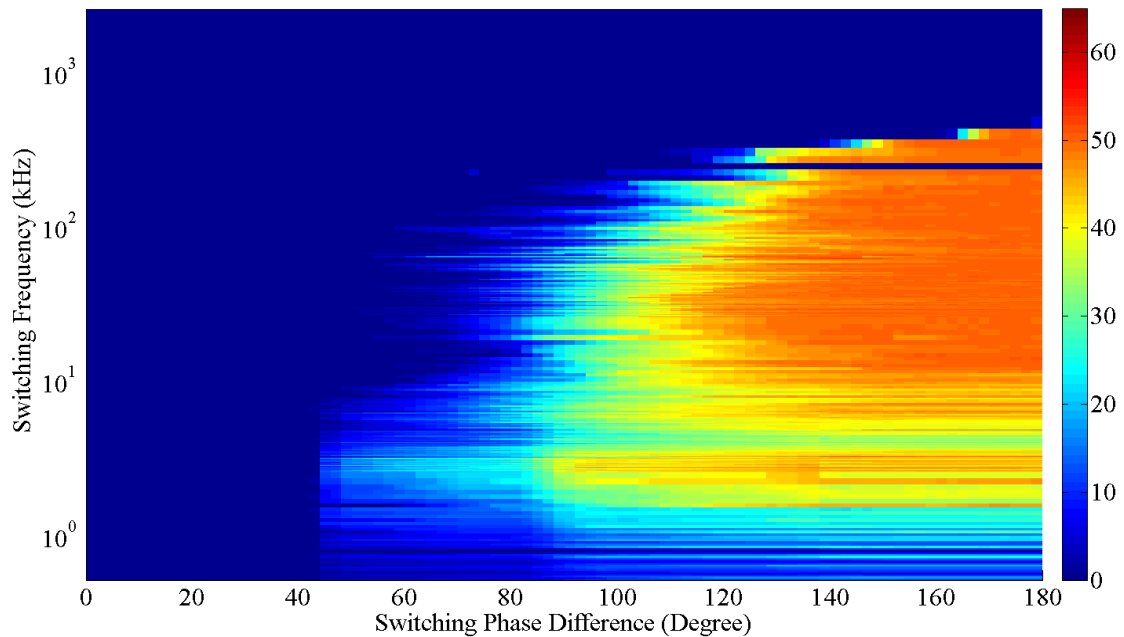


**Figure 5-21: BER (%) using Bandwidth Filter of 405kHz with Interleaving**

When the bandwidth of receiver filter is double the GSM bandwidth (540kHz), the resulting 2-D BER is shown in Figure 5-22.

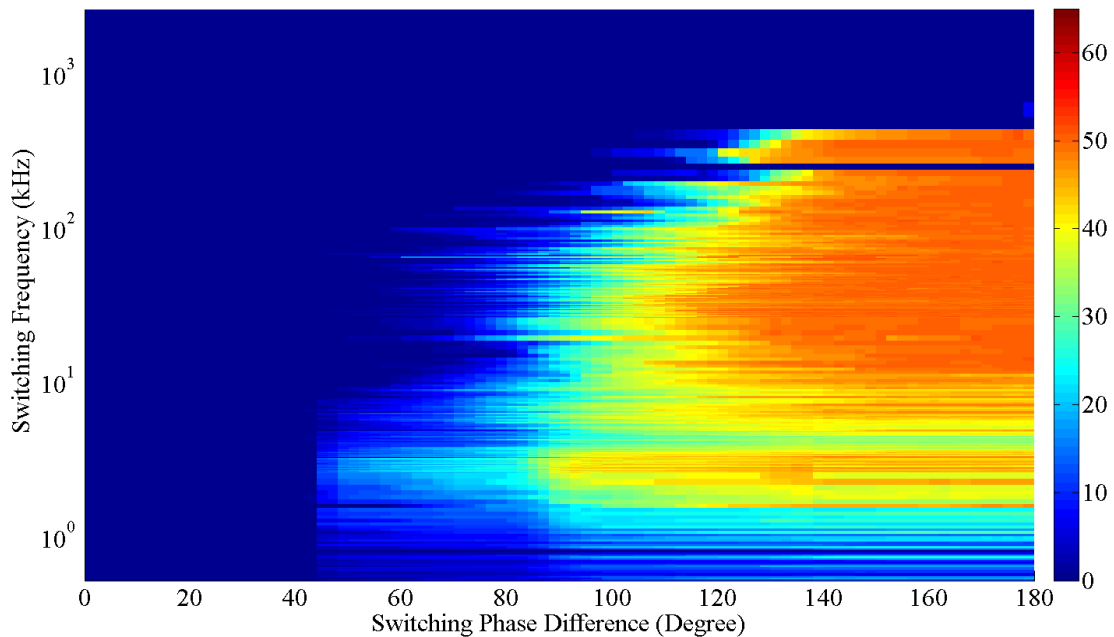


**Figure 5-22: BER (%) using Bandwidth Filter of 540kHz with Interleaving**

It can be seen from Figure 5-19 to Figure 5-22 that significant BER can be achieved over a large range of switching frequency and transmission phases. Particular regions of interest are the low and high frequency “cut-off”. It can be seen that some signal impairment occurs for switching frequencies as low as 1 kHz for different bandwidths of receiver filter, but the high frequency cut-off varies depending on the different bandwidth of the receiver filter. When the bandwidth of the receiver filter is increased above the normal GSM bandwidth, the high frequency cut-off increases due to side band energy interference. An example of this can be seen when the phase difference is  $120^\circ$ ; the high frequency cut off at which the BER starts to fall back to zero is 150.5kHz when the bandwidth is 135kHz, 270.8kHz when the bandwidth is 270kHz, 386.9kHz when the bandwidth is 405kHz and 541.7kHz when the bandwidth is 540kHz. This means when the bandwidth of the receiver filter is increased, the high frequency cut-off also increases due to the signal ‘in band’ being degraded causing inaccurate data recovery.

#### 5.4 Frequency Spectrum of Channel without Interleaving

Next the results of a randomly generated data stream without interleaving are shown, after GSM modulation and entering the GSM Channel. This is then compared with the channel being switched and filtered with the bandwidth of the filter being 270kHz. As before the switching was between  $\pm 60^\circ$ , only the switching frequency varies from Figure 5-23 to Figure 5-25 . The first example is a switching frequency at 271kHz. Figure 5-23 shows the red line, representing the filter in the receiver, with the BER being zero in this case.

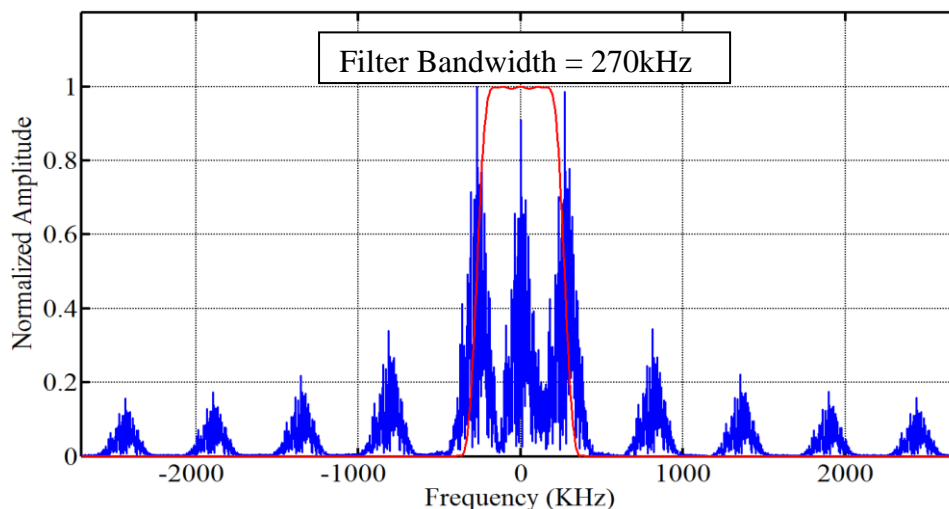


*Figure 5-23: The Signal as Switching Frequency at 271 kHz*

If the switching frequency is 135.5kHz as in Figure 5-24, the BER increases to 49%.

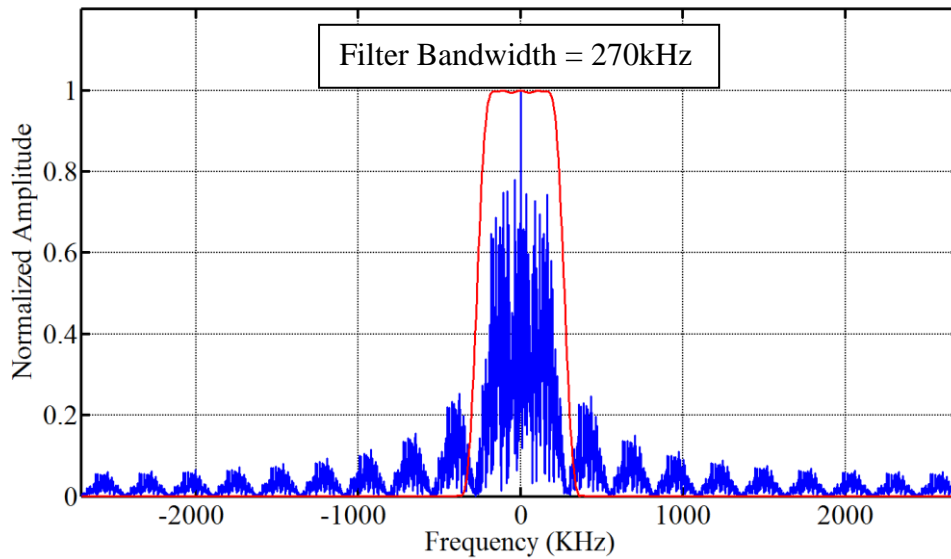


*Figure 5-24: The Signal as Switching Frequency at 135.5kHz*

If the switching frequency is 67.75kHz as in Figure 5-25, the BER increases further to 51%.

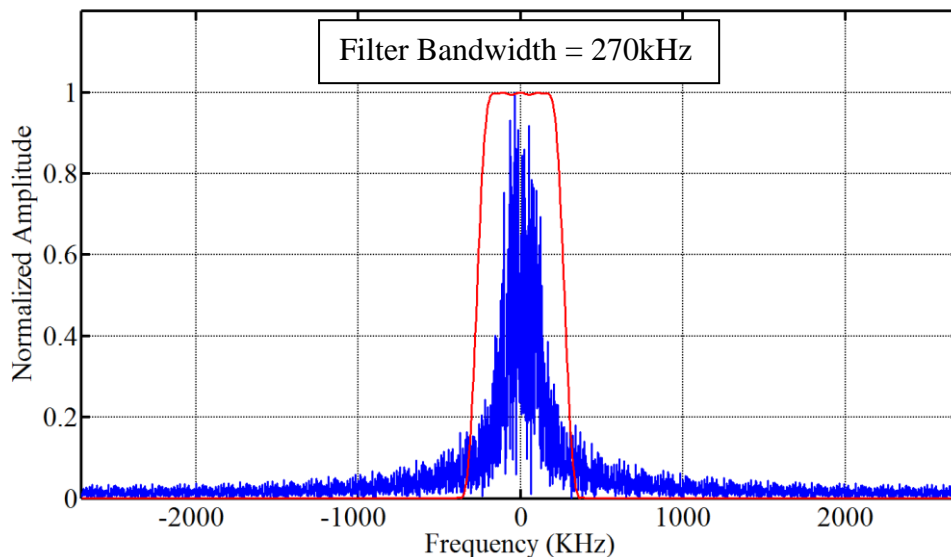


*Figure 5-25: The Signal as Switching Frequency at 67.75kHz*

Comparing the results of ‘interleaving on’ and ‘interleaving off’ on the frequency spectrum of the different switching frequency with an applied bandwidth filter of 270kHz, when the switching frequency is 271kHz, the BER is zero for both of ‘interleaving on’

and ‘interleaving off’, due to the sideband signal not being significantly distorting the ‘in band’ signal. When the switching frequencies decrease, the sideband signals are contained in the bandwidth of the receiver filter, and the signal cannot be recovered by the GSM system. Examples of this can be seen at 135.5kHz, with a BER of 42% for the ‘interleaving on’ case and a BER of 49% for the ‘interleaving off’ case. When the switching frequencies are 67.75kHz, the BER is 44.6% for the ‘interleaving on’ case and the BER is 51% for the ‘interleaving off’ case. So from these examples, the ‘interleaving off’ case results in a greater BER than the ‘interleaving on’ case.

### 5.5 2-D Surface Plots of BER without Interleaving

Figure 5-23 to Figure 5-25 have been shown as an example of switching with a two state FSS between phase of  $60^\circ$  and  $-60^\circ$  without interleaving to observe the effects on the frequency spectrum. The wide range of effects at different switching phases across different switching frequencies without interleaving are plotted in the 2-D surface of the BER. The x-axis is the switching frequency in kHz, the y-axis is the phase difference in degrees between two states i.e.  $\pm 60^\circ$  equals  $120^\circ$  and the z-axis is the BER which is represented as a percentage. The BER shown is the average taken from a set number of randomly generated GSM signals tested at a given frequency and phase switching sample. The 2-D surfaces of BER are plotted in Figure 5-26 to Figure 5-29 which are simulated in MATLAB using 100 random seeds.

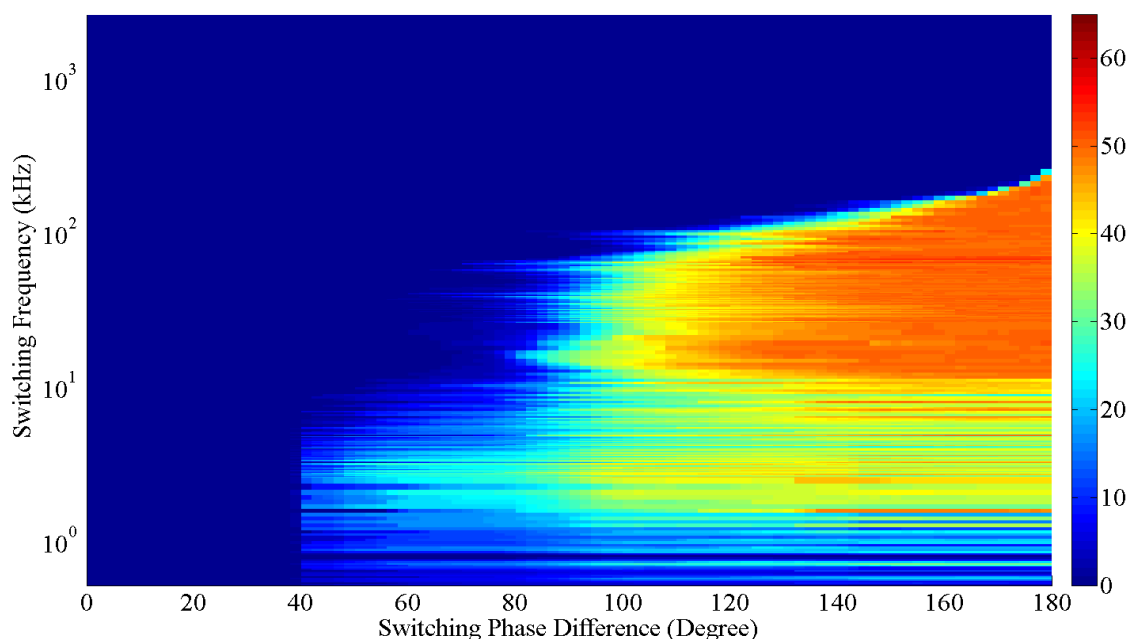


*Figure 5-26: BER (%) using Bandwidth Filter of 135kHz without Interleaving*

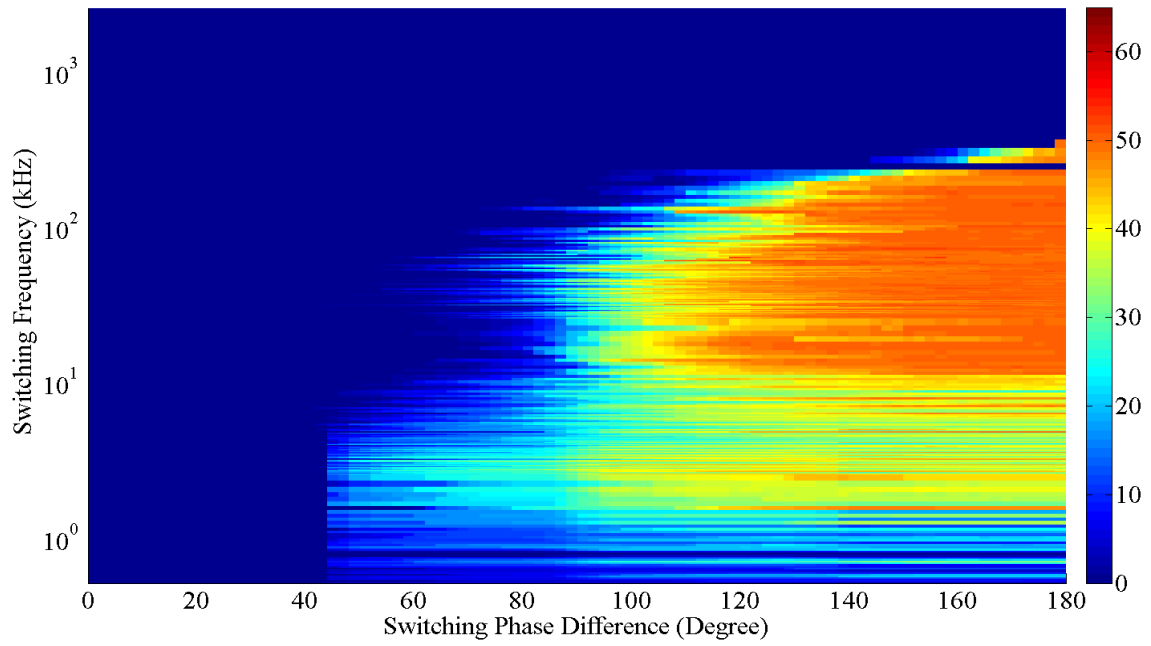


**Figure 5-27: BER (%) using Bandwidth Filter of 270kHz without Interleaving**

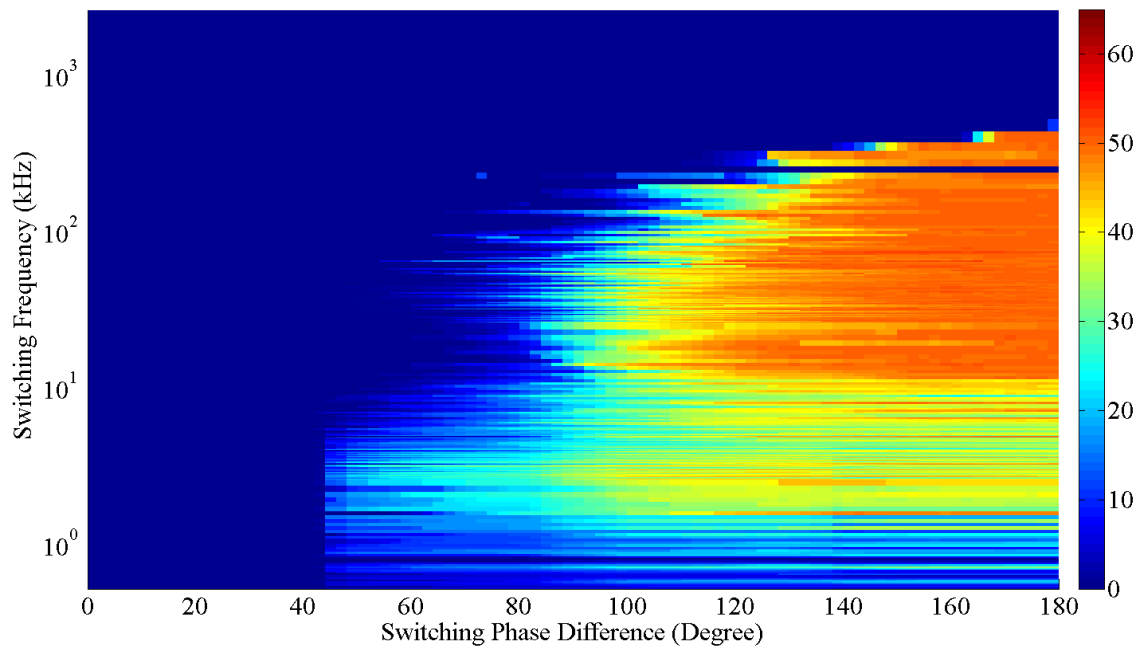


**Figure 5-28: BER (%) using Bandwidth Filter of 405kHz without Interleaving**

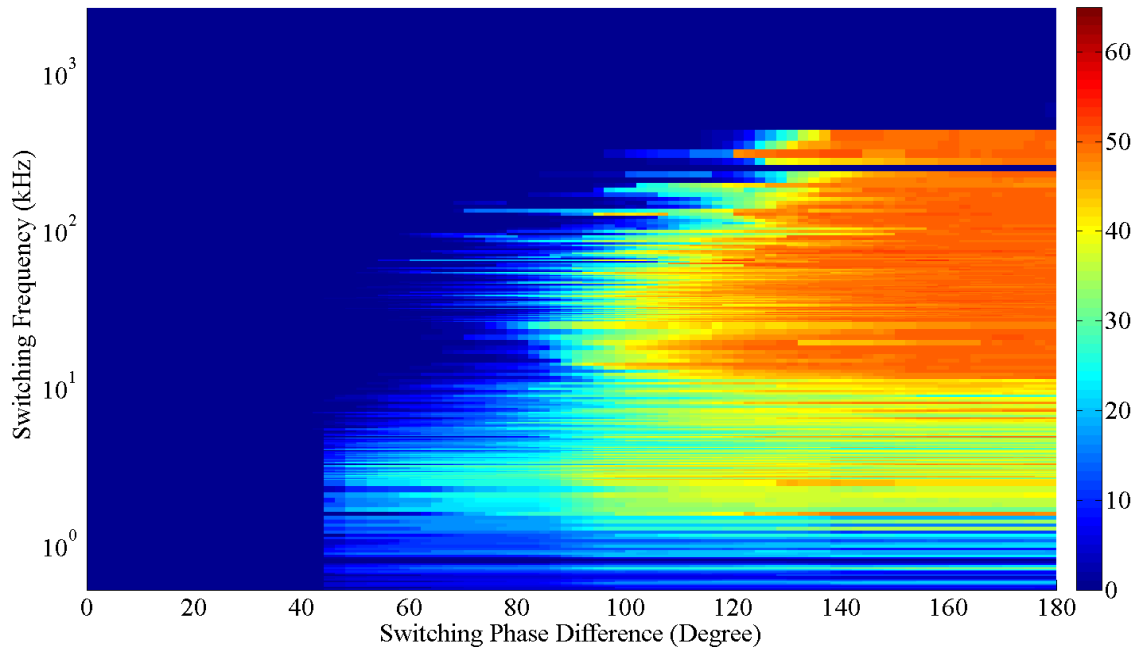


*Figure 5-29: BER (%) using Bandwidth Filter of 540kHz without Interleaving*

When comparing the ‘on’ and ‘off’ modes of interleaving the outer perimeter trend of the BER plot appears to be same as shown in Table 5-1 . When the sending signal is interleaved, the receiver operates more effectively after decoding for recovery, which is observed with the BER being lower at small phase shifts and at slower switching frequencies.

| Bandwidth of Receiver Filter | With Interleaving |                |                 | Without Interleaving |                |                 |
|------------------------------|-------------------|----------------|-----------------|----------------------|----------------|-----------------|
|                              | $F_{min}(kHz)$    | $F_{Max}(kHz)$ | $\Phi$ (Degree) | $F_{min}(kHz)$       | $F_{Max}(kHz)$ | $\Phi$ (Degree) |
| <b>135kHz</b>                | 0.85              | 300.9          | 36              | 0.85                 | 300.9          | 36              |
| <b>270kHz</b>                | 0.85              | 451.4          | 40              | 0.85                 | 451.4          | 40              |
| <b>405kHz</b>                | 0.85              | 541.7          | 40              | 0.85                 | 541.7          | 40              |
| <b>540kHz</b>                | 0.85              | 677.1          | 40              | 0.85                 | 677.1          | 40              |

*Table 5-1: Comparison of the 'on' and 'off' Mode of Interleaving*

## 5.6 Summary

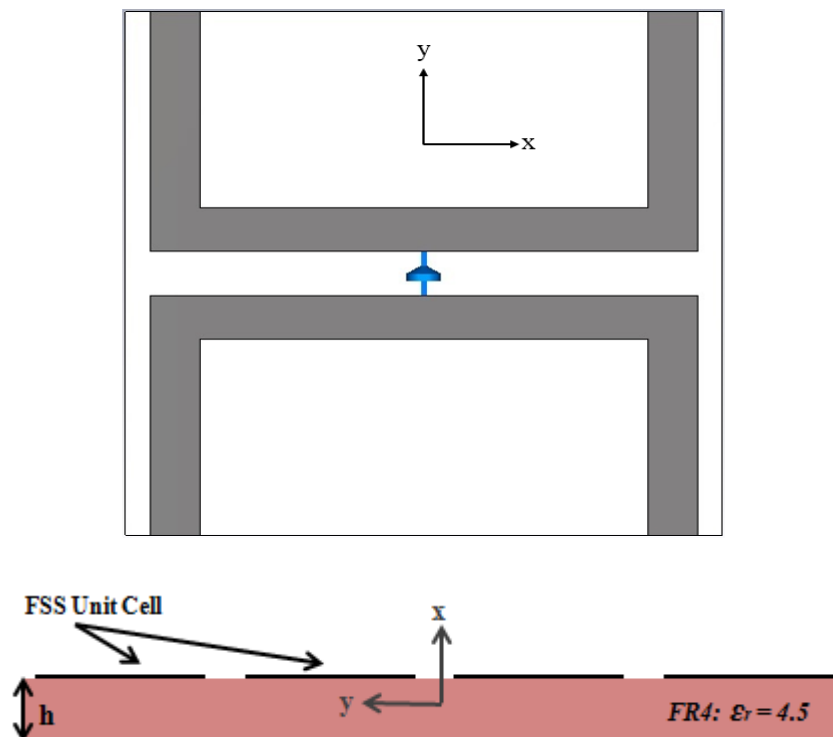
This chapter follows on from the GSM systems explained in Chapter 4, where phase switching can be achieved by using a reconfigurable switched FSS over the GSM channel. The maximum switching frequency of the FSS is 2.71MHz. The frequency spectrum of the switched GSM channel would represent the phase switching technique that shifts the energy at the carrier frequency to the sidebands. Observations are concluded on how the overall BER is affected by using different bandwidths of the receiver filter as well as variation of the switched frequencies between the phase states. Simulation results from MATLAB showed when the switching frequency decreases, the BER would be increased. 2-D surface plots varying the switching frequency and transmission phase have also been given, with the switching frequency of signal impairment starting from a lower boundary at 1kHz and upper boundary which would depend on the bandwidth of the receiver filter. This was seen when the bandwidth of the filter was increased, the upper boundary also increased up to the point at which higher frequencies irrelevant to the recovery of a GSM transmitted signal.

# CHAPTER 6 SYSTEM MEASUREMENT TO TEST SWITCHING FSS WITH GSM SIGNALS

In this chapter, the design and test of two reconfigurable switching FSS panels are discussed, with the measurement setups being introduced as well. Finally, 2-D surface plots of the BER results for the measurements are shown.

## 6.1 Reconfigurable Single Polarization FSS Unit Cell Design

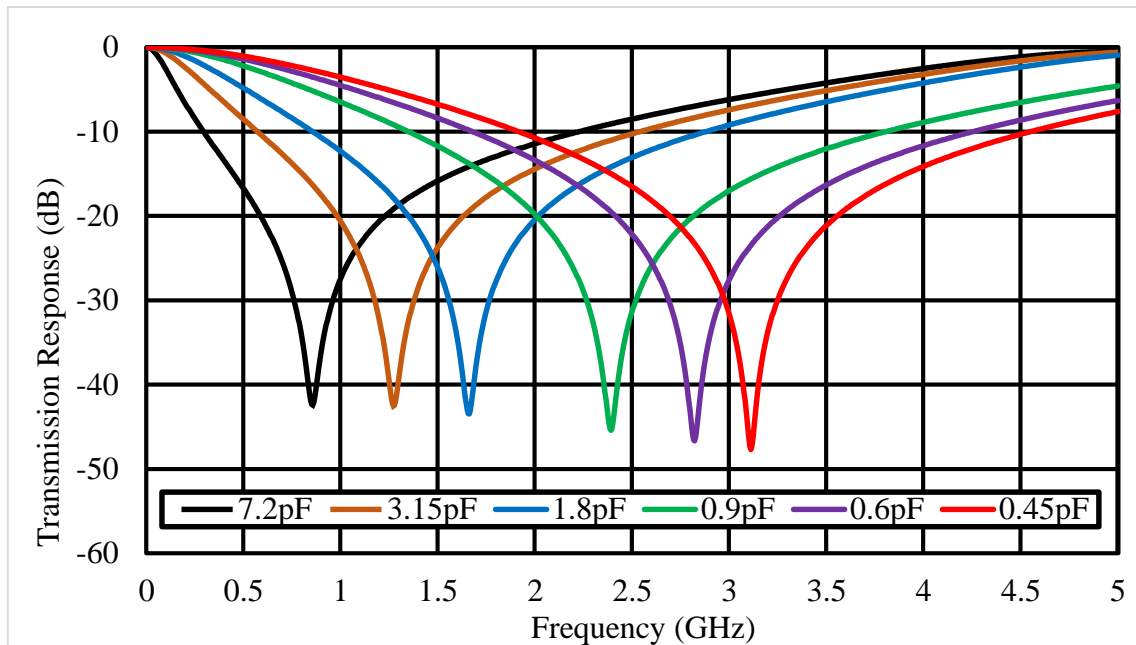
Reconfigurable single polarization FSS unit cell design and simulations were carried out using CST microwave studio as illustrated in Figure 6-1. Square loop has been employed as a band-stop filter, with the periodicity of the unit cell being 12mm; the width of the loop being 1mm and the gaps between unit cells being 1mm. The loop is fabricated on 1.6mm FR4 dielectric ( $\epsilon_r = 4.5$ ,  $\tan\delta = 0.01$ ) substrate with the gap between each unit cell being linked by a BB857 silicon tuning diode (Appendix V), used as a tuning element with its capacitance change being controlled from 0.45pF to 7.2pF.



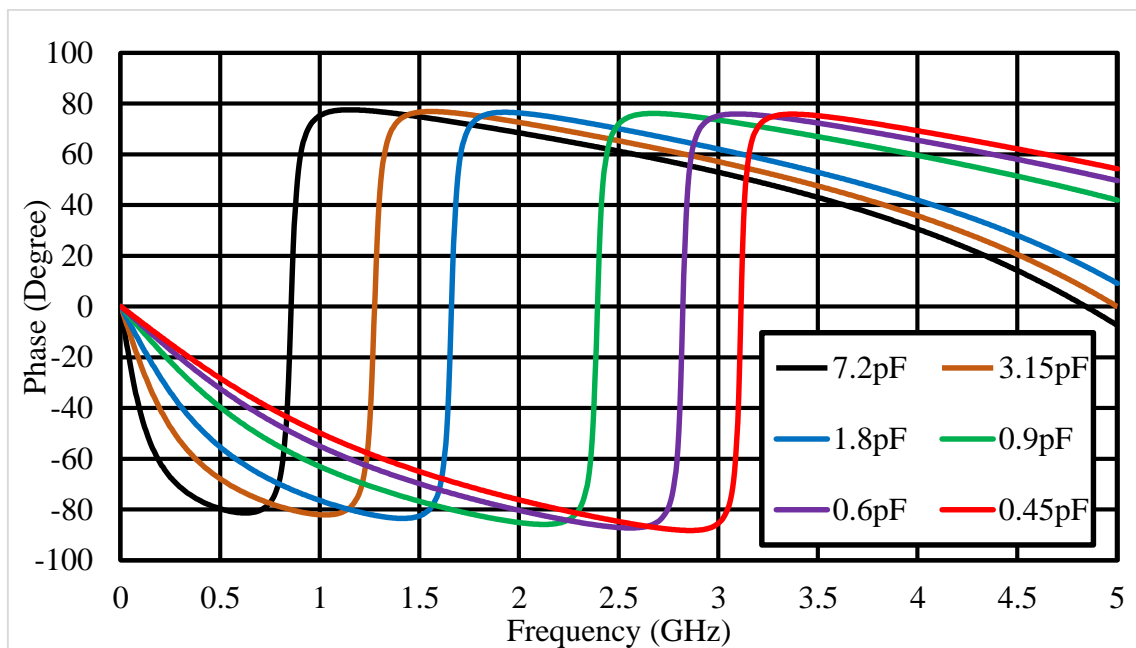
Substrate: FR4, Thickness ( $h$ ): 1.6mm

Figure 6-1: Front and Side View of the Reconfigurable Signal Polarization FSS Unit Cell

From Figure 6-2 and Figure 6-3, the reconfigurable FSS can be seen to sweep the frequency response from 0.9GHz to 3.1GHz by varying the capacitance which could cover the 2G and 3G mobile phone signal frequency range. Additionally, from the data sheet (Appendix V) for the tuning diode, when the voltage increases, the capacitance is reduced. Therefore for the operation of the transmission response, the desired resonant frequency of the band-stop filter increases as the voltage is increased across the diode.



*Figure 6-2: Transmission Response for Reconfigurable Signal Polarization FSS Unit Cell*



*Figure 6-3: Phase Response for Reconfigurable Signal Polarization FSS Unit Cell*

For this section the focus will be on the 2G GSM protocol at 1.8GHz. To achieve this the capacitance of the diode has been swept in CST to find the optimum attenuation at the resonance frequency of 1.8GHz. After sweeping, the capacitance is found to be 1.5pF at the resonance frequency with the attenuation being 43.8dB which is shown in Figure 6-4. The phase response can also be seen in Figure 6-5, with the positive phase response being  $76^\circ$  and  $-84^\circ$ , giving an overall phase difference of  $160^\circ$ . Figure 6-6 shows the single polarization reconfigurable FSS only influencing GSM signals around the tuned selective frequency of 1.8GHz. i.e when the voltage is varied between two states the capacitance change causes a difference in phase of  $160^\circ$  around 1.8GHz. However in the Tetra band range (400MHz), the phase difference is very small being only  $13^\circ$ , which is not enough to produce a significant BER.

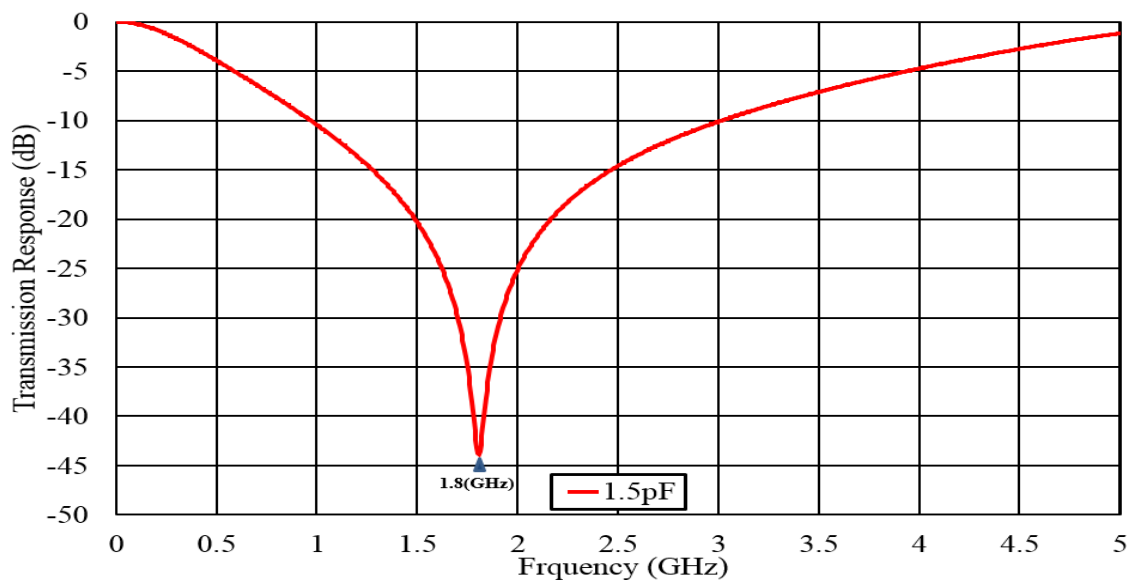


*Figure 6-4: Transmission Response of FSS Unit Cell Tuned at 1.8GHz*

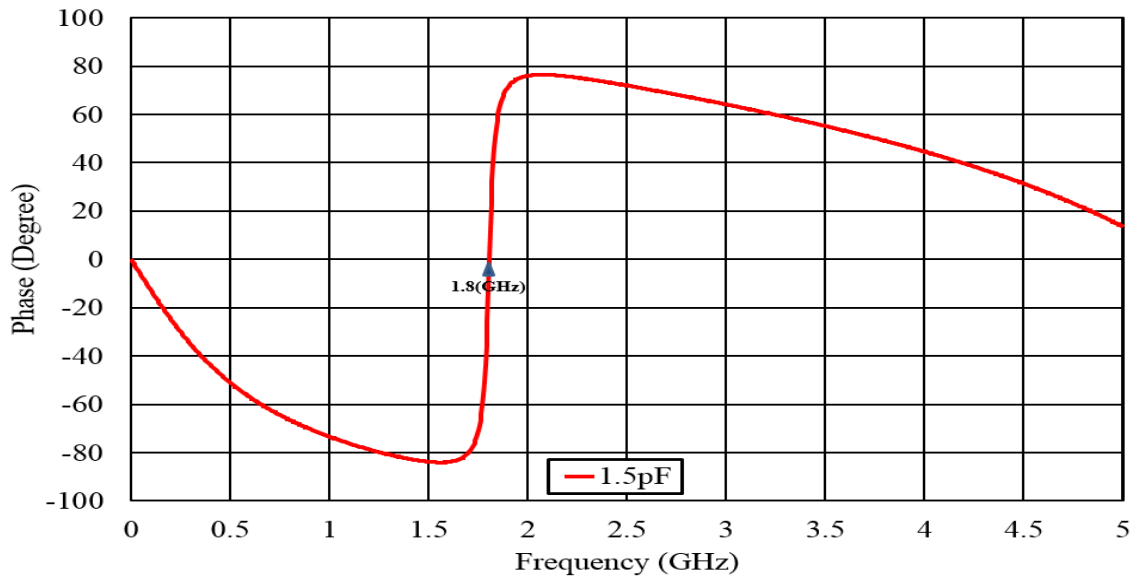


Figure 6-5: Phase Response of FSS Unit Cell Tuned at 1.8GHz

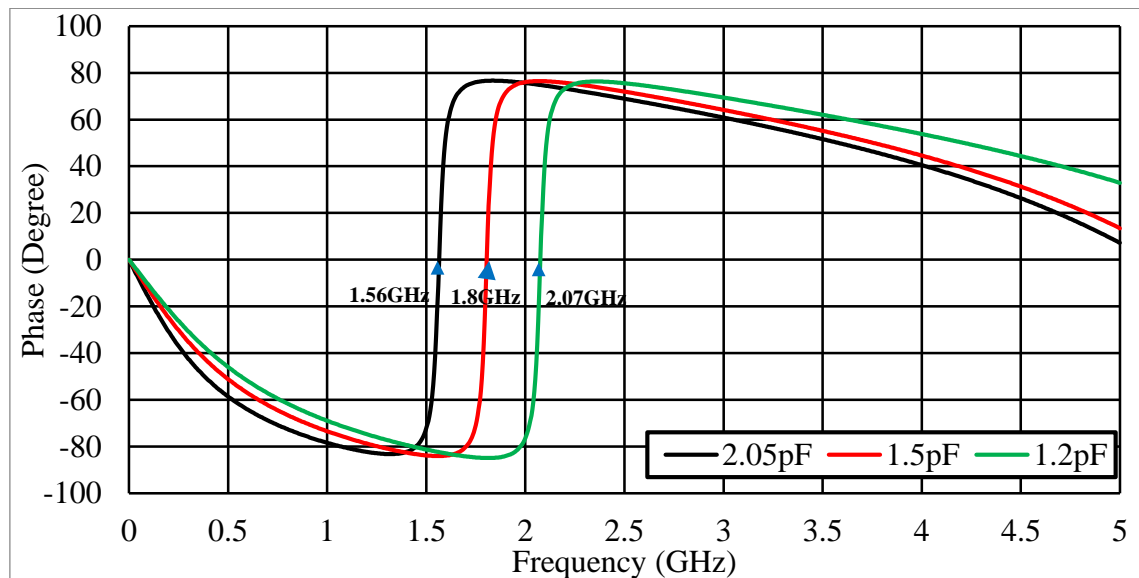
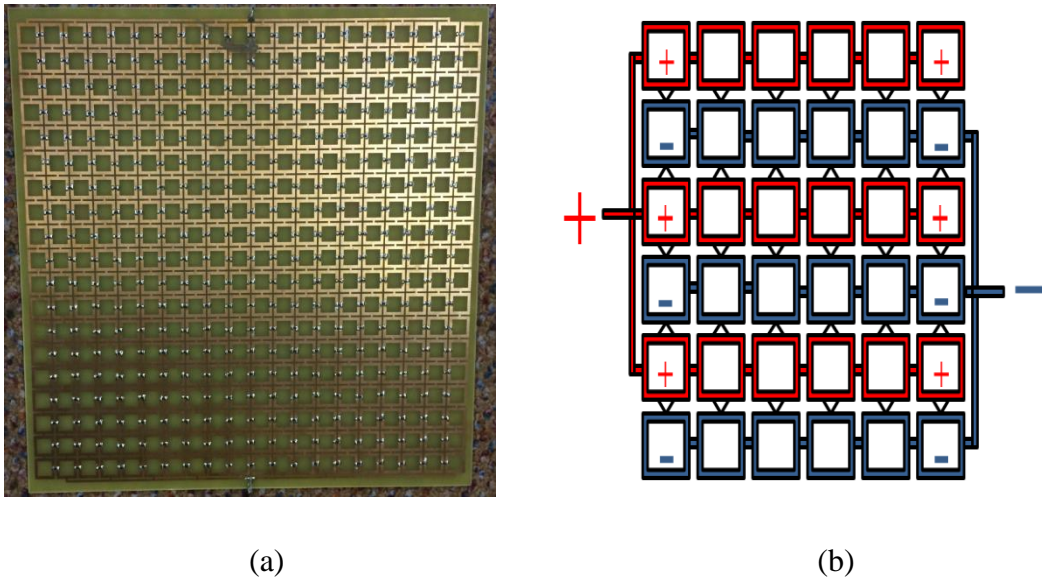


Figure 6-6: Phase Response of FSS Unit Cell at varying Capacitances

## 6.2 Reconfigurable Single Polarization FSS Panel Design

The single-polarized reconfigurable FSS panel has been manufactured into a prototype FSS shown in Figure 6-7 (a). The size of board is 24.5cm x 24.2cm, comprising of 20x19 individual unit cells linked by 380 variable capacitance diodes (BB857) soldered onto the PCB board. The surrounding traces are to be utilised for the power terminals. A simplified version of the FSS panel structure can also be seen graphically in Figure 6-7 (b), where all red coloured unit cells connect to the positive terminal of power supply, and the blue coloured unit cells connect to the negative terminal of power supply.



*Figure 6-7: Reconfigurable Single Polarization FSS Panel*

### 6.3 Reconfigurable Single Polarization FSS System Measurement

Measurements will be carried out to validate the simulation results. The setup of the measurement is shown in Figure 6-8. The transmission properties were characterized using a free-space measurement technique, consisting of two wideband horn antennas connected to an HP8720 vector network analyser. The transmit antenna was mounted above and the FSS, at a distance of approximately 60cm from the FSS. The FSS was placed on the centre of the metal plate which has an aperture to fit the FSS in. The FSS and metal plate were placed on a low permittivity foam spacer. The receive antenna was mounted 60cm below the FSS. This provides RF illumination close to normal incidence.

The system was calibrated by measuring the transmitted power over frequency range when the FSS was not present, by doing this, diffraction which is measured from the edges of the finite metal sheet are included in the calibration when the FSS was in plate, by varying the voltage across the varactor diodes the amplitude and phase of the transmission coefficient can be altered as the resonant frequency of the FSS is tuned.

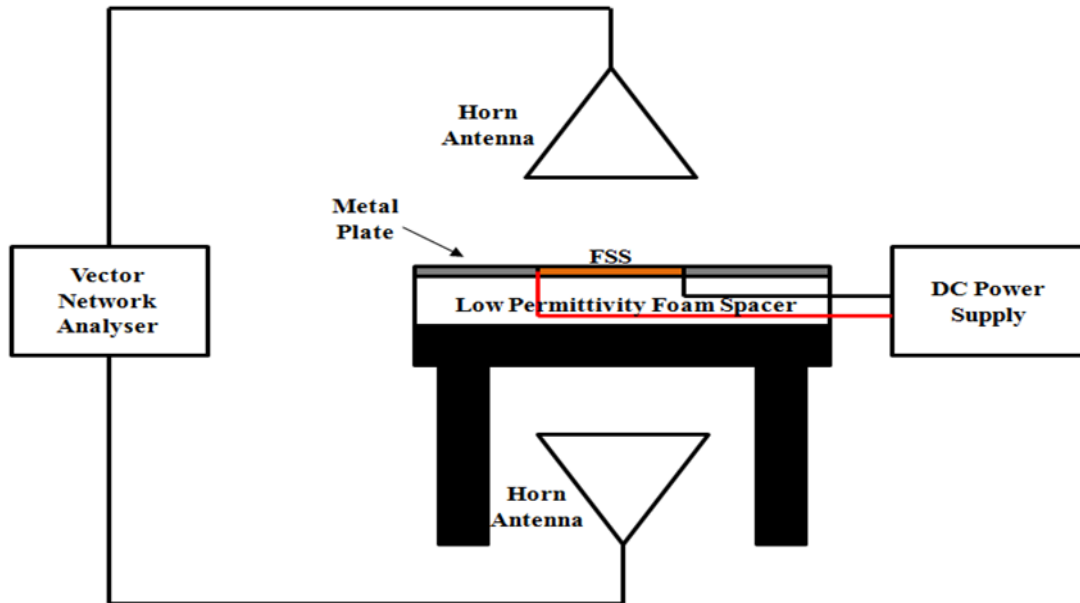


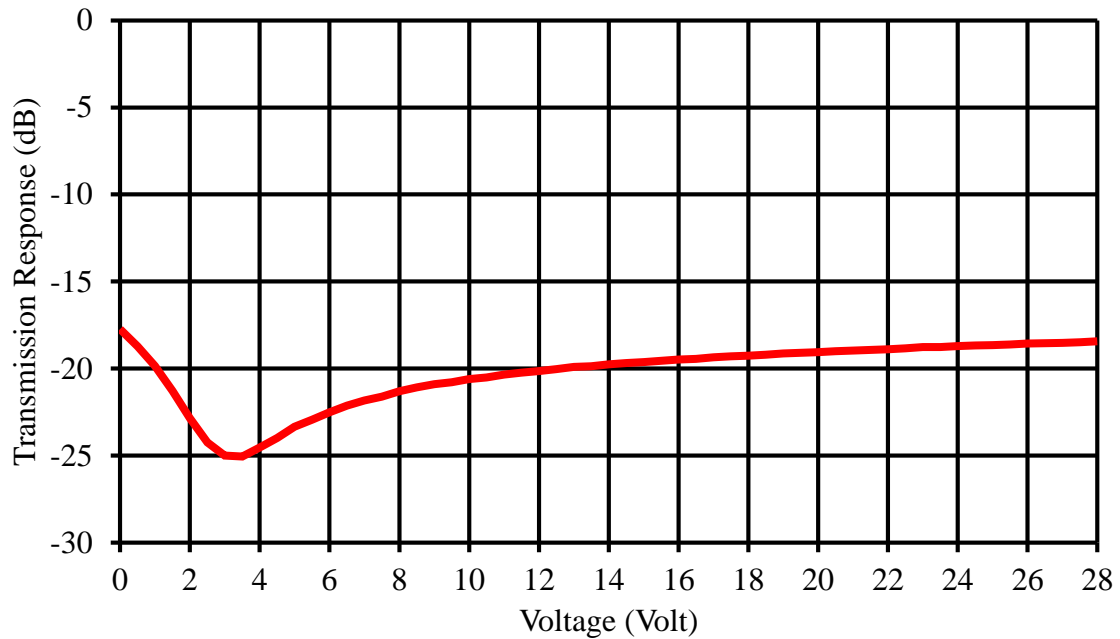
Figure 6-8: Measurement Set Up for Reconfigurable FSS Panel

The data for transmission and phase response are shown in Table 6-1.

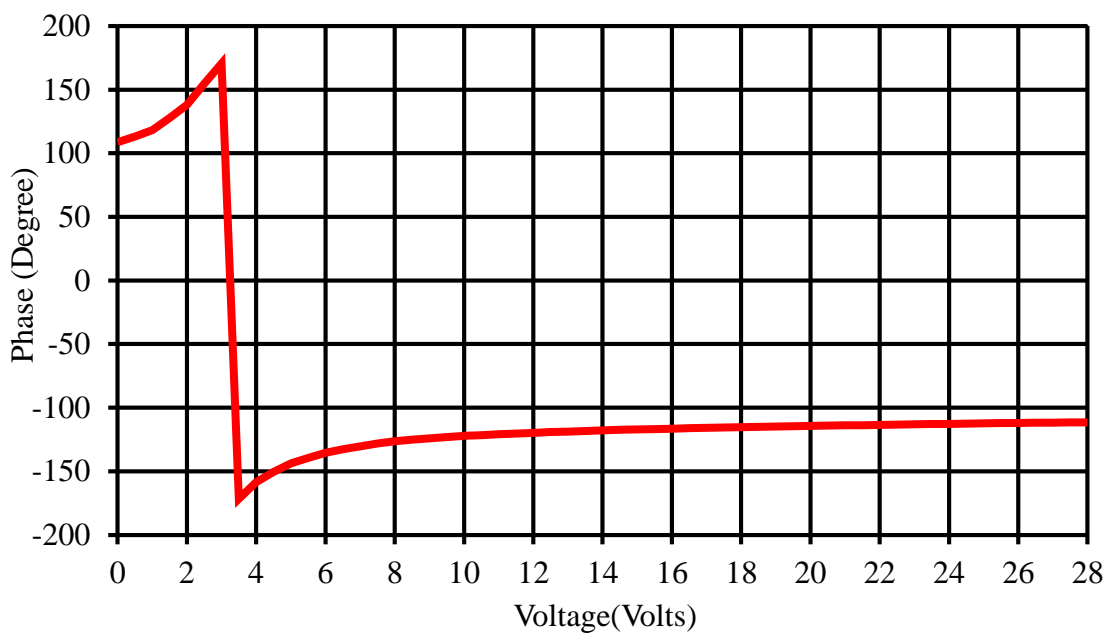
| Voltage (V) | Transmission Response (dB) | Phase (Degree) | Voltage (V) | Transmission Response (dB) | Phase (Degree) | Voltage (V) | Transmission Response (dB) | Phase (Degree) |
|-------------|----------------------------|----------------|-------------|----------------------------|----------------|-------------|----------------------------|----------------|
| 0           | -17                        | 108            | 9.5         | -20                        | -123           | 19          | -19                        | -114           |
| 0.5         | -18                        | 113            | 10          | -20                        | -122           | 19.5        | -19                        | -114           |
| 1           | -19                        | 118            | 10.5        | -20                        | -121           | 20.0        | -19                        | -114           |
| 1.5         | -21                        | 127            | 11          | -20                        | -120           | 20.5        | -19                        | -114           |
| 2           | -22                        | 138            | 11.5        | -20                        | -120           | 21          | -18                        | -113           |
| 2.5         | -24                        | 154            | 12          | -20                        | -119           | 21.5        | -18                        | -113           |
| 3           | -24                        | 170            | 12.5        | -20                        | -119           | 22          | -18                        | -113           |
| 3.5         | -25                        | -171           | 13          | -19                        | -118           | 22.5        | -18                        | -113           |
| 4           | -24                        | -158           | 13.5        | -19                        | -118           | 23          | -18                        | -113           |
| 4.5         | -23                        | -150           | 14          | -19                        | -117           | 23.5        | -18                        | -112           |
| 5           | -23                        | -143           | 14.5        | -19                        | -117           | 24          | -18                        | -112           |
| 5.5         | -22                        | -139           | 15          | -19                        | -116           | 24.5        | -18                        | -112           |
| 6           | -22                        | -135           | 15.5        | -19                        | -116           | 25          | -18                        | -112           |
| 6.5         | -22                        | -132           | 16          | -19                        | -116           | 25.5        | -18                        | -112           |
| 7           | -21                        | -130           | 16.5        | -19                        | -116           | 26          | -18                        | -111           |
| 7.5         | -21                        | -128           | 17          | -19                        | -115           | 26.5        | -18                        | -111           |
| 8           | -21                        | -126           | 17.5        | -19                        | -115           | 27          | -18                        | -111           |
| 8.5         | -21                        | -125           | 18          | -19                        | -115           | 27.5        | -18                        | -111           |
| 9           | -20                        | -124           | 18.5        | -19                        | -115           | 28          | -18                        | -111           |

Table 6-1: The Transmission and Phase Response for the FSS against Voltage

In Table 6-1, the DC voltage has been varied from 0V to 28V which provided attenuation variation between 17.74 dB to 25.06 dB and a phase variation between  $+170^\circ$  to  $-171^\circ$ , where the highlighted red result indicates the phase change for the resonant frequency of 1.8GHz at 3.5V. These measurement results are clearly shown in Figure 6-9 and Figure 6-10.



*Figure 6-9: Transmission Response for Reconfigurable Single Polarization FSS Panel*



*Figure 6-10: Phase Response for Reconfigurable Single Polarization FSS Panel*

## 6.4 BER Measurement for the Reconfigurable Signal Polarization FSS Panel

The setup of the measurement is shown in Figure 6-11. To test the FSS against a GSM signal being transmitted from the antenna; the free space measurement system described above was connected to a Rohde & Schwarz SMBV 100A signal generator. The signal generator was configured to transmit a standard GSM signal at a data rate of 270.833kbits/s at a carrier frequency of 1.8GHz and power level of 0dBm. The data element of the GSM burst was a continuously repeating 11 bit pseudo random binary sequence. The receiving antenna was connected to a Rohde & Schwarz FSV vector signal analyser (VSA). The VSA has the capability to demodulate the GSM signal and compute the Bit Error Rate (BER) of the received signal. The BER is computed from prior measurement of the 11 bit pseudo random sequence when the FSS is not present i.e. the received signal has a high Signal to Noise Ratio (SNR).

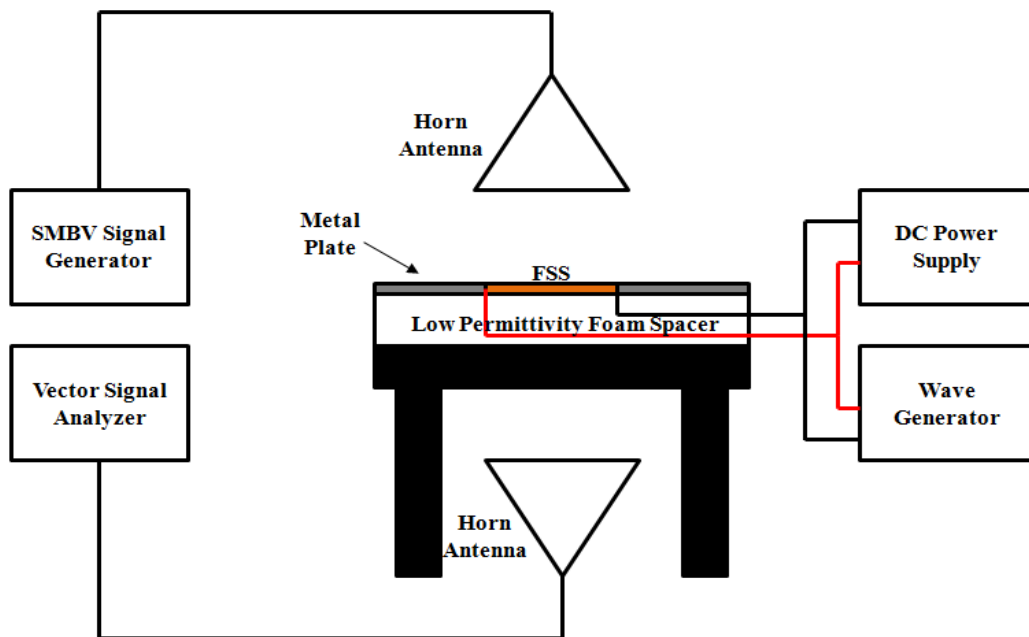
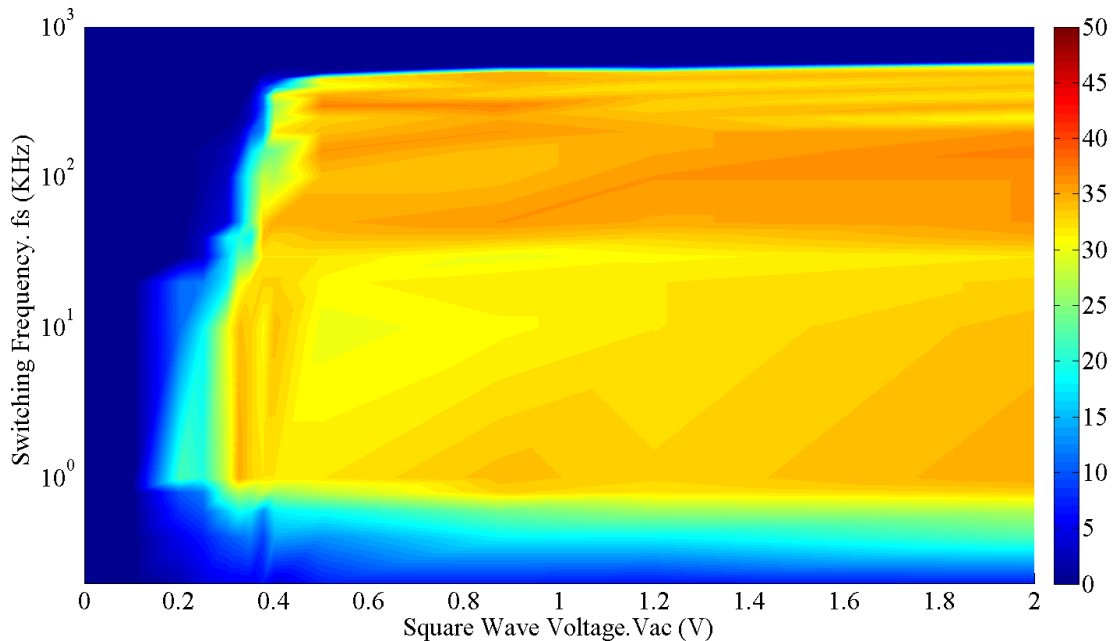


Figure 6-11: BER Measurement Set Up for Reconfigurable Single Polarization FSS Panel

To test the hypothesis of using a time varying FSS transmission response an AC signal generator was used to apply a square wave voltage with a DC voltage offset, such that the voltage applied across the varactor diode was of the form:

$$V_{varactor} = V_{dc} \pm V_{ac} \quad (6-1)$$

This was to ensure that the resonant frequency of the FSS was at 1.8GHz ( $V_{dc} = 3.5V$ ) and the square wave would provide transmission phase perturbations. BER measurements were carried out for a range of square wave switching frequencies and voltage amplitudes. Figure 6-12 shows a contour plot of the measured BER in percentage versus switching frequency and square wave voltage.



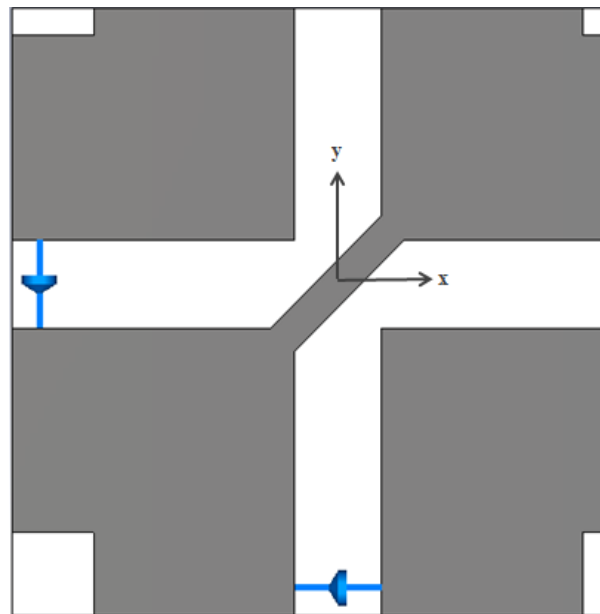
**Figure 6-12: GSM Signal BER (%) of Reconfigurable Single Polarization FSS Panel**

Figure 6-12 shows that the BER varies between 0-35% depending on the switching frequency and the applied square wave voltage. There are three particular regions of interest in Figure 6-12. The first is the low switching frequency limit, below which the BER rapidly reduces to 0%. This occurs between 700-1000Hz, depending on the amplitude of the switching waveform. Below this switching frequency the FSS will not change its phase response for all GSM bursts. The second region of interest is the high frequency limit, which is approximately 600kHz. Above this frequency the GSM signal is not impaired. The reason for this is that the received signal frequency spectrum comprises of the original baseband data plus harmonics spaced  $n \cdot f_s$  apart, where  $n$  is an odd integer in the ideal case. For high switching frequencies these harmonics are filtered out by the GSM receiver and hence only the original, attenuated, baseband message remains. This attenuated baseband signal can be easily received, assuming it is not attenuated beyond the sensitivity of the receiver. The third region of interest is the low switching voltage amplitude limit, which controls the phase change of the FSS. This

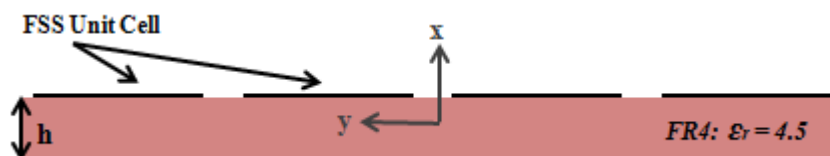
occurs between 0.3-0.5V, which equates to a phase change of approximately  $\pm 10^\circ$  to  $\pm 15^\circ$ . The solution presented demonstrates its robustness as there are large ranges of switching frequencies and voltages, which will give a high BER.

### 6.5 Reconfigurable Dual Polarization FSS Unit Cell Design

The dual polarization FSS unit cell has been designed in Figure 6-13. The square loop has been employed as a band-stop filter, with the periodicity of the unit cell being 11mm; the width of the tracks being 0.6mm and the gaps between unit cells being 1.6 mm. The loop is fabricated on 1.6mm FR4 dielectric ( $\epsilon_r = 4.5$ ,  $\tan\delta = 0.01$ ) substrate with the gap between each unit cell being linked by a BB131 VHF variable capacitance diode (Appendix VI), used as a tuning element due to its capacitance variance being controlled from 0.7pF to 1.7pF.



*Overall size:  $11 \times 11 \text{mm}^2$ , Loop thickness: 3.7mm, Line thickness: 0.6mm*



*Substrate: FR4, Thickness (h): 1.6mm*

**Figure 6-13: Front and Side View of the Reconfigurable Dual Polarization FSS Unit Cell**

To estimate the performance range for the minimum and maximum values for the tuneable capacitance that links each unit cell FSS, the transmission and phase response are simulated in CST using the frequency domain, fixing the capacitance of 0.7pF and 17pF respectively which are shown in Figure 6-14 and Figure 6-15.

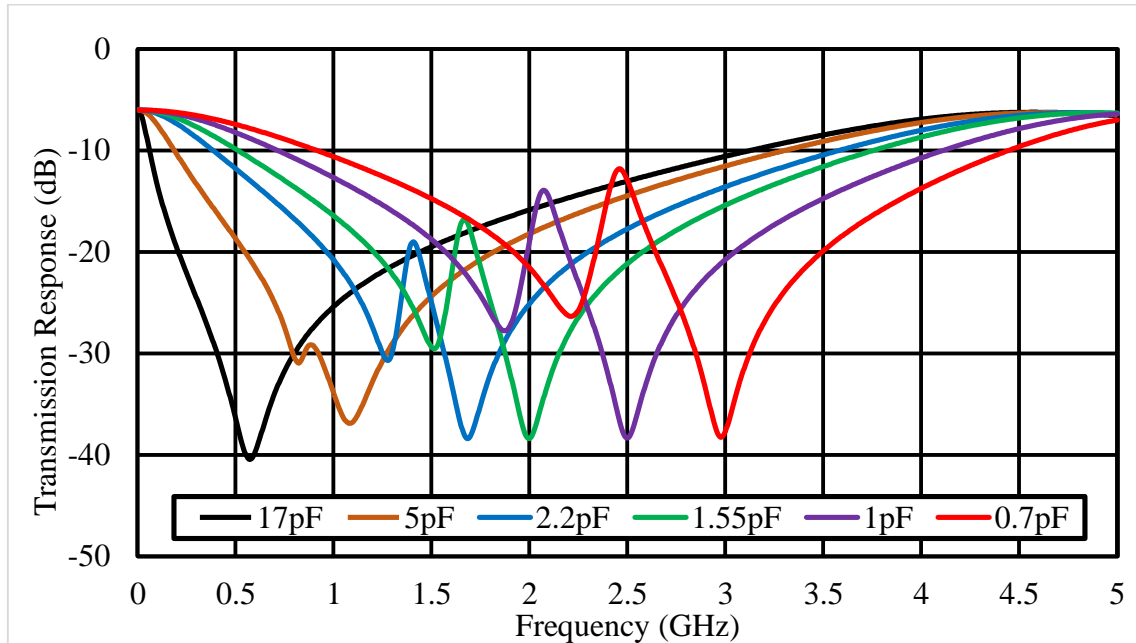


*Figure 6-14: Transmission Response for Reconfigurable Dual Polarization FSS Unit Cell*

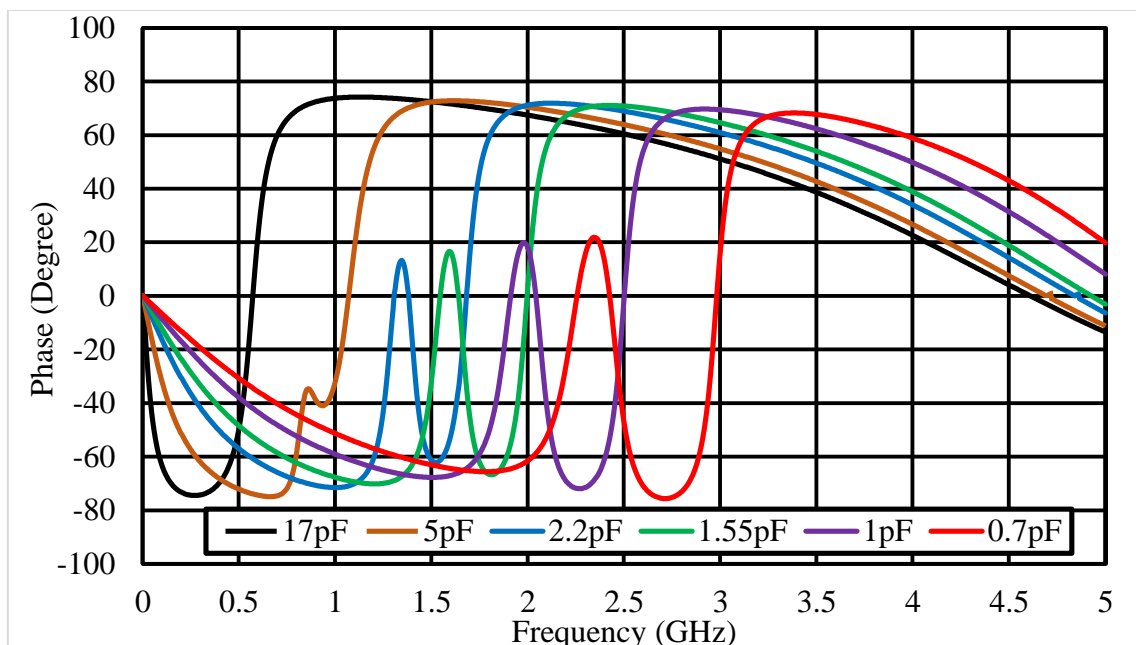


*Figure 6-15: Phase Response for Reconfigurable Dual Polarization FSS Unit Cell*

From Figure 6-14 and Figure 6-15, the reconfigurable FSS can sweep the frequency response from 0.6GHz to 2.98GHz by varying the capacitance which could cover the 2G and 3G mobile phone signal frequency range. Additionally, from the data sheet (Appendix VI) for the tuning diode, when the voltage increases, the capacitance is reduced. Therefore for the operation of the transmission response will be that the desired resonant frequency of the band-stop filter will increase as the voltage is increased across the diode.

For this research the focus will be on the 2G GSM protocol at 1.8GHz. To achieve this the capacitance of the diode has been swept in CST to find the optimum attenuation at the resonance frequency of 1.8GHz. After sweeping, the capacitance is found to be 1.92pF at the resonance frequency with the attenuation being 38.39dB which is shown in Figure 6-16. The phase response can also be seen in Figure 6-17, with the positive phase response of  $72^\circ$  and the negative phase response of  $64^\circ$ , giving an overall phase difference of  $136^\circ$ . Figure 6-18 shows the dual polarization reconfigurable FSS only influencing GSM signals around the tuned selective frequency of 1.8GHz. i.e when the voltage is varied between two states the capacitance change causes a difference in phase of  $136^\circ$  around 1.8GHz. However in the Tetra band range (400MHz), the phase difference is very small being only  $16^\circ$ , which is not enough to produce a significant BER.

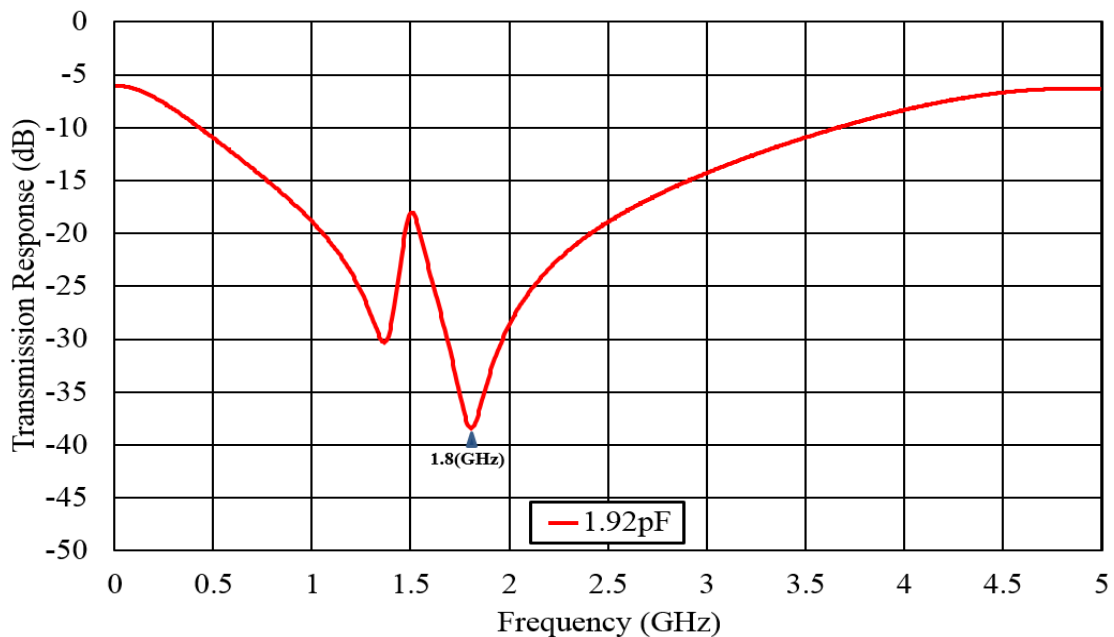


*Figure 6-16: Transmission Response of FSS Unit Cell Tuned at 1.8GHz*

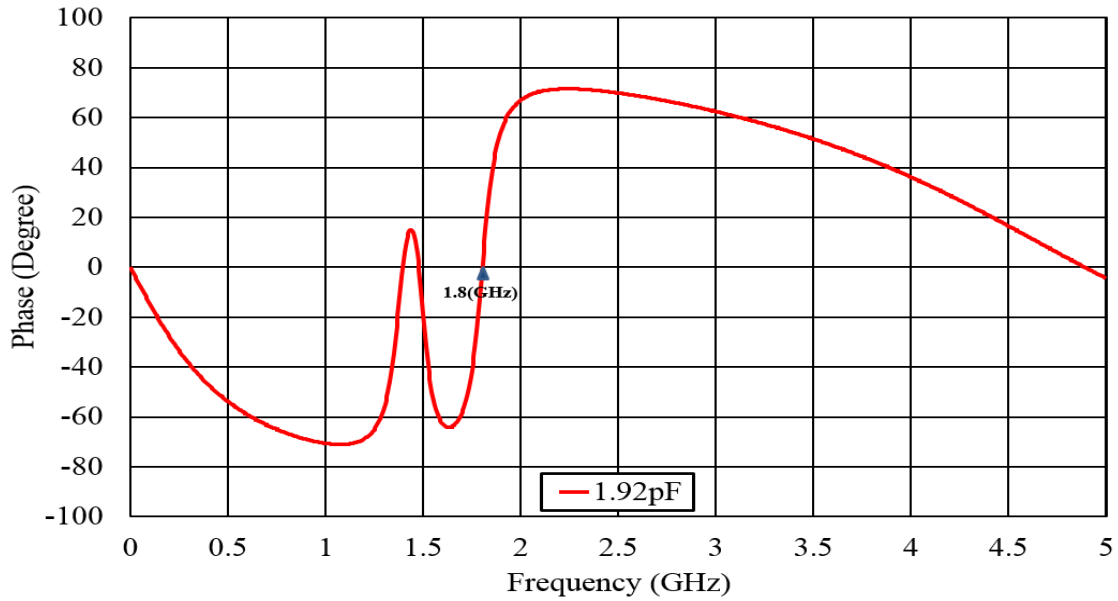


Figure 6-17: Phase Response of FSS Unit Cell Tuned at 1.8GHz

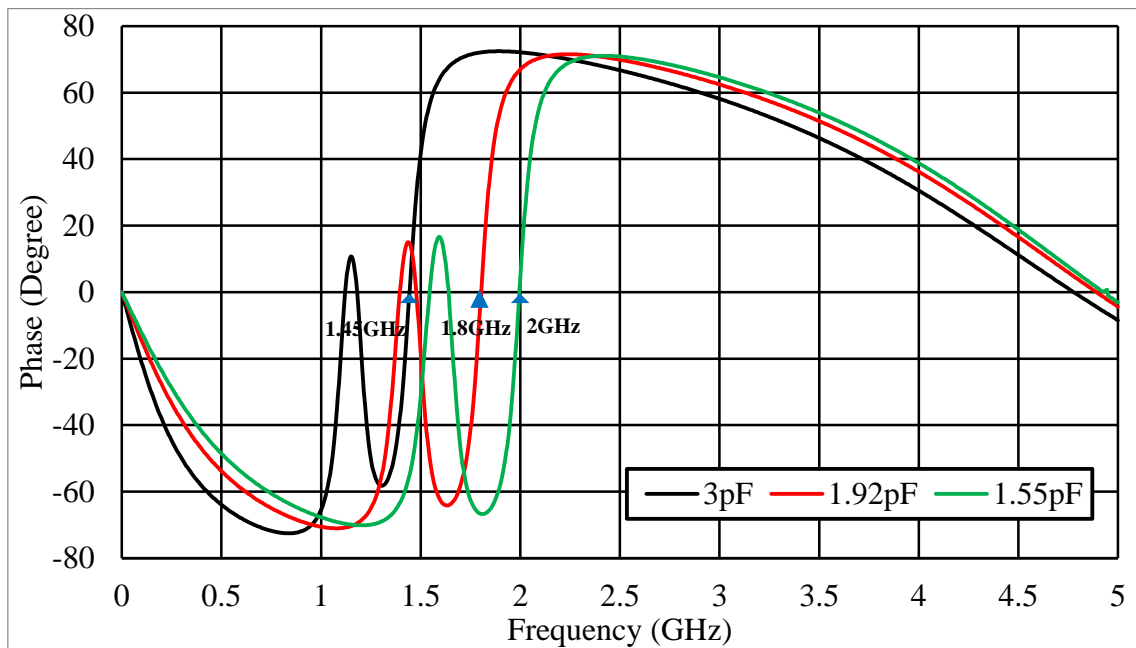
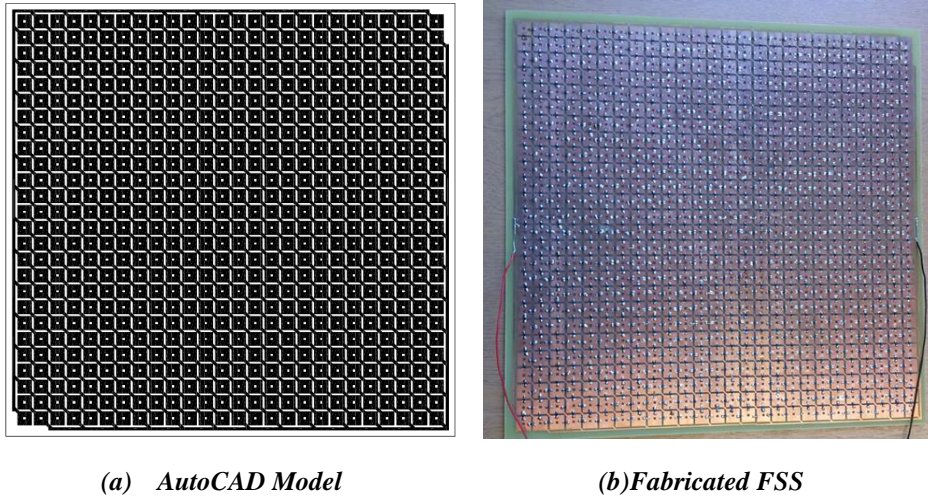


Figure 6-18: Phase Response of FSS Unit Cell at varying Capacitances

## 6.6 Reconfigurable Dual Polarization FSS Panel Design

The dual-polarized reconfigurable FSS panel has been designed in CST Microwave Studio. This can be converted into a mask using AutoCAD as illustrated in Figure 6-19 (a), which can then be manufactured into a prototype FSS shown Figure 6-19 (b). The size of board is 30cm x 30cm, comprising of 26x26 individual unit cells linked by 1300 variable capacitance diodes (BB131) soldered onto the PCB board. The surrounding traces are to be utilised for the power terminals.



**Figure 6-19: Reconfigurable Dual Polarization FSS Panel**

A simplified version of the FSS panel structure can also be seen graphically in Figure 6-20 (a), where all red coloured unit cells connect to the positive terminal of the power supply, and the blue coloured unit cells connect to the negative terminal. The odd diagonals of red unit cells contain diodes which are connected to their neighbours on the board in reverse biased operation via connections at the top edge of the PCB board. The even column of diodes on the board are also reverse biased via connections at the bottom edge of the PCB board connected to their neighbours. The individual unit cells are connected diagonally with small metallic tabs to simplify biasing, as illustrated in Figure 6-20 (b). In this configuration the FSS operates when the incident electric field is two different polarizations (parallel or perpendicular) to the diode orientation in order to demonstrate a polarization insensitivity of the FSS panel.

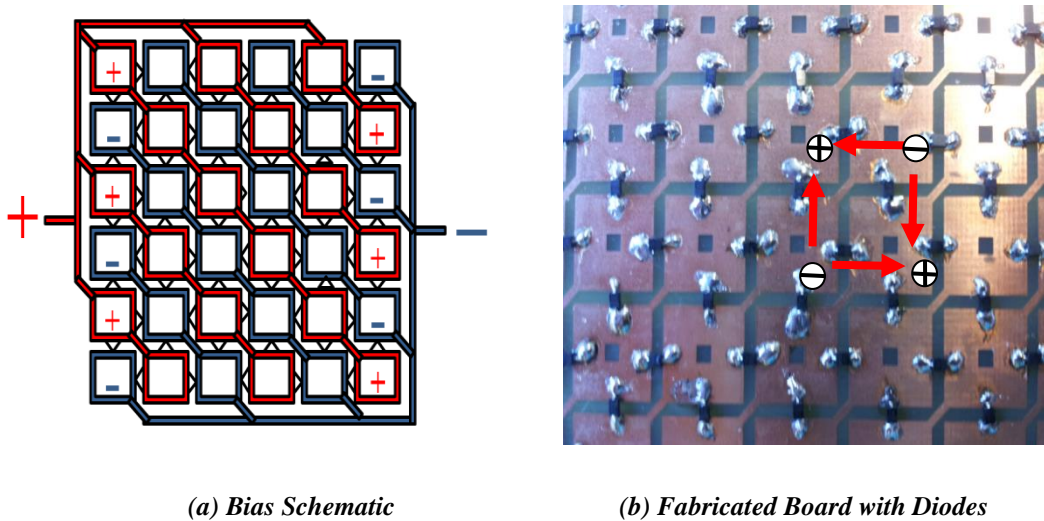


**Figure 6-20: The structure of the FSS Panel**

## 6.7 Reconfigurable Dual Polarization FSS System Measurement

The measurement for the dual polarization FSS panel is to validate its simulation results. The setup of the process is the same as the single polarization FSS panel shown in Figure 6-8. The difference is that after measuring the transmission response for one polarization, the horn antennas were kept stationary while the FSS was rotated  $90^\circ$ , where the initial position of the FSS panel was marked on the metal plate as a reference.

On the initial position of the FSS panel, the data for transmission and phase response were shown in Table 6-2.

| Voltage (V) | Transmission Response (dB) | Phase (Degree) | Voltage (V) | Transmission Response (dB) | Phase (Degree) | Voltage (V) | Transmission Response (dB) | Phase (Degree) |
|-------------|----------------------------|----------------|-------------|----------------------------|----------------|-------------|----------------------------|----------------|
| 0.5         | -21                        | 130            | 10.5        | -27                        | -105           | 20.5        | -20                        | -123           |
| 1           | -21                        | 132            | 11          | -29                        | -91            | 21          | -20                        | -120           |
| 1.5         | -21                        | 135            | 11.5        | -31                        | -79            | 21.5        | -19                        | -118           |
| 2           | -21                        | 137            | 12          | -33                        | -67            | 22          | -19                        | -116           |
| 2.5         | -21                        | 139            | 12.5        | -38                        | -52            | 22.5        | -19                        | -114           |
| 3           | -22                        | 142            | 13          | -51                        | -29            | 23          | -19                        | -113           |
| 3.5         | -22                        | 145            | 13.5        | -44                        | 136            | 23.5        | -19                        | -112           |
| 4           | -22                        | 148            | 14          | -35                        | 153            | 24          | -19                        | -110           |
| 4.5         | -22                        | 152            | 14.5        | -31                        | 163            | 24.5        | -18                        | -109           |
| 5           | -23                        | 155            | 15          | -28                        | 173            | 25          | -18                        | -108           |
| 5.5         | -23                        | 160            | 15.5        | -26                        | -176           | 25.5        | -18                        | -107           |
| 6           | -23                        | 166            | 16          | -25                        | -168           | 26          | -18                        | -106           |
| 6.5         | -23                        | 172            | 16.5        | -24                        | -161           | 26.5        | -18                        | -106           |
| 7           | -23                        | 179            | 17          | -23                        | -153           | 27          | -18                        | -105           |
| 7.5         | -24                        | -172           | 17.5        | -22                        | -148           | 27.5        | -18                        | -104           |
| 8           | -24                        | -162           | 18          | -22                        | -142           | 28          | -17                        | -103           |
| 8.5         | -24                        | -151           | 18.5        | -21                        | -137           | 28.5        | -17                        | -102           |
| 9           | -25                        | -141           | 19          | -21                        | -132           | 29          | -17                        | -102           |
| 9.5         | -25                        | -130           | 19.5        | -20                        | -129           | 29.5        | -17                        | -101           |
| 10          | -26                        | -117           | 20          | -20                        | -125           | 30          | -17                        | -101           |

*Table 6-2: The Transmission and Phase Response for the FSS against Voltage at initial position*

From Table 6-2, the DC voltage has been varied from 0.5V to 30V which provided attenuation variation between 17dB to 51dB and a phase variation between  $-172^\circ$  to  $+173^\circ$ , These measurement results are clearly shown in Figure 6-21 and Figure 6-22.

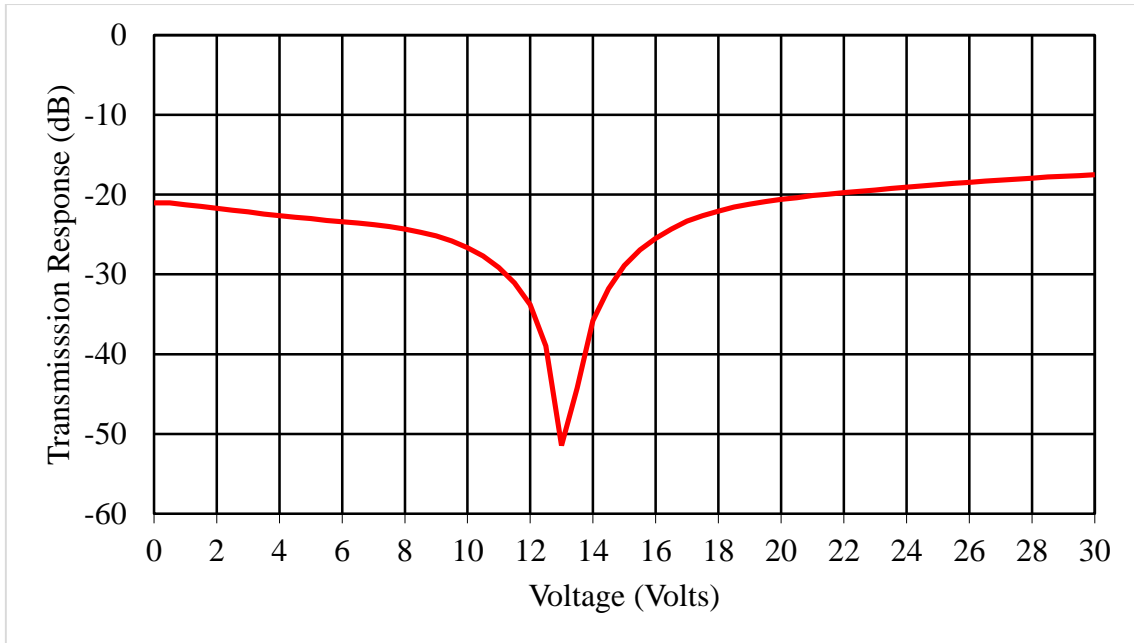


*Figure 6-21: Transmission Response for Initial Position of the FSS Panel*

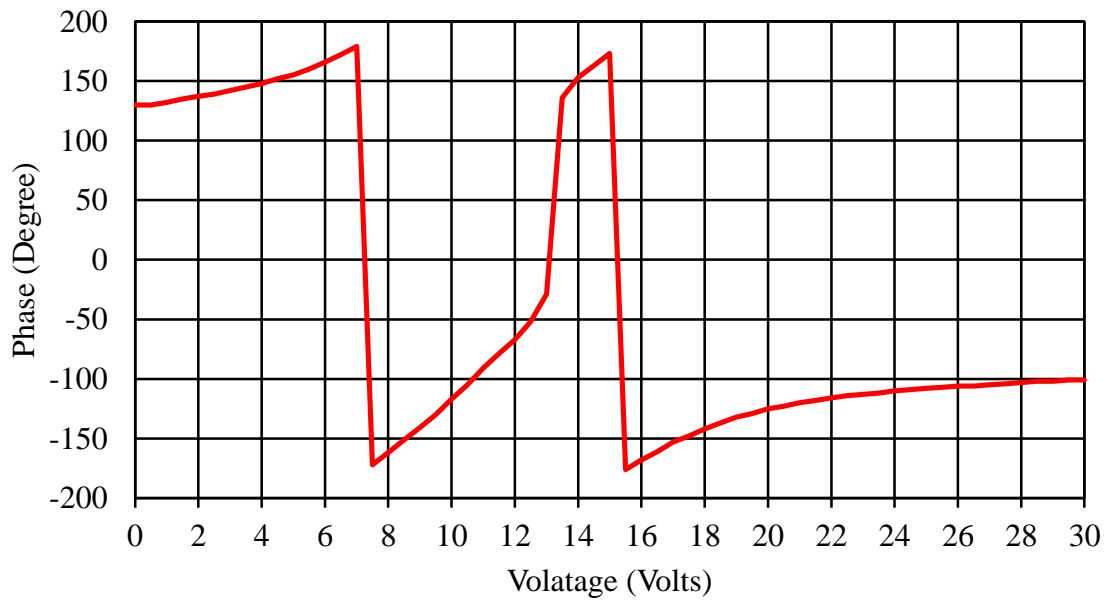


*Figure 6-22: Phase Response for Initial Position of the FSS Panel*

The Figure 6-23 and Figure 6-24 show the transmission response and phase response against frequency from 11V to 14V. From these two figures, at 1.8GHz the maximum attenuation was measured at 51.4dB and a phase variation between  $+3^\circ$  to  $-150^\circ$  at 13V.

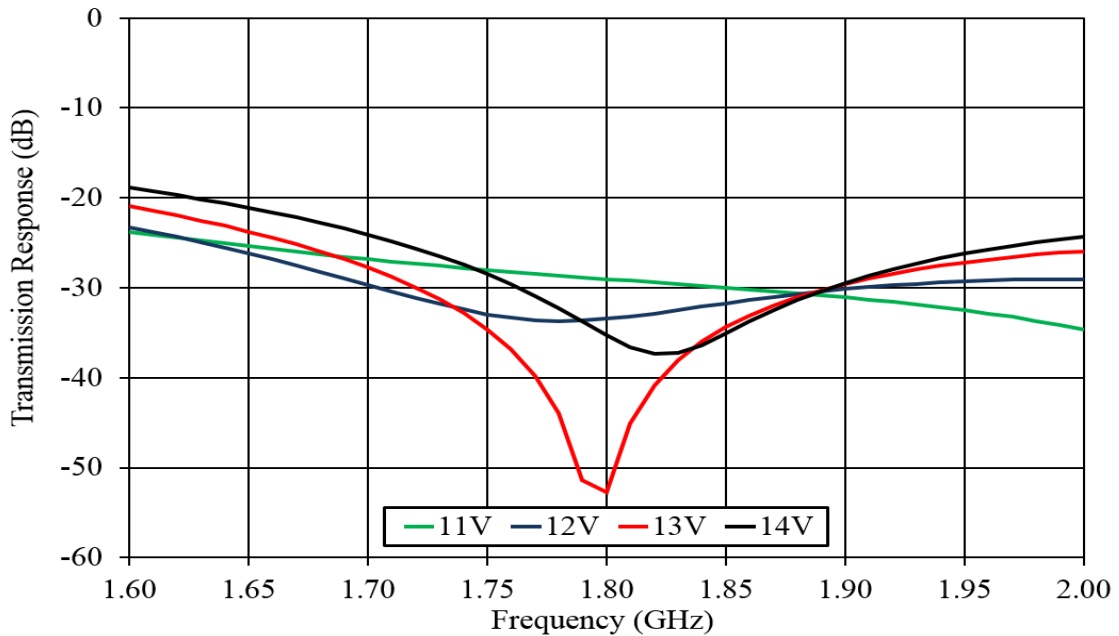


**Figure 6-23: Transmission Response against Frequencies at Initial Position of FSS Panel**

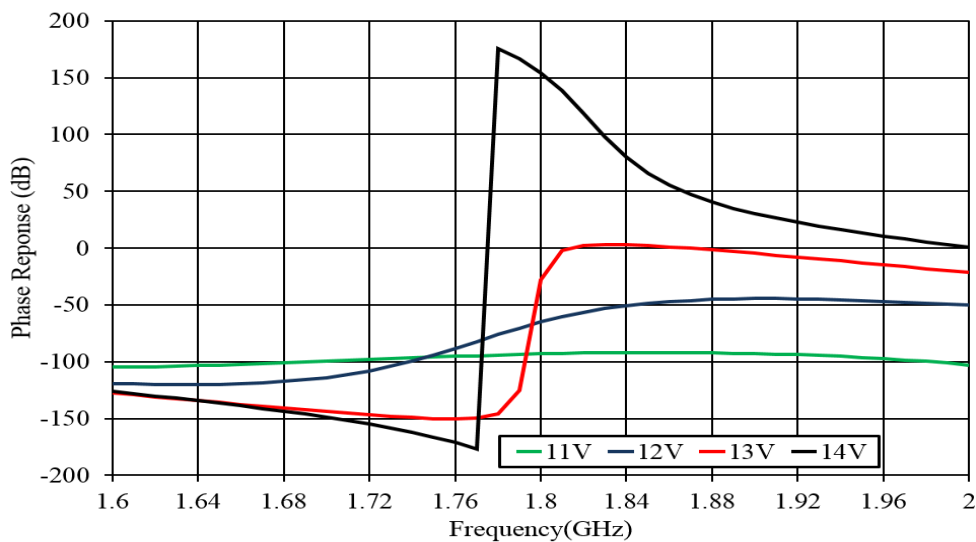


**Figure 6-24: Phase Response against Frequencies at Initial Position of FSS Panel**

After the initial position of the FSS panel has been measured, the FSS was carefully rotated  $90^\circ$ . All measurement procedures were repeated. The data for transmission and phase response are shown in Table 6-3.

| Voltage (V) | Transmission Response (dB) | Phase (Degree) | Voltage (V) | Transmission Response (dB) | Phase (Degree) | Voltage (V) | Transmission Response (dB) | Phase (Degree) |
|-------------|----------------------------|----------------|-------------|----------------------------|----------------|-------------|----------------------------|----------------|
| 0.5         | -20                        | 130            | 10.5        | -26                        | -80            | 20.5        | -20                        | -126           |
| 1           | -21                        | 133            | 11          | -26                        | -62            | 21          | -20                        | -124           |
| 1.5         | -21                        | 135            | 11.5        | -27                        | -44            | 21.5        | -20                        | -121           |
| 2           | -21                        | 138            | 12          | -28                        | -25            | 22          | -19                        | -119           |
| 2.5         | -21                        | 141            | 12.5        | -30                        | -1             | 22.5        | -19                        | -117           |
| 3           | -22                        | 143            | 13          | -31                        | 26             | 23          | -19                        | -115           |
| 3.5         | -22                        | 146            | 13.5        | -32                        | 56             | 23.5        | -19                        | -114           |
| 4           | -22                        | 150            | 14          | -31                        | 89             | 24          | -19                        | -113           |
| 4.5         | -22                        | 153            | 14.5        | -30                        | 118            | 24.5        | -18                        | -111           |
| 5           | -22                        | 158            | 15          | -28                        | 140            | 25          | -18                        | -110           |
| 5.5         | -23                        | 162            | 15.5        | -26                        | 157            | 25.5        | -18                        | -109           |
| 6           | -23                        | 169            | 16          | -25                        | 171            | 26          | -18                        | -108           |
| 6.5         | -23                        | 176            | 16.5        | -24                        | -175           | 26.5        | -18                        | -107           |
| 7           | -23                        | -174           | 17          | -23                        | -165           | 27          | -18                        | -106           |
| 7.5         | -23                        | -164           | 17.5        | -22                        | -156           | 27.5        | -18                        | -105           |
| 8           | -23                        | -151           | 18          | -22                        | -150           | 28          | -17                        | -104           |
| 8.5         | -24                        | -139           | 18.5        | -21                        | -143           | 28.5        | -17                        | -104           |
| 9           | -24                        | -128           | 19          | -21                        | -138           | 29          | -17                        | -103           |
| 9.5         | -24                        | -111           | 19.5        | -21                        | -133           | 29.5        | -17                        | -102           |
| 10          | -25                        | -97            | 20          | -20                        | -130           | 30          | -17                        | -102           |

*Table 6-3: The Transmission and Phase Response for the FSS against Voltage after rotated 90°*

In Table 6-3, the DC voltage has been varied from 0.5V to 30V which provided attenuation variation between 17 to 32dB and a phase variation between -174° to 171°. These measurement results are clearly shown in Figure 6-25 and Figure 6-26.

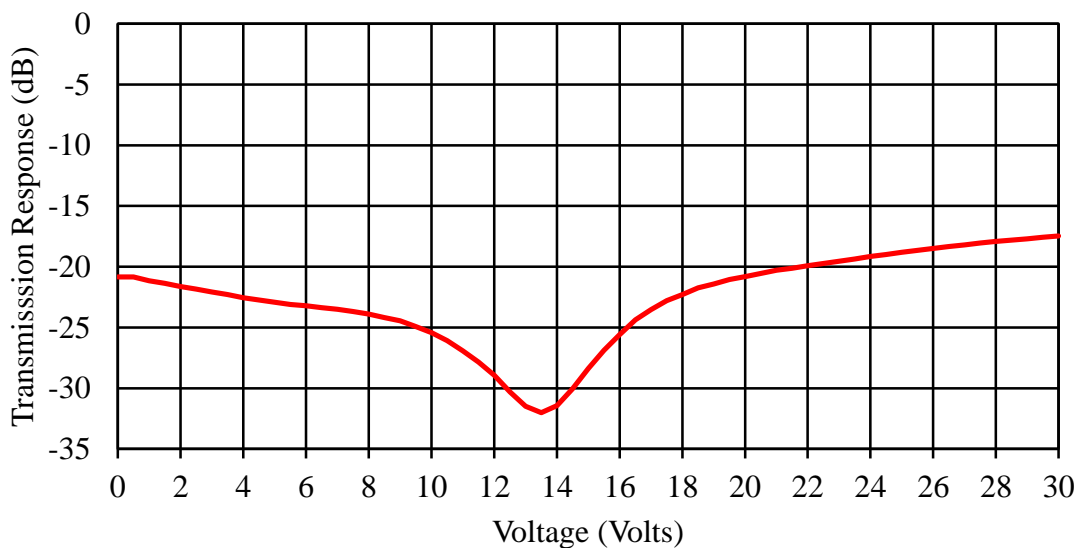


**Figure 6-25: The Transmission Response of FSS Panel Rotate 90°**

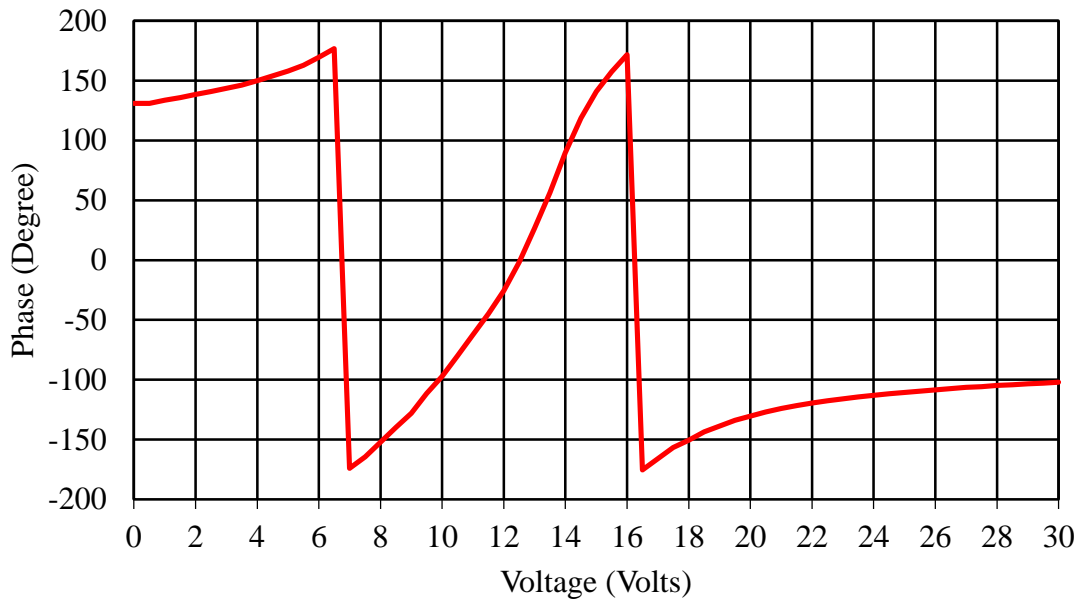


**Figure 6-26: The Phase Response of the FSS Panel Rotate 90°**

Figure 6-27 and Figure 6-28 show the transmission response and phase response against frequency from 11V to 14V. From these two figures, at 1.74GHz the maximum attenuation was measured at 43dB and a phase variation between +38° to +174° at 13V.

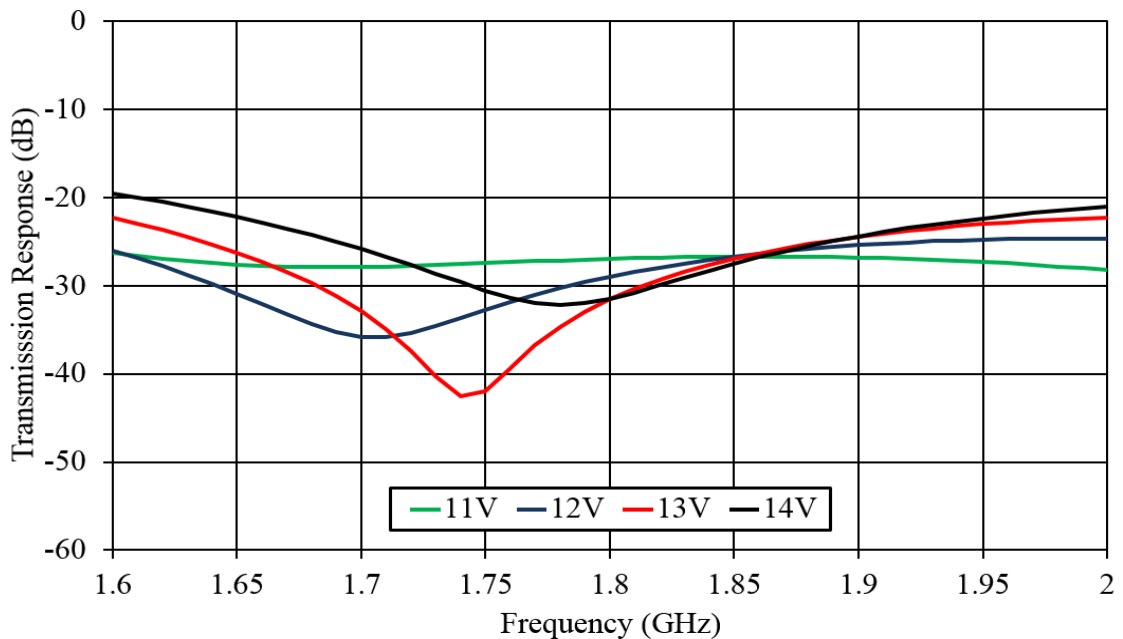


**Figure 6-27: Transmission Response against Frequencies after FSS Panel Rotated 90°**

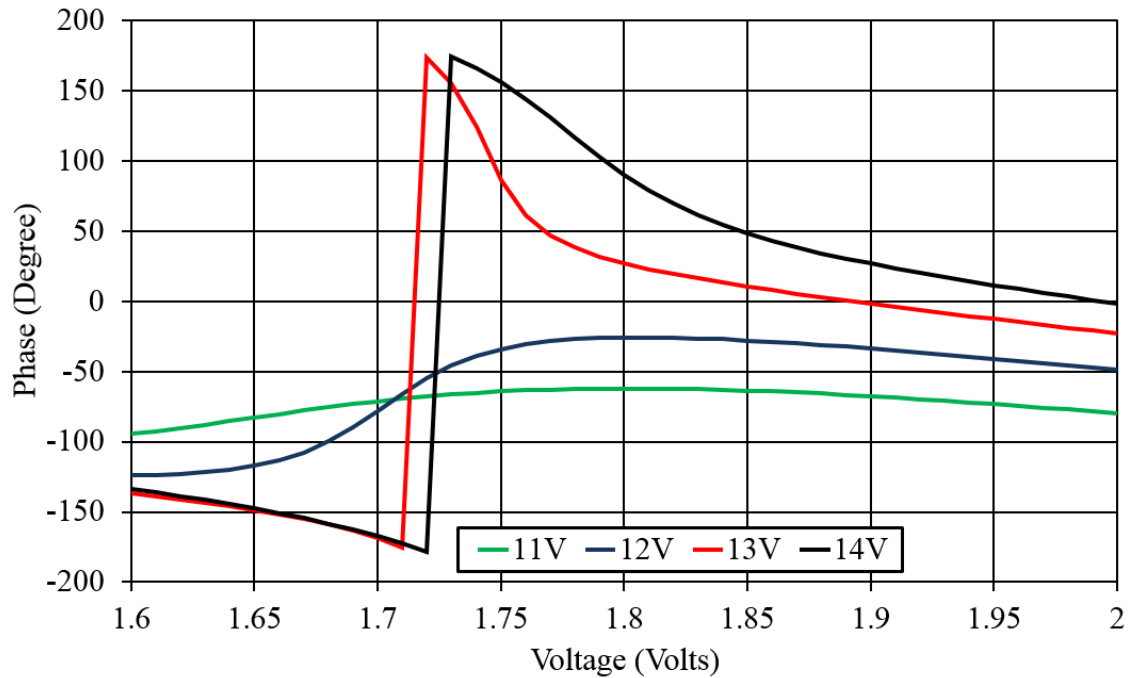


*Figure 6-28: Phase Response against Frequencies after FSS Panel Rotated 90°*

So from the results above in Figure 6-23, the simulation results in Figure 6-16 are matched at 1.8GHz when a voltage of 13V is applied. Also the measurement results of the initial position of the FSS panel is very similar as the measurement results of the FSS panel after turning 90° but has a slight frequency shift to the left at the resonant frequency response.

## 6.8 BER Measurement for the Reconfigurable Dual Polarization FSS

The setup of the BER measurement for the reconfigurable dual polarization FSS panel is the same as the single polarization FSS panel shown in Figure 6-11. To test the FSS against a GSM signal being transmitted from the antenna, the free space measurement system is used as described above, connected to a Rohde & Schwarz SMBV 100A signal generator. The data element of the GSM burst was a continuously repeating 11 bit pseudo random binary sequence. The receiving antenna was connected to a Rohde & Schwarz FSV vector signal analyser (VSA). The VSA has the capability to demodulate the GSM signal and compute the Bit Error Rate (BER) of the received signal. The BER is computed from prior measurement of the 11 bit pseudo random sequence when the FSS is not present i.e. the received signal has a high Signal to Noise Ratio (SNR).

BER measurements were initially carried out when the FSS was placed between the transmitter and receiver antennas, and a DC bias voltage of 13 Volts was applied across the varactor diodes to provide maximum attenuation. The received signal power in this case was approximately -60dBm as shown in Figure 6-29. This is also above the sensitivity limit of the VSA, therefore in initial measurement the BER was zero, as expected.

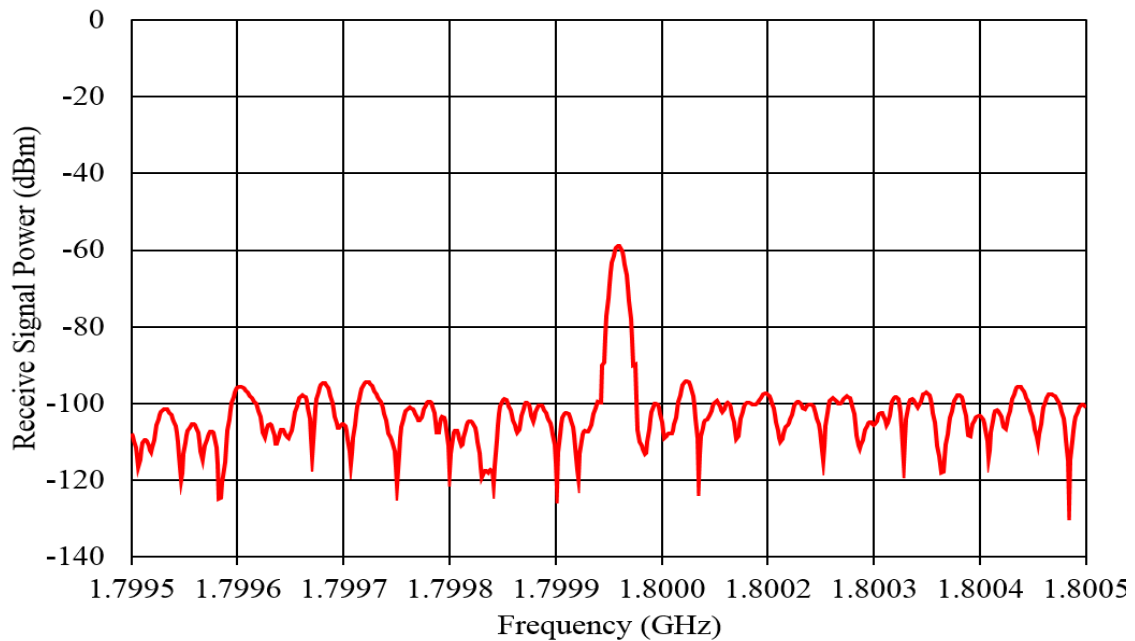


*Figure 6-29: Received Signal power against Frequencies*

To measure the BER of the reconfigurable dual polarization FSS panel, the resonant frequency of the FSS is kept at 1.8GHz using the DC voltage offset ( $V_{dc}$ ) of 13V being applied. A square wave voltage ( $V_{ac}$ ) is then applied from an AC signal generator at different ranges of switching frequencies ( $f_s$ ).

Figure 6-30 and Figure 6-31 shows a contour plot of the measured BER in percentage for  $0^\circ$  and  $90^\circ$  rotation of the FSS.

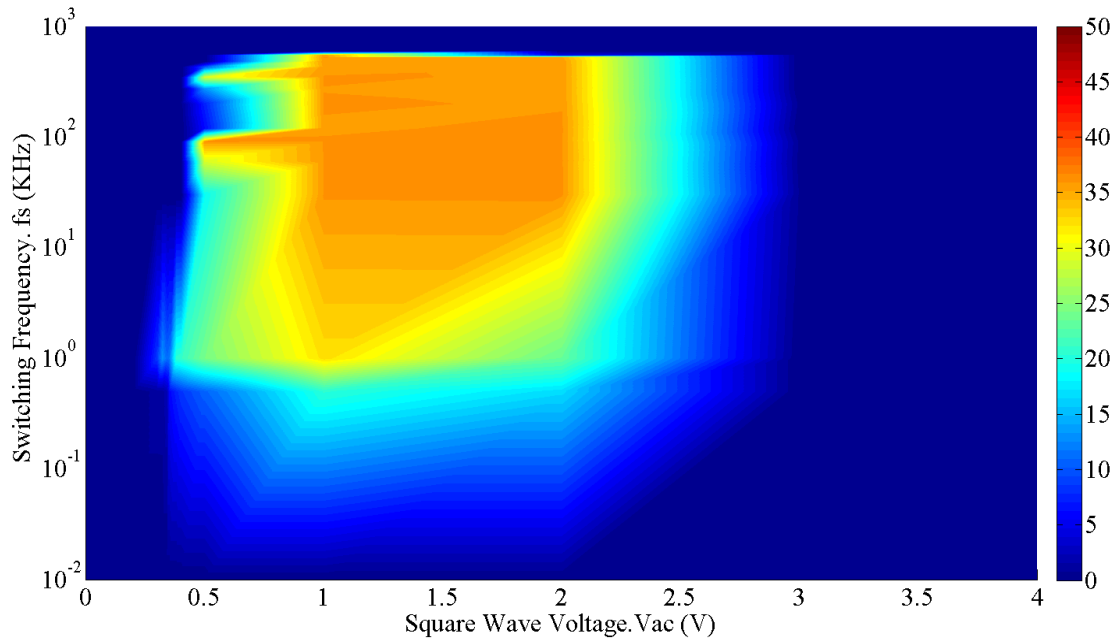


*Figure 6-30: GSM Signal BER (%) of Reconfigurable Dual Polarization FSS Panel*

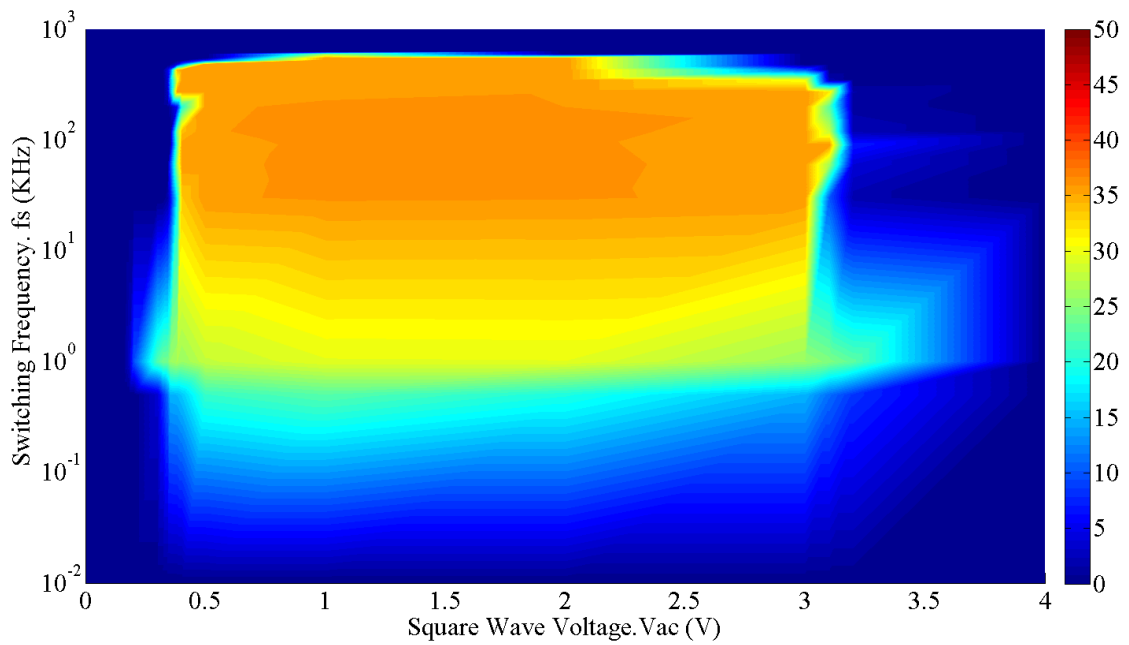
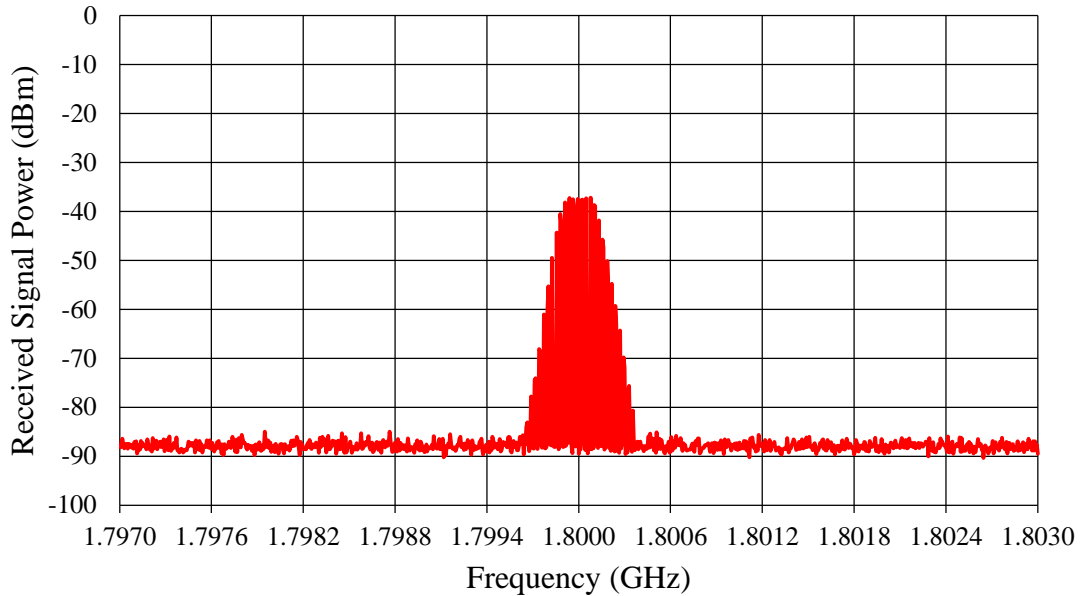


*Figure 6-31: GSM Signal BER (%) of Reconfigurable Dual Polarization FSS Panel rotated 90°*

From Figure 6-30 and Figure 6-31, when the switching frequency and square wave voltage changes, the BER can increase up to 36%. The results compare with the single polarization switching FSS, with the results following the same trend. Firstly, they have similar low switching frequency limits which are between 700-1000Hz and high frequency limits around 600kHz. If the BER is observed below or above these frequency limits the BER rapidly reduces to 0%, meaning the GSM signal is not impaired and the correct mobile phone signal will be received. The solution presented demonstrates its robustness as there are large ranges of switching frequencies and voltages, which will give a high level of BER, which can make sure the mobile phones do not receive the correct signal. This solution has better performance compared with passive FSS, as it is not limited to the strength of the signal received from the base station.

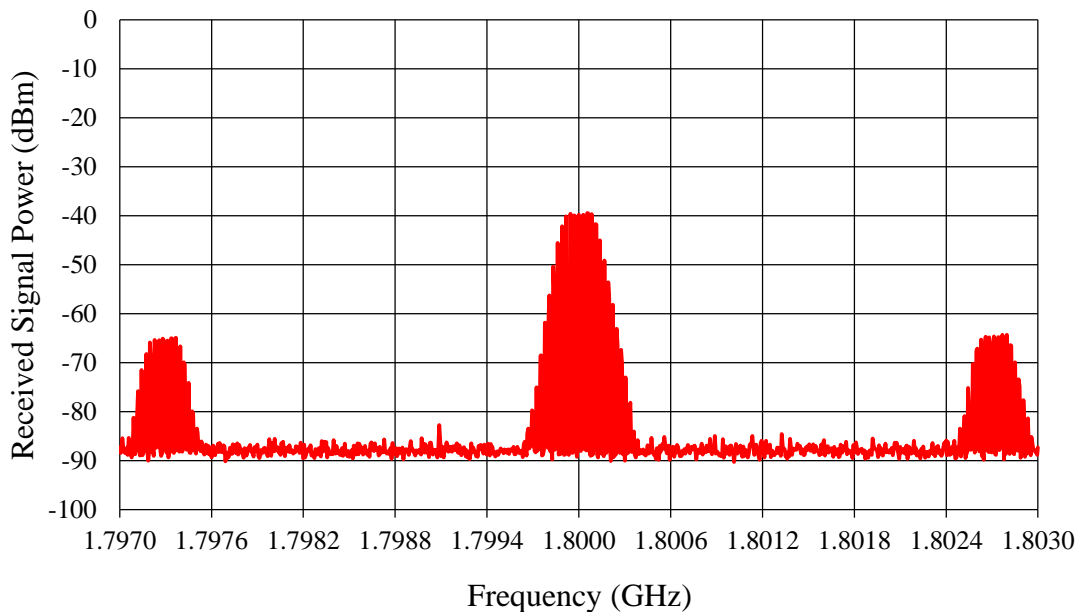
## **6.9 Frequency Spectrum Measurements for the Reconfigurable Dual Polarization FSS**

Shown in Figure 6-32 to Figure 6-36 is the effects on the frequency spectrum as the reconfiguration dual polarization FSS is switch at different frequencies. These measurements were obtained using a fixed offset of 13 volts DC and a square wave switched signal of 1 volt peak-to-peak. To observe a more stable spectrum, the GSM data selected was set at all ones, with a sweep time of 1s being set on all measurements measured by a vector signal analyser as previously shown in Figure 6-11. Figure 6-32 shows the FSS at its normal passive state where not external voltage is applied, illustrating only the received signal at 1.8 GHz.



**Figure 6-32** Frequency Spectrum for Reconfigurable Dual Polarization FSS – No Switching

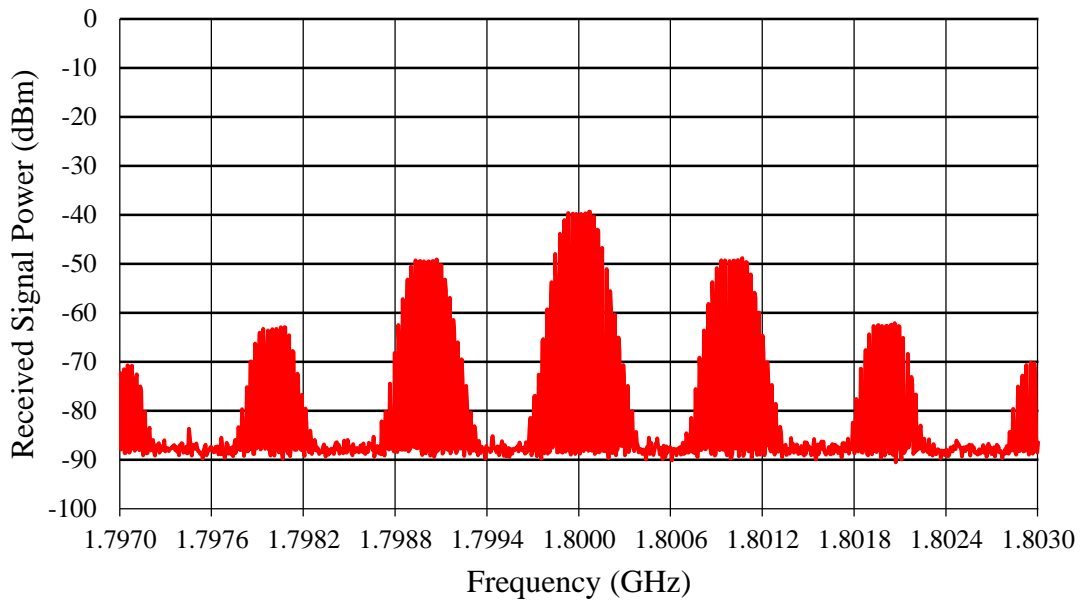
Figure 6-33 shows when the FSS is actively switched at 2.71 MHz causing the signal to shift from the centre frequencies into the sidebands at equally spaced harmonics. As the harmonics are not within the original spectrum a bit error rate of zero can still be obtained.



**Figure 6-33** Frequency Spectrum for Reconfigurable Dual Polarization FSS – Switching At 2.71 MHz

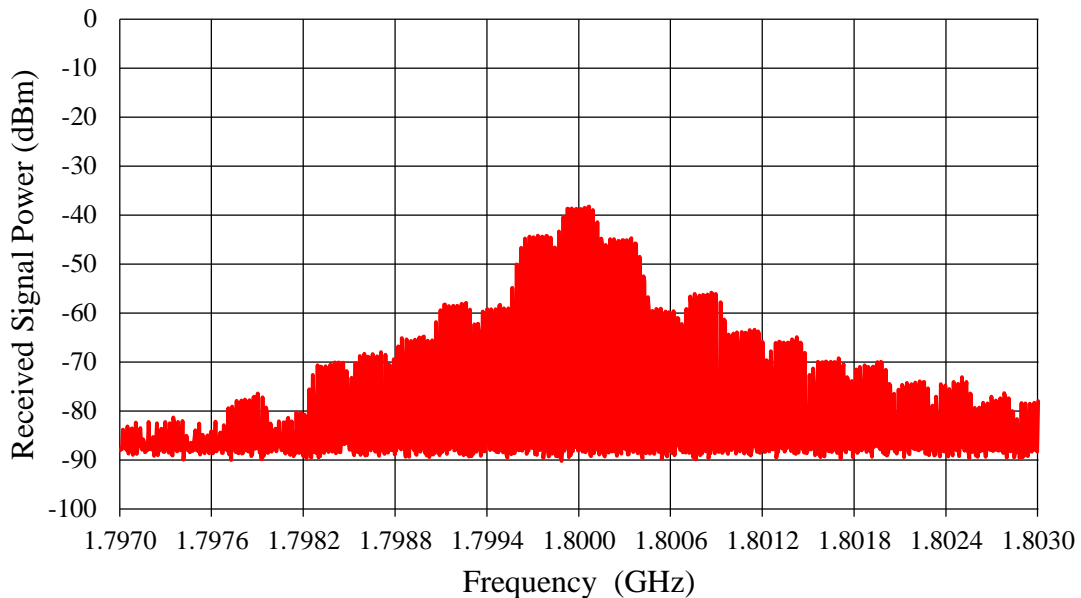
Figure 6-34 again shows when the FSS is actively switched at a lower rate of 1 MHz causing even more harmonics equally spaced around the centre frequency of 1.8 GHz.

As the harmonics are not within the original spectrum a bit error rate of zero can still be obtained.



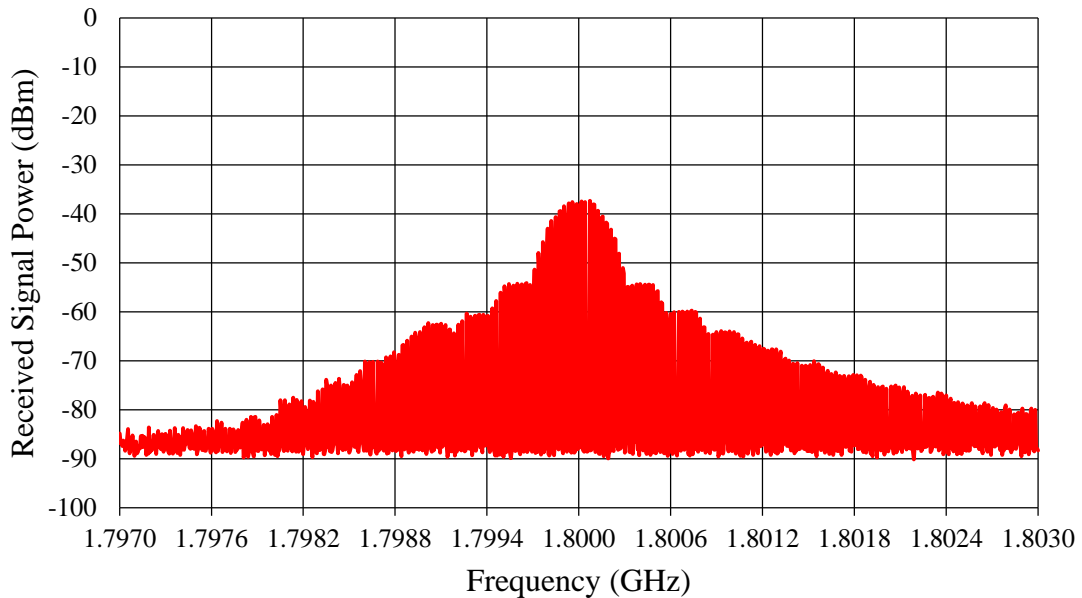
**Figure 6-34** Frequency Spectrum for Reconfigurable Dual Polarization FSS – Switching At 1 MHz

Figure 6-35 show when the FSS is switched at a much lower frequency of 271 kHz, causing the equally spaced apart harmonics to interfere with the original frequency spectrum. Due to this reasons a bit error rate of 44.3% can be observed at this switching frequency.



**Figure 6-35** Frequency Spectrum for Reconfigurable Dual Polarization FSS – Switching At 271 kHz

Figure 6-36 shows the final measured switching frequency of 135.5 kHz. Again as observed at the switching frequency of 271 kHz the equally spaced apart harmonics are interfering with the original centre frequencies at 1.8 GHz causing a bit error rate of 44.2% being measured.



*Figure 6-36 Frequency Spectrum for Reconfigurable Dual Polarization FSS – Switching At 135.5 kHz*

The above measurements all follow the same observations that were simulated in Figure 5-5 to Figure 5-7, where the sideband harmonics interfere causing bit errors when being too close to the original centre frequency spectrum.

## 6.10 Summary

Two reconfigurable switching FSS panels were manufactured for measurement. One for single polarization and the other dual polarization, 2-D surface plots of their measurements all follow the same trend as the simulation results obtained in MATLAB.

# CHAPTER 7      DIFFRACTION FROM FREQUENCY SELECTIVE SURFACES FOR SECURE BUILDING APPLICATION

A Frequency Selective Surface (FSS) can be used to control mobile phone signal propagation both in and out of buildings. When an FSS is to be designed to be attached to a building surface, such as a window, there are two main aspects which affect its performance. The common research interest is to design a FSS that can alter the specular attenuation for a range of angles and polarizations. For secure buildings applications the level of attenuation needed to stop signals propagating into a room requires the need to investigate the level of diffraction scattering from the FSS. This chapter focuses on the diffraction issues associated with a FSS design when used for secure building applications.

In order to design a FSS to block mobile phone frequency, an assessment needs to be made on the power levels expected in a room or building that is required to be secure. This can be carried out using various modelling techniques. Depending on the level of attenuation needed by the FSS solution it may be required to assess not only the specular response but also non-specular diffraction to determine its impact on system performance. Non-specular scattering will be of importance for Non Line of Sight when very high attenuation levels are required.

## **7.1 FSS Non-Specular Scattering Scenario**

A scenario is considered in which an FSS is placed across a window of a building to reduce the power between a Base Transceiver Station (BTS) and a mobile device as shown in Figure 7-1, which CST model is illustrated in Figure 7-2. The received signal will comprise of the direct path and the diffraction from the FSS/metal interface. It is assumed that the rest of the room consists of metallic surfaces and is perfectly isolating. The simulations were carried out using the time domain solver within CST Microwave Studio.

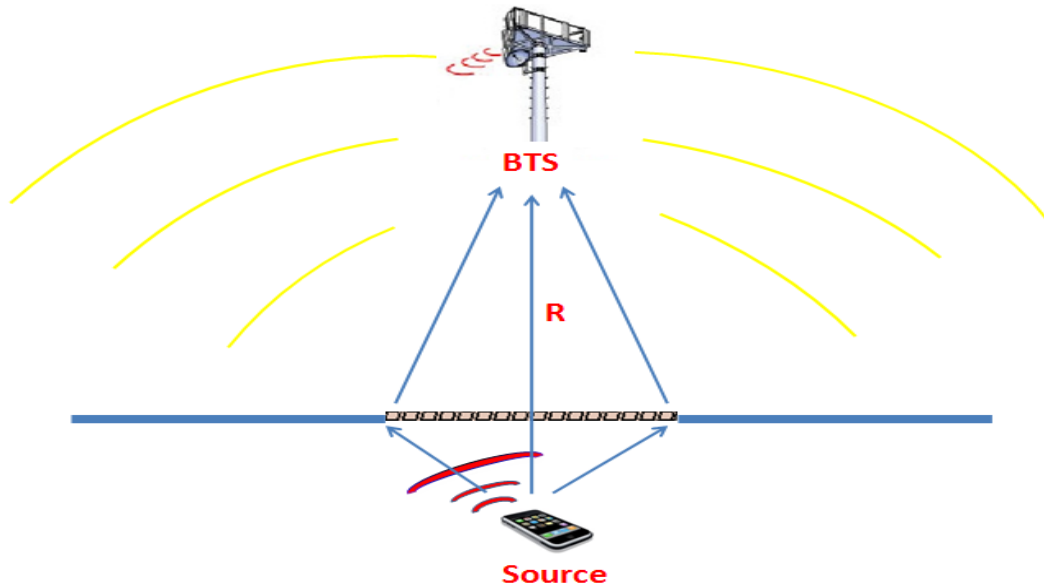


*Figure 7-1: The Signal Received by Base Station*

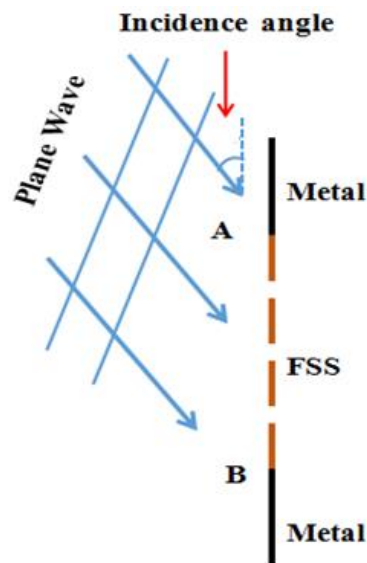
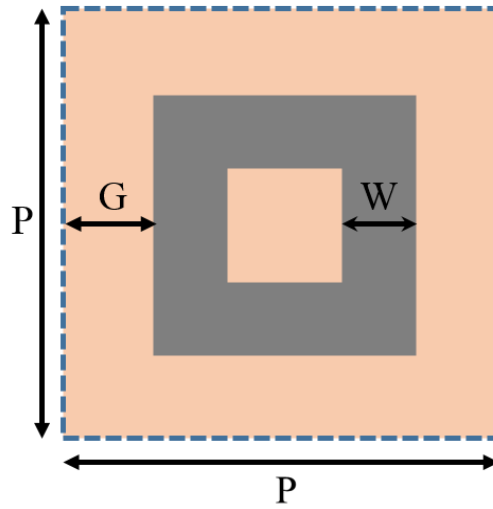


*Figure 7-2: Illustration of an FSS in a Secure Room*

In order to simulate the diffraction from the FSS/metal interfaces, a 3D simulated wall surface model was produced, which is illustrated in Figure 7-4. The size of the wall is 2m x 2m which has an aperture 0.5m x 0.5m in the middle, with the FSS panel containing 100 FSS unit cells being attached to this aperture. Each FSS simulation comprises of a square metallic loop with a unit cell periodicity of 50mm, loop size of 46.5mm and the

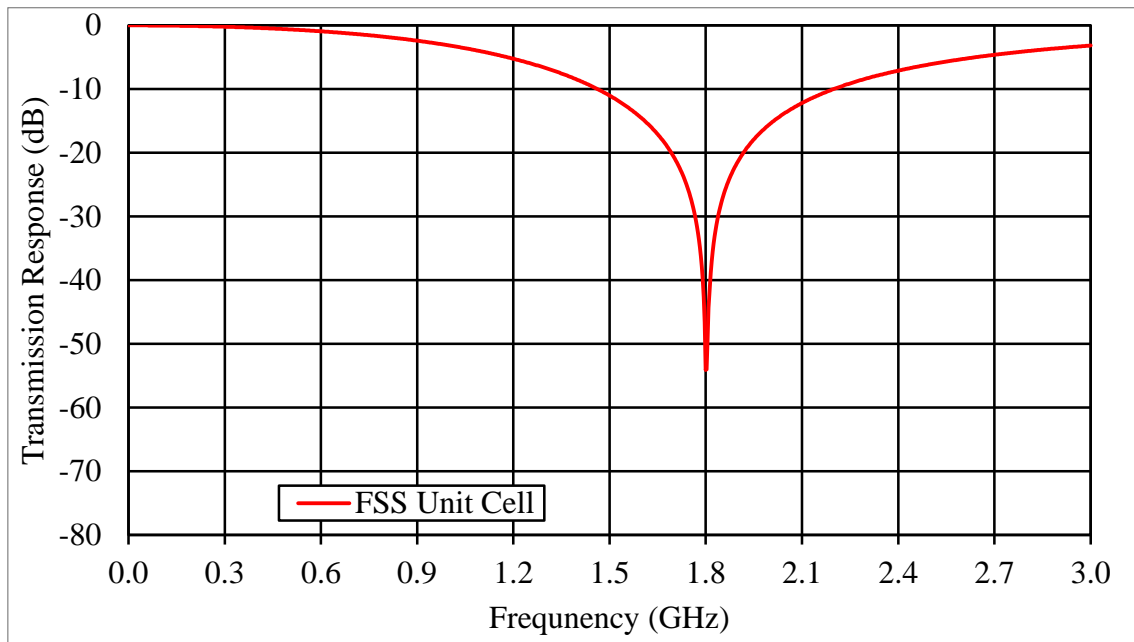
width of the metallic loop being 4.25mm and tuned to operate at 1.8GHz, the attenuation is 54dB for normal incidence in Figure 7-3.



(a) Unit Cell

| FSS Type               | P(mm) | G(mm) | W(mm) |
|------------------------|-------|-------|-------|
| Single Square Loop FSS | 50    | 1.75  | 4.25  |

(b) Dimensions



(c) Simulation Transmission Response

Figure 7-3: The Transmission Response for the Unit Cell

A simulated 1V/m plane wave illuminates the structure at varying angles from the surface of the FSS with the E-field parallel to the FSS/metal interface. The scattered E-field is

monitored at a fixed distance of 1.2m from the metal wall. To assess the far field scattering of the structure diffraction from the wall surface was removed by replacing the FSS with a continuous PEC sheet. This flat PEC sheet represents a perfect reflector, where the entire of the incident signal would be reflected. For fair comparison, this size of the PEC sheet needs to have the exact same dimensions as a metal wall containing an FSS panel. The scattering radiation simulated from the far field scenarios with and without the FSS were subtracted to provide the scattering from the FSS region only.

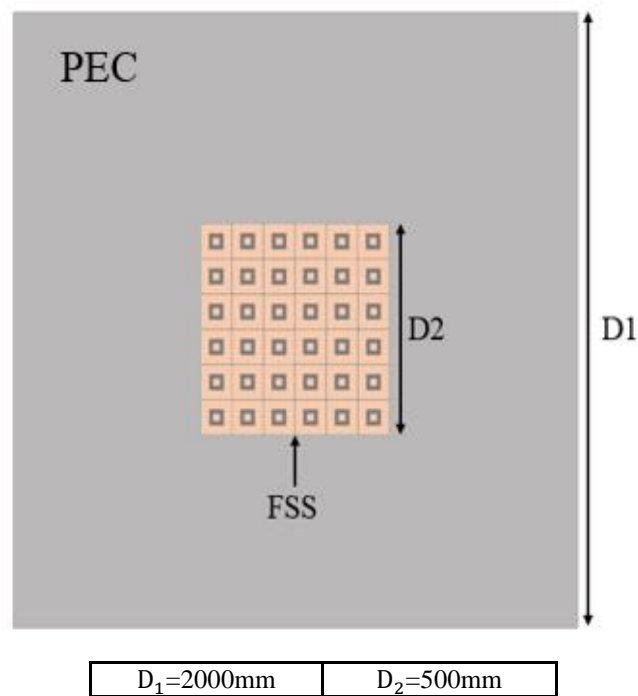


*Figure 7-4: 3-D Wall Surface*

## 7.2 FSS Non-Specular Scattering Radiation Pattern Analysis

A scenario is considered in which an FSS is placed across a window of a building to reduce the power between a Base Transceiver Station (BTS) and a mobile device as illustrated in Figure 7-1. The scattered E-field is monitored at a fixed distance of 1.2m around metal wall by a far field monitor simulated in CST software.

Scattering pattern results need to be employed to analyse the diffraction scattering from different incident angles. Figure 7-5 (a) is an illustration for a plane wave with incident angle of  $20^\circ$  from the vertical wall surface. Figure 7-5 (b) is the 3-D simulated result,

which shows the E-field of the wall surface when subject to a 1V/m plane wave for all forward and back scattering angles.

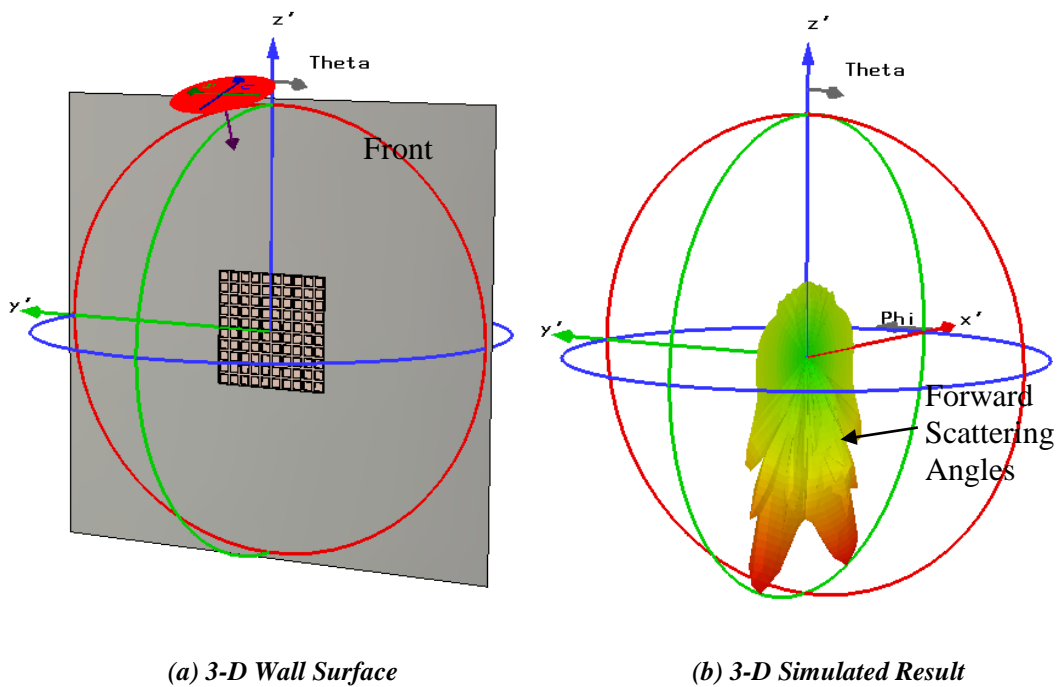


**Figure 7-5: 20° Incident Angle from the Wall Surface with 3-D Simulation Result**

A field monitor has been used to monitor the E-field in the far-field from 0 to 3GHz. The plot in Figure 7-5 (b) represents the scattered field at 1.8GHz. This research focuses on the scattering field inside a building, ranging from  $-180^\circ$  to  $0^\circ$  (forward scattering angles). Additionally, the results are normalised to the scattered E-Field from a PEC surface of the same dimensions in the specular direction which equates to a reflection coefficient of -1. This research focuses on observing diffraction scattering from varying incident angles, using four different incident angles ( $20^\circ$ ,  $40^\circ$ ,  $60^\circ$ ,  $80^\circ$ ) as examples. The radiation patterns for the PEC sheet at different angles have been simulated using CST which are shown in Figure 7-6, where the main lobe magnitudes are 15dBm/V at  $20^\circ$ , 22dBm/V at  $40^\circ$ , 25dBm/V at  $60^\circ$  and 26dBm/V at  $80^\circ$ . When the results are normalised, they need to be subtracted using different peak magnitudes of the main beam depending on their simulated incident angle.

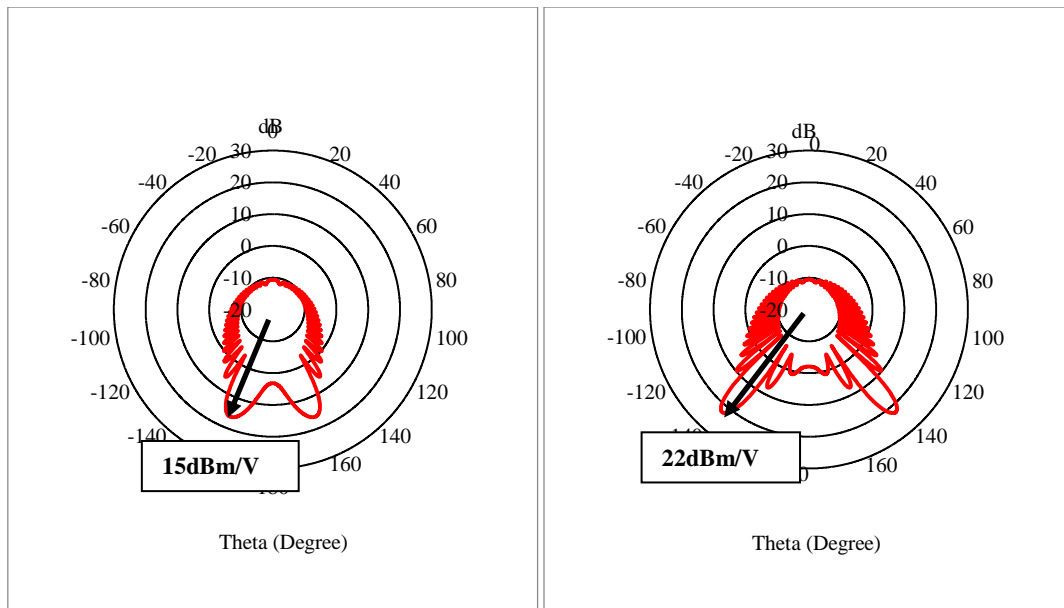
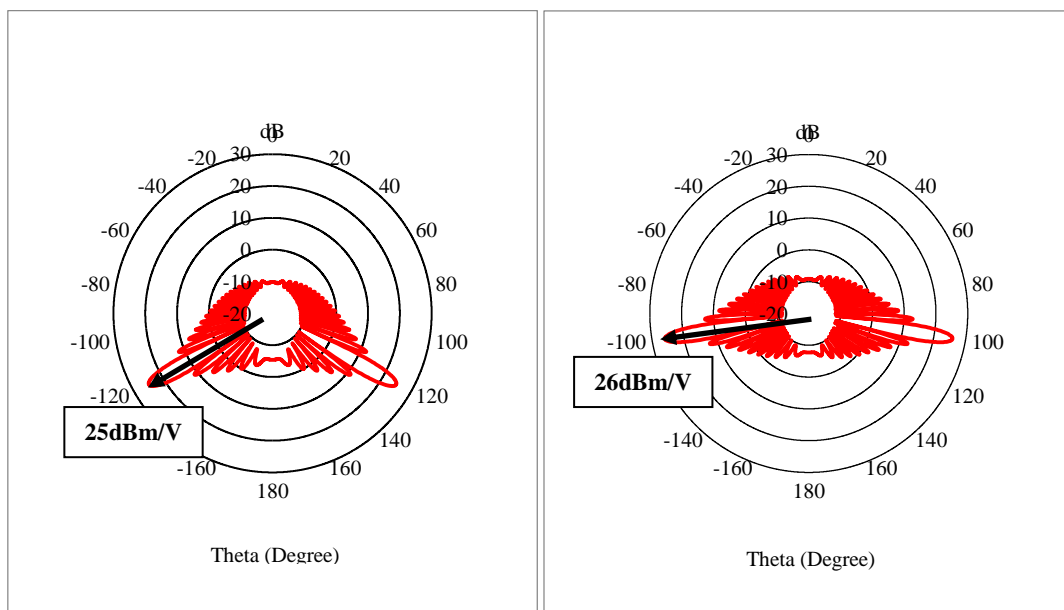
(a) Incident Angle at  $20^\circ$ (b) Incident Angle at  $40^\circ$ (c) Incident Angle at  $60^\circ$ (d) Incident Angle at  $80^\circ$ **Figure 7-6: Radiation Pattern Flat PEC Sheet at Different Incident Angles**

Figure 7-7 to Figure 7-10 show the normalised scattered field Cartesian plot results for different incidence angles ranging from  $20^\circ$  to  $80^\circ$  over the whole angular range of interest at 1.8GHz for the scatter field. The scattering with, or without, a FSS on the wall surface were subtracted in the far field to provide the scattering from the FSS region only. The results show the effective scattering field of the FSS to a 1V/m plane wave for all

forward scattering angles. As expected there are peaks in the response at the specular angles, which are a combination of the standard transmission response plus the diffraction from the FSS edges.

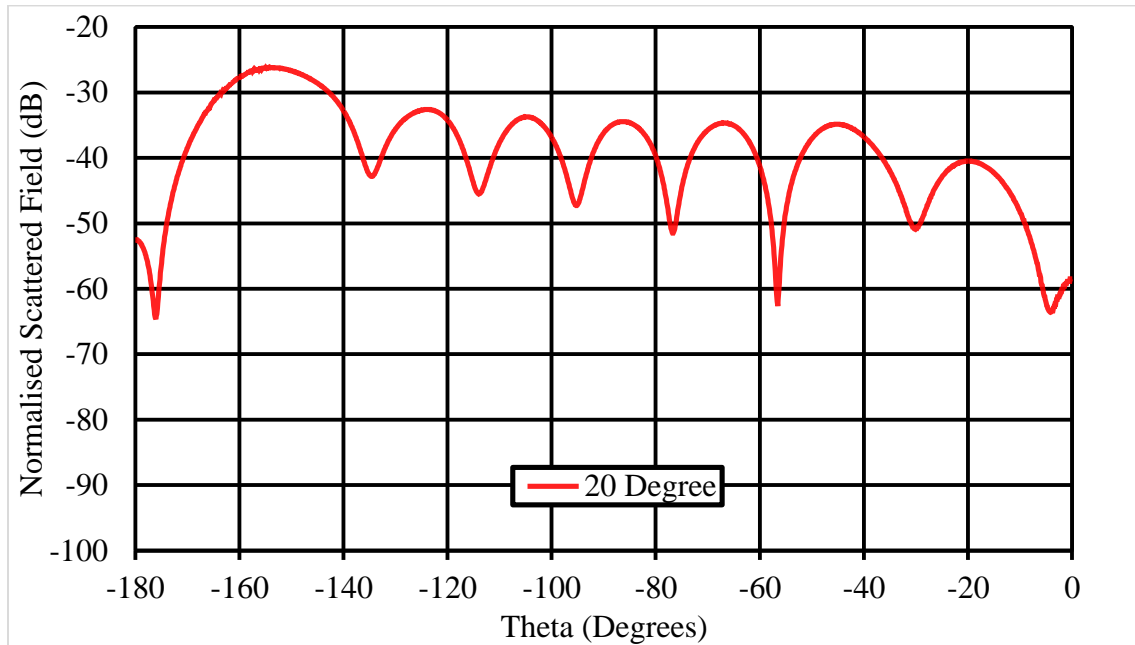


Figure 7-7: Incident Angle at 20° for the scatter field

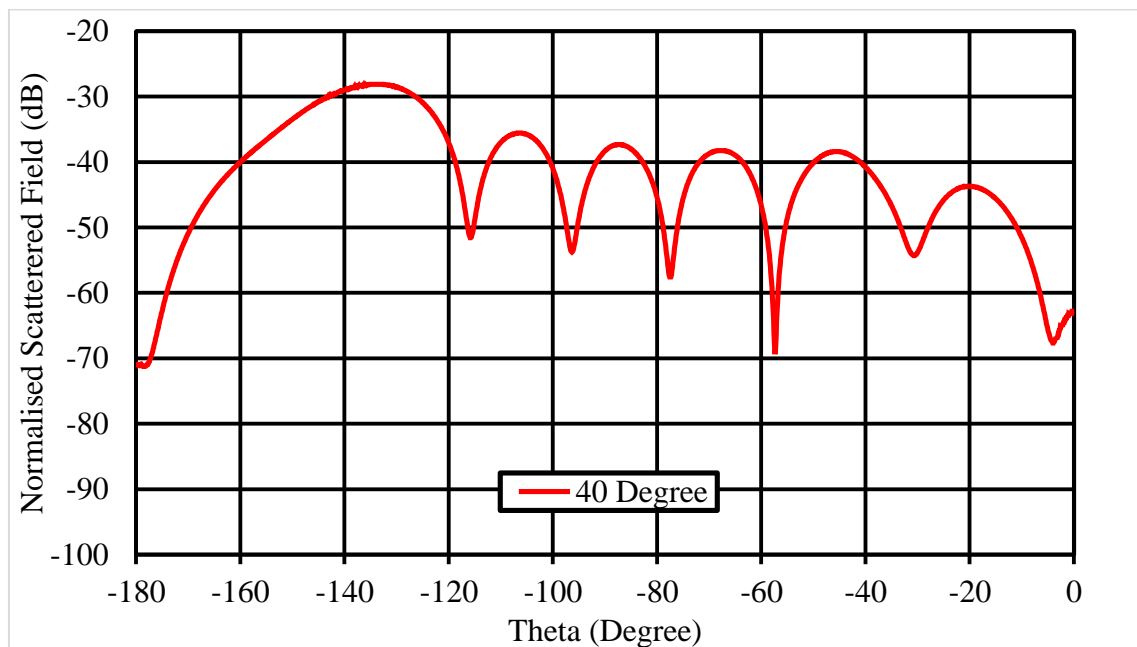
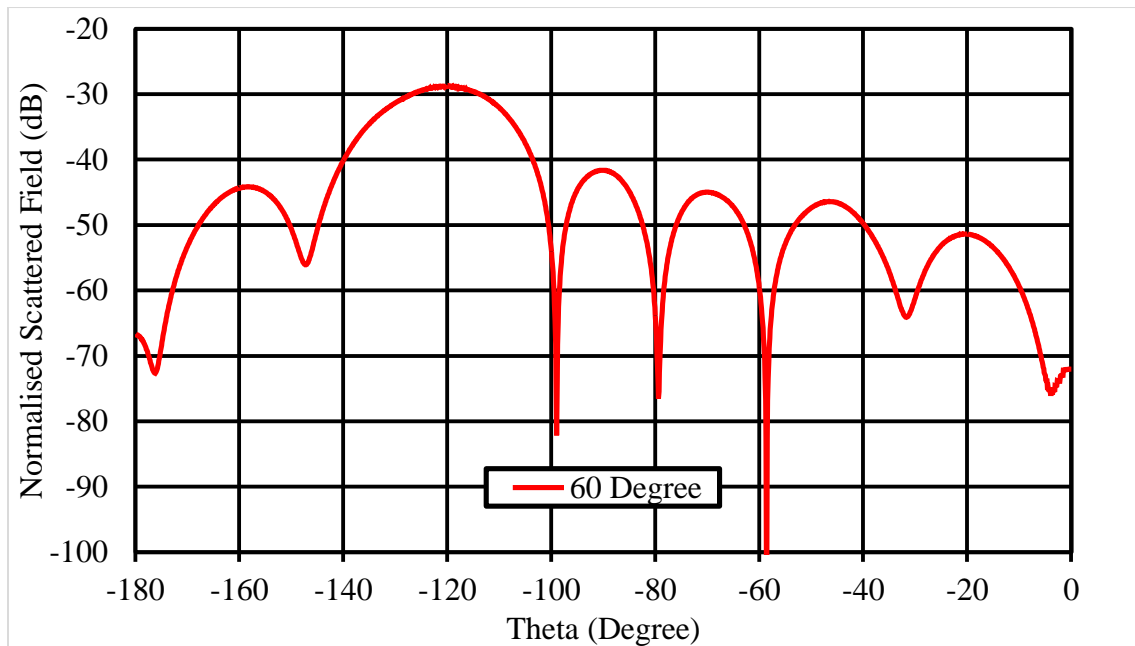
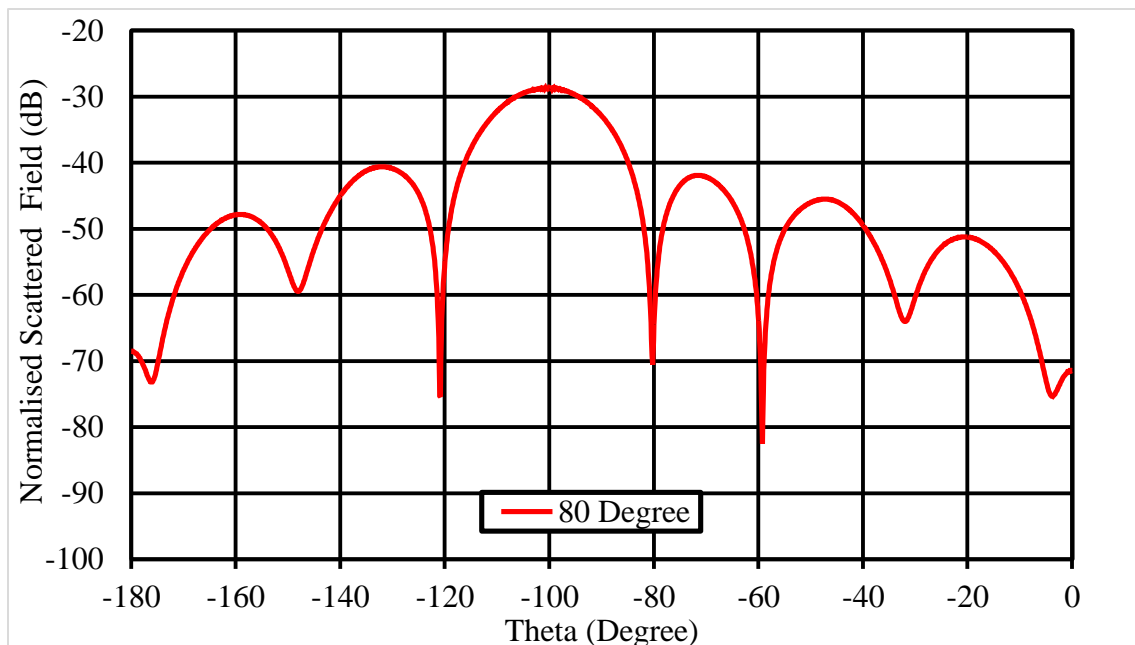


Figure 7-8: Incident Angle at 40° for the scatter field



*Figure 7-9: Incident Angle at 60° for the scatter field*



*Figure 7-10: Incident Angle at 80° for the scatter field*

From Figure 7-7 to Figure 7-10, the peaks can be found at around  $-160^\circ$ ,  $-140^\circ$ ,  $-120^\circ$  and  $-100^\circ$  for incidence angles of  $20^\circ$ ,  $40^\circ$ ,  $60^\circ$  and  $80^\circ$  respectively. The small spikes in the data near the forward scattering direction are due to minor variations of the mesh within CST. This is particularly important when carrying out the subtraction of the PEC surface so that the scattering of the FSS region alone can be carried out.

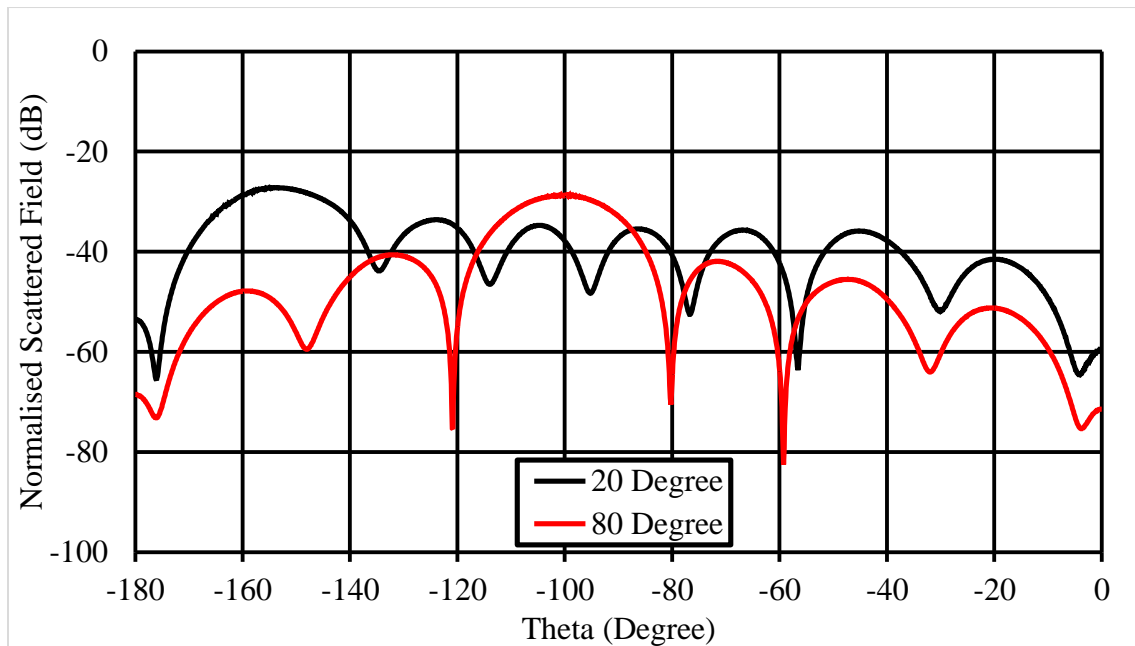


*Figure 7-11: Comparison of Incident Angle at 20° and 80°*

Figure 7-11 compares the scattered field results for 20° and 80° with the results illustrating that for the non-specular angles the diffraction from the FSS is an important factor. Figure 7-12 shows the transmission response for the FSS unit cell at different incident angles.

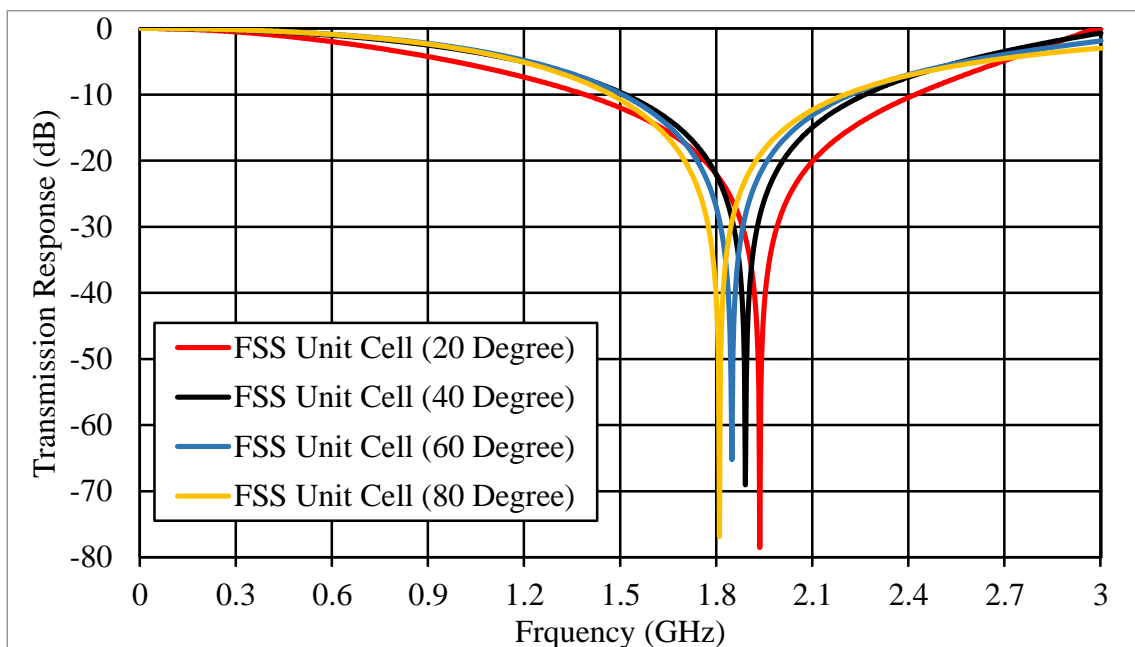


*Figure 7-12: The Transmission Responses of the Large Unit Cell*

The specular scattering of the FSS unit cell at 1.8GHz have been listed in Table 7-1. Measurements were taken from the internal and external areas of the Mappin building at the University of Sheffield, where the values obtained showed that a secure room would require levels of attenuation over 60dB in order to prevent wireless communication. This table indicated that the normalised scattered field is between -37dB to -51dB, which would potentially still allow a mobile phone inside the secure building to receive the transmitted base station signals.

| Incidence angles (Degrees) | Specular Scattering (dB) | Normalised Scattered Field (dB) |      |      |      |
|----------------------------|--------------------------|---------------------------------|------|------|------|
|                            |                          | -90°                            | -70° | -50° | -20° |
| 20°                        | -22                      | -37                             | -36  | -38  | -41  |
| 40°                        | -22                      | -38                             | -38  | -40  | -43  |
| 60°                        | -27                      | -41                             | -44  | -47  | -51  |
| 80°                        | -41                      | -32                             | -42  | -46  | -51  |

*Table 7-1: Specular Scattering and Normalised Scattered Field*

This can be further expanded by comparing the difference in forward scattering in two different scenarios. The first scenario would be the metal wall with a FSS on the window aperture as seen above, and second would be the metal wall with an window aperture with the FSS removed. The comparisons will be for the far field at different specular angles. Incident angles of 60° and 80° have been simulated as examples and results are illustrated in Figure 7-13 and Figure 7-14. For fair comparison, the aperture has been created with the same size as the FSS panel. The results show the specular performance of the FSS being unaltered, as expected; but there is a reduction for the metal wall with FSS present where the non-specular scattering can introduced an additional 5dB in field strength.

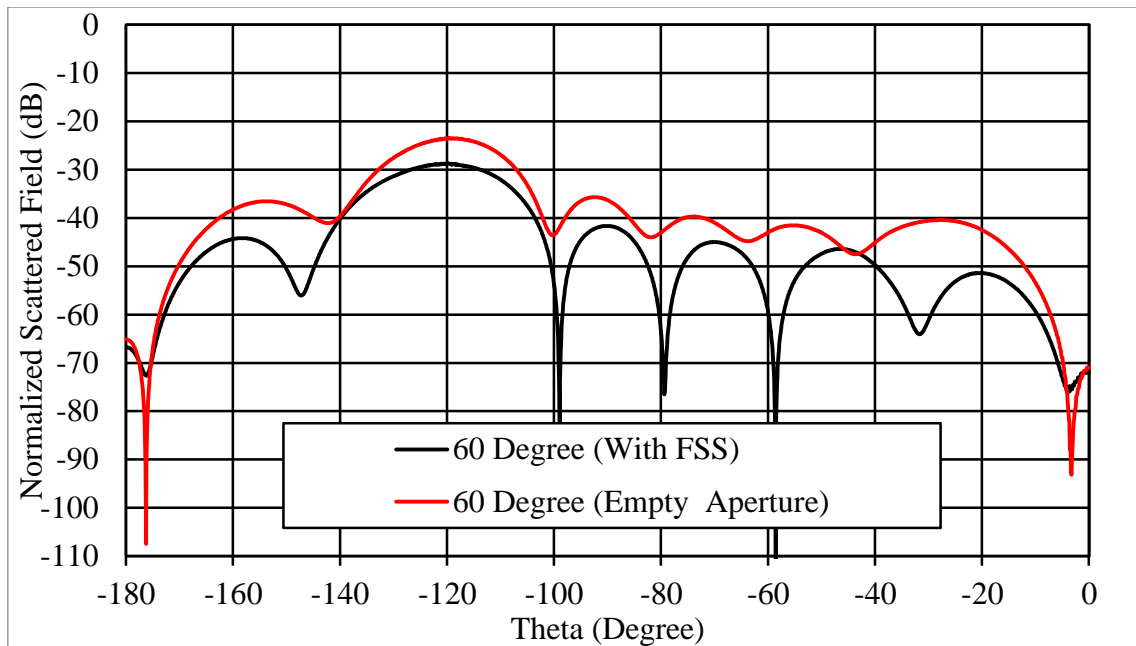


Figure 7-13: Comparison Metal Wall with FSS and With Aperture Cases at Specular Angle at 60°

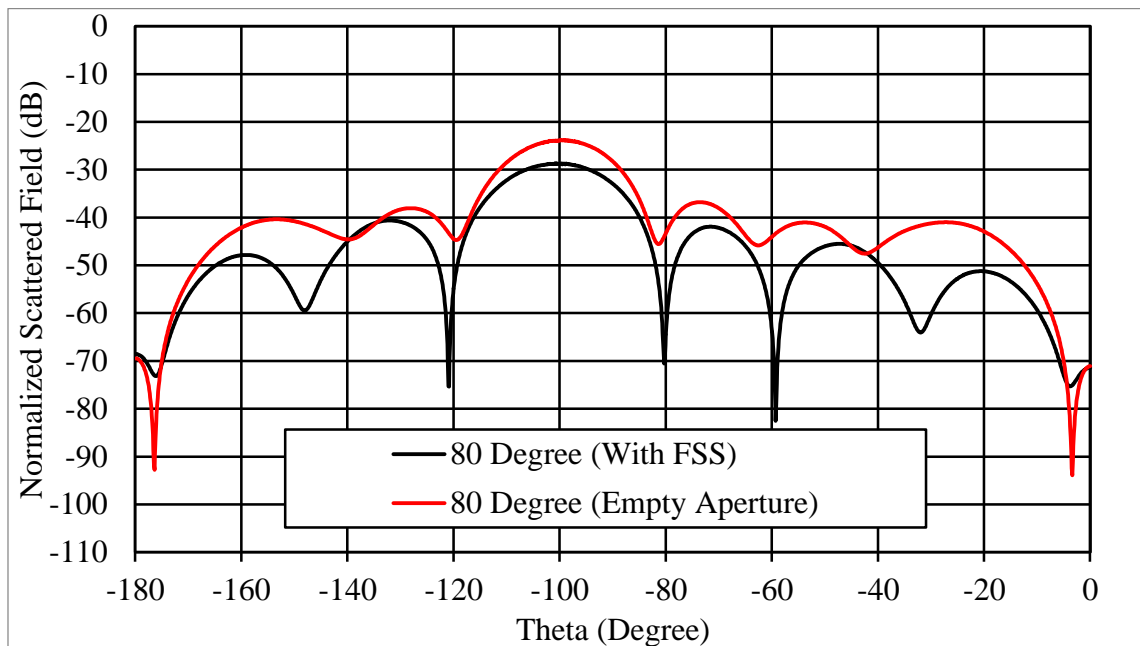
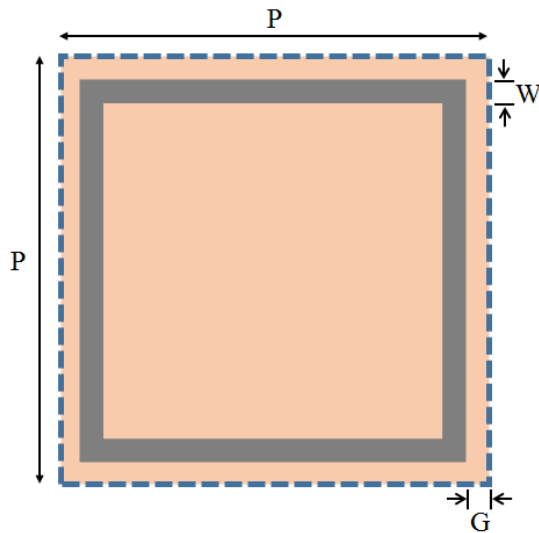


Figure 7-14: Comparison Metal Wall with FSS and With Aperture Cases at Specular Angle at 80°

In order to reduce the non-specular scattering, the FSS unit cell design was altered, as shown in Figure 7-15. The FSS is now half the size of the original one, but the normal incidence specular performance of the small FSS still operates at 1.8GHz as shown in Figure 7-16.



| FSS Type               | P(mm) | G(mm) | W(mm) |
|------------------------|-------|-------|-------|
| Single Square Loop FSS | 25    | 0.5   | 1.26  |

Figure 7-15: Small Unit Cell

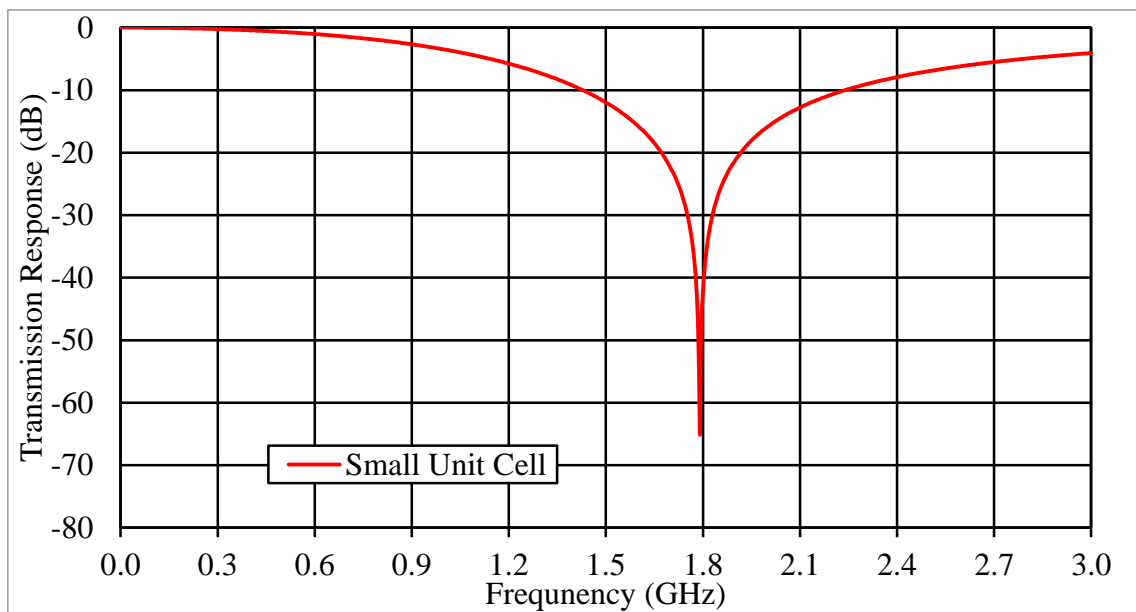
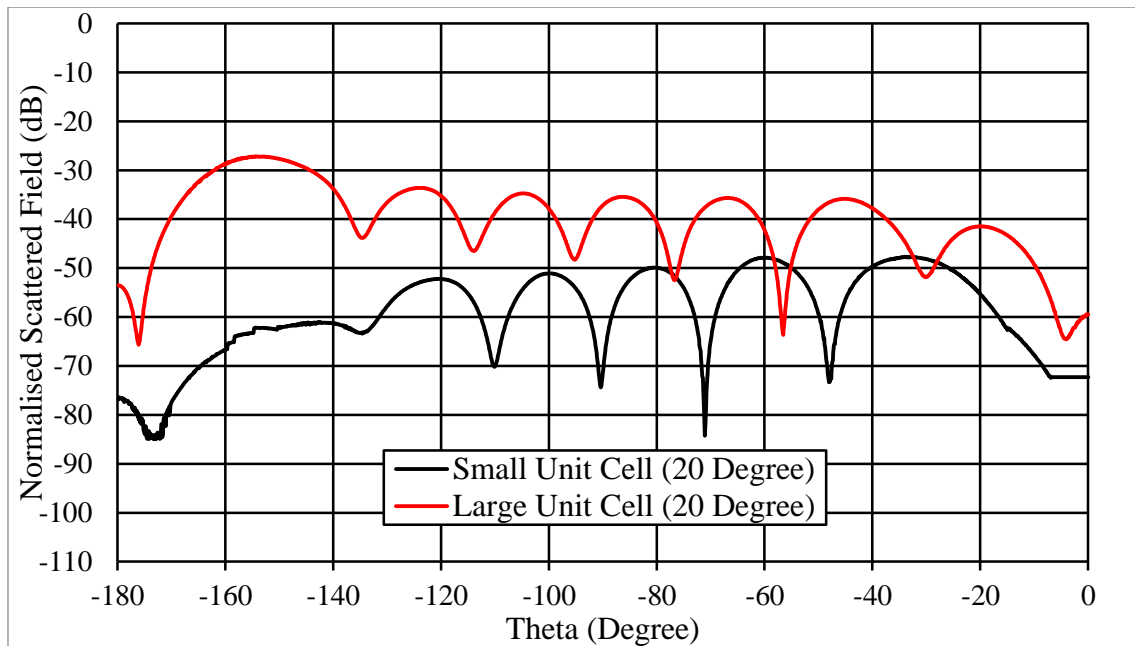


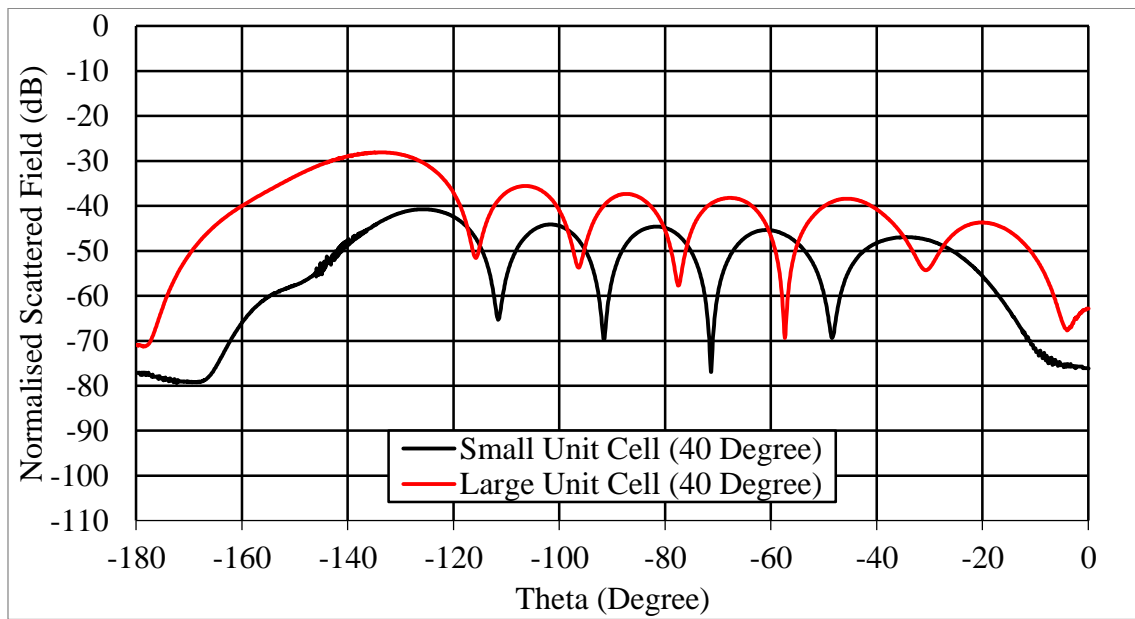
Figure 7-16: Transmission Response for a Smaller Unit Cell

Figure 7-17 to Figure 7-20 compare the forward scattering performance between the redesigned 25mm and previous 50mm designed unit cell, over different incident angles. It can also be seen that the non-specular scattering of the smaller designed unit cells is smaller than the previous designed unit cell in all incident angle scenarios. This means

the smaller element redesigned FSS panel has less leakage compared with the larger previous FSS panel place over the window aperture.



*Figure 7-17: Comparison of 25mm and 50mm Unit Cell at incident angle of 20°*



*Figure 7-18: Comparison of 25mm and 50mm Unit Cell at incident angle of 40°*

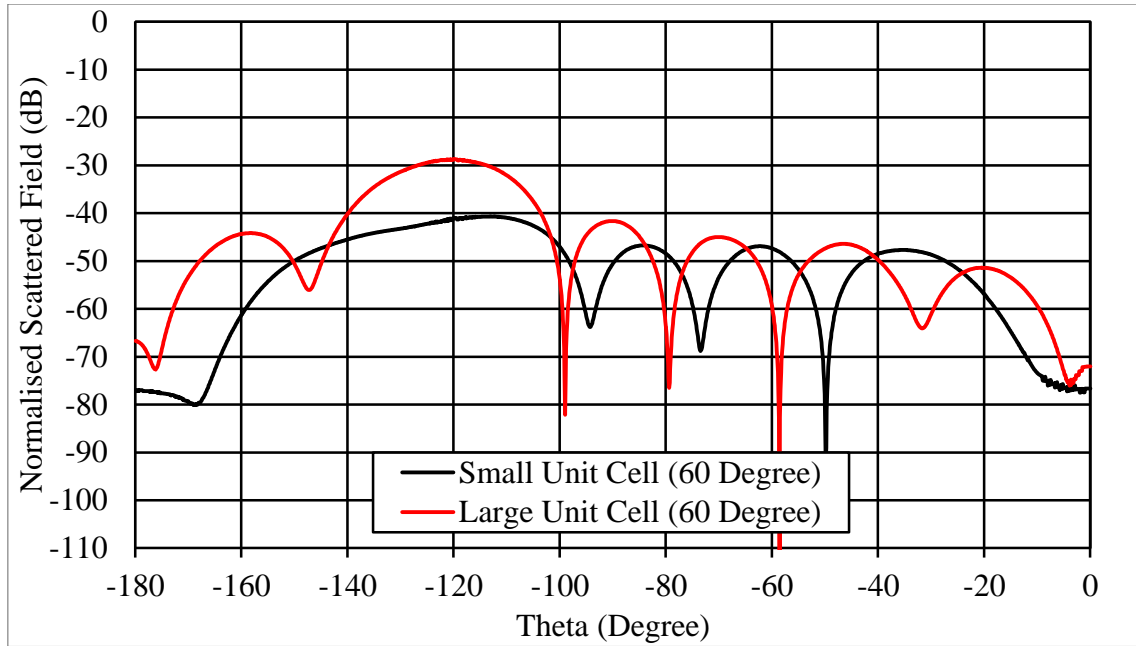


Figure 7-19: Comparison of 25mm and 50mm Unit Cell at incident angle of 60°

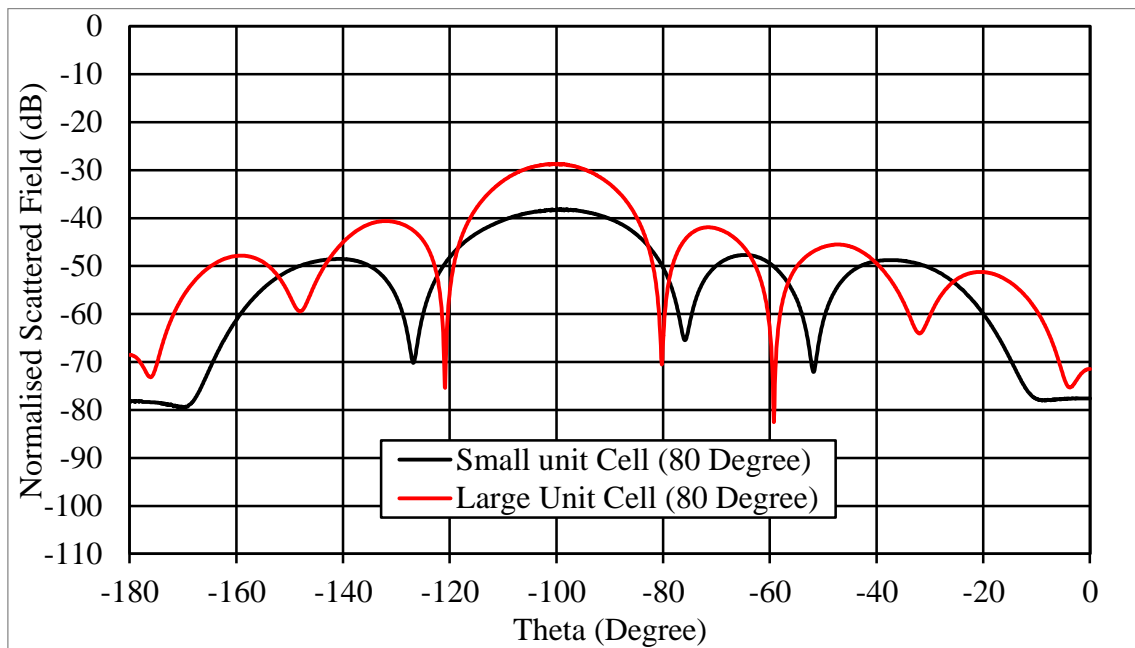
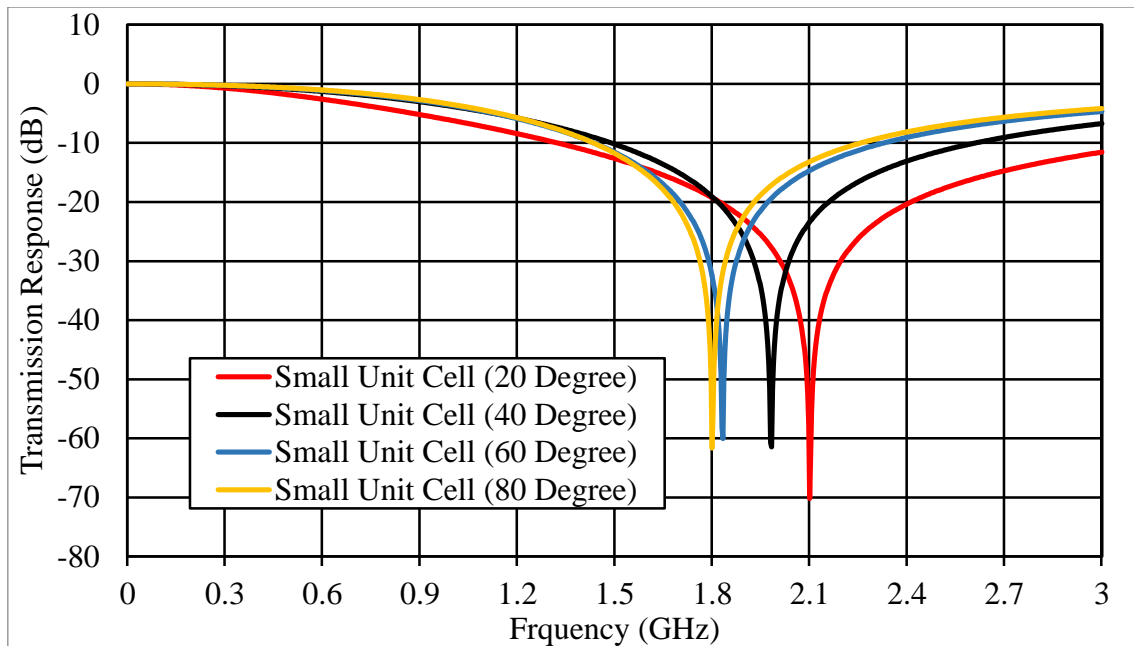


Figure 7-20: Comparison of 25mm and 50mm Unit Cell at incident angle of 80°

Figure 7-21 shows the transmission response for the smaller unit cell design at different incident angles.



**Figure 7-21: Transmission Responses for the Small Unit Cell**

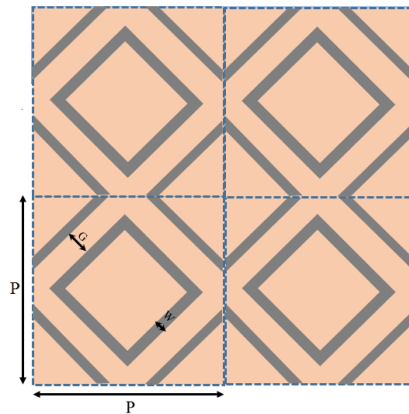
Table 7-2 summarises the specular scattering and normalised scattered field at 1.8GHz, where it needs to be kept in mind that a secure room requires at least 60dB of attenuation to stop wireless communication. As previously obtained to compare with, the normalised scattered field is between -37dB to -51dB for the large unit cell design. The normalised scattered field for the small unit cell design ranges between -50dB to -82dB. Although the performance is improved with less leakage from the FSS unit cell design, a mobile phone contained within a secure building, still may pick up the signals from the base station.

| Incidence angles (Degrees) | Specular Scattering (dB) for Small Unit cell | Small Unit Cell Normalised Scattered Field (dB) |      |      |      | Large Unit Cell Normalised Scattered Field (dB) |      |      |      |
|----------------------------|--|---|------|------|------|---|------|------|------|
|                            |  | -90°  | -70° | -50° | -20° | -90°  | -70° | -50° | -20° |
| 20°                        | -18  | -71   | -64  | -59  | -55  | -37   | -36  | -38  | -41  |
| 40°                        | -18  | -56   | -59  | -59  | -55  | -38   | -38  | -40  | -43  |
| 60°                        | -30  | -50   | -53  | -82  | -56  | -41   | -44  | -47  | -51  |
| 80°                        | -41  | -40   | -49  | -61  | -60  | -32   | -42  | -46  | -51  |

**Table 7-2: Specular Scattering and Normalised Scattered Field of Small and Large Unit Cell**

In order to reduce the non-specular scattering issues observed, other improved FSS designs should be considered. This research will explore two design methods that could achieve this: First a FSS unit cell the same size as the original design, which has been rotated by  $45^\circ$ , and the second metal teeth are added to the original design around the window part that interfaces with the FSS.

The first rotated FSS unit cell as shown in Figure 7-22 keeping its transmission response operating at 1.8GHz as simulated in Figure 7-23.



| FSS Type               | P(mm) | G(mm) | W(mm) |
|------------------------|-------|-------|-------|
| Single Square Loop FSS | 50    | 3.5   | 4.25  |

*Figure 7-22: Rotate Unit Cell  $45^\circ$*

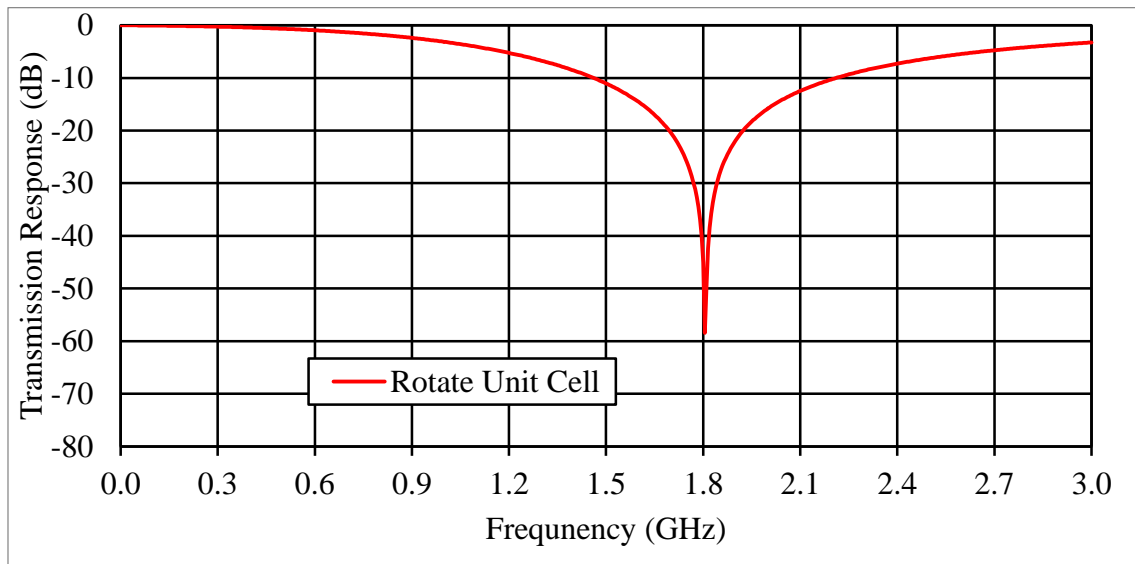


*Figure 7-23: Transmission Response for Rotate FSS  $45^\circ$*

Figure 7-24 to Figure 7-27, compare the scattering performance of the original unit cell and its rotated counterpart at  $45^\circ$  over different incident angles. From the simulation results, when the incident angle is smaller, the reduction of scattering appears more significant, for example the unit cells that has been rotated through  $45^\circ$  will become a rhombus. The plane wave would "see" the sharp point of the rhombus. If the angle is further increased to  $90^\circ$  (normal incidence), the plane wave would "see" the whole rhombus as a flat surface.

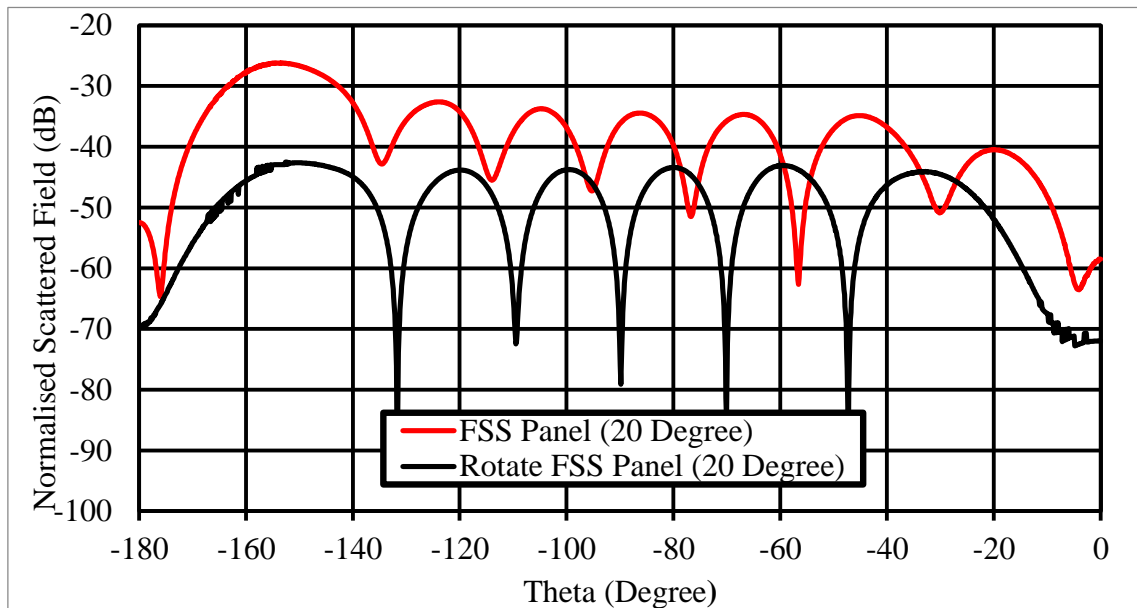


Figure 7-24: Comparison of Original and Rotated Unit Cell at Incident Angle of  $20^\circ$

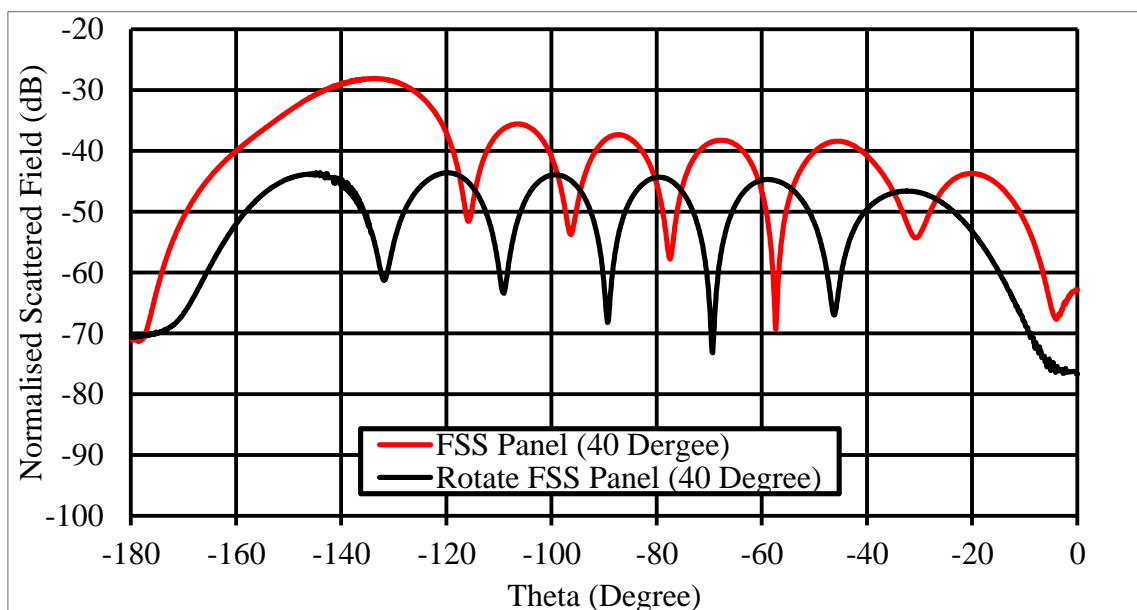


Figure 7-25: Comparison of Original and Rotated Unit Cell at Incident Angle of  $40^\circ$

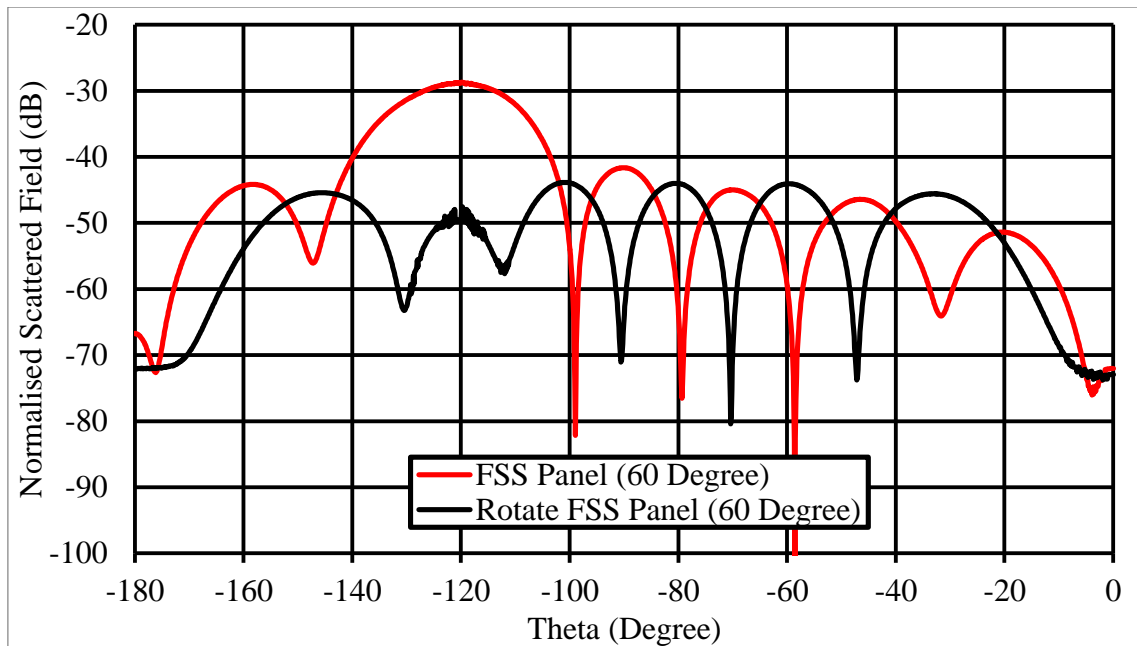


Figure 7-26: Comparison of Original and Rotated Unit Cell at Incident Angle of  $60^\circ$

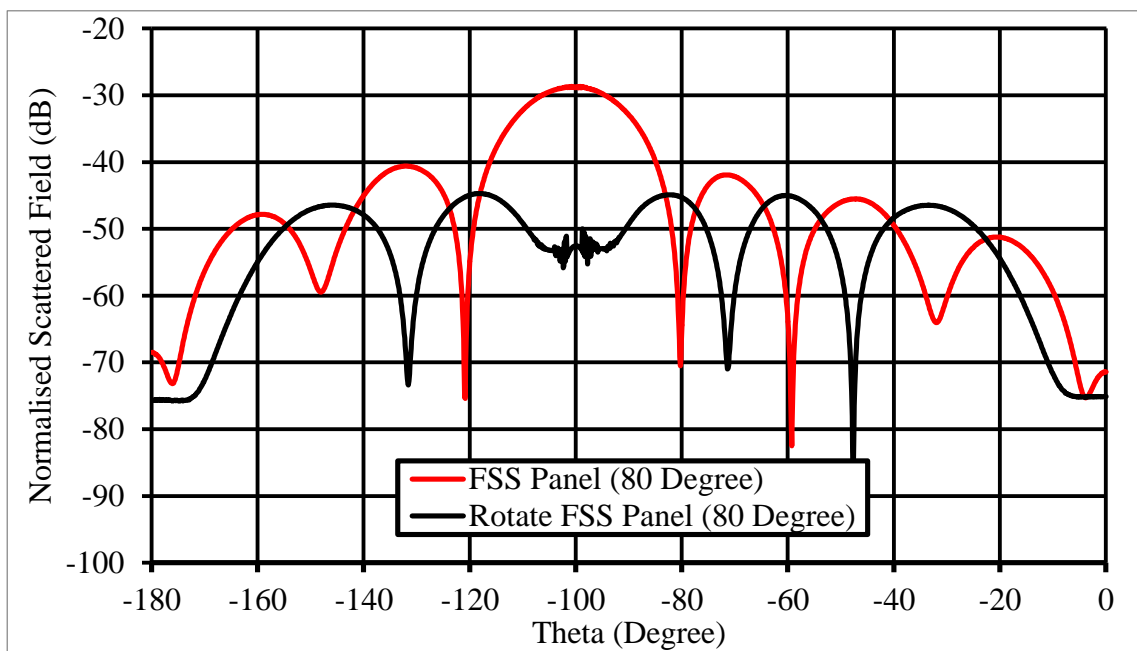


Figure 7-27: Comparison of Original and Rotated Unit Cell at Incident Angle of  $80^\circ$

Figure 7-28 shows the transmission response for the rotated unit cell at different incident angles.

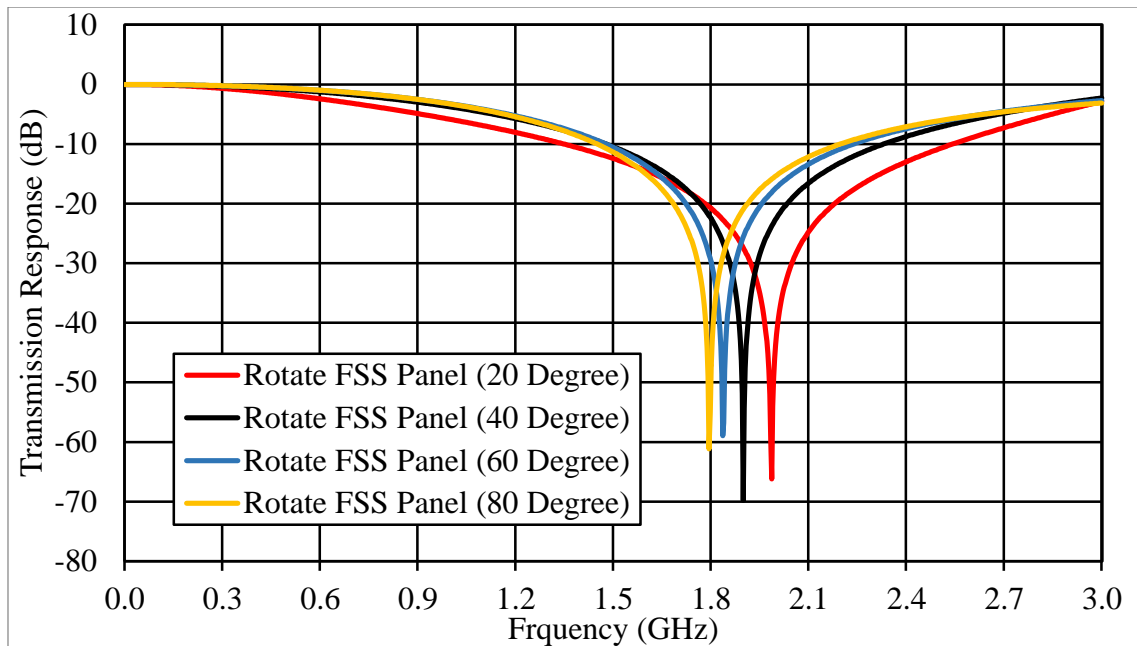


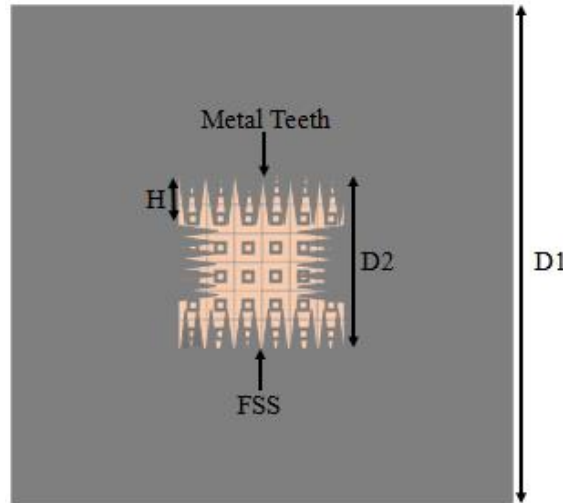
Figure 7-28: The Transmission Response for the Rotate FSS Panel

Table 7-3 compares the previous large panel FSS design with the new rotated panel for the specular scattering at 1.8GHz and normalised scattered field. It can be clearly seen that the rotated design has significantly improved the diffraction scattering ranging between -49dB to -76dB for the normalised scattered field. Although scattered fields are reduced, some values for the receiver angle (Theta) are still above the 60dB attenuation level to stop wireless communication.

| Incidence angles (Degrees) | Specular Scattering (dB) for Rotate Unit Cell | Normalised Scattered Field for Rotated Unit Cell (dB) |      |      |      | Normalised Scattered Field for Large Unit Cell (dB) |      |      |      |
|----------------------------|---|---|------|------|------|---|------|------|------|
|                            |   | -90°  | -70° | -50° | -20° | -90°  | -70° | -50° | -20° |
| 20°                        | -21   | -75   | -76  | -52  | -52  | -36   | -35  | -37  | -40  |
| 40°                        | -22   | -62   | -65  | -51  | -53  | -38   | -38  | -40  | -43  |
| 60°                        | -29   | -63   | -69  | -53  | -53  | -41   | -44  | -47  | -51  |
| 80°                        | -47   | -49   | -59  | -56  | -54  | -32   | -42  | -46  | -51  |

Table 7-3: Specular Scattering and Normalised Scattered Field of Rotated and Large Unit Cell FSS

The second method of adding metal teeth surrounding the window part that interfaces with the FSS will also help to reduce the scattering. This is shown in Figure 7-29, with the height of each metal tooth being 125mm and the FSS panel attached to the window part still operating at 1.8GHz.



|                     |                    |                  |
|---------------------|--------------------|------------------|
| $D_1=2000\text{mm}$ | $D_2=500\text{mm}$ | $H=125\text{mm}$ |
|---------------------|--------------------|------------------|

*Figure 7-29: FSS Panel with Metal Teeth attached to a Metal Wall*

The simulation results in Figure 7-30 to Figure 7-33 are the comparison of the FSS panel being attached to the window part with and without the metal teeth surrounding the interfacing window part at different incident angles. The scattered field levels are recorded in in Table 7-4 and they clearly show that the metal teeth surrounding the FSS will reduce the non-specular scattering.

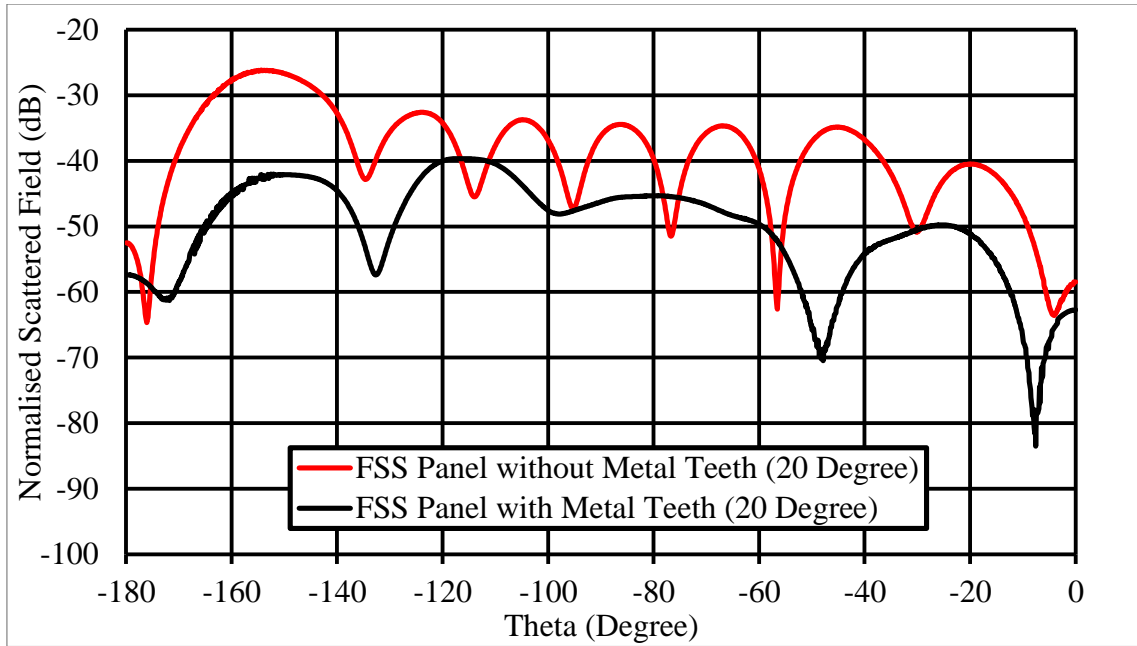


Figure 7-30: Comparison of FSS Panel , with and without Metal Teeth at Incident Angle of  $20^\circ$

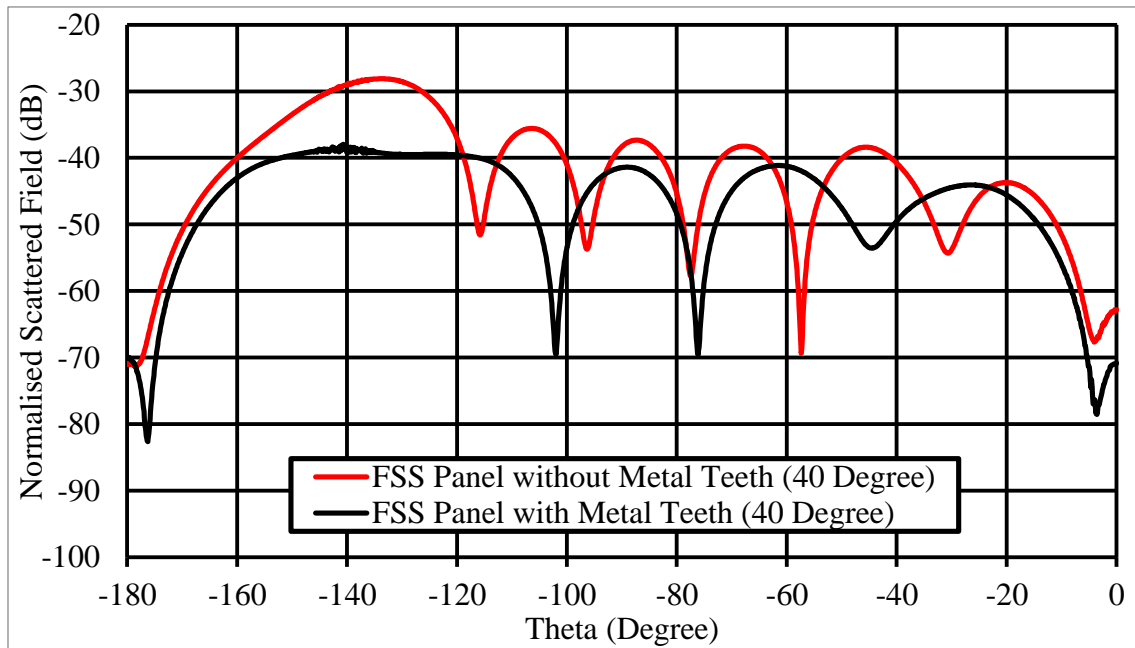


Figure 7-31: Comparison of FSS Panel , with and without Metal Teeth at Incident Angle of  $40^\circ$

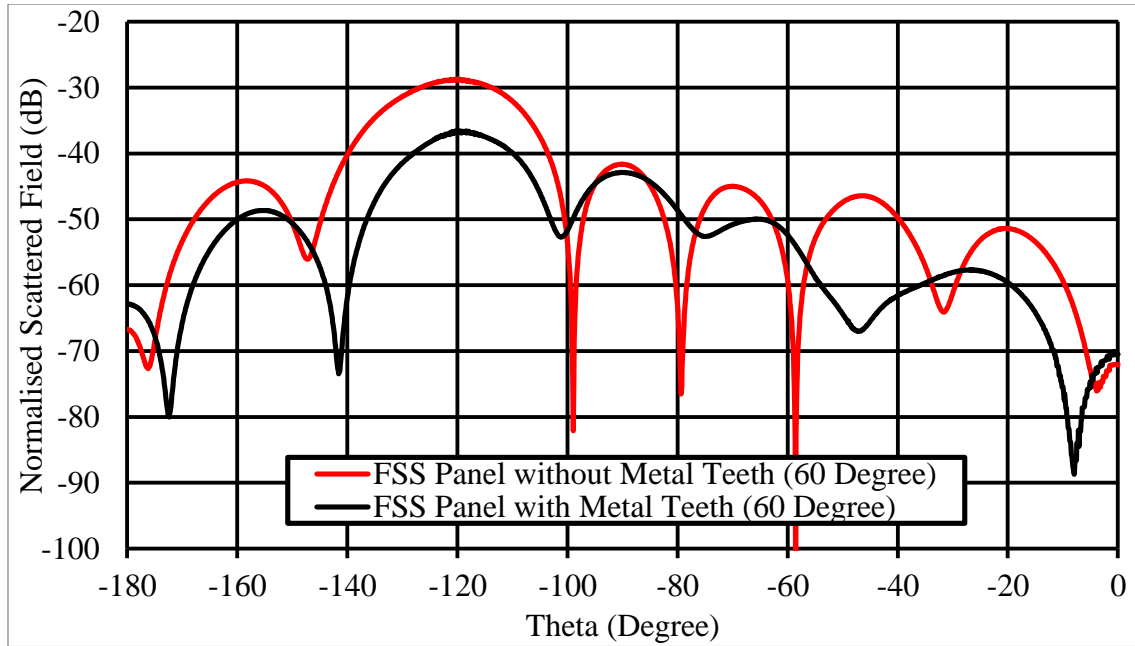


Figure 7-32: Comparison of FSS Panel , with and without Metal Teeth at Incident Angle of 60°

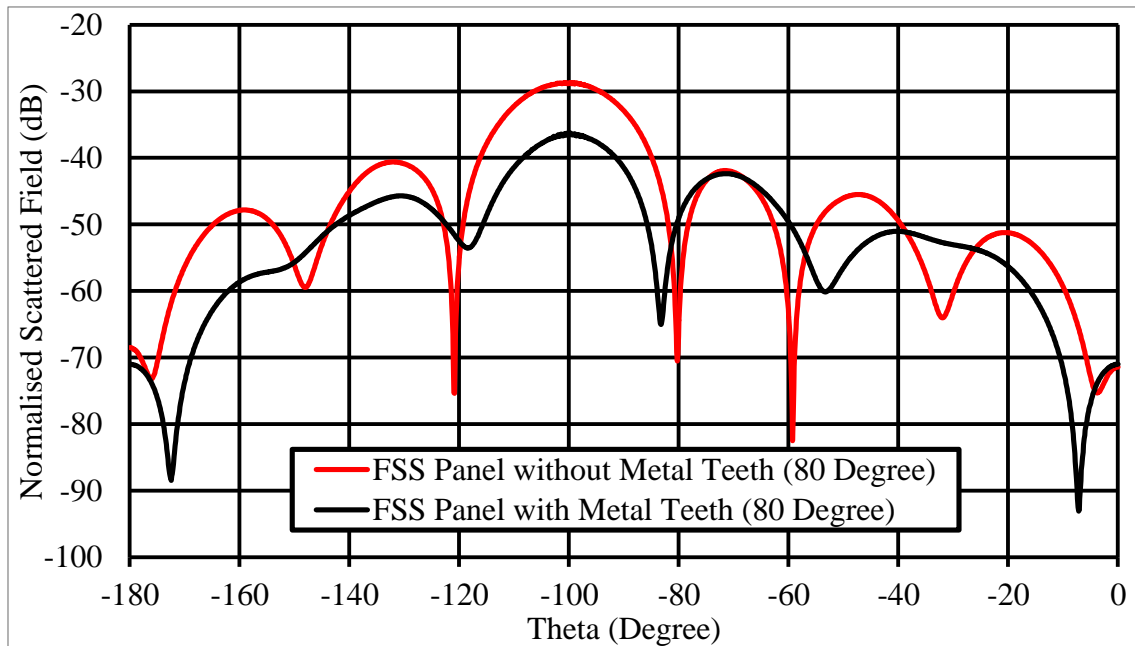


Figure 7-33: Comparison of FSS Panel , with and without Metal Teeth at Incident Angle of 80°

| Incidence angles (Degrees) | Normalised Scattered Field for Metal Teeth Panel (dB) |      |      |      | Normalised Scattered Field for Large Unit Cell Panel (dB) |      |      |      |
|----------------------------|---|------|------|------|---|------|------|------|
|                            | -90°  | -70° | -50° | -20° | -90°  | -70° | -50° | -20° |
| 20°                        | -46   | -46  | -65  | -51  | -36   | -35  | -37  | -40  |
| 40°                        | -41   | -44  | -47  | -45  | -38   | -38  | -40  | -43  |
| 60°                        | -42   | -50  | -64  | -59  | -41   | -44  | -47  | -51  |
| 80°                        | -41   | -42  | -56  | -56  | -32   | -42  | -46  | -51  |

*Table 7-4: Specular Scattering and Normalised Scattered Field of Metal Teeth and Large Unit Cell Panel*

### 7.3 Summary

This chapter illustrates the importance of FSS diffraction scattering for secure building applications in high signal strength areas. Measured results of a typical building show that attenuation levels of FSS may need to be greater than 60dB, in order to stop mobile communications. In such cases the methods for reducing the non-specular scattering mechanisms as well as traditional FSS design should be considered. For this reason, a 3D simulated wall surface model was produced in CST modelling software to observe a FSS non-specular scattering scenario. The scattered field of the wall surface is observed from different incident angles ranging from 20° to 80° by using radiation patterns in the format of a Cartesian plot. It has also been shown that suitable FSS design concepts are capable of reducing the non-specular scattering. e.g. smaller unit cells, rotated unit cells and metal teeth added to the perimeter of the FSS panel.

## CHAPTER 8 CONCLUSION

The objective of this research is to investigate the use of a FSS, for a special building application, e.g. for a prison, where a FSS could be used to block three mobile phone frequency bands GSM800 (890MHz - 960MHz), GSM1800 (1710MHz - 1875MHz) and UMTS (1920MHz - 2170MHz), but still allow TETRA (380MHz - 420MHz) which enables emergency calls to pass through.

Different types of classical passive FSS structures which could be used on buildings have been researched, where attenuation is normally between -30dB to -60dB depending on their shape and material. Current research shows that mobile phones can operate with received power levels as low as -120dBm. So to assess power levels to secure a build in different locations, a total of 249 prisons in the UK were analysed in order to work out the 2G cellular network signal quality. After analysing the power levels of different level security prisons from mobile operator's websites; it can be seen that a large proportion of prisons have a rated excellent signal quality and so a field test would need to be conducted in order to find out an average level of attenuation for this signal quality. These measurements were conducted using a portable spectrum analyser for both inside and outside of the Sir Frederick Mappin Building at the University of Sheffield. This location also had a rating of an excellent signal quality for fair comparison. Electric field strength measurements were carried out at 900MHz and 1800MHz for the 2G mobile networks. So from these obtained results, the possibility for a secured room would require at least an attenuation above 60dB in order to filter out the required signal bands in an excellent signal quality area.

Passive FSS are limited to attenuate a mobile phone signal to the required levels from the field tests. For this reason, innovation of a reconfigurable switching FSS structure has been designed and tested, which assumes the walls of the building have been perfectly shielded, and the signal can only propagate where the FSS is applied on a building aperture such as window. Also this aperture is assumed to be large enough with respect to the wavelength of the incoming signal such that diffraction effects can be ignored.

Two reconfigurable FSS panels have been designed, one is a reconfigurable single polarization FSS system, and another is a reconfigurable dual polarization FSS system. These two systems both use varactor diodes embedded into the FSS structure which are controlled by an external bias voltage. This change in voltage can rapidly change the

complex transmission response causing corruption to a received mobile phone signal. This means that the receiver inside the building cannot determine the data which was transmitted from outside the building from a base station.

Initially, these reconfigurable systems have been simulated in CST, where the capacitance of the diode can be controlled by an external bias voltage. The reconfigurable single polarization design uses diode (BB857), with capacitance varied from 0.45pF to 7.2pF. This allows for a reconfigurable single polarization FSS swept frequency response from 0.9GHz to 3.1GHz. The reconfigurable dual polarization FSS uses diode (BB131), with capacitance varied in a different range of 0.7pF to 1.7pF. This allowed for a reconfigurable dual polarization FSS swept frequency response from 0.6GHz to 2.98GHz by varying the capacitance. If the voltage is increased across the diode, the desired resonant frequency will be also increased. Both swept frequency ranges would be able cover the 2G and 3G mobile phone signal frequency ranges.

Further to this, the switching FSS design have been tested against the GSM protocol which has been simulated by coding in MATLAB. The design of this GSM framework is introduced in Chapter 4. Once GSM protocol is understood, the MATLAB simulation was configured to transmit a standard GSM signal at a data rate of 270.833kbits/s. The modulation scheme used is GMSK, with a GSM frame being split into eight bursts. As a frame time of 4.6ms is used a burst time of 0.577ms is calculated, with a total bit duration of 3.692  $\mu$ s.

Twelve elements of the GSM system are used in this research which are listed as follows: speech signal, convolutional coding, interleaving, differential encoding, GSMK modulation, channel, low-pass filtering, GSMK demodulation, MLSE, Differential decoding, de-interleaving and convolutional decoding. The function of each element has been introduced and comparisons of simulation results with results done by the previous work are performed.

To simulate results a random data stream is switched over a GSM channel, for a unit transmission coefficient magnitude of the FSS. The study focused on observations of varying phase. The bandwidth of the filter may vary depending on the receiver topology which is very important as it impacts the overall BER. The frequency spectrum of a switched GSM channel shows this phase switching technique shifts the energy at the carrier frequency to the sidebands, with these sidebands being odd multiples of the switching frequency. The frequency spectrum near the carrier (0Hz) is also an

attenuated version of the original baseband spectrum. e.g. When the switching frequency is 2.7MHz, the spectrum contains the original baseband data plus harmonics spaced  $n \cdot f_s$  apart, where  $n$  is an odd integer and the first harmonics being at 2.7 MHz, second at 8.1MHz and so on. If the receiver simulated uses a filter bandwidth of 270 kHz, the in-band signal is retained when filtered by the receiver. This allows for the attenuated baseband signal to be recovered, giving a BER of 0%. If the switching frequency is changed to 135 kHz, the low frequency switching causes the sidebands to be retained when filtered by the receiver. This makes it difficult to filter out the unwanted sideband energy, and therefore a BER of 42% is obtained.

2-D surface plots of the BER generated by MATLAB show the averaged BER for all GSM signals transmitted through the surface. Results are achieved by using 100 random seeds being switched in the same way using different phase values. Significant BER can be achieved over a large range of switching frequency and transmission phases. e.g. the signal impairment can be seen for switching frequencies as low as 1kHz and a high frequency cut-off being approximately 270 kHz when using a receiver filter with cutoff of 270 kHz.

The research continues by constructing a reconfigurable FSS to validate the MATLAB GSM protocol simulations. This is achieved by using a square wave being set at the required external bias voltage to imitate the phase switching performed in MATLAB. BER results seen varied between 0 and 35% depending on the applied voltage and the frequency in which the square wave is generated. These results closely matched the simulated results.

Additionally, the level of diffraction scattering from the edge of an FSS panel on the window aperture has been investigated. Non-specular scattering will be important for Non Line of Site, especially in high signal strength areas. A scenario has been created which assumed that the room is made of metal and is isolating, and that the mobile phone signal can only transmit through the window. To assess the far field scattering of the structure, the scattering radiation simulated from the far field scenarios of with and without the FSS were subtracted to provide the scattering from the FSS region only.

As previously discovered, a secure room required attenuation levels of over 60dB to prevent wireless communication. After comparison of the incident angle at different angles, the normalized scattered field of the example large unit cell was between -37dB to -51dB, causing a mobile phone to still pick up signals inside a secure building from

the base station. Methods to reduce non-specular scattering were investigated by creating three different types of FSS panels. The first design simulated was to alter the size of FSS unit cell to half the size of the original. Next a unit cell design rotated by  $45^\circ$  was simulated. Finally a design in which metal teeth were added to perimeter of the simulated FSS panel. All three designs kept the unit cell transmission response at 1.8GHz at normal incidence, with all having a reduction in the non-specular scattering to help prevent the signal leakage in the window aperture.

## CHAPTER 9 FUTURE WORK

### 9.1 Smart FSS design

In this research reconfigurable FSS has been designed and simulated in the CST simulation software, but has been modelled using cost effective materials which don't have transparent properties. Transparent reconfigurable FSS designs will need to be considered for use in window apertures to let the sunlight propagate through the surface.

Future work will also investigate multiband reconfigurable FSS to provide operation over a number of bands in present and future spectral usage. Techniques for enhancing and impairing wireless signals through time varying FSS performance will be investigated.

Additionally, future work will address issues such as FSS maintenance, durability and cost, with respect to the proposed lifetime of the technology.

### 9.2 3D building simulation

Realistic 3D models of scenarios such as offices, corridors, cupboards etc. will need to be implemented in commercial electromagnetic packages (CST, FEKO) to estimate the performance that a FSS designed in previous research work could deliver.

A combination of full field modelling and complex signal processing will be employed to evaluate and optimise the performance.

### 9.3 Verifying theoretical results with measurement results

To obtain reliable results, measurements will need to be carried out to validate the simulation results. A representative "building", which could be a scaled version of adjoining rooms or by modifying existing rooms, needs to be constructed. State of the art communications equipment will be used to transmit and receive signals in the representative building to assess the FSS performance. The communications group has manufactured a representative office space at its Buxton site, which will be used on this future project.

#### **9.4 Measurement of different concrete materials**

In more recent building structure designs, new composite concrete materials are to be used, which includes varying the different percentage of steel fibres contained within the concrete to improve strength. For future study, when a suitable FSS has been designed, the effect of this concrete material as a background also needs to be considered. The total attenuation can be measured by attaching the FSS in front of the concrete.

#### **9.5 Investigate Diffraction Scattering from FSS Panel with Missing Elements**

Traditional methods to manufacture a FSS involve chemically etching a metal film to form the required pattern. This can be expensive, so cheaper fabrication would be required for building application, such as inkjet technology; during this printing process, some elements may be missing from the FSS panel, and so in this case, the diffraction scattering needs to be investigated to calculate how much power will leak inside a room.

#### **9.6 Reconfigurable Switching FSS Switch over Different Modulation Schemes**

In this research, the modulation scheme GSMK has been employed for GSM. The concept has been to corrupt the mobile phone signal by phase switching. This method could be applied to other phase modulation schemes, such as: Quadrature Phase Shift Keying, for future research studies. The simulation and measurement for different phase modulation schemes will be investigated.

## BIBLIOGRAPHY

- [1] H. GRUBER, *The economics of mobile telecommunications*. US: Cambridge University Press, 2005.
- [2] (September 8, 2014). Can I use my mobile phone in an NHS hospital? Available:  
<http://www.nhs.uk/chq/pages/2146.aspx?CategoryID=68&SubCategoryID=162>
- [3] D. Walker. (May 22, 2014). Right to silence. Available:  
<http://news.bbc.co.uk/1/hi/magazine/3738652.stm>
- [4] (March 11, 2014). RF Shielding Products. Available: [http://www.mwt-materials.com/Products/RF\\_Shielding/rf\\_shielding.html](http://www.mwt-materials.com/Products/RF_Shielding/rf_shielding.html)
- [5] L. Hui Lai, K. L. Ford, and R. J. Langley, "Design Methodology for a Miniaturized Frequency Selective Surface Using Lumped Reactive Components," *Antennas and Propagation, IEEE Transactions on*, vol. 57, pp. 2732-2738, 2009.
- [6] Y. Ming and A. Brown, "Simulation of propagation through a frequency selective wall at 3 GHz," in *Antennas and Propagation (EuCAP), 2010 Proceedings of the Fourth European Conference on*, 2010, pp. 1-5.
- [7] J. C. Batchelor, E. A. Parker, B. Sanz-Izquierdo, J. B. Robertson, I. T. Ekpo, and A. G. Williamson, "Designing FSS for wireless propagation control within buildings," in *Antennas & Propagation Conference, 2009. LAPC 2009. Loughborough, 2009*, pp. 14-17.
- [8] B. Sanz-Izquierdo, J. B. Robertson, E. A. Parker, and J. C. Batchelor, "Minimal size of operation of fractal FSS," in *Antennas and Propagation Society International Symposium, 2009. APSURSI '09. IEEE, 2009*, pp. 1-4.
- [9] (September 9, 2013). Prisoner Category. Available:  
<http://www.offendersfamilieshelpline.org/index.php/prisoner-category/>
- [10] B. M. a. P. Turki, Edward A. and Ziai, Mohamed A. and Batchelor, John C. and Sanchez-Romaguera, Veronica and Yeates, Stephen, "Study of Clusters of Defects in Low-cost Digitally Fabricated Frequency Selective Surfaces," presented at the EuCAP 2014, Dan Haag, 2014.
- [11] M. Raspopoulos and S. Stavrou, "Frequency Selective Buildings Through Frequency Selective Surfaces," *Antennas and Propagation, IEEE Transactions on*, vol. 59, pp. 2998-3005, 2011.
- [12] B. Sanz-Izquierdo and E. A. Parker, "Dual Polarized Reconfigurable Frequency Selective Surfaces," *Antennas and Propagation, IEEE Transactions on*, vol. 62, pp. 764-771, 2014.
- [13] B. Sanz-Izquierdo, E. A. Parker, J. B. Robertson, and J. C. Batchelor, "Singly and Dual Polarized Convolved Frequency Selective Structures," *Antennas and Propagation, IEEE Transactions on*, vol. 58, pp. 690-696, 2010.
- [14] R. Mittra, C. H. Chan, and T. Cwik, "Techniques for analyzing frequency selective surfaces-a review," *Proceedings of the IEEE*, vol. 76, pp. 1593-1615, 1988.
- [15] B. A. Munk, *Frequency selective surfaces: theory and design* 2000.
- [16] B. Hooberman, "Everything You Ever Wanted to Know About Frequency-Selective Surface Filters but Were Afraid to Ask," 2005.
- [17] F. Bayatpur and K. Sarabandi, "Single-Layer High-Order Miniaturized-Element Frequency-Selective Surfaces," *Microwave Theory and Techniques, IEEE Transactions on*, vol. 56, pp. 774-781, 2008.

- [18] T.K.WU, Frequency Selective Surface and Grid Array: John Wiley & Sons Inc, 1995.
- [19] M. Raspopoulos and S. Stavrou, "Frequency selective surfaces on building materials - air gap impact," *Electronics Letters*, vol. 43, pp. 700-702, 2007.
- [20] (March 5, 2013). Notch Filter. Available: [http://tempest.das.ucdavis.edu/mmwave/notch\\_filter/notchfilter.htm](http://tempest.das.ucdavis.edu/mmwave/notch_filter/notchfilter.htm)
- [21] S. W. Lee and T. T. Fong, "Electromagnetic Wave Scattering from an Active Corrugated Structure," *Journal of Applied Physics*, vol. 43, pp. 388-396, 1972.
- [22] S. N. Azemi, K. Ghorbani, and W. S. T. Rowe, "A Reconfigurable FSS Using a Spring Resonator Element," *Antennas and Wireless Propagation Letters, IEEE*, vol. 12, pp. 781-784, 2013.
- [23] A. Munir, V. Fusco, and O. Malyuskin, "Tunable Frequency Selective Surfaces Characterisation," in *Microwave Conference, 2008. EuMC 2008. 38th European, 2008*, pp. 813-816.
- [24] B. Philips, E. A. Parker, and R. J. Langley, "Active FSS in an experimental horn antenna switchable between two beamwidths," *Electronics Letters*, vol. 31, pp. 1-2, 1995.
- [25] B. M. Cahill and E. A. Parker, "Field switching in an enclosure with active FSS screen," *Electronics Letters*, vol. 37, pp. 244-245, 2001.
- [26] G. I. Kiani, K. L. Ford, L. G. Olsson, K. P. Esselle, and C. J. Panagamuwa, "Switchable Frequency Selective Surface for Reconfigurable Electromagnetic Architecture of Buildings," *Antennas and Propagation, IEEE Transactions on*, vol. 58, pp. 581-584, 2010.
- [27] D. William C.Lee, N.J., "Covert Communication Sysrem," *United States Patent*, 1984.
- [28] B. Chambers, A. Melnikov, and A. Tennant, "Performance of a phase switched screen against a pulse compression radar system," in *Antennas and Propagation Society International Symposium, 2004. IEEE, 2004*, pp. 4248-4251 Vol.4.
- [29] B. Chambers and A. Tennant, "Influence of switching-waveform characteristics on the performance of a single-layer-phase switched screen," *Electromagnetic Compatibility, IEEE Transactions on*, vol. 44, pp. 434-441, 2002.
- [30] B. Chambers and A. Tennant, "General analysis of the phase-switched screen .1. The single layer case," *Radar, Sonar and Navigation, IEE Proceedings -*, vol. 149, pp. 243-247, 2002.
- [31] B. Chambers and A. Tennant, "Single layer phase-switched screen using double-diode switching elements," *Electronics Letters*, vol. 39, pp. 1150-1152, 2003.
- [32] B. Chambers and A. Tennant, "The phase-switched screen," *Antennas and Propagation Magazine, IEEE*, vol. 46, pp. 23-37, 2004.
- [33] A. Tennant and B. Chambers, "Experimental two-layer adaptive phase-switched screen," *Electronics Letters*, vol. 37, pp. 1379-1380, 2001.
- [34] A. Tennant and B. Chambers, "Space-time analysis of phase-switched screens," in *Antennas and Propagation Society International Symposium, 2007 IEEE, 2007*, pp. 6035-6038.
- [35] A. Tennant and B. Chambers, "Experimental performance of a phase-switched screen against modulated microwave signals," *Radar, Sonar and Navigation, IEE Proceedings -*, vol. 152, pp. 29-33, 2005.
- [36] B. Chambers and A. Tennant, "A smart radar absorber based on the phase-switched screen," *Antennas and Propagation, IEEE Transactions on*, vol. 53, pp. 394-403, 2005.
- [37] A. Tennant, "Reflection properties of a phase modulating planar screen," *Electronics Letters*, vol. 33, pp. 1768-1769, 1997.

- [38] E. A. a. A. Parker, C. and Simpson, N.E., "Microwave band FSS in optically transparent conducting layers: Performance of ring element arrays," *Microwave and Optical Technology Letters*, vol. 16, 1997.
- [39] C. T. C. Mias, C. Oswald, "An Investigation into the Feasibility of designing Frequency Selective Windows employing periodic structures," The Nottingham Trent University, UK2001.
- [40] J. Hirai and I. Yokota, "Electromagnetic shielding glass of frequency selective surfaces," in *Electromagnetic Compatibility, 1999 International Symposium on*, 1999, pp. 314-316.
- [41] K. Yong-Jin, N. Sung-Soo, and L. Hong-Min, "Frequency selective surface superstrate for wideband code division multiple access system," in *Wireless Technology Conference, 2009. EuWIT 2009. European*, 2009, pp. 33-36.
- [42] B. Sanz-Izquierdo, E. A. Parker, J. B. Robertson, J. C. Batchelor, M. J. Neve, and A. G. Williamson, "Interwoven loops for electromagnetic architecture of buildings," in *Antennas and Propagation Society International Symposium (APSURSI), 2010 IEEE*, 2010, pp. 1-4.
- [43] J. Y. Dongho Kim, and Jaekick Choi, "Compact Spatial Triple-Band-Stop Filter for Cellular/PCS/IMT-2000 Systems," *ETRI*, vol. 30, 2008.
- [44] D. C. K. Lee, K. W. Sowerby, and M. J. Neve, "Shielding strategies for interference mitigation in indoor wireless communications with frequency selective surfaces," in *Antennas and Propagation Society International Symposium, 2005 IEEE*, 2005, pp. 260-263 vol. 3B.
- [45] S. Stavrou and S. R. Saunders, "Review of constitutive parameters of building materials," in *Antennas and Propagation, 2003. (ICAP 2003). Twelfth International Conference on (Conf. Publ. No. 491)*, 2003, pp. 211-215 vol.1.
- [46] G. H. H. Sung, K. W. Sowerby, and A. G. Williamson, "The impact of frequency selective surfaces applied to standard wall construction materials," in *Antennas and Propagation Society International Symposium, 2004. IEEE*, 2004, pp. 2187-2190 Vol.2.
- [47] R. Piesiewicz, C. Jansen, D. Mittleman, T. Kleine-Ostmann, M. Koch, and T. Kurner, "Scattering Analysis for the Modeling of THz Communication Systems," *Antennas and Propagation, IEEE Transactions on*, vol. 55, pp. 3002-3009, 2007.
- [48] R. A. Dalke, C. L. Holloway, P. McKenna, M. Johansson, and A. S. Ali, "Effects of reinforced concrete structures on RF communications," *Electromagnetic Compatibility, IEEE Transactions on*, vol. 42, pp. 486-496, 2000.
- [49] A. C. M. Austin, M. J. Neve, G. B. Rowe, and R. J. Pirkl, "Modeling the Effects of Nearby Buildings on Inter-Floor Radio-Wave Propagation," *Antennas and Propagation, IEEE Transactions on*, vol. 57, pp. 2155-2161, 2009.
- [50] H. Oka, K. Narita, H. Osada, and K. Seki, "Experimental results on indoor electromagnetic wave absorber using magnetic wood," *Journal of Applied Physics*, vol. 91, pp. 7008-7010, 2002.
- [51] K. Kimura and O. Hashimoto, "Three-layer wave absorber using common building material for wireless LAN," *Electronics Letters*, vol. 40, pp. 1323-1324, 2004.
- [52] P. Jaturatussanai, M. Chamchoy, and S. Promwong, "Characteristics of UWB propagation through building materials," in *Communications and Information Technology, 2005. ISCIT 2005. IEEE International Symposium on*, 2005, pp. 987-990.

- [53] I. K. Appleton, "The GSM protocol stack," in *The Design of Digital Cellular Handsets* (Ref. No. 1998/240), IEE Colloquium on, 1998, pp. 9/1-9/5.
- [54] M. W. Siegmund H. Redl, Malcolm W. Oliphant, *An Introduction to GSM First Edition* edition ed. London: Artech House, Incorporated, 1995.
- [55] E. B. Tchikaya, A. Rashid, F. Khalil, H. Aubert, H. Legay, and N. J. G. Fonseca, "Multi-scale approach for the electromagnetic modeling of metallic FSS grids of finite thickness with non-uniform cells," in *Microwave Conference, 2009. APMC 2009. Asia Pacific, 2009*, pp. 1485-1488.
- [56] Y. Ming and A. K. Brown, "A Hybrid Model for Radio Wave Propagation Through Frequency Selective Structures (FSS)," *Antennas and Propagation, IEEE Transactions on*, vol. 58, pp. 2961-2968, 2010.
- [57] (2001 February 6, 2013). How Mobile Phone Networks Work Available: <http://www.ofcom.org.uk/static/archive/ra/topics/mpsafety/school-audit/mobilework.htm>
- [58] (February 6, 2013). Mobile Phone Technology. Available: <http://www.dti.gov.uk/files/file35411.pdf>
- [59] A. Ray and S. Prakriya, "A subspace based approach for channel estimation and equalization in GSM receivers," in *Personal Wireless Communications, 2002 IEEE International Conference on*, 2002, pp. 134-137.
- [60] M. Drutarovsky, "GSM Channel Equalization Algorithm - Modern DSP Coprocessor Approach " *Radioengineering*, vol. 8, p. 27, 1999.
- [61] M. Drutarovsky, "GSM Channel Equalization Algorithm - Modern DSP Coprocessor Approach," 1999.
- [62] L. H. C. Lee and P. G. Farrell, "Concatenated coding and interleaving for half-rate GSM digital mobile radio system," *Electronics Letters*, vol. 27, pp. 1274-1276, 1991.
- [63] S. G. Ibrahim M. M. EL EMARY, Hamzeh AL-JAZAZZI, "Testing the performance of GSM using a proposed semi automated method," *Scientific Bulletin of the University of Pitesti*, vol. 2, p. 45, 2009.
- [64] (March 5, 2012). Digital Modulation and GMSK. Available: <http://www.emc.york.ac.uk/reports/linkpcp/appD.pdf>
- [65] M. Pukkila, "Channel Estimation Modeling," *Nokia Research Center* 2000.
- [66] (May 6, 2012). Digital cellular telecommunications system. Available: [http://www.etsi.org/deliver/etsi\\_ts/100900\\_100999/100908/08.11.00\\_60/ts\\_100908v081100p.pdf](http://www.etsi.org/deliver/etsi_ts/100900_100999/100908/08.11.00_60/ts_100908v081100p.pdf)
- [67] J. Brøndum, "GSM data receiver structures," Technical report, Institute for Electronic Systems Department of Communication Technology 1993.
- [68] G. J. Wheeler, *Introduction to Microwaves*: Prentice-Hall, 1963.
- [69] R. J. Langley and E. A. Parker, "Double-Square Frequency-Selective Surfaces and their Equivalent-Circuit," *Electronics Letters*, vol. 19, pp. 675-677, 1983.
- [70] K. Sarabandi and N. Behdad, "A frequency selective surface with miniaturized elements," *IEEE Transactions on Antennas and Propagation*, vol. 55, pp. 1239-1245, May 2007.
- [71] H. L. Liu, K. L. Ford, and R. J. Langley, "Design Methodology for a Miniaturized Frequency Selective Surface Using Lumped Reactive Components," *IEEE Transactions on Antennas and Propagation*, vol. 57, pp. 2732-2738, Sep 2009.
- [72] K. L. Ford and B. Chambers, "Improvement in the low frequency performance of geometric transition radar absorbers using square loop impedance layers," *IEEE Transactions on Antennas and Propagation*, vol. 56, pp. 133-141, Jan 2008.

- 
- [73] E. A. Parker, J. C. Batchelor, R. Chiang, A. G. Williamson, B. Sanz-Izquierdo, M. J. Neve, et al., "Frequency selectively screened office incorporating convoluted FSS window," *Electronics Letters*, vol. 46, pp. 317-U24, Mar 2010.
- [74] J. Roberts, J. M. Rigelsford, and K. L. Ford, "Diffraction from Frequency Selective Surfaces for secure building applications," in *Antennas and Propagation (EUCAP), 2012 6th European Conference on*, 2012, pp. 2388-2391.

## APPENDIX I: PRISON LIST

| Prison Name               | Address  | Post Code | Category | OP-A | OP-B | OP-C | OP-D |
|---------------------------|--|-----------|----------|------|------|------|------|
| HMP MANCHESTER            | Southall Street, Strangeways,<br>MANCHESTER                            | M60 9AH   | A        | 5    | 5    | 2    | 5    |
| HMP ALTCOURSE             | Higher Lane, Fazakerley,<br>LIVERPOOL                                  | L9 7LH    | A        | 5    | 5    | 2    | 5    |
| HMP/YOI<br>DONCASTER      | Off North Bridge, Marshgate,<br>DONCASTER, South<br>Yorkshire          | DN5 8UX   | A        | 5    | 5    | 2    | 5    |
| HMP BOWHOUSE              | Mauchline Road,<br>Bowhouse, KILMARNOCK,<br>East Ayrshire              | KA1 5AA   | A        | 5    | 3    | 1    | 5    |
| HMP & IDC<br>MAGHABERRY   | 17, Old Road,<br>Upper Ballinderry,<br>LISBURN, Co.Antrim              | BT28 2PT  | A        | 5    | 4    | 2    | 5    |
| HMP SHOTTS NIC            | HMP Shotts<br>Newmill & Canthill Road,<br>SHOTTS,<br>North Lanarkshire | ML7 4LE   | A B      | 3    | 4    | 1    | 4    |
| HMP PETERHEAD             | South Road,<br>PETERHEAD,<br>Aberdeenshire                             | AB42 2YY  | A B      | 5    | 4    | 1    | 5    |
| HMP GLENOCHIL             | King O'Muir Road,<br>Tullibody, ALLOA,<br>Clackmannanshire             | FK10 3AD  | A B C    | 5    | 5    | 1    | 5    |
| HMP/YOI<br>EDMUNDS HILL   | Stradishall, NEWMARKET,<br>Suffolk                                     | CB8 9YG   | A B C D  | 5    | 2    | 2    | 3    |
| HMP PERTH                 | 3, Edinburgh Road,<br>PERTH,<br>Perthshire & Kinross                   | PH2 8AT   | A C      | 5    | 5    | 2    | 5    |
| HMP ALBANY                | 55, Parkhurst Road,<br>Parkhurst, NEWPORT,<br>Isle of Wight            | PO30 5RS  | B        | 4    | 5    | 2    | 5    |
| HMP PRESTON               | 2 Ribbleton Lane,<br>PRESTON,<br>Lancashire                            | PR1 5AB   | B        | 5    | 5    | 2    | 5    |
| HSH BROADMOOR<br>HOSPITAL | The Terrace, Upper<br>Broadmoor Road,<br>CROWTHORNE,<br>Berkshire      | RG45 7EG  | B        | 5    | 5    | 2    | 5    |
| HMYOI<br>WERRINGTON       | Werrington, STOKE-ON-<br>TRENT,<br>Staffordshire                       | ST9 0DX   | B        | 5    | 5    | 2    | 5    |
| HMYOI<br>AYLESBURY        | Bierton Road,<br>AYLESBURY,<br>Bucks                                   | HP20 1EH  | B        | 5    | 5    | 2    | 5    |
| HMP BEDFORD               | St. Loyes Street,<br>BEDFORD   | MK40 1HG  | B        | 5    | 5    | 2    | 5    |
| HMP BIRMINGHAM            | Winson Green Road,<br>BIRMINGHAM                                       | B18 4AS   | B        | 5    | 4    | 2    | 5    |
| HMP<br>BLAKENHURST        | Hewell Lane, REDDITCH,<br>Worcestershire                               | B97 6QS   | B        | 5    | 4    | 1    | 5    |
| HMP BLUNDESTON            | Lakeside Rise, Blundeston,<br>LOWESTOFT, Suffolk                       | NR32 5BG  | B        | 5    | 5    | 1    | 4    |

|                       |  |          |   |   |   |   |   |
|-----------------------|--|----------|---|---|---|---|---|
| HMP BRISTOL           | 19, Cambridge Road,<br>Horfield,<br>BRISTOL                      | BS7 8PS  | B | 5 | 5 | 2 | 5 |
| HMP BRIXTON           | PO Box 369, Jebb Avenue,<br>LONDON                               | SW2 5XF  | B | 5 | 5 | 2 | 5 |
| HMP BRONZEFIELD       | Woodthorpe Road,<br>Ashford, STAINES<br>London                   | TW15 3JZ | B | 5 | 5 | 2 | 5 |
| HMP BULLINGDON        | PO Box 50,<br>Patrick Haugh Road, Arncoth,<br>Nr. BICESTER, Oxon | OX6 0PZ  | B | 5 | 3 | 2 | 5 |
| HMP/RC CARDIFF        | Knox Road, CARDIFF   | CF24 0UG | B | 5 | 5 | 2 | 5 |
| HMP/YOI<br>CHELMSFORD | 200, Springfield Road,<br>CHELMSFORD,<br>Essex                   | CM2 6LQ  | B | 5 | 5 | 2 | 5 |
| HMP DOVEGATE          | off Moreton Lane,<br>Marchington, UTTOXETER,<br>Staffordshire    | ST14 8XR | B | 5 | 4 | 2 | 5 |
| HMP/YOI EXETER        | New North Road, EXETER,<br>Devon                                 | EX4 4EX  | B | 5 | 5 | 2 | 5 |
| HMP GARTH             | Ulnes Walton Lane, Leyland,<br>PRESTON, Lancashire               | PR26 8NE | B | 4 | 4 | 1 | 5 |
| HMP GARTREE           | Gallow Field Road,<br>MARKET HARBOROUGH,<br>Leicestershire       | LE16 7RP | B | 5 | 3 | 1 | 5 |
| HMP/YOI<br>GLOUCESTER | Barrack Square,<br>GLOUCESTER                                    | GL1 2JN  | B | 5 | 5 | 2 | 5 |
| HMP GRENDON           | Edgcott,<br>AYLESBURY, Bucks                                     | HP18 0TL | B | 4 | 3 | 1 | 4 |
| HMP HOLME<br>HOUSE    | Holme House Road,<br>STOCKTON-ON-TEES,<br>Cleveland              | TS18 2QU | B | 5 | 5 | 2 | 5 |
| HMP KINGSTON          | 122, Milton Road,<br>PORTSMOUTH, Hampshire                       | PO3 6AS  | B | 5 | 5 | 2 | 5 |
| HMP LEEDS             | 2, Gloucester Terrace,<br>Armley, LEEDS, West<br>Yorkshire       | LS12 2TJ | B | 5 | 5 | 2 | 5 |
| HMP LEICESTER         | Welford Road, LEICESTER  | LE2 7AJ  | B | 5 | 5 | 2 | 5 |
| HMP/YOI LEWES         | 1, Brighton Road,<br>LEWES, East Sussex                          | BN7 1EA  | B | 5 | 5 | 2 | 5 |
| HMP LIVERPOOL         | 68, Hornby Road,<br>LIVERPOOL                                    | L9 3DF   | B | 5 | 5 | 2 | 5 |
| HMP LOWDHAM<br>GRANGE | Lowdham, NOTTINGHAM,<br>Nottinghamshire                          | NG14 7DA | B | 4 | 4 | 1 | 5 |
| HMP MAIDSTONE         | 36, County Road,<br>MAIDSTONE,<br>Kent                           | ME14 1UZ | B | 5 | 5 | 2 | 5 |
| HMP NOTTINGHAM        | Perry Road, Sherwood,<br>NOTTINGHAM                              | NG5 3AG  | B | 5 | 5 | 2 | 5 |
| HMP/YOI PARC          | Heol Hopcyn John, Coity,<br>BRIDGEND, Mid-<br>Glamorgan          | CF35 6AR | B | 5 | 3 | 2 | 5 |

|                         |   |          |   |   |   |   |   |
|-------------------------|---|----------|---|---|---|---|---|
| HMP PARKHURST           | Clissold Road,<br>Parkhurst, NEWPORT,<br>Isle of Wight  | PO30 5NX | B | 4 | 5 | 2 | 5 |
| HMP PENTONVILLE         | Caledonian Road, LONDON   | N7 8TT   | B | 5 | 5 | 2 | 5 |
| HMP<br>PETERBOROUGH     | Saville Road,<br>Westwood,<br>PETERBOROUGH,<br>Cambridgeshire   | PE3 7PD  | B | 5 | 5 | 2 | 5 |
| HMP RYE HILL            | Willoughby, RUGBY<br>Warwickshire   | CV23 8SZ | B | 5 | 4 | 1 | 5 |
| HMP SHREWSBURY          | The Dana, SHREWSBURY,<br>Shropshire   | SY1 2HR  | B | 5 | 5 | 2 | 5 |
| HMP SWALESIDE           | Barbazon Road, Eastchurch,<br>SHEERNESS, Isle of<br>Sheppey,<br>Kent  | ME12 4AX | B | 4 | 3 | 1 | 5 |
| HMP SWANSEA             | 200, Oystermouth Road,<br>SWANSEA,<br>West Glamorgan  | SA1 3SR  | B | 5 | 5 | 2 | 5 |
| HMP<br>WANDSWORTH       | PO Box 757, Heathfield<br>Road,<br>Wandsworth LONDON  | SW18 3HS | B | 5 | 5 | 2 | 5 |
| HMP WINCHESTER          | Romsey Road,<br>WINCHESTER,<br>Hampshire  | SO22 5DF | B | 5 | 5 | 2 | 5 |
| HMP WOLDS               | Sands Lane, Everthorpe,<br>BROUGH, East Yorkshire   | HU15 2JZ | B | 4 | 2 | 2 | 5 |
| HMP WORMWOOD<br>SCRUBS  | PO Box 757, Du Cane Road,<br>LONDON   | W12 0AE  | B | 5 | 5 | 2 | 5 |
| HSH ASHWORTH<br>EAST    | School Lane,<br>Parkbourn, Maghull,<br>LIVERPOOL  | L31 1HW  | B | 5 | 5 | 2 | 5 |
| MSU EDENFIELD<br>Centre | Prestwich Hospital,<br>Valley Park Road,<br>off Bury New Rd (A56),<br>Prestwich, MANCHESTER                                 | M25 3BL  | B | 5 | 5 | 2 | 5 |
| STC BRENTWOOD           | Nr. St. Charles Road,<br>off Weald Road,<br>BRENTWOOD, Essex  | CM14 4TP | B | 5 | 5 | 2 | 5 |
| STC GLYNNEATH           | Nr. Derifach (B4242),<br>Glynneath Business Park,<br>Cwmgwrach, Glyn-Neath,<br>Vale of Neath, NEATH,<br>Neath & Port Talbot | SA11 5PY | B | 3 | 4 | 2 | 5 |
| STC<br>HASOCKFIELD      | Corbridge Road, Medomsley,<br>CONSETT, County Durham  | DH8 6QY  | B | 5 | 5 | 1 | 5 |
| STC MEDWAY              | off Sir Evelyn Road,<br>Chatham, ROCHESTER,<br>Kent   | ME1 3YB  | B | 5 | 5 | 2 | 5 |
| STC OAKHILL             | Tattenhoe Street,<br>Woodhill, MILTON<br>KEYNES,<br>Bucks   | MK5 6AH  | B | 4 | 4 | 1 | 5 |
| STC RAINSBROOK          | Willoughby, Nr. RUGBY,<br>Warwickshire  | CV23 8SY | B | 5 | 4 | 1 | 5 |
| HMP BARLINNIE           | 81, Lee Avenue,<br>Barlinnie,<br>GLASGOW  | G33 2QX  | B | 5 | 5 | 2 | 5 |

|                     |   |          |     |   |   |   |   |
|---------------------|---|----------|-----|---|---|---|---|
| HMP/YOI FOREST BANK | Agecroft Road, Pendlebury, MANCHESTER   | M27 8FB  | B C | 5 | 5 | 2 | 5 |
| MSU CANE HILL       | Brighton Road, Coulsdon, CROYDON, Kent  | CR5 3YL  | B C | 4 | 5 | 2 | 5 |
| MSU CHADWICK LODGE  | Chadwick Drive, Eaglestone, MILTON KEYNES, Buckinghamshire                                    | MK6 5LS  | B C | 5 | 5 | 2 | 5 |
| MSU COASTLANDS      | Northgate Hospital, Great Yarmouth, Norfolk   | NR30 1BU | B C | 5 | 4 | 2 | 5 |
| MSU CROZIER TERRACE | 1, Crozier Terrace, Hackney, LONDON   | E9 6BE   | B C | 5 | 5 | 2 | 5 |
| MSU GUILD LODGE     | Guild Park, Whittingham Lane, Goosnargh, PRESTON Lancashire                                   | PR3 2JH  | B C | 4 | 3 | 1 | 5 |
| MSU LANGDALE        | Whittingham Hospital, Whittingham Lane, Goosnargh, PRESTON Lancashire                         | PR3 3JH  | B C | 3 | 5 | 0 | 5 |
| MSU RAVENSWOOD      | Ravenswood House, Knowle Hospital, FAREHAM, Hampshire   | PO17 5NA | B C | 4 | 4 | 1 | 5 |
| MSU REASIDE Clinic  | Reaside Drive, Birmingham Great Park, Bristol Road South, Rubery, BIRMINGHAM                  | B45 9BE  | B C | 4 | 5 | 2 | 5 |
| HMP CORNTON VALE    | Cornton Road, STIRLING, Stirling  | FK9 5NU  | B C | 5 | 5 | 2 | 5 |
| MSU BLAIR UNIT      | Royal Cornhill Hospital, Grampian University NHS Trust, Cornhill Road, ABERDEEN Aberdeenshire | AB9 2ZH  | B C | 5 | 5 | 2 | 5 |
| MSU PERTH           | Murray Royal Hospital, Muirhall Road, Kinnoull, PERTH, Perthshire & Kinross                   | PH2 7BH  | B C | 5 | 3 | 2 | 5 |
| MSU ORCHARD CLINIC  | Royal Edinburgh Hospital, 51, Morningside Place, Morningside, EDINBURGH                       | EH10 5HF | B C | 5 | 5 | 2 | 5 |
| MSU PAISLEY         | Dykebar Hospital Grahamston Road, Dykebar, PAISLEY, Renfrewshire                              | PA2 7DE  | B C | 5 | 5 | 2 | 5 |
| MSU STOBHILL        | Stobhill NHS Trust Hospital, 133, Balornock Road, Springburn, GLASGOW                         | G21 3UW  | B C | 5 | 5 | 2 | 5 |
| RSU SHANNON CLINIC  | Knockbracken Healthcare Park, Saintfield Road, BELFAST  | BT8 8BH  | B C | 4 | 5 | 2 | 5 |
| HMP DORCHESTER      | North Square, DORCHESTER, Dorset  | DT1 1JD  | B C | 5 | 5 | 2 | 5 |

|                         |  |          |       |   |   |   |   |
|-------------------------|--|----------|-------|---|---|---|---|
| HMYOI LOW NEWTON        | Finchale Avenue, Framwellgate Moor, Brasside, DURHAM                     | DH1 5SD  | B C   | 5 | 5 | 2 | 5 |
| HMP/YOI NORWICH         | Knox Road, Mousehold, NORWICH, Norfolk                                   | NR1 4LU  | B C   | 5 | 5 | 2 | 5 |
| MCTC COLCHESTER         | Berechurch Hall Road, COLCHESTER, Essex                                  | CO2 9NU  | B C   | 4 | 4 | 1 | 4 |
| HMP LOW MOSS            | 190, Crosshill Road, Bishopbriggs, GLASGOW                               | G64 2QB  | B C   | 5 | 5 | 1 | 5 |
| HMYOI POLMONT           | Redding Road, Brightons, FALKIRK, Stirlingshire                          | FK2 0AB  | B C   | 5 | 4 | 2 | 5 |
| HMP MAGILLIGAN          | Point Road, Magilligan, LIMAVADY, Co.(London)derry                       | BT49 0LR | B C   | 5 | 3 | 0 | 5 |
| RS ST. MARY'S KENMURE   | St. Mary's Road, Bishopbriggs, GLASGOW, East Dunbartonshire              | G64 2EH  | B C D | 5 | 5 | 2 | 5 |
| HMP CANTERBURY          | 46, Longport, CANTERBURY, Kent   | CT1 1PJ  | C     | 5 | 5 | 2 | 5 |
| HMP/YOI CASTINGTON      | Wansbeck Road, Acklington, Nr. Amble, MORPETH, Northumberland            | NE65 9XG | C     | 4 | 3 | 1 | 4 |
| HMYOI DEERBOLT          | Bowes Road, BARNARD CASTLE, County Durham                                | DL12 9BG | C     | 4 | 5 | 2 | 5 |
| HMYOI/RC FELTHAM        | Bedfont Road, FELTHAM, Middlesex   | TW13 4ND | C     | 5 | 4 | 2 | 5 |
| HMYOI/RC GLEN PARVA     | 10, Tigers Road, Wigston, LEICESTER                                      | LE18 4TN | C     | 5 | 5 | 2 | 5 |
| HMP HINDLEY             | Gibson Street, Bickershaw, WIGAN, Lancashire                             | WN2 5TH  | C     | 5 | 5 | 2 | 5 |
| HMP/YOI LANCASTER FARMS | Far Moor Lane, Stone Row Head, off Quernmore Road, LANCASTER, Lancashire | LA1 3QZ  | C     | 5 | 4 | 1 | 5 |
| HMYOI NORTHALLERTON     | 15a, East Road, NORTHALLERTON, North Yorkshire                           | DL6 1NW  | C     | 5 | 5 | 2 | 5 |
| HMYOI ONLEY             | Willoughby, RUGBY, Warwickshire  | CV23 8AP | C     | 5 | 4 | 1 | 5 |
| HMYOI PORTLAND          | Easton, PORTLAND, Dorset   | DT5 1DF  | C     | 5 | 4 | 2 | 5 |
| HMYOI & RC READING      | Forbury Road, READING, Berks   | RG1 3HY  | C     | 5 | 5 | 2 | 5 |
| HMYOI STOKE HEATH       | Stoke Heath, MARKET DRAYTON, Shropshire                                  | TF9 2JL  | C     | 3 | 2 | 2 | 5 |
| HMYOI SWINFEN HALL      | Swinfen, LICHFIELD, Staffs   | WS14 9QS | C     | 5 | 5 | 1 | 5 |
| HMYOI WETHERBY          | York Road, WETHERBY, West Yorkshire                                      | LS22 5ED | C     | 5 | 5 | 2 | 5 |
| YTC GLENTHORNE          | Kingsbury Road, Erdington, BIRMINGHAM                                    | B24 9SA  | C     | 5 | 5 | 2 | 5 |
| YTC ST. CHARLES         | Nr. St. Charles Road, off Weald Road, BRENTWOOD, Essex                   | CM14 4TP | C     | 5 | 5 | 2 | 5 |

|                            |   |          |   |   |   |   |   |
|----------------------------|---|----------|---|---|---|---|---|
| STOKE HOUSE                | Lloyd Crescent,<br>Wyken,<br>COVENTRY                               | CV2 5NY  | C | 5 | 5 | 2 | 5 |
| HMP BELFAST                | Landscape Terrace,<br>Crumlin Road (A52),<br>BELFAST                | BT14 6AD | C | 5 | 5 | 2 | 5 |
| HMP & YOC<br>HYDEBANK WOOD | Hospital Road,<br>Hydebank Wood,<br>BELFAST                         | BT8 8NA  | C | 5 | 5 | 2 | 5 |
| IDU CRUMLIN<br>ROAD        | Landscape Terrace,<br>Crumlin Road (A52),<br>BELFAST                | BT14 6AD | C | 5 | 5 | 2 | 5 |
| JJC ST. PATRICK'S          | Glen Road (A55),<br>West Belfast,<br>BELFAST, Co.Antrim             | BT11 8BX | C | 5 | 5 | 2 | 5 |
| JJC RATHGAEL               | School Avenue,<br>Newtownards Road (A21),<br>BANGOR, Co.Down        | BT19 1TA | C | 5 | 4 | 2 | 5 |
| SARK ISLAND<br>PRISON      | Mill Lane,<br>La Collinette,<br>Sark, GUERNSEY                      | GY9 0SA  | C | 5 | 5 | 2 | 5 |
| HMP ACKLINGTON             | Wansbeck Road, Acklington,<br>Nr. Amble,<br>MORPETH, Northumberland | NE65 9XF | C | 4 | 3 | 0 | 4 |
| HMP ASHWELL                | OAKHAM, Rutland   | LE15 7LF | C | 4 | 4 | 1 | 5 |
| HMYOI BRINSFORD            | New Road, Featherstone,<br>WOLVERHAMPTON,<br>Staffs                 | WV10 7PY | C | 5 | 5 | 2 | 5 |
| HMP BROCKHILL              | Hewell Grange,<br>REDDITCH, Worcestershire                          | B97 6RD  | C | 5 | 4 | 2 | 5 |
| HMP BUCKLEY<br>HALL        | Buckley Farm Lane,<br>ROCHDALE,<br>Lancashire                       | OL12 9DP | C | 5 | 5 | 2 | 5 |
| HMP CAMP HILL              | High Road,<br>Parkhurst, NEWPORT,<br>Isle of Wight                  | PO30 5PB | C | 4 | 5 | 1 | 5 |
| HMP CHANNINGS<br>WOOD      | Denbury, NEWTON<br>ABBOT,<br>Devon                                  | TQ12 6DW | C | 3 | 3 | 1 | 5 |
| HMP COLDINGLEY             | Shaftesbury Road, Bisley,<br>WOKING, Surrey                         | GU24 9EX | C | 4 | 5 | 2 | 5 |
| HMP DARTMOOR               | Princetown, YELVERTON,<br>Devon                                     | PL20 6RR | C | 5 | 3 | 1 | 5 |
| HMP ELMLEY                 | Church Road, Eastchurch,<br>SHEERNESS, Isle of<br>Sheppey,<br>Kent  | ME12 4DZ | C | 4 | 3 | 1 | 5 |
| HMP ERLESTOKE              | DEVIZES, Wiltshire  | SN10 5TU | C | 4 | 3 | 0 | 4 |
| HMP EVERTHORPE             | BROUGH, East Yorkshire  | HU15 1RB | C | 4 | 2 | 2 | 5 |
| HMP<br>FEATHERSTONE        | New Road,<br>WOLVERHAMPTON,<br>Staffs                               | WV10 7PU | C | 5 | 5 | 2 | 5 |
| HMP/YOI GUYS<br>MARSH      | SHAFTESBURY, Dorset   | SP7 0AH  | C | 4 | 2 | 1 | 5 |
| HMP HAVERIGG               | MILLOM, Cumbria   | LA18 4NA | C | 5 | 3 | 1 | 5 |
| HMP HIGHPOINT              | Stradishall, NEWMARKET,<br>Suffolk                                  | CB8 9YG  | C | 5 | 2 | 2 | 3 |

|                         |   |          |   |   |   |   |   |
|-------------------------|---|----------|---|---|---|---|---|
| HMYOI HUNTERCOMBE       | Huntercombe Place, Nuffield, HENLEY-ON-THAMES, Oxfordshire      | RG9 5SB  | C | 3 | 5 | 0 | 4 |
| HMP LANCASTER CASTLE    | The Castle, LANCASTER, Lancashire                               | LA1 1YL  | C | 5 | 5 | 2 | 5 |
| HMP LINCOLN             | Greetwell Road, LINCOLN   | LN2 4BD  | C | 5 | 5 | 2 | 5 |
| HMP LINDHOLME           | Bawtry Road, Hatfield Woodhouse, DONCASTER                      | DN7 6EE  | C | 4 | 4 | 2 | 5 |
| HMP LITTLEHEY           | Crow Spinney Lane, West Perry, HUNTINGDON, Cambridgeshire       | PE28 0SR | C | 5 | 3 | 1 | 5 |
| HMP/YOI MOORLAND CLOSED | Bawtry Road, Nr. Hatfield Woodhouse, DONCASTER, South Yorkshire | DN7 6BW  | C | 4 | 4 | 2 | 5 |
| HMP THE MOUNT           | Molyneaux Avenue, Bovingdon, HEMEL HEMPSTEAD, Herts             | HP3 0NZ  | C | 5 | 5 | 2 | 5 |
| HMP RANBY               | A620 Straight Mile Road, Nr. Ranby, RETFORD, Nottinghamshire    | DN22 8EU | C | 4 | 5 | 0 | 5 |
| HMP RISLEY              | 617, Warrington Road, Risley, WARRINGTON, Cheshire              | WA3 6BP  | C | 5 | 5 | 2 | 5 |
| HMP SEND                | Ripley Road, Send, WOKING, Surrey                               | GU23 7LJ | C | 4 | 4 | 2 | 5 |
| HMP SHEPTON MALLET      | Cornhill, SHEPTON MALLET, Somerset                              | BA4 5LU  | C | 5 | 5 | 2 | 5 |
| HMP STAFFORD            | 54, Gaol Road, STAFFORD   | ST16 3AW | C | 5 | 5 | 2 | 5 |
| HMP STOCKEN             | Stocken Hall Road, Stretton, OAKHAM, Rutland                    | LE15 7RD | C | 4 | 4 | 1 | 5 |
| HMP THE VERNE           | The Verne, PORTLAND, Dorset                                     | DT5 1EQ  | C | 4 | 5 | 2 | 5 |
| HMYOI WARREN HILL       | Rectory Road, Hollesley, WOODBRIDGE, Suffolk                    | IP12 3JW | C | 5 | 5 | 2 | 5 |
| HMP WAYLAND             | Griston, THETFORD, Norfolk                                      | IP25 6RL | C | 5 | 4 | 1 | 5 |
| HMP THE WEARE           | Portland Dock, Rotherham Road, Fortuneswell, PORTLAND, Dorset   | DT5 1PZ  | C | 4 | 3 | 1 | 4 |
| HMP WELLINGBOROUGH      | Millers Park, Doddington Road, WELLINGBOROUGH, Northants        | NN8 2NH  | C | 5 | 5 | 2 | 5 |
| HMP WHATTON             | 14, Cromwell Road, NOTTINGHAM                                   | NG13 9FQ | C | 5 | 3 | 1 | 5 |
| HMP WYMOTT              | Ulnes Walton Lane, Leyland, PRESTON                             | PR26 8LW | C | 4 | 4 | 2 | 5 |
| IRC DOVER               | The Citadel, Western Heights, DOVER, Kent                       | CT17 9DR | C | 5 | 5 | 1 | 5 |
| IRC HASLAR              | 2, Dolphin Way, GOSPORT, Hampshire                              | PO12 2AW | C | 5 | 5 | 2 | 5 |

|                        |  |          |   |   |   |   |   |
|------------------------|--|----------|---|---|---|---|---|
| HMYOI COLCHESTER       | Berechurch Hall Road,<br>COLCHESTER,<br>Essex                                | CO2 9NU  | C | 4 | 4 | 1 | 4 |
| MSU DENIS HILL         | Bethlem Royal Hospital,<br>Orchard Road, Beckenham,<br>KENT                  | BR3 3BX  | C | 5 | 5 | 2 | 5 |
| MSU FROMESIDE          | Blackberry Hill Hospital,<br>Manor Road, Fishponds,<br>BRISTOL               | BS16 2EW | C | 5 | 5 | 2 | 5 |
| RSU SCOTT CLINIC       | Rainhill Road,<br>ST. HELENS, Merseyside                                     | WA9 5BD  | C | 5 | 5 | 2 | 5 |
| MSU WALLINGFORD Clinic | Fair Mile Hospital,<br>Reading Road,<br>Cholsey, WALLINGFORD,<br>Oxfordshire | OX10 9HH | C | 5 | 5 | 2 | 5 |
| LASCH ALDINE HOUSE     | 75, Limb Lane,<br>Dore, SHEFFIELD  | S17 3ES  | C | 5 | 5 | 2 | 5 |
| LASCH ATKINSON UNIT    | Atkinson Close,<br>Beacon Lane,<br>EXETER, Devon                             | EX4 8NA  | C | 5 | 4 | 2 | 5 |
| LASCH AYCLIFFE         | Copelaw,<br>NEWTON AYCLIFFE,<br>County Durham                                | DL5 6JB  | C | 5 | 3 | 2 | 5 |
| LASCH BARTON MOSS      | Barton Moss Road,<br>Chat Moss, Eccles,<br>MANCHESTER                        | M30 7RL  | C | 5 | 5 | 2 | 5 |
| LASCH BEECHFIELD       | Effingham Road,<br>Cophorne, CRAWLEY,<br>West Sussex                         | RH10 3HZ | C | 5 | 4 | 2 | 5 |
| LASCH BRIARS HAY       | Mill Lane,<br>Rainhill,<br>ST. HELENS,<br>Merseyside                         | L35 6NE  | C | 5 | 5 | 2 | 5 |
| LASCH BRUNEL UNIT      | 125c, Market Street,<br>Clay Cross,<br>CHESTERFIELD,<br>Derbyshire           | S45 9LX  | C | 5 | 5 | 2 | 5 |
| LASCH CLARE LODGE      | 104, Welmore Road,<br>Glington, PETERBOROUGH,<br>Cambridgeshire              | PE6 7LU  | C | 4 | 4 | 1 | 5 |
| LASCH CLAYFIELDS HOUSE | 18-20, Moorbridge Lane,<br>Stapleford, NOTTINGHAM                            | NG9 8GU  | C | 5 | 5 | 2 | 5 |
| LASCH DALES HOUSE      | Normoss Road,<br>Flyde Community,<br>BLACKPOOL<br>Lancashire                 | FY3 0BE  | C | 5 | 4 | 2 | 5 |
| LASCH EARLSWOOD        | 18, Gravelly Hill North,<br>Erdington, BIRMINGHAM,<br>West Midlands          | B23 6BQ  | C | 5 | 5 | 2 | 5 |
| LASCH EAST MOOR        | East Moor Lane,<br>Adel, LEEDS,<br>West Yorkshire                            | LS16 8EB | C | 4 | 5 | 1 | 5 |
| LASCH GLADSTONE HOUSE  | Dyson Hall Campus,<br>Higher Lane, Fazakerly,<br>LIVERPOOL                   | L9 7HB   | C | 5 | 5 | 2 | 5 |
| LASCH HILLSIDE         | off Burnside, Cimla,<br>NEATH,<br>Neath & Port Talbot                        | SA11 1UL | C | 5 | 5 | 1 | 5 |

|                       |  |          |   |   |   |   |   |
|-----------------------|--|----------|---|---|---|---|---|
| LASCH KYLOE HOUSE     | Netherton Park,<br>Stannington, MORPETH,<br>Northumberland                       | NE61 6DE | C | 5 | 3 | 2 | 5 |
| LASCH LANSDOWNE       | Hawks Town Close,<br>Hawks Road, Magham,<br>HAILSHAM,<br>East Sussex             | BN27 1HT | C | 4 | 4 | 2 | 5 |
| LASCH LEVERTON HALL   | Dark Lane,<br>Nr. Great Warley,<br>BRENTWOOD,<br>Essex                           | CM14 5LL | C | 5 | 5 | 2 | 5 |
| LASCH LINCOLNSHIRE    | Rookery Avenue,<br>SLEAFORD,<br>Lincolnshire                                     | NG34 7TY | C | 5 | 4 | 1 | 5 |
| LASCH RED BANK        | Winwick Road,<br>NEWTON-LE-WILLOWS,<br>Merseyside                                | WA12 8EA | C | 5 | 5 | 2 | 5 |
| LASCH REDSANDS        | Oak House,<br>251, Crewe Road,<br>Willaston, NANTWICH,<br>Cheshire               | CW5 6NE  | C | 4 | 5 | 2 | 5 |
| LASCH ST. JOHN'S      | St. John's Road,<br>Tiffield, TOWCESTER,<br>Northamptonshire                     | NN12 8AA | C | 5 | 2 | 2 | 5 |
| LASCH STAMFORD HOUSE  | 206, Goldhawk Road,<br>Sheppards Bush,<br>LONDON                                 | W12 9PA  | C | 5 | 5 | 2 | 5 |
| LASCH SUTTON PLACE    | 347, Saltshouse Road,<br>HULL, North Humberside                                  | HU8 9HR  | C | 5 | 5 | 2 | 5 |
| LASCH SWANWICK LODGE  | Glen Road, off Swanwick<br>Lane,<br>Lower Swanwick,<br>SOUTHAMPTON,<br>Hampshire | SO31 7HD | C | 5 | 5 | 2 | 5 |
| LASCH THORNBURY HOUSE | 40, The Moors,<br>KIDLINGTON,<br>Oxon  | OX5 2AL  | C | 5 | 4 | 2 | 5 |
| LASCH VINNEY GREEN    | Emersons Green Lane,<br>Mangotsfield, Nr. BRISTOL,<br>South Gloucestershire      | BS16 7AA | C | 5 | 5 | 2 | 5 |
| LASCH WATLING HOUSE   | Watling Street,<br>Gailey, STAFFORD,<br>Staffordshire                            | ST19 5PR | C | 5 | 5 | 2 | 5 |
| HMP CRAIGINCHES       | 4, Grampian Place,<br>Craiginchies, ABERDEEN<br>Aberdeenshire                    | AB11 8FN | C | 5 | 5 | 1 | 5 |
| HMP DUMFRIES          | Terregles Street,<br>DUMFRIES,<br>Dumfries & Galloway                            | DG2 9AX  | C | 5 | 5 | 1 | 5 |
| HMP EDINBURGH         | 33, Stenhouse Road,<br>EDINBURGH   | EH11 3LN | C | 5 | 5 | 2 | 5 |
| HMP GREENOCK          | 85, Old Inverkip Road,<br>Gateside, GREENOCK,<br>Inverclyde                      | PA16 9AJ | C | 5 | 5 | 2 | 5 |
| HMP KERR HOUSE        | HMP Shotts<br>Newmill & Canthill Road,<br>SHOTTS,<br>North Lanarkshire           | ML7 4LE  | C | 3 | 4 | 1 | 4 |
| HMP FOYLEVIEW         | HMP MAGILLIGAN, Point<br>Road, Magilligan,<br>LIMAVADY,<br>Co.(London)derry      | BT49 0LR | C | 5 | 3 | 0 | 5 |

|   |   |          |      |   |   |   |   |
|---|---|----------|------|---|---|---|---|
| JJC LISNEVIN                            | 2, Drumfad Road, Millisle, NEWTOWNA RDS, Co. Down                     | BT22 2JQ | C    | 5 | 3 | 0 | 5 |
| JJC NORTHERN IRELAND                    | School Avenue, Newtownards Road (A21), BANGOR, Co. Down               | BT19 1TA | C    | 5 | 4 | 2 | 5 |
| HMP PORTERFIELD                         | Duffy Drive, INVERNESS, Highland                                      | IV2 3HH  | C ~D | 5 | 5 | 2 | 5 |
| LAH HOWDENHALL                          | Braid Unit, 39, Howdenhall Road, EDINBURGH                            | EH16 6TY | C ~D | 5 | 5 | 2 | 5 |
| RS KIBBLE                               | Goudie Street, PAISLEY, Renfrewshire                                  | PA3 2LG  | C ~D | 5 | 5 | 2 | 5 |
| RS OAKBANK                              | Midstocket Road, ABERDEEN, Aberdeenshire                              | AB15 5XP | C ~D | 5 | 4 | 2 | 5 |
| LAH ST. KATHERINE'S                     | Guthrie Unit, 29b, Balmwell Terrace EDINBURGH                         | EH16 6PS | C ~D | 5 | 5 | 2 | 5 |
| HMP BLANTYRE HOUSE                      | Goudhurst, CRANBROOK, Kent  | TN17 2NH | C D  | 3 | 5 | 1 | 5 |
| HMP/YOI DRAKE HALL                      | Patterson Avenue, Sturbridge, Nr. Eccleshall, STAFFORD, Staffordshire | ST21 6LQ | C D  | 4 | 5 | 2 | 5 |
| HMP MORTON HALL                         | Swinderby, LINCOLN  | LN6 9PT  | C D  | 4 | 4 | 1 | 5 |
| HMP ROCHESTER                           | 1 Fort Road, ROCHESTER, Kent  | ME1 3QS  | C D  | 5 | 5 | 2 | 5 |
| RS LINN MOOR                            | Nr. PETERCULTER, Aberdeen, Aberdeenshire                              | AB14 0PJ | C D  | 5 | 4 | 1 | 4 |
| HMP LATCHMERE HOUSE                     | Church Road, Ham Common, RICHMOND, Surrey                             | TW10 5HH | C D  | 5 | 4 | 1 | 5 |
| HMP USK                                 | 47, Maryport Street, USK, Gwent                                       | NP15 1XP | C D  | 4 | 5 | 2 | 5 |
| HMP WEALSTUN                            | WETHERBY, West Yorkshire  | LS23 7AZ | C D  | 4 | 5 | 1 | 5 |
| LASCH ORCHARD LODGE                     | within grounds of Orchard School, William Booth Road, Anerley, LONDON | SE20 8BG | C D  | 5 | 5 | 2 | 5 |
| LASCH ST. CATHERINE'S                   | off Blackbrook Road, Blackbrook, ST. HELENS, Merseyside               | WA11 9RJ | C D  | 5 | 5 | 2 | 5 |
| LAH THE ELMS                            | Elm Court, 317, South Road, Lochee, DUNDEE, Angus                     | DD2 2RT  | C D  | 5 | 5 | 2 | 5 |
| RS GOOD SHEPHERD                        | Greenock Road, BISHOPTON, Renfrewshire                                | PA7 5PF  | C D  | 5 | 5 | 2 | 5 |
| RS KERELAW                              | Kerelaw Campus, Kerelaw Road, STEVENSTON, North Ayrshire              | KA20 4JY | C D  | 4 | 5 | 2 | 5 |
| RS ROSSIE Secure Accommodation Services | Westerton, Nr. MONTROSE, Angus  | DD10 9TW | C D  | 5 | 4 | 1 | 5 |

|                             |   |          |       |   |   |   |   |
|-----------------------------|---|----------|-------|---|---|---|---|
| RS ST. PHILIP'S             | Beechwood House,<br>Plains, by AIRDRIE,<br>North Lanarkshire            | ML6 7SF  | C D   | 4 | 5 | 2 | 5 |
| RS SPRINGBOIG ST.<br>JOHN'S | 1190, Edinburgh Road,<br>Shettleston, GLASGOW                           | G33 4EH  | C D   | 5 | 5 | 2 | 5 |
| HMP/YOI ASKHAM<br>GRANGE    | Askham Richard, YORK  | YO23 3FT | D     | 5 | 4 | 2 | 4 |
| HMP/YOI EAST<br>SUTTON PARK | Sutton Valence,<br>MAIDSTONE,<br>Kent                                   | ME17 3DF | D     | 3 | 4 | 1 | 5 |
| HMP FORD                    | ARUNDEL, West Sussex  | BN18 0BX | D     | 5 | 5 | 1 | 5 |
| HMP HEWELL<br>GRANGE        | REDDITCH, Worcs   | B97 6QQ  | D     | 4 | 3 | 2 | 5 |
| HMP KIRKHAM                 | Freckleton Road, PRESTON,<br>Lancashire                                 | PR4 2RN  | D     | 5 | 5 | 2 | 5 |
| HMP LEYHILL                 | Cromhall, WOTTON-<br>UNDER-EDGE,<br>Gloucestershire                     | GL12 8BT | D     | 4 | 5 | 1 | 4 |
| HMP/YOI<br>MOORLAND OPEN    | Thorne Road, Hatfield,<br>DONCASTER,<br>South Yorkshire                 | DN7 6EL  | D     | 5 | 5 | 2 | 5 |
| HMP NORTH SEA<br>CAMP       | Croppers Lane,<br>Freiston, BOSTON,<br>Lincolnshire                     | PE22 0QX | D     | 3 | 1 | 0 | 4 |
| HMP SPRING HILL             | Edgcott,<br>AYLESBURY, Bucks  | HP18 0TH | D     | 4 | 3 | 1 | 4 |
| HMP STANDFORD<br>HILL       | Church Road,<br>Eastchurch, SHEERNESS,<br>Isle of Sheppey, Kent         | ME12 4AA | D     | 4 | 3 | 1 | 4 |
| HMP SUDBURY                 | Sudbury,<br>ASHBOURNE, Derbyshire                                       | DE6 5HW  | D     | 5 | 5 | 2 | 5 |
| HMYOI THORN<br>CROSS        | Arley Road, Appleton Thorn,<br>WARRINGTON, Cheshire                     | WA4 4RL  | D     | 5 | 5 | 2 | 5 |
| HMP CASTLE<br>HUNTLY        | Longforgan,<br>DUNDEE, Angus  | DD2 5HL  | D     | 5 | 2 | 2 | 5 |
| HMP NORANSIDE               | Fern,<br>FORFAR,<br>Angus   | DD8 3QY  | D     | 3 | 2 | 1 | 4 |
| HMP WAKEFIELD               | 5 Love Lane, WAKEFIELD,<br>West Yorkshire                               | WF2 9AG  | M A   | 5 | 5 | 2 | 4 |
| HMP HIGH DOWN               | Highdown Lane, off Sutton<br>Lane,<br>Belmont, SUTTON,<br>Surrey/London | SM2 5PJ  | M A   | 5 | 4 | 2 | 5 |
| HSH ASHWORTH<br>NORTH       | School Lane,<br>Parkbourn, Maghull,<br>LIVERPOOL                        | L31 1HW  | M A   | 5 | 5 | 2 | 5 |
| HMP BELMARSH                | Western Way, Thamesmead,<br>LONDON                                      | SE28 0EB | M A   | 5 | 4 | 2 | 5 |
| HMP FRANKLAND               | Brasside, DURHAM  | DH1 5YD  | M A   | 5 | 4 | 2 | 5 |
| HMP WOODHILL                | Tattenhoe Street,<br>Woodhill, MILTON<br>KEYNES,<br>Bucks               | MK4 4DA  | M A   | 3 | 4 | 1 | 5 |
| HMP SHOTTS                  | Newmill & Canthill Road,<br>SHOTTS,<br>North Lanarkshire                | ML7 4LE  | M A   | 3 | 4 | 1 | 4 |
| HMP WHITEMOOR               | Longhill Road, MARCH,<br>Cambs  | PE15 0PR | M A B | 4 | 5 | 1 | 5 |
| HMP HULL                    | Hedon Road, HULL,<br>North Humberside                                   | HU9 5LS  | M A B | 5 | 5 | 2 | 5 |

|                        |   |          |       |   |   |   |   |
|------------------------|---|----------|-------|---|---|---|---|
| HSH RAMPTON HOSPITAL   | Flemming Drive, Woodbeck, RETFORD, Nottinghamshire                              | DN22 0PD | M A B | 4 | 5 | 1 | 4 |
| HSH THE STATE HOSPITAL | 110, Lampits Road, Carstairs Junction, Nr. Carstairs, LANARK, South Lanarkshire | ML11 8RP | M A B | 4 | 2 | 2 | 5 |
| HMP DURHAM             | 19b, Old Elvet, DURHAM  | DH1 3HU  | M A B | 5 | 5 | 2 | 4 |
| HMP FULL SUTTON        | Full Sutton, YORK   | YO41 1PS | M A B | 4 | 3 | 1 | 5 |
| HMP LONG LARTIN        | South Littleton, EVESHAM, Worcestershire  | WR11 8TZ | M B   | 4 | 3 | 2 | 4 |
| HMP/YOI ASHFIELD       | Shortwood Road, Pucklechurch, BRISTOL   | BS16 9QJ |       | 5 | 5 | 2 | 5 |
| HMYOI BULLWOOD HALL    | High Road, HOCKLEY, Essex   | SS5 4TE  |       | 4 | 5 | 2 | 5 |
| HMP COOKHAM WOOD       | Sir Evelyn Road, Chatham, ROCHESTER, Kent                                       | ME1 3LU  |       | 5 | 5 | 2 | 5 |
| HMP DOWNVIEW           | Highdown Lane, off Sutton Lane, Belmont, SUTTON, Surrey/London                  | SM2 5PD  |       | 5 | 5 | 2 | 5 |
| HMP/YOI EASTWOOD PARK  | Falfield, WOTTON-UNDER-EDGE, Gloucestershire                                    | GL12 8DB |       | 5 | 3 | 2 | 5 |
| HMP FOSTON HALL        | Foston, DERBY, Derbyshire   | DE65 5DN |       | 5 | 3 | 2 | 5 |
| HMP/YOI HOLLOWAY       | Parkhurst Road, LONDON  | N7 0NU   |       | 5 | 5 | 2 | 5 |
| HMP/YOI NEW HALL       | Dial Wood, Flockton, WAKEFIELD, West Yorkshire                                  | WF4 4AX  |       | 5 | 5 | 2 | 5 |
| HMP/YOI PRESCOED       | 47, Maryport Street, USK, Gwent   | NP15 1XP |       | 4 | 5 | 2 | 4 |
| HMP/YOI STYAL          | Styal, WILMSLOW, Cheshire   | SK9 4HR  |       | 5 | 5 | 2 | 5 |
| HMU PETERHEAD          | PETERHEAD, Aberdeenshire  | AB42 2YY |       | 5 | 4 | 1 | 5 |
| HMU SHOTTS             | HMP Shotts Newmill & Canthill Road, SHOTTS, North Lanarkshire                   | ML7 4LE  |       | 3 | 4 | 1 | 4 |
| IDC DUNGAVEL           | STRATHAVEN, South Lanarkshire   | ML10 6RF |       | 4 | 5 | 1 | 5 |

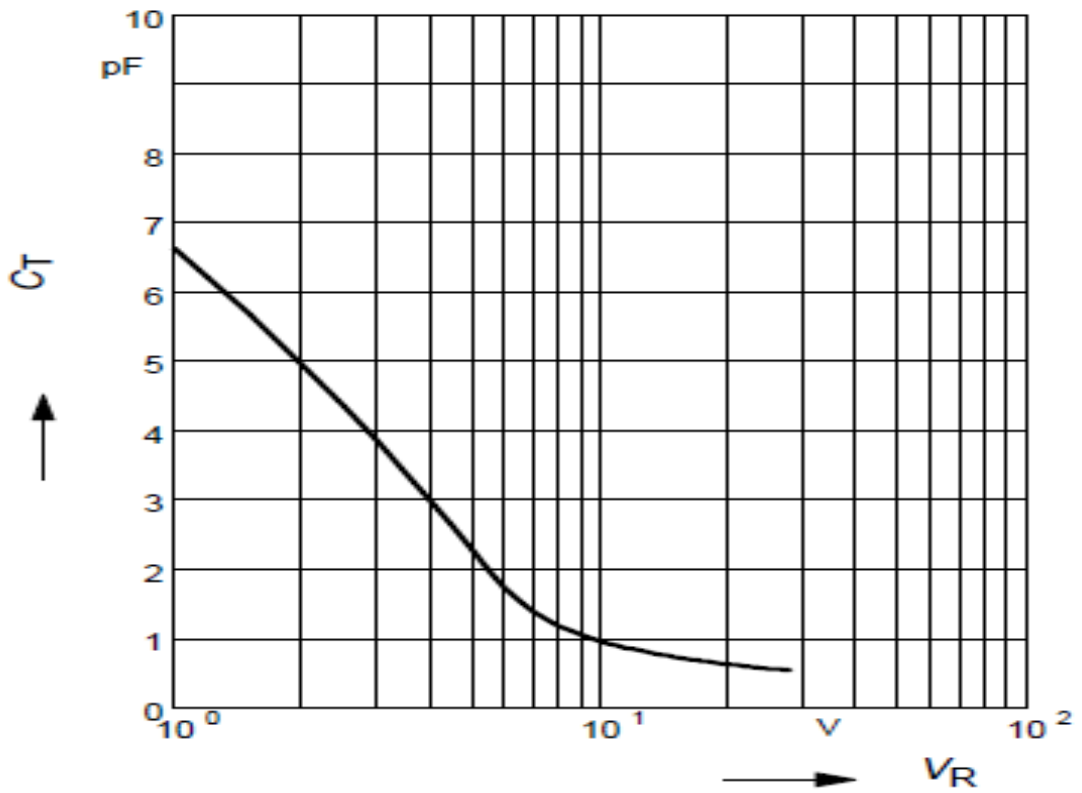
## APPENDIX II: PRISON CELL WITH FSS ON THE WINDOW



# APPENDIX III: BB857 DIODE DATA SHEET

Electrical Characteristics at  $T_A = 25^\circ\text{C}$ , unless otherwise specified

| Parameter  | Symbol           | Values |      |      | Unit     |
|--|------------------|--------|------|------|----------|
|  |                  | min.   | typ. | max. |          |
| <b>DC Characteristics</b>  |                  |        |      |      |          |
| Reverse current  | $I_R$            | -      | -    | 10   | nA       |
| $V_R = 30\text{ V}$  |                  | -      | -    | 10   |          |
| $V_R = 30\text{ V}, T_A = 85^\circ\text{C}$                                      |                  | -      | -    | 200  |          |
| <b>AC Characteristics</b>  |                  |        |      |      |          |
| Diode capacitance  | $C_T$            |        |      |      | pF       |
| $V_R = 1\text{ V}, f = 1\text{ MHz}$   |                  | 6      | 6.6  | 7.2  |          |
| $V_R = 25\text{ V}, f = 1\text{ MHz}$  |                  | 0.5    | 0.55 | 0.65 |          |
| $V_R = 28\text{ V}, f = 1\text{ MHz}$  |                  | 0.45   | 0.52 | -    |          |
| Capacitance ratio  | $C_{T1}/C_{T25}$ | 10.2   | 12   | -    | -        |
| $V_R = 1\text{ V}, V_R = 25\text{ V}, f = 1\text{ MHz}$                          |                  |        |      |      |          |
| Capacitance ratio  | $C_{T1}/C_{T28}$ | 9.7    | 12.7 | -    | -        |
| $V_R = 1\text{ V}, V_R = 28\text{ V}, f = 1\text{ MHz}$                          |                  |        |      |      |          |
| Capacitance matching <sup>1)</sup>   | $\Delta C_T/C_T$ | -      | -    | 5    | %        |
| $V_R = 1\text{ V} \dots 28\text{ V}, f = 1\text{ MHz}, 7\text{ diodes sequence}$ |                  |        |      |      |          |
| Series resistance  | $r_S$            | -      | 1.5  | -    | $\Omega$ |
| $V_R = 5\text{ V}, f = 470\text{ MHz}$   |                  |        |      |      |          |
| Series inductance  | $L_S$            | -      | 0.6  | -    | nH       |



# APPENDIX IV: BB131 DIODE DATA SHEET

VHF variable capacitance diode

BB131

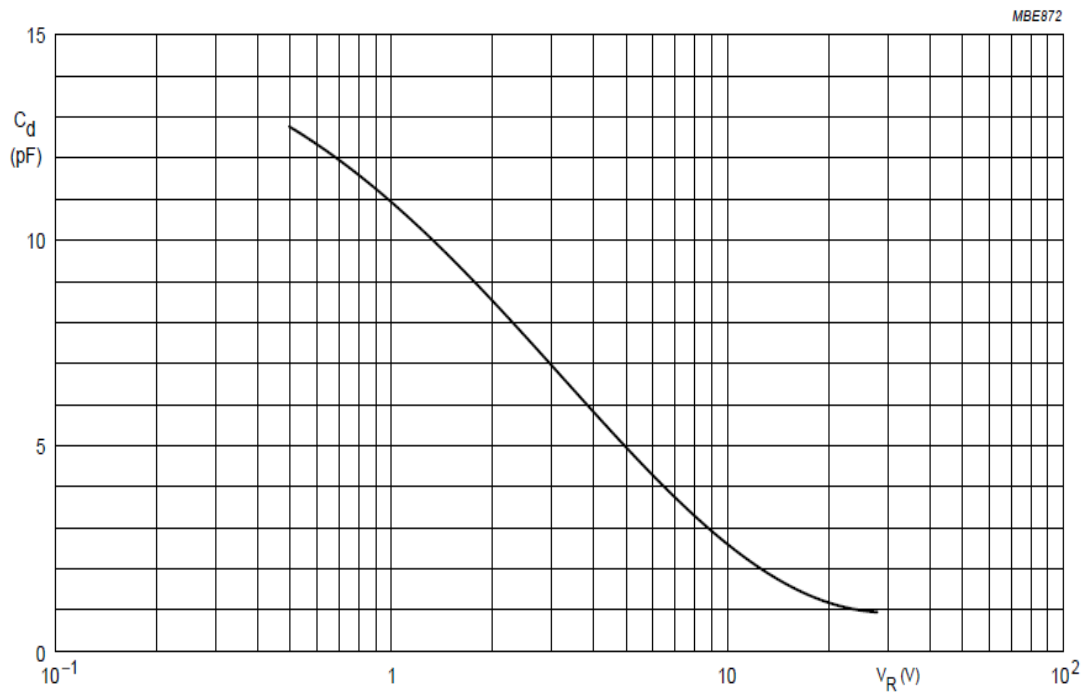
## CHARACTERISTICS

$T_j = 25\text{ °C}$  unless otherwise specified.

| SYMBOL                           | PARAMETER               | CONDITIONS   | MIN. | MAX.  | UNIT     |
|----------------------------------|-------------------------|--|------|-------|----------|
| $I_R$                            | reverse current         | $V_R = 30\text{ V}$ ; see Fig.3                              | –    | 10    | nA       |
|                                  |                         | $V_R = 30\text{ V}$ ; $T_j = 85\text{ °C}$ ; see Fig.3       | –    | 200   | nA       |
| $r_s$                            | diode series resistance | $f = 470\text{ MHz}$ ; note 1                                | –    | 3     | $\Omega$ |
| $C_d$                            | diode capacitance       | $V_R = 0.5\text{ V}$ ; $f = 1\text{ MHz}$ ; see Figs 2 and 4 | 8    | 17    | pF       |
|                                  |                         | $V_R = 28\text{ V}$ ; $f = 1\text{ MHz}$ ; see Figs 2 and 4  | 0.7  | 1.055 | pF       |
| $\frac{C_{d(0.5V)}}{C_{d(28V)}}$ | capacitance ratio       | $f = 1\text{ MHz}$   | 12   | 16    |          |

### Note

- $V_R$  is the value at which  $C_d = 9\text{ pF}$ .



$T_j = 25\text{ °C}$ ;  $f = 1\text{ MHz}$ .

Diode capacitance as a function of reverse voltage; typical values.